SYNTHETIC RECEPTOR-ENGINEERED T LYMPHOCYTES FOR CANCER

PRE-CLINICAL DEVELOPMENT OF SYNTHETIC RECEPTOR-ENGINEERED T LYMPHOCYTES FOR THE TREATMENT OF CANCER: NOVEL RECEPTORS AND UNDERSTANDING TOXICITY

By JOANNE A. HAMMILL, Hons.B.Sc.

A Thesis Submitted to the School of Graduate Studies in Partial Fulfilment of the Requirements for the Degree Doctor of Philosophy

McMaster University DOCTOR OF PHILOSOPHY (2017) Hamilton, Ontario (Medical Sciences)

TITLE: Pre-clinical development of synthetic receptor-engineered T lymphocytes for the treatment of cancer: novel receptors and understanding toxicity

AUTHOR: Joanne A. Hammill, Hons.B.Sc. (McMaster University)

SUPERVISOR: Professor Jonathan L. Bramson

NUMBER OF PAGES: xix, 200

Lay Abstract:

The human immune system has the unique capacity to "seek and destroy" tumor cells throughout the body. A novel class of drugs, immuno-oncology agents, harness this ability to fight cancer. Within this class is a new cellular drug where genetic engineering is used to create killer immune cells (called T cells) capable of recognizing and eliminating tumors. Two of these cellular drugs have recently received FDA approval, supporting the feasibility of this approach. However, further research is needed to improve the safety of engineered-T cells and increase the number of patients whom can benefit from their use. This thesis uses laboratory investigations to better understand the side-effects associated with anti-cancer engineered-T cells and evaluate new engineering strategies. We anticipate that these results will contribute towards the development of next-generation engineered-T cell drugs which retain the ability to function systemically against cancer but offer an enhanced safety profile.

Abstract:

Advances in our understanding of the molecular events leading to cancer have facilitated the development of next-generation targeted therapies. Among the most promising new approaches is immuno-oncology, where therapeutic agents engage the immune system to fight cancer. One exciting strategy therein is the adoptive transfer of *ex vivo* cultivated tumor-specific T lymphocytes into a cancer patient. Tumor-specific T cells can be produced by engineering a patient's own T cells with synthetic receptors (e.g. chimeric antigen receptors (CARs)) designed to redirect T cell cytotoxicity against a tumor target. CAR-engineered T cells (CAR-T cells) were expected to be a non-toxic cellular therapy which would seek out and specifically eliminate disseminated tumors. The clinical experience supports the promise of CAR-T cell therapy (striking efficacy has been observed in the treatment of hematological malignancies), while highlighting areas for improvement; CAR-T cell use has been associated with a host of toxicities and robust clinical efficacy has yet to be replicated in solid tumors.

This thesis uses pre-clinical models to describe previously unappreciated aspects of CAR-T cell-associated toxicity and novel synthetic receptor strategies, including:

i. The capacity of NKG2D-based CAR-T cells to mediate toxicity.
ii. The utility of designed ankyrin repeat proteins as CAR antigen-binding domains.
iii. The discovery that variables intrinsic to human CAR-T cell products contribute to toxicity.
iv. A novel synthetic receptor capable of redirecting T cell specificity against a tumor target – the T cell antigen coupler (TAC). Unlike equivalent CAR-T cells, TAC-T cells are capable of mediating efficacy against a solid tumor in the absence of toxicity.

We anticipate that these results will contribute towards the development of next-generation synthetic receptor-engineered T cell products that can deliver upon the promise of safe, systemic cancer therapeutics.

Acknowledgements:

Modern science is a team sport. I have been incredibly fortunate to have had the support of individuals and organizations, members of "my team", which have impacted upon the work in this thesis and my graduate student experience for the better. I would like to offer each of them my sincere thanks.

First and foremost, to my mentor Dr. Jonathan Bramson. I can confidently say that my trainee experience has been more fortunate than most because of his mentorship. Jonathan leads by example, and as much as I've been deliberately taught by him, I've taken away more from having had the opportunity to observe his approach to science and leadership from "the inside". While, on a practical level, my work has benefited from Jonathan's intellectual guidance and ability to garner funding, it's been his mastery of the field, comfortability and confidence in speaking about science, and ability to evolve (both in his science and career), that have been inspirational. Simply put, working with Jonathan has made me want to be a better scientist. JB – words do little justice to the strength of your character and calibre of science/mentorship. Thank you for everything.

To Dr. Yonghong Wan, Dr. John Hassell, and Dr. Mark Levine. Thank you for taking the time to act as members of my graduate supervisory committee. Your collective efforts have served to further my development as a scientist and are deeply appreciated. Each of you has caused me to consider a unique perspective on my project. Wan – thank you for offering a second source of expertise in the immuno-oncology arena and being my first insight into the power of academic collaboration through your relationship with Jonathan. John – thank you for pushing me on the cancer biology side of immuno-oncology and asking the tough questions. Mark – thank you for providing a window into the clinical world and humanizing cancer patients.

To members of the Bramson Lab, past and present, whom have made our research group a supportive, intellectually challenging, and enjoyable place to work. What we have is special – a big thanks goes to all of you. In particular, Dr. Heather VanSeggelen, who was my go-to peer mentor and comrade-in-arms early in the CAR project – thank you. Also, to Dr. Alina Lelic, for endless advice on human T cells, flow cytometry, and how to finish a thesis – thank you.

To my co-authors and collaborators who fall outside of the aforementioned groups and contributed to the manuscripts in this thesis (as listed in the Preface). Thank you for contributing both physical and intellectual resources, and taking the time to share your expertise (Dr. Anna Dvorkin-Gheva and Dr. Jacek Kwiecien were particularly generous).

I am grateful to the funding sources that have generously supported both me and the work within this thesis: the Ontario Graduate Scholarship program, the Canadian Cancer Society (formerly the Canadian Breast Cancer Foundation), the Canadian Institutes for Health Research, the Terry Fox Foundation, the Samuel Family Foundation, and Triumvira Immunologics.

Lastly, I would like to extend personal thanks to my family. To my parents – thank you for holding me accountable to my own potential, being overwhelmingly supportive (most of the time), and making every effort to understand my work/the world of academia. To my sister – I was lucky to be given a best friend by birth, I was even luckier when you went to grad school so we could commiserate. You've kept me sane.

Table of Contents:

Preliminary Pages:

Main Text:

Lists of Figures and Tables:

Notes: S denotes supplementary. In the case of a figure/table legend appearing on a different page than the corresponding the figure/table, the location of the legend is indicated in brackets.

List of all Abbreviations and Symbols:

Abbreviations:

ACT	adoptive cell transfer
ANOVA	analysis of variance
AP-1	activated protein 1
AR	ankyrin repeat
B-ALL	B cell acute lymphoblastic leukemia
BCMA	B cell maturation antigen
BiTE	bispecific T cell engager
CAIX	carbonic anhydrase IX
CAR	chimeric antigen receptor
CAR-T cell	CAR-engineered T cell
CD	cluster of differentiation
CLL	chronic lymphocytic leukemia
CRS	cytokine release syndrome
CTLA-4	cytotoxic T lymphocyte-associated protein 4
CTX	cyclophosphamide
d	day
DARPin	designed ankyrin repeat protein
DART	dual-affinity retargeting protein
DNA	deoxyribonucleic acid
E:T	effector:target
EF-1α	elongation factor-1 alpha
EpCAM	epithelial cell adhesion molecule
FBS	fetal bovine serum
FDA	US Food and Drug Administration
GM-CSF	granulocyte-macrophage colony-stimulating factor
H&E	hematoxylin and eosin
HAMA	human anti-mouse antibody
HER2	human epidermal growth factor receptor 2
HLA	human leukocyte antigen
huUCHT1	humanized UCHT1
IC	intracellular
IFN	interferon
IgG	immunoglobulin G
IHC	immunohistochemistry
IL	interleukin
ITAM	immunoreceptor tyrosine-based activation motif
LEUK	commercial leukapheresis product

MAC	McMaster adult cohort
mCMV	minimal cytomegalovirus
MCP-1	monocyte chemoattractant protein-1
MHC	major histocompatibility complex
NFAT	nuclear factor of activated T cells
NF-κB	nuclear factor-κB
NGFR	nerve growth factor receptor
NHL	non-Hodgkin lymphoma
NK cell	natural killer cell
NKG2D	natural killer group 2, member D
NKG2DL	NKG2D ligand
NRG	NOD.Cg-Rag1^{tm1Mom} Il2rg^{tm1Wjl}/SzJ
NS	not significant
OV	oncolytic virus
PBMC	peripheral blood mononuclear cell
PBS	phosphate buffered saline
PC	principle component
PCA	principle component analysis
PCR	polymerase chain reaction
PD-1	programmed cell death protein 1
PD-L1/2	programmed death ligand 1 or 2
PLAT-E	platinum-E
pMHC	peptide-MHC complex
r/r	relapsed/refractory
RAG	recombination activation gene
RCC	renal cell carcinoma
RNA	ribonucleic acid
RV	retrovirus
scFv	single chain variable fragment
sCRS	severe CRS
SD	standard deviation
SE	standard error (see SEM)
SEM	standard error of the mean
SPADE	spanning-tree progression analysis of density-normalized events
SPICE	simplified presentation of incredibly complex evaluations
TAA	tumor associated antigen
TAC	T cell antigen coupler
TAC-T cell	TAC-engineered T cell
TCR	T cell receptor
TGF	transforming growth factor

TIL	tumor infiltrating lymphocyte
TLS	tumor lysis syndrome
TM	transmembrane
TNF	tumor necrosis factor
tNGFR	truncated nerve growth factor receptor
TSA	tumor specific antigen

Symbols:

α	alpha
β	beta
°C	degrees celcius
Δ	delta
γ	gamma
κ	kappa
%	percent
ζ	zeta

Declaration of Academic Achievement:

I, Joanne Hammill, declare that I have independently authored and assembled the contents of this thesis, with editorial assistance from Professor Bramson. Regarding the scholarly works presented in Chapters Two – Five; for a detailed breakdown of my own academic contributions, as well as those of my co-authors, please see the Preface.

Preface:

The body of this thesis contains four scholarly co-authored works (Chapters Two – Five). My own academic contributions (**bold text**) towards each of those works, as well as those of manuscript co-authors, are detailed below.

Chapter Two: VanSeggelen, H, **Hammill, JA**, Dvorkin-Gheva, A, Tantalo, DGM, Kwiecien, JM, Denisova, GF, Rabinovich, B, Wan, Y, Bramson, JL. (2015). T cells engineered with chimeric antigen receptors targeting NKG2D ligands display lethal toxicity in mice. *Molecular Therapy*. 23(10):1601-1610. doi: 10.1038/mt.2015.119.

- HV, **JAH**, and JLB **conceived of these studies, designed experiments, and wrote the manuscript**. HV and **JAH executed *in vitro* and *in vivo* experiments**. HV analyzed data and prepared figures. ADG performed PCA. DGMT assisted with *in vitro* experiments. JMK performed pathological analysis of murine tissues. GFD made contributions to receptor design. BR made contributions to retroviral design. YW made intellectual contributions to the direction of this study. All authors read and approved the final manuscript.
- Joni's contributions to the work represented by this manuscript were conducted from January 2013 – October 2014.

Chapter Three: **Hammill, JA**, VanSeggelen, H, Helsen, CW, Denisova, GF, Evelegh, C, Tantalo, DGM, Bassett, JD, Bramson, JL. (2015). Designed ankyrin repeat proteins are effective targeting elements for chimeric antigen receptors. *Journal for ImmunoTherapy of Cancer*. 3:55. doi: 10.1186/s40425-015-0099-4.

- **JAH helped to coordinate and plan the study, was involved in all aspects of its execution (murine/human CAR-T cell studies, CAR retrovirus design and preparation, CAR lentivirus preparation, and cytotoxicity assays), and drafted/revised the manuscript.** HV assisted with CAR retrovirus preparation and murine CAR-T cell studies. CWH designed CAR lentiviruses and executed human CAR-T cell studies. GFD designed CAR retroviruses. CE executed CAR lentivirus generation. DGMT assisted with CAR lentivirus generation and cytotoxicity assays. JDB assisted with CAR retrovirus preparation and murine CAR-T cell studies. JLB conceived of the study, participated in its coordination and planning, and contributed to the drafting/revision of the manuscript. All authors read and approved the final manuscript.
- The work represented by this manuscript was conducted from December 2011 – October 2015.

Chapter Four: **Hammill, JA**, Kwiecien, JM, Dvorkin-Gheva, A, Bezverbnaya, K, Aarts, C, Helsen, CW, Denisova, GF, Derocher, H, Milne, K, Nelson, BH, Bramson, JL (2018). Chimeric antigen receptor driven toxicity is mediated by co-stimulation of $CD4^+$ T cells in a donor-specific manner. In submission: *The Journal of Clinical Investigation*.

- **JAH** and JLB **conceived of these studies, designed experiments, and wrote the manuscript. JAH acquired and analyzed all data (unless otherwise stated).** JMK performed pathological analysis of murine tissues. ADG performed PCA and hierarchical clustering. KB and CA assisted with *in vivo* experiments. CWH and GFD made contributions to receptor design. HD and KM performed and analyzed multicolour IHC as designed by BHN, KM, and JLB.
- The work represented by this manuscript was conducted from November 2014 – June 2017.

Chapter Five: Helsen, CW, **Hammill, JA**, Mwawasi, KA, Lau, VWC, Afsahi, A, Bezverbnaya, K, Newhook, L, Hayes, DL, Aarts, C, Bojovic, B, Denisova, GF, Kwiecien, JM, Brain, I, Derocher, H, Milne, K, Nelson, BH, Bramson, JL. (2017). A novel chimeric T cell receptor that delivers robust anti-tumor activity and low off-tumor toxicity. In submission, under peer-review: *Nature Communications*.

- CWH, **JAH**, KAM, VWCL, and JLB **conceived of various aspects of these studies and designed experiments.** CWH invented the TAC receptor architecture. GFD made contributions to receptor design. CWH, **JAH,** KAM, VWCL, AA, KB, LN, DLH, and BB **performed *in vitro* TAC assays. JAH performed *in vitro* CAR assays**. VWCL performed phenotypic analysis of checkpoint receptors and memory markers. **JAH**, KB, and CA **performed *in vivo* experiments in the HER2 model**. CA performed *in vivo* experiments in the CD19 model. JMK and IB performed pathological analysis and scoring of murine tissues, respectively. HD and KM performed multicolour IHC as designed by BHN, KM, and JLB. CWH, **JAH**, KAM, VWCL, AA, KB, LN, DLH and JLB **prepared the manuscript (figure design, writing, editing).** All authors reviewed the final manuscript prior to submission.
- Joni's contributions to the work (comparing anti-HER2 DARPin-targeted CAR and TAC T cells *in vitro* and *in vivo*) represented by this manuscript were conducted from November 2014 – April 2017.

1.0 Chapter One – Introduction

1.1 Overview

The current mainstays of cancer therapy, surgery, chemotherapy, and radiation therapy, have been in use for decades. While their introductions revolutionized cancer therapy, and advancements therein have contributed to steadily increasing survivorship rates, their utility is limited by the localized and/or non-specific nature of the therapies. This makes treating metastatic disease a clinical challenge and results in a host of unpleasant side effects incurred as a result of damage to non-tumor tissues. As such, there is a critical need for novel therapeutic strategies.

Over the past century, the capacity of the immune system (in particular, T lymphocytes, *aka T cells*), to identify and eliminate cancerous cells has been established. The immune system naturally functions systemically to discriminately eliminate target cells while sparing healthy tissue, making immunotherapies ideal anti-cancer agents. Immuno-oncology aims to harness the power of the immune system and establish a state of immune control of tumor growth within cancer patients.

The infusion of *ex vivo*-cultivated, tumor-specific T cells into a cancer patient, a type of adoptive cell transfer (ACT), is a promising immunotherapeutic strategy. Spontaneously occurring tumor-specific T cells can be isolated from cancer patients for this purpose, although these populations can be rare, limiting the feasibility and applicability of this approach. Tumor-specificity can be conferred upon T cells via genetically engineering the expression of a tumor-specific receptor. Chimeric antigen receptors (CARs) are particularly useful for this purpose given that they can redirect T cell specificity against tumor targets in an MHC-independent manner. CARs are recombinant proteins composed of an extracellular antigen-binding domain, with specificity for a tumor antigen, and intracellular signaling domains that trigger the activation of T cell effector functions (e.g. cytotoxicity) upon ligation of the antigen-binding domain. CAR-engineered T cells (CAR-T cells) have demonstrated the ability to induce staggering clinical efficacy when targeted against CD19 for the treatment of $CD19^+$ hematological malignancies. However, their use in treating solid tumors has yet to generate the same level of excitement. In addition, the clinical use of CAR-T cells has become synonymous with a constellation of toxicities, ranging in severity from mild to lethal.

It is our belief that *these are surmountable challenges and T cells engineered to express synthetic tumor-targeting receptors remain poised to deliver upon the promise of safe, systemically functioning cancer therapeutics*. *Development of these next-generation synthetic receptor-engineered T cell products will be informed, in part, by the use of pre-clinical models; herein I share my experiences.*

1.2 Background

1.2.1 Prologue: the advent of cancer immunotherapy

In 1890, bone surgeon Dr. William Coley was treating one of his first patients at New York City's Memorial Hospital (now known as Memorial Sloan Kettering Cancer Center). Elizabeth Dashiell, a previously healthy young adult, had developed a metacarpal bone sarcoma. Despite amputation of the limb at the middle forearm, distal metastases were observed several weeks later, and the patient succumbed to her disease just six months after the initial onset of symptoms. Dr. Coley was struck by how rapidly the disease had progressed to claim Elizabeth's life and was left acutely aware of just how little he could do for his patient (at the time, standard of care options for a cancer diagnosis were limited to surgical resection and palliative care) (1).

While combing through hospital records in the search for new treatment ideas, Coley uncovered the case of an incomplete sarcoma resection that had spontaneously undergone complete regression after the patient experienced two bouts of erysipelas (a skin infection usually caused by bacteria of the *Streptococcus* genus (2)). A subsequent literature search uncovered numerous observations of spontaneous tumor regressions occurring after bouts of infectious disease and pioneering physicians who were inoculating malignant patients with purified cultures of "*Streptococcus erysipelatis*" bacteria, reporting regressions and even cures. Thus, Coley embarked upon efforts to treat his own patients with streptococcal cultures in 1891 (1) and it became his life's work.

"*Nature often gives us hints to her profoundest secrets, and it is possible that she has given us a hint which, if we will but follow, may lead us on to the solution of this difficult problem*" – William B. Coley, 1891 (1)

Over time, Coley progressed from potentially fatal treatments with live bacteria (3) to a heat-killed mixture of *Streptococcus pyogenes* and *Serratia marcescens*, which became known as Coley's toxins (4, 5).

Although Coley believed his therapeutic to be directly tumoricidal (1), we now know it likely acted as a powerful immune stimulant, signaling through innate immune receptors to trigger release of inflammatory cytokines and promote adaptive immune responses (6). As such, Dr. William Coley has become known as the "father of immunotherapy" (7).

Unfortunately, due to the simultaneous advent of radiotherapy (which became the preferred approach), inconsistent results, and the toxic nature of Coley's therapy (7, 8), progress in the development of cancer immunotherapies (agents

which aim to "[activate] the immune system for therapeutic benefit in cancer" (4)) would stall for decades.

A note from the author

I have chosen to open my thesis with the story of Dr. Coley for two reasons. First, because Dr. Coley embarked upon his research, inspired by his patient, to address a clinical need; it's a story that puts patients first. As a bench scientist working in the pre-clinical development of cancer therapeutics (using *in vitro* assays and small animal models as a proxy), we are removed from the clinical implications of our work. However, it's important for translational and motivational purposes that our work is conducted with the end goal of helping cancer patients in mind. Second, as is only casually mentioned above, Coley's toxins were in and of themselves toxic to patients. This association between efficacy and toxicity is a common thread amongst cancer therapies and is a central component of this thesis.

1.2.2 A modern view of cancer and its treatment

What is cancer?

Cancer is an umbrella term for the >100 unique diseases (as defined by tissue of origin and histological characterization) arising from the uncontrolled division of cells with the capacity to invade surrounding tissues, resulting in the formation of tumors[1] (9). Even with advanced prevention, detection, and treatment strategies, one in two Canadians will develop cancer in their lifetime and one in four will die of the disease (10).

The prevailing theory of carcinogenesis, the process by which a normal cell transforms into a cancerous cell, posits that mutations arising in the genomic material of a single cell (whether inherited or spontaneous (11)) allow it to escape proliferative controls giving rise to cancerous progeny which propagate the mutations and together form and cultivate a tumor mass[2] (12, 13). The ongoing process of mutation accumulation that can occur during the proliferation of these progeny contributes to the heterogeneity that exists both intra-tumorally (within cells of the same tumor mass) (14, 15) and inter-tumorally (between tumor masses in the case of metastatic disease) (15, 16) within a single cancer patient and across cancer patients.

[1] For the purposes of this thesis, usage of the nomenclature "tumor" is solely in reference to malignancy and not benign tumors.

[2] The vast majority of cancers are a solid mass/tumor, the exception being liquid (or blood) tumors, such as leukemias.

The tumor microenvironment

In addition to malignant cells, the local environment within a tumor contains non-transformed cells and factors released by both of these cell types; together this is called the tumor microenvironment. Non-transformed cells within the tumor microenvironment include stromal cells (such as cancer associated fibroblasts and cells of the vasculature) and immune cells, among others (17). Dynamic interplay between these non-transformed cells and malignant cells contributes to tumor formation (18, 19).

Treating cancer – the big three: surgery, radiation, and chemotherapy

The current mainstays of cancer therapy are surgery, radiation therapy, chemotherapy, and various combinations thereof (20). Since the exact therapeutic agents, combinations, and timelines enacted by oncologists over the course of treatment depend on a number of factors (such as type and stage of malignancy, or whether the treatment is curative or palliative in intent), we will only briefly comment on general properties of each.

The development of surgical resection techniques to remove tumors were bolstered in the mid-nineteenth century with the discovery of anesthesia (21). Today, surgery aims to remove a tumor mass, as well as a surrounding margin of healthy tissue and (in some cases) local lymph nodes to reduce the chances of recurrence or metastatic spread (22).

Radiation therapy (or radiotherapy) for the treatment of cancer was first discovered in the 1890s (21, 23). Radiotherapy aims to deliver a dose of cytotoxic, DNA-damaging radiation to cancer cells, while sparing healthy tissues, by the precise aiming of external beams or localized delivery (an oversimplification that will suffice for the purposes herein) (24, 25).

Chemotherapy, by the truest definition of the term, refers to the use of any drug to treat any disease. However, it has become colloquially associated with the treatment of cancer via the administration of small molecules that are directly cytotoxic to rapidly dividing cells, such as tumor cells. Chemotherapeutics are described using non-mutually exclusive classes based on their mechanism of action, structure, or source (22); for example, alkylating drugs, such as cyclophosphamide, work by covalently altering DNA bases (26, 27).

Since their advent, combinatorial therapies have further bolstered the success of these individual therapeutic techniques; from adjuvant chemo- or radiotherapy provided after surgical resection (28, 29) to combination chemotherapy treatment regimens which reduce the likelihood of chemo-resistant tumor cell formation (30).

However, none of these therapies are specific for tumor cells. This means that they are either limited to use as a localized therapy to spare healthy tissues (as

is the case for surgery and radiotherapy[3]), and thus are generally ineffective in the treatment of disseminated, metastatic disease, or are associated with toxic side effects arising from their systemic administration (as is the case for the hair loss and gastrointestinal distress, among others, associated with chemotherapeutic treatment (22)).

Treating cancer – modern therapeutics in the era of precision medicine

With an increased understanding of the role of the tumor microenvironment, along with the genetic, epigenetic, and molecular alterations that underpin malignant transformation, novel classes of anti-cancer therapeutics have been developed over the past few decades which directly target these changes, theoretically offering improved specificity and reduced toxicity.

However, cancer (even within the same type) can vary on a cellular and molecular level from patient to patient – meaning these targeted therapeutics only work in select patient populations. As such, increasingly so, cancer is treated with a personalized, or precision, medicine approach; matching the choice of therapeutic(s) to the patient's tumor in order to achieve the greatest benefit (31, 32).

Examples include: hormone therapies (33, 34), kinase inhibitors (35, 36), and anti-angiogenic approaches (37). In most cases these therapies are not administered in isolation, but as combination regimens alongside traditional strategies. The most exciting new class of therapeutics to enter this foray are immunotherapies (38).

1.2.3 Cancer as an immunological target

The presence of an immune infiltrate within the microenvironment of an established (clinically diagnosable) tumor in a cancer patient represents only a snapshot at the end stage of a dynamic process. Modern theory regarding the active contribution of the immune system to the process of tumor formation and elimination has relied heavily on data derived from human studies and evidence from small animal tumor models. It has revealed avenues to exploit these pathways as therapeutic targets, thus giving rise to a new field: immuno-oncology.

The theory of immunosurveillance

In the early 1900s, Paul Ehrlich was the first to hypothesize that aberrant cells with the potential to generate a tumor would regularly arise within humans but, in the majority of cases, intrinsic host factors would prevent tumor formation (39-41). However, it would take almost a century to develop the experimental evidence and framework of immunological knowledge that could substantiate this claim.

[3] In some cases radiotherapy is delivered systemically, and in these instances would not be considered a localized therapy.

Critically, experiments performed with carcinogen-induced tumors in murine models were among some of the first to prove immunization against a tumor was possible and that the immune response was directed against antigens which were unique to the tumors themselves (42, 43). Thus, the immune system was capable of triggering tumor rejection.

These concepts were synthesized into the immunological surveillance hypothesis by Frank Burnet who postulated that the immune system, in particular lymphocytes, played a critical role surveying the body to detect and eliminate neoplastic cells that arose as a result of somatic mutations (whether triggered by carcinogens, arising as a result of viral infection, or occurring spontaneously) before they became a clinical tumor (44, 45).

If the immunosurveillance hypothesis were true, by extension, a deficit in immunity would be characterized by an increased rate of tumor formation. Indeed, severely immunocompromised mice develop tumors sooner and at a higher rate than their wild type counterparts (46). In humans, inherited immunodeficiencies (47) and long term immunosuppression (such as that experienced by solid organ transplant patients) (48) are risk factors for the development of cancer. This evidence, amongst others (further discussed below), has helped transition the immunosurveillance hypothesis into a widely accepted theory.

Tumor immunoediting

The process by which transformed cells escape immunosurveillance and give rise to a tumor has been dubbed *immunoediting* (45). Immunoediting describes the dynamic interaction between a developing tumor and the immune system and encompasses the Janus-like role of immunity in tumor formation where it serves both to protect the host against tumor growth and, in some circumstances, it serves to cultivate tumor formation. The process of immunoediting is divided into three distinct phases: elimination, equilibrium, and escape.

The *elimination phase* is equivalent to immunosurveillance; innate (e.g. natural killer cells and dendritic cells) and adaptive (e.g. T cells) immune cells contribute to the complete elimination of tumors as they develop. Those tumors which are not eliminated, considered to be a rare event, enter the *equilibrium phase*. During equilibrium a balance between pro- and anti-tumor immune responses keep tumor growth in check resulting in a dormancy that may last for years. It is during this stage that the constant presence of anti-tumor immunity imposes a selective pressure on tumor cells, selecting for those cells which are able to subvert the anti-tumor immune response and enter the *escape phase*. In this phase tumor progression dominates, supported by increased tumor growth, increased immunosuppression in the tumor microenvironment, and/or decreased immunogenicity of tumor cells.

By the time a tumor is diagnosed clinically it has already reached the escape phase. This makes the observation of elimination and equilibrium phases in humans nearly impossible; as such, much of the evidence supporting the theory of immunoediting comes from the documentation of the existence of anti-tumor

immunity in humans and analyses of the dynamic nature of the process in murine models (described in (49-51)). However, this evidence is so compelling that escape from immune-mediated suppression is considered one of the hallmarks of cancer (13).

The function of immune cells in the tumor microenvironment:

The tumor microenvironment can contain a multitude of different immune cells and immune signalling molecules (such as cytokines, i.e. small secreted proteins) which can contribute to tumor regression (anti-tumorigenic factors; those generally dominant in the elimination and equilibrium phases) or tumor progression (pro-tumorigenic factors; these dominate the escape phase).

i) anti-tumorigenic factors

Some of the main contributors to the anti-tumor immune response are effector T cells (Section 1.2.4 provides a primer on T cell biology).

$CD8^+$ T cells have the capacity to be directly cytotoxic towards tumor cells (52, 53). Indeed, across a variety of human malignancies, an increase in $CD8^+$ T cells within the tumor infiltrate is correlated with improved prognosis (54-59). Furthermore, tumor-specific $CD8^+$ T cells can often be isolated from cancer patients (60-65).

Effector $CD4^+$ T cells, particularly those of the T_H1 subset, can also contribute towards anti-tumor immunity. $CD4^+$ T cells recognizing MHC-II-restricted tumor antigens have been described in a variety of human malignancies (66, 67). Given the absence of MHC class II on many solid tumors, the primary functionality of anti-tumor $CD4^+$ T cells is believed to be mediated through their ability to provide help to cytotoxic CD8+ anti-tumor T cells (68) and other immune cell populations (e.g. M1 macrophages (69)). However, $CD4^+$ T cells are also capable of mediating anti-tumor efficacy, even in the absence of $CD8^+$ T cells, through both indirect (70) and direct (71) cytolytic mechanisms.

While the evidence has solidly placed T cells as the critical mediators of anti-tumor immunity, other immune cell populations which play a role in anti-tumor immunity have also been described, including M1 macrophages (72, 73), mature dendritic cells (74), and natural killer cells (75).

Many of the aforementioned cell types contribute to anti-tumor immunity via the release of cytokines. The cytokine milieu typically associated with tumor regression is biased towards IL-12 (76), type I and type II interferons (IFN-α/β and IFN-γ) (77), and TNF-α (6), amongst others .

ii) pro-tumorigenic factors

Pro-tumorigenic factors are those which are immunosuppressive; i.e. they dampen the anti-tumor immune response.

In terms of immune cell populations, contributors include myeloid derived suppressor cells (78), tumor associated macrophages (i.e. M2-polarized macrophages) (79), and regulatory T cells (80, 81).

Cellular and non-cellular mediators of an immunosuppressive tumor microenvironment can originate from numerous cells within the tumor, including: immune cells, stromal cells, and the cancerous cells themselves. For example, both tumor cells and immunosuppressive immune cells can upregulate the expression of immune checkpoint ligands (e.g. PD-L1) (82) which function to inhibit T cell activity through binding to checkpoint (or coinhibitory) receptors (e.g. PD-1) (83). The untreated tumor microenvironment is rich in immunosuppressive cytokines. For example, TGF-β is a master regulator of intratumoral immunosuppression (84); it can be released by both tumor cells and immune cells (e.g. regulatory T cells, myeloid derived suppressor cells) and has inhibitory effects on multiple immune cell populations. Although IL-10 has historically been associated with immunosuppression and tumor progression, it can also contribute to anti-tumor immune functions given its pleiotropic nature (85, 86) (this latter point illustrates the over-simplification of attempting to categorize all tumor immune mediators (cellular or otherwise) as either pro- or anti-tumorigenic; the reality is much more complicated and depends on a balance rather than any one factor in isolation).

1.2.4 The induction of an endogenous T cell response; a brief foray into T cell biology

In order to appreciate the intricacies and consequences of cancer immunotherapy and anti-tumor T cell responses, we must first cover some basic T lymphocyte (T cell) biology.

T cell biology basics

T cells are one arm of the adaptive immune system. Adaptive immunity is characterized by immune cells (deemed lymphocytes) which *acquire* functional receptors during development; these receptors are *specific* for their ligands.

With regards to T lymphocytes, this functional receptor is called a T cell receptor (TCR). The TCR[4] is a heterodimeric structure composed of transmembrane glycoproteins; a single TCRα chain linked to a single TCRβ chain through a disulfide bond. When expressed on the T cell surface, the TCR is found in a complex with CD3 (the TCR-CD3 complex). While the CD3 chains (CD3δ, CD3γ, CD3ε, and CD3ζ) are invariant across T cells, the two TCR chains are highly variable; it is this variability that affords T cells, as a collective, the ability to recognize a large diversity of antigens (87).

[4] For the sake of simplicity, we will only be considering archetypal αβ TCRs herein. We will not be discussing γδ T cells.

T cells only recognize antigens, short peptide sequences, presented in the context of self-major histocompatibility complex (MHC) on the surface of host cells (called a peptide-MHC complex (pMHC)). Formation of a TCR:pMHC complex is stabilized by the involvement of a TCR co-receptor, either CD4 or CD8 (transmembrane proteins found on the surface of a T cell), which can bind MHC. CD4 shows specificity for MHC-II, which is only expressed by antigen presenting cells (innate immune cells, such as macrophages and dendritic cells, as well as B cells), and CD8 shows specificity for MHC-I, which is expressed by all nucleated cells. The peptides being presented by MHC can originate from endogenous host cell proteins or foreign peptides (as may be the case in a virally infected cell, after bacterial phagocytosis, etc.).

Each T cell expresses an estimated ~4×10^4-10^5 copies of a single TCR[5] clone (88) on its surface (89-91). All T cells which express the same TCR at the genetic level (whether by chance or by expansion) are said to be clonotypes. The incredible diversity of antigens recognized by T cells arises from the maintenance of ~10^{11}-10^{12} T cells in the human body (92-94), composed of an estimated 10^6-10^8 (but possibly as high as 10^{10}) unique TCR clonotypes (some clones are present at higher frequencies than others) (92, 95). TCRs recognize pMHC complexes degenerately and are capable of cross-reacting against multiple pMHC complexes (96).

Although a small fraction of T cells can be found circulating in the blood and lymphatics, the vast majority are located in secondary lymphoid organs (such as the lymph nodes and mucosa-associated lymphoid tissue) (97, 98).

T cell development

T cell development begins when hematopoietic stem cells in the bone marrow differentiate into multipotent progenitor cells that traffic to the thymus where they commit to the T cell lineage (99, 100).

Within the thymus, these T cell precursors progress through a series of developmental stages during which they begin to express a TCR. The variability in the sequences of the TCRα and β chains arise at this stage as a result of a combination of somatic recombination and nucleotide addition/deletion events. Simply put, a set number of smaller gene segments (known as variable (V), diversity (D), joining (J), and constant (C) regions) are mixed-and-matched together like building blocks to form whole TCRs; this process is initiated by recombination activation gene (RAG) proteins (101).

If TCRα and TCRβ chain gene rearrangements were successful (yielded full length proteins), developing T cells bearing mature αβTCRs proceed through the processes of positive and negative selection. In short, the ability of the TCR to bind self-pMHC is tested. A minimum threshold of signaling through the TCR:self-

[5] While in the majority of cases T cells do express a single TCR, this statement is an oversimplification … in actuality, up to 30% of T cells can simultaneously express two TCRs.

pMHC is required to trigger *positive selection*, where T cells that can bind self-MHC with a moderate degree of specificity are permitted to survive, thus ensuring that mature T cells in periphery are restricted by the host MHC. However, if the interaction of the TCR with self-pMHC is too strong, indicating potential reactivity to self-antigen in healthy tissues, an apoptotic program is induced in the corresponding T cell through a process known as *negative selection*, which serves to eliminate potentially autoreactive T cells from the repertoire. It is during this time that T cells will become single positive for either CD4 or CD8, dependent upon whether they were selected through MHC-II or MHC-I, respectively (102).

Following the selection process, the surviving T cells (termed *naïve* T cells) exit the thymus though the lymphatics or vasculature (103, 104).

T cell activation

In the periphery, naïve T cells circulate amongst secondary lymphoid organs, including the lymph nodes, via the vasculature and lymphatics systems. The lymph nodes facilitate interactions between immune cell populations; here naïve T cells encounter antigen presenting cells, typically dendritic cells. T cells will then scan pMHC complexes on antigen presenting cells via their TCR seeking a match (97). If the interaction between TCRs and pMHCs is of sufficient strength/affinity signaling a match (that the antigenic peptide has been recognized by the TCR) (105) an immunological synapse is formed triggering T cell activation (83, 106).

T cell activation is dependent upon transmission of two signals; a stimulatory signal delivered through the TCR-CD3 complex via its interaction with pMHC (deemed *signal one*) and a co-stimulatory signal (*signal two*) (101). Signal two is generated when co-stimulatory receptors on the T cell surface bind to cognate ligands on the surface of mature antigen presenting cells; the archetypal example being the co-stimulatory receptor CD28 binding to ligands CD80/CD86 (83). In their default state, antigen presenting cells are considered *immature* and do not express co-stimulatory molecules; maturation of the antigen presenting cell is triggered by exposure to pathogen- or damage-associated molecular patterns (107). Through the requirement of evidence of infection and/or damage, innate immune cells control adaptive immune responses. Delivery of signal one in the absence of signal two, as in the case of a TCR that matches a pMHC with self-antigen, triggers T cell *anergy* (a state of long term non-responsiveness (108)) rather than activation, which serves to prevent adaptive immune responses against innocuous antigens and limit the activation of potentially auto-reactive T cells.

These extracellular ligation events are transmitted intracellularly through signaling cascades that culminate in the activation and nuclear translocation of transcription factors – nuclear factor of activated T cells (NFAT), activated protein 1 (AP-1), and nuclear factor-κB (NF-κB). The earliest membrane proximal signaling events of the TCR-CD3 complex are of particular importance to this thesis (101, 109). Immediately after matching a pMHC, the intracellular immunoreceptor tyrosine-based activation motifs (ITAMs) of CD3 are phosphorylated by the Src

family tyrosine kinases Lck and Fyn allowing the recruitment of ZAP-70, which initiates the signaling cascade. Lck is recruited to the immunological synapse through its interaction with co-receptors CD4 or CD8 and is also responsible for the phosphorylation of ZAP-70.

Activated T cell fates

The initial activation of a naïve T cell by an antigen presenting cell is called *priming*. Activation of a T cell triggers production of the T cell growth cytokine IL-2 causing proliferation and differentiation (101). Following the priming event, the T cell is referred to as *antigen experienced*.

The proliferating daughter T cells acquire phenotypic and functional changes that distinguish them from the original naïve T cell. The progeny are grouped into subsets based on their fates, functions, and biological properties; all are either classified as memory or effector cells. Memory cells persist in the long term and facilitate the generation of rapid immune responses upon re-exposure to the same antigen. Currently, there are four recognized subsets of memory T cells: stem cell memory (T_{SCM}), central memory (T_{CM}), effector memory (T_{EM}), and tissue-resident memory (T_{RM}). Effector cells (T_{Eff}) are short lived mediators with high functionality against target cells expressing the target pMHC (110, 111). While the processes by which a single naïve T cell gives rise to these diverse populations are still being elucidated, they can be thought of as a series of intermediary states between naïve and terminal effector cells (112, 113).

Helper ($CD4^+$) T cells become polarized towards various functional lineages dependent upon signals received from the local cytokine milieu; fates include T_H1, T_H2, and inducible[6] regulatory T cells, amongst others (114, 115). $CD4^+$ T cells are considered to be plastic, meaning their polarization can change over their lifetime (115, 116); this may be of particular concern in an immunosuppressive tumor microenvironment (TGFβ polarizes cells towards the regulatory lineage (117)).

Effector T cell mechanisms

An experienced T cell does not require co-stimulation (i.e. signal two) to trigger effector functions; signal one (i.e. TCR recognition of pMHC on a target cell) is sufficient (101).

$CD8^+$ T cells are also referred to as cytotoxic[7], or killer, T cells given their ability to cause target cell death. They orient their effector mechanisms towards a target cell via polarization that occurs during the formation of an immunological synapse. Target cell cytotoxicity is directly mediated by degranulation (release of

[6] These are unique from thymic derived, natural regulatory T cells.

[7] It should be noted that while the vast majority of $CD8^+$ T cells are cytotoxic in nature, exceptions (such as $CD8^+$ immunosuppressive T cells) do exist.

perforin and granzymes) (118, 119) and expression of Fas ligand (118), and is aided by cytokine release (e.g. IFN-γ, TNF-α) (6, 77, 118).

$CD4^+$ T cells have been designated as *helpers* since their primary mechanism of action is to modulate the functionality of other immune cell populations through the release of cytokines and stimulation via ligands such as CD154. The cytokines released, and thus the effector mechanisms triggered, are dependent upon polarization. T_H1 cells are associated with the release of IFN-γ and macrophage activation (114). T_H2 cells primarily release IL-4, IL-5, and IL-13 and can impact B cells and eosinophils (114). Regulatory T cells primarily release IL-10 and TGF-β and function to dampen inflammation through the direct inhibition of effector T cell responses (120).

1.2.5 Cancer immunotherapy

Cancer immunotherapy (also called immuno-oncology) is an umbrella term encompassing any therapy which aims to "[activate] the immune system for therapeutic benefit in cancer" (4). The goal is to return the tumor microenvironment to a state promoting tumor elimination, rather than escape; this is accomplished by either promoting anti-tumorigenic factors or inhibiting pro-tumorigenic factors.

Immunological consequences of traditional cancer therapeutics

Although they do not fall under the broad categorization of immunotherapies, chemotherapy and radiation therapy have been shown to modulate the tumor immune microenvironment in ways that can promote tumor regression, likely contributing to their efficacy (reviewed in (121-123)). For example, both chemo- and radiotherapies have been shown to increase the release of damage-associated molecular patterns by dying tumor cells to modulate dendritic cell activity (124), and chemotherapeutic agents have been demonstrated to eliminate immunosuppressive cell populations such as myeloid derived suppressor cells (125) and regulatory T cells (126).

Modern immuno-oncology (moving beyond Coley's toxins)

The first success story in the modern resurgence of interest in treating cancer using an immunomodulatory approach, which rapidly accelerated in the 1980s, is the systemic administration of IL-2 (best summarized in (127)).

In short, systemic administration of high-dose IL-2 triggers the growth and activation of T cells and natural killer cells promoting anti-tumor immunity (128, 129). Repeated intravenous infusions of high-dose recombinant human IL-2 produced an objective clinical response in 15-17% of metastatic melanoma and renal cell carcinoma (RCC) patients treated, with 6-8% of patients experiencing durable complete regressions (130). These numbers, though seemingly low, were considered impressive given that the responses were occurring in patients whom

had failed to respond to standard therapies. However, the treatment was synonymous with severe toxicities manifesting as fever, hypotension, gastrointestinal distress, and weight gain resulting from vascular leakage and a systemic cytokine storm (130, 131).

Despite the associated toxicities and a lack of striking efficacy (for the most part) in other malignancies, the success and FDA approval of systemic IL-2 therapy for metastatic melanoma and RCC proved that immunotherapy was a valid approach to treating cancer and paved the way for the development of modern immunotherapeutics.

i) Monoclonal antibody-based therapies

- *Tumor-targeted antibodies*

Tumor-targeted monoclonal antibodies (typically immunoglobulin G (IgG) class) bind cell surface antigens on malignant cells or components of the tumor stroma. Their exact mechanism of action varies, but can include immunomodulatory effects (e.g. activation of antibody-dependent cellular cytotoxicity, complement-dependent cytotoxicity, and opsonisation), and direct anti-tumor functionality (e.g. inhibition of cell surface receptors delivering proliferative or survival signals) (132, 133). The first monoclonal antibody to receive FDA approval for the treatment of cancer (in 1997) was rituximab, an anti-CD20 antibody indicated for use in treating non-Hodgkin lymphoma (NHL) and chronic lymphocytic leukemia (CLL) (132); the approval of anti-HER2 (trastuzumab) followed shortly thereafter.

- *Bispecific antibodies*

Bispecific antibodies are antibody-derived molecules manufactured to permit the simultaneous binding of two different antigens (134). In the treatment of cancer, bispecific antibodies generally permit the binding of a tumor antigen and recruitment of an immune effector cell. Types of bispecific antibodies in use or development for the treatment of cancer include: bispecific T cell engagers (BiTEs; e.g. anti-CD3/anti-CD19, blinatumomab) (135, 136), trifunctional antibodies (e.g. anti-CD3/anti-EpCAM, catumaxomab) (137), and dual-affinity retargeting proteins (DARTs) (138).

- *Checkpoint blockade*

Often referred to as “releasing the brakes” on T cells, checkpoint inhibition/blockade strategies use monoclonal antibodies against checkpoint receptors (also called coinhibitory receptors) or their ligands to block interactions that can lead to the inhibition of anti-tumor T cells (139). Checkpoint blockade relies on the presence of endogenous anti-tumor T cells capable of recognizing tumor cells through the formation of a TCR:pMHC complex. The first-in-class therapeutic to receive FDA approval was ipilimumab (anti-CTLA-4) for the treatment of metastatic melanoma (CTLA-4 is a coinhibitory receptor upregulated

by T cells shortly after activation). Other approved checkpoint blockade strategies target the interaction between PD-1 and its ligands PD-L1 and PD-L2 (e.g. pembrolizumab and nivolumab (anti-PD-1); while their initial approval was indicated for use in advanced melanomas, this has since expanded to include other malignancies (e.g. non-small cell lung cancer).

While these therapies were able to demonstrate striking efficacy in a small subset of patients treated, many did not experience this benefit. Thus, identification of those patients who would most benefit from treatment via the use of biomarkers (e.g. intratumoral CD8+ T cells and PD-L1 expression in the tumor microenvironment) is becoming an important aspect of the implementation of checkpoint blockade (140, 141).

Checkpoint blockade strategies, have demonstrated significant treatment-associated toxicities (142). In healthy humans, coinhibitory signals delivered to T cells play an important role in maintaining immune homeostasis and peripheral tolerance by inhibiting the T cell response against self-tissues. Since checkpoint blockade strategies release the breaks on all T cells, regardless of specificity, its usage can trigger severe autoimmune pathologies.

ii) Oncolytic Virotherapy

Oncolytic viruses (OVs) are naturally occurring viruses (which may have been further genetically manipulated) used to exploit the unique biology of tumors, which are no longer able to activate anti-viral mechanisms. As a result, OVs selectively replicate within tumor cells, leading to OV amplification and tumor cell lysis, while sparing healthy cells (143). In addition to their direct lytic capacity, treatment of a tumor with an OV results in a reversal of the immunosuppressive microenvironment and induction of novel anti-tumor immune responses, thus earning classification as an immunotherapy (144, 145). This latter property occurs through the release of tumor antigens (products of tumor lysis) into an immunostimulatory microenvironment rich in viral pathogen-associated molecular patterns (from the OV) and damage-associated molecular patterns (released by tumor cells upon lysis). In 2015, T-VEC became the first-in-class oncolytic virus to receive FDA approval (for the treatment of advanced melanoma) (146). Interestingly, T-VEC is engineered to express the cytokine GM-CSF, which is believed to promote the local development of dendritic cells which, in turn, acquire tumor antigen and activate T cells within the local environment and draining lymph nodes. As another strategy to promote T cell responses following oncolytic virotherapy, viruses have been engineered to carry defined tumor antigens resulting in a virus with a dual purpose: 1) to lyse the tumor and 2) to directly activate T cells against the virally encoded tumor antigen via infection of antigen presenting cells (147).

iii) Cancer Vaccines

Cancer vaccines are (for the most part) therapeutic vaccination strategies which aim to activate an endogenous anti-tumor cytotoxic $CD8^+$ T cell response in a cancer patient (148). This is accomplished through the inoculation of a patient with a source of tumor antigen(s) and signals triggering immune activation (e.g. adjuvants). This strategy also relies on the availability of anti-tumor T cells, either naïve or experienced, within the host.

Cancer vaccine strategies in various stages of pre-clinical and clinical testing have evaluated different routes of administration, tumor antigen(s), and types of vaccines (e.g. antigen-loaded dendritic cells, protein/peptides, killed tumor cells/lysates, DNA/RNA, genetically engineered viruses, etc.) in a variety of indications (148-150). The single commonality has been an underwhelming performance in clinical trials; only a single cancer vaccine has ever received FDA approval (sipuleucel-T (151) – approved in 2010 for the treatment of castration-resistant metastatic prostate cancer, despite only providing a modest survival benefit of 4 months).

The general failure of cancer vaccines is a multifaceted phenomenon. Many of the contributing factors are likely to dampen the success of all immunotherapies which rely on endogenous anti-tumor T cells (e.g. MHC downregulation or antigen loss by tumor cells, and a T cell pool restricted by central tolerance).

iv) Adoptive T cell transfer

Most of the aforementioned classes of cancer immunotherapies (checkpoint blockade, oncolytic immunotherapy, and cancer vaccines) rely on the activation of an anti-tumor T cell response *in vivo*. Concerns over the ability to control the development of a T cell response *in vivo* (152), particularly in an immunosuppressive environment (153), and the need to rapidly overpower a tumor prior to any therapy-thwarting adaptation (154) give rationale for a different class of immunotherapy: adoptive cell transfer (ACT).

In adoptive cell transfer, patients are treated with cell populations that have been expanded *ex vivo* and are delivered as a bolus to rapidly inundate a tumor. With respect to T cells[8], ACT therapies fall into one of two categories as defined by the origin of the tumor-specific T cell population: (i) endogenous or (ii) engineered.

The general schema for the clinical implementation of both of these strategies is the same (155). In short:

(i) T cells are isolated from a cancer patient[9]

[8] Adoptive cell transfer (sometimes called adoptive cell therapy) isn't limited to use of a T cell population as the cellular product. For example, the transfer of *ex vivo* cultivated NK cells is also considered a form of ACT for cancer treatment. However, this falls outside the scope of this thesis.
[9] Efforts to use modified allogeneic T cells for the purposes of ACT are also being pursued.

(ii) T cells are either selected (endogenous) or engineered for tumor specificity
(iii) tumor-specific T cell cultures are expanded *ex vivo* (enabled by the provision of activation signals (e.g. anti-CD3) and growth cytokines (e.g. IL-2))
(iv) the patient receives a lymphodepleting preparative regimen (e.g. chemotherapy)
(v) tumor-specific T cells are administered to the patient *en masse*[10] (most often systemically through the intravenous route)

Anti-tumor T cells can be isolated from the peripheral blood of cancer patients or their excised tumors, the latter being referred to as tumor infiltrating lymphocyte (TIL) therapy. These represent the pioneering forms of anti-tumor ACT, first developed in the 1980s (156, 157). Modern TIL therapy has experienced particular success in clinical trials for the treatment of metastatic melanoma (158-161); and strides are being made to adapt TIL for use in treating other malignancies (e.g. cervical cancer (162), gastrointestinal cancer (163), and bile duct cancer (164)).

TIL therapy has been incredibly impressive for the treatment of metastatic melanoma; trials regularly achieve objective response rates of ~50% (158, 159, 161) and treatment can be successful even after other immunotherapies (e.g. checkpoint blockade) have failed (165). However, the therapy requires access to a resectable tumor (which isn't always possible) and considerable manipulation *ex vivo* to identify tumor-specific T cell populations (that cannot always be obtained from all patients). In addition, it appears melanoma may be uniquely poised to benefit from therapies which rely on endogenous anti-tumor T cells (including checkpoint blockade, etc.) (166). Melanomas have high mutational loads (167), likely contributing to a greater number of neoantigens[11], which are not subject to central tolerance (168), leading to a larger pool of peripheral T cells with the potential to recognize these antigens with a high avidity.

One potential strategy to circumvent these problems is the genetic engineering of bulk T cells (readily accessible in the peripheral blood), conferring upon them the necessary specificity against tumor antigens. This can be achieved through introduction of either a tumor-specific T cell receptor (TCR) or a chimeric antigen receptor (CAR)[12].

TCR-engineered T cells (reviewed in (169)) have been clinically evaluated in a variety of malignancies (e.g. melanoma (170, 171) and synovial cell sarcoma (171)) with specificity against a variety of antigenic targets (e.g. NY-ESO-1 (171), MART-1 (170), and gp100 (170)). The use of TCR-engineered T cells is limited by the need to match the patient's MHC to the engineered TCR. Given the broad

[10] In some cases, supportive systemic cytokine therapy (e.g. IL-2), is provided simultaneously.
[11] Neoantigen = new antigen. These are mutant peptide sequences arising in tumors (not present in non-tumor tissues) as a result of genetic mutations in tumor cells.
[12] These receptors are generally expressed by the T cell *in addition* to a natural TCR, which is often of unknown specificity.

diversity of MHC, many TCRs must be available to cover the diversity; a limited patient population can benefit from each TCR. Further, down regulation of MHC is a common mechanism of immune evasion that is well documented on cancer cells (172-174), which would *negate the efficacy of any immunotherapeutic strategies which rely upon TCR-mediated tumor recognition*.

1.3 Chimeric antigen receptor-engineered T cells for the treatment of cancer

1.3.1 CAR-T cell overview

Chimeric antigen receptors (CARs; recently reviewed in (175-178)) are recombinant proteins designed to direct T cells against a target of interest in an MHC-independent manner, regardless of the specificity of the endogenous TCR.

The general structure of a CAR consists of a series of functional domains, appropriated from endogenous protein sequences, linked together like beads on a string (at a genetic level) to create a novel cell surface receptor. Listed in order from

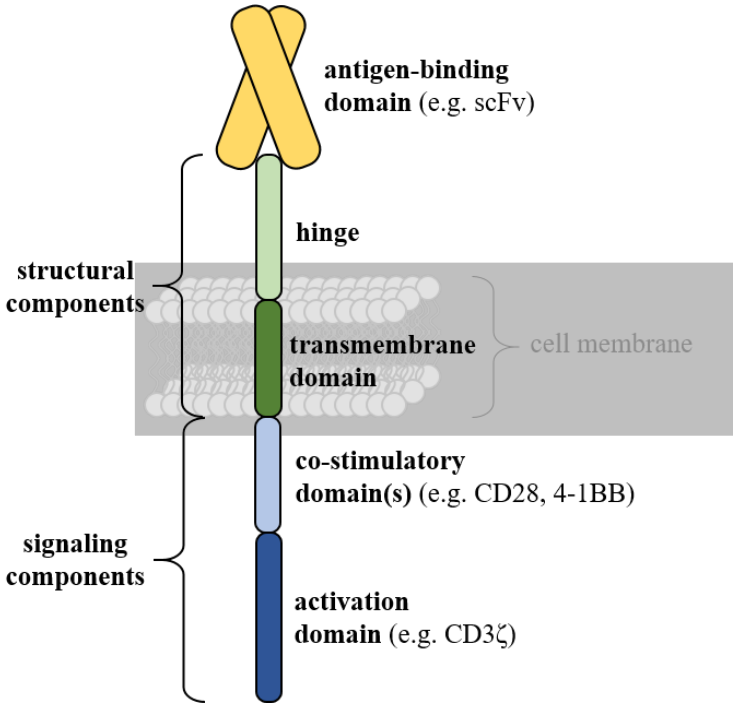

Figure 1. Schematic of a chimeric antigen receptor. The general schema for the structure of a CAR in relation to the cell membrane.

extracellular to intracellular, these generally include: an antigen-binding domain, a hinge, a transmembrane domain, an intracellular co-stimulatory domain(s), and an activation domain (see **Fig. 1**). The extracellular antigen-binding domain, as the

name would imply, functions to afford the CAR-T cell an ability to bind a target of interest on the surface of a tumor cell (see section 1.3.3 *CAR-T cell domains* for a deeper exploration of CAR antigen-binding domains). The hinge (frequently of CD8 or IgG origin) serves to extend the antigen-binding domain away from the cell membrane and afford flexibility to facilitate target binding. The transmembrane domain serves to anchor the CAR in the T cell membrane (it is usually from a native T cell surface protein and is frequently an extension of either the hinge or intracellular signaling CAR domains, e.g. CD8 or CD28). Intracellular activation and co-stimulatory domains (equivalent to signals *one* and *two* of T cell activation, respectively; discussed in Section 1.2.4) are initiators of intracellular signaling pathways triggering T cell effector functionality, amongst others (discussed further below). CARs are modular by nature; multiple options for each of the above domains can be mixed and matched together generating novel receptors with unique properties.

A patient's own T cells, collected from the peripheral blood, are genetically engineered (through a variety of mechanisms, but most often using retroviruses[13] (179)) to express the CAR, at which point they are referred to as CAR-T cells. CAR-T cells are considered a form of personalized medicine as the drug, a cell product, is produced on a patient-by-patient basis from the individual patient's cells[14]. However, the CARs themselves can be used to generate CAR-T cells in any patient whose tumor is positive for the CAR-target.

1.3.2 A brief history of CAR-T cells

The genesis for a TCR-mimetic receptor that could redirect T cells in an MHC-independent manner was the work of Zelig Eshhar (180) whose *T-body* approach fused a single-chain variable fragment (scFv; a synthetic fusion of the variable regions of the heavy and light chains of an antibody, connected by a linker) to CD3ζ or Fc receptor γ chain; expression of the receptor on a murine T cell hybridoma cell line successfully redirected cytotoxicity and IL-2 production against cells positive for the scFv target (181). These earliest CARs, which include only a singular intracellular signaling domain (to recapitulate signal one of T cell activation), are referred to as *first generation*.

First generation CAR-T cells were evaluated in the clinic against a variety of malignancies and tumor associated targets, e.g. anti-CD20 in lymphoma (182), anti-GD2 in neuroblastoma (183, 184), anti-folate receptor in ovarian cancer (185), and anti-carbonic anhydrase IX (CAIX) in renal cell carcinoma (186). These trials were characterized by an inability of CAR-T cells to expand *in vivo*, limited CAR-

[13] A family of viruses which incorporate their own genetic information into the host cell genome.
[14] This excludes the concept of universal CAR-T cells, which are produced from an allogeneic T cell donor along with genetic editing to eliminate endogenous MHC and/or TCR expression, preventing CAR-T cell rejection and/or graft versus host disease.

T cell persistence (on the scale of days to weeks), and underwhelming anti-tumor efficacy.

Chimeric antigen receptor technology was significantly bolstered with the advent of *second* and *third generation* CARs, which included one or two intracellular co-stimulatory domains (to deliver the second signal of T cell activation), respectively (187-189). It was a second generation CAR encoding the intracellular signaling domain for CD137 (aka 4-1BB) in addition to the CD3ζ signaling domain, targeted against CD19 with an scFv, that provided the first compelling evidence that CAR-T cells were capable of exerting potent anti-tumor efficacy and triggering complete remissions in humans (in the setting of chronic lymphocytic leukemia) (190, 191).

1.3.3 CAR-T cell domains and functionality

Antigen-binding domains

The antigen-binding domain functions to bring the CAR-T cell into close contact with a tumor cell by binding an antigen on the tumor cell surface. As such, there are two key considerations to make. Which antigen should be a target, and what extracellular domain will facilitate its binding by the CAR?

i) Choosing an antigen

Target selection has been identified as one of the biggest challenges associated with CAR-T cell strategies (192). Chimeric antigen receptors have access to a limited pool of potential tumor antigens – those which are expressed on the tumor cell[15] surface (exceptions which allow the targeting of intracellular antigens do exist, but these strategies require tumor cells to retain MHC expression (193-195)). The ideal tumor target would be a tumor specific antigen (TSA); an antigen whose expression is absolutely restricted to tumor cells (e.g. neoantigens and virally associated antigens). This would, in theory, prevent CAR-T cell cytotoxicity against healthy tissues. However, as shared[16] TSAs expressed on the tumor cell surface are limited, the vast majority of CARs developed to date target tumor associated antigens (TAA); those antigens which are highly expressed by a tumor but also show restricted patterns of expression on non-tumor tissues (either at much lower levels or limited to "non-essential" tissues). In addition, an ideal

[15] Strategies targeting CAR-T cells against pro-tumorigenic cells in the tumor microenvironment (e.g. tumor-associated fibroblasts and vasculature), rather than tumor cells themselves, have also been explored.

[16] In order to keep CARs as an off-the-shelf product, they must be developed to target antigens which are shared amongst many cancer patients.

target antigen would be a tumor driver[17], reducing the chances of tumor escape via antigen loss.

ii) Choosing an antigen-binding domain

The earliest chimeric antigen receptors were almost exclusively targeted against tumor antigens using scFvs. However, any protein capable of directly or indirectly causing binding to a tumor antigen can be utilized as the extracellular antigen-binding domain of a CAR. An array of CAR-targeting strategies have been employed in CARs in various stages of development from *in vitro* systems to clinical trials. For example, the antigen-binding domain can be a/an: scFv (184, 196, 197), naturally occurring ligand (198) or ligand-binding domain (199-201), avidin-based (202), etc. This topic has recently been reviewed in depth by our lab (203).

It is worth noting that the majority of interactions between CAR antigen-binding domains and their tumor antigens are of a much greater affinity than the recognition of a tumor antigen as a pMHC via an endogenous TCR (204). In addition, consideration must be made for the origin of the antigen-binding domain; development of an immune response against foreign components of a CAR (e.g. against an scFv of murine origin) can contribute to reduced CAR-T cell persistence, for example (205).

Intracellular signaling domains

The intracellular signaling domains of CARs are designed to recapitulate the endogenous signals a T cell receives upon activation (discussed in Section 1.2.4) such that T cell effector functions will be activated upon tumor cell ligation via the antigen-binding domain. Most CARs utilize the intracellular domain of CD3ζ (an ITAM-containing component of the TCR-CD3 complex) to deliver *signal one*. T cells carry a host of co-stimulatory receptors (83); the intracellular signaling domains of most of these receptors have been evaluated for their utility as *signal two* when incorporated into a CAR (see (206)). Unlike endogenous T cell signaling, CAR-T cells integrate both signaling domains into a single cell surface receptor, disrupting the natural spatial and temporal regulation of these signalling components; the exact consequences of this disrupted regulation remain to be fully elucidated.

[17] Tumor drivers include mutations, epigenetic changes, etc. that directly contribute to carcinogenesis.

The inclusion of a co-stimulatory domain in a chimeric antigen receptor[18] is now recognized as a critical step to promote the *in vivo* expansion and persistence of CAR-T cells (both of which correlate with improved anti-tumor efficacy) (207). Most CAR-T cells in pre-clinical or clinical development utilize CD28, CD137, or a combination of both (a third generation CAR) as a source of co-stimulation. CD28 and CD137 belong to different families of co-stimulatory molecules (immunoglobulin superfamily and TNF receptor superfamily, respectively), meaning they activate different intracellular signaling pathways to affect T cell activation (83). This translates to differential properties among CD28 vs CD137 co-stimulated second generation CAR-T cells. For example, in CAR-T cells, CD28 vs CD137 co-stimulation variants display differential induction of cytokine production (187). And, comparatively, CD28 co-stimulation is associated with increased CAR-T cell functionality, whereas CD137 is associated with improved CAR-T cell persistence *in vivo* (189, 208, 209).

1.3.4 Anti-CD19 CAR-T cells for the treatment of hematological malignancies – a success story

Anti-CD19 CAR-T cells in the clinic

CAR-T cells targeted against the B cell lineage marker CD19 have proven widely successful in clinical trials targeting $CD19^+$ hematological malignancies across a variety of CAR configurations, institutions, and malignancies (see **Table 1**, below). Indeed, the majority of CAR-T cell clinical data collected to date has arisen from the use of anti-CD19 modalities. Perhaps most striking, complete response rates of over 90% are being achieved in patient populations whose malignancies have relapsed and/or are refractory (r/r) to front-line therapies. This success has proven so robust that two different CD19-targeted CAR-T cell platforms have recently received FDA approval for the treatment of r/r pediatric and young adult B cell acute lymphoblastic leukemia (B-ALL) (210) and r/r adult large B cell lymphoma (211), respectively.

Table 1. Recent clinical trial results with CD19-CAR-T cell treatment. Evaluated in relapsed/refractory B cell malignancies.

Center	Disease	Pre-conditioning regimen	CAR co-stimulatory domain	Dosing	Outcome	Ref.
MSKCC	adult B-ALL	cyclo	CD28	3×10^6 CAR-T cells/kg	14/16 (88%) CR	(212)

[18] Or the delivery of a co-stimulatory signal to the CAR-T cell through some other means.

UPenn/ CHOP	pediatric + adult B-ALL	various	CD137	1-10×10^7 T cells/kg	27/30 (90%) CR	(213)
NCI/NIH	pediatric + young adult B-ALL + NHL	cyclo + flu	CD28	1×10^6 or 3×10^6 CAR-T cells/kg	14/21 (67%) CR	(214)
FHCRC	adult B-ALL	cyclo ± flu	CD137	2×10^5, 2×10^6, or 2×10^7 CAR-T cells/kg	27/29 (93%) CR	(205)
FHCRC	adult NHL	cyclo ± flu	CD137	2×10^5, 2×10^6, or 2×10^7 CAR-T cells/kg	10/30 (33%) CR	(215)
FHCRC	adult CLL	cyclo ± flu	CD137	2×10^5, 2×10^6, or 2×10^7 CAR-T cells/kg	4/24 (17%) CR 17/24 (71%) ORR	(216)
Multiple	adult NHL	cyclo + flu	CD28	2×10^6 CAR-T cells/kg	4/7 (57%) CR	(196)
NCI/NIH	adult NHL + CLL	cyclo + flu	CD28	1-5×10^6 CAR-T cells/kg	8/15 (53%) CR	(217)

CAR-T cells were delivered as a single infusion or over multiple infusions and were administered as undefined or defined (FHCRC; 1:1 $CD4^+$:$CD8^+$) composition products. MSKCC = Memorial Sloan-Kettering Cancer Center; UPenn = University of Pennsylvania; CHOP = Children's Hospital of Philadelphia; NCI = National Cancer Institute (NCI); NIH = National Institutes of Health; FHCRC = Fred Hutchinson Cancer Research Center; B-ALL = B cell acute lymphoblastic leukemia; NHL = non-Hodgkin lymphoma; CLL = chronic lymphocytic leukemia; cyclo = cyclophosphamide; flu = fluridabine; CR = complete response rate; ORR = overall response rate

Pre-conditioning regimens

Prior to the administration of CAR-T cells, patients are often preconditioned with a chemotherapeutic lymphodepletion regimen, as in TIL therapies (218, 219). The inclusion of a preconditioning regimen serves to generate a niche by eliminating endogenous leukocytes increasing the availability of homeostatic cytokines (e.g. IL-7 and IL-15) to support the engraftment and functionality of adoptively transferred CAR-T cells (220). In addition, as previously discussed (see section 1.2.5, *Immunological consequences of traditional cancer therapeutics*), chemotherapies can contribute to the reversal of the characteristically immunosuppressive microenvironment, likely to the benefit of CAR-T cells.

CAR-T cells for CD19-negative hematological malignancies

CAR-T cells for the treatment of CD19-negative hematological malignancies or antigen-loss relapses after CD19-CAR-T cell therapies (221) are under development against a variety of tumor targets (see Table 2 in (175)). Early results are beginning to emerge from first-in-man and phase I clinical trials: e.g. CD22 (222), CD20 (223, 224), CD123 (225), and B cell maturation antigen (BCMA) (226). The observation of robust partial and complete responses (223, 226) as well as increasing response rates in recent trials (222, 227, 228), suggest that CAR-T cell therapy will be amenable to other hematological malignancies.

1.3.5 Challenges associated with CAR-T cell therapy

Treatment of solid tumors

CAR-T cell treatment of solid tumors in clinical trials have thus far failed to replicate the response rates observed in the treatment of hematological malignancies (229). However, the success of TIL and TCR-engineered T cell therapies in the treatment of melanoma support the use of ACT for the treatment of solid tumors. Furthermore, first generation CAR-T cells targeted against GD2 in neuroblastoma patients saw 27% of patients achieve complete remission (183), supporting the feasibility of this platform for treating solid tumors.

In part, the lack of CAR-T cell success in the solid tumor arena has been attributed to a lack of clinical trials with second or third generation constructs (176). Early trials of the technology in solid tumors were conducted using first generation CAR-T cells, which unsurprisingly (in retrospect) produced poor results. One of the first reports of a solid tumor patient treated with CAR-T cells incorporating co-stimulatory signaling domains (a metastatic colon cancer patient treated with a third generation CAR-T cell targeted against HER2 containing intracellular signaling domains from CD28, CD137, and CD3ζ) was of a fatality attributed to CAR-T cell toxicity arising as a result of on-target off-tumor toxicity against low levels of HER2 expression on pulmonary tissue (197). This fatality put a damper on CAR-T cell clinical trials and refocused efforts on targeting tumor antigens whose expression was limited to tumors or only shared with non-essential tissues. CD19 emerged as one of these candidates and the widespread success of second generation anti-CD19 CAR-T cells in treating hematological malignancies has reinvigorated the field. A large number of clinical trials of CAR-T cells against various targets in solid tumors are currently underway (see Table 4 in (230)).

Results of two trials and one case study have been reported (231-233). All three reports concluded that second generation CAR-T cell (anti-HER2, anti-mesothelin, or anti-carcinoembryonic antigen) treatment of solid tumors could be safe; however this may come at the expense of efficacy, as all had underwhelming

response rates. Lower than expected efficacy was likely due to lower CAR-T cell doses and/or a lack of chemotherapeutic preconditioning; both were precautions taken in trials after the fatality in the third generation HER2-CAR study.

Other considerations proposed to hinder CAR-T cell efficacy in treating solid tumors have been the challenges of infiltrating a solid mass and overcoming the local immunosuppressive microenvironment (234).

CAR-T cell associated toxicities

The promise of CAR-T cell technology was a therapeutic agent that could seek out and discriminately target tumor cells while avoiding collateral damage to non-tumor tissues. Thus far, the clinical reality has failed to achieve this goal; CAR-T cells have become synonymous with a constellation of associated toxicities.

i) Types of CAR-T cell associated toxicities

CAR-T cell toxicities are categorized based on what antigen and antigen-bearing cell population are causing CAR-T cell activation to mediate the toxicity.

- *Off-target toxicities*

While theoretically possible, cross-reactivity of a CAR-T cell against an unexpected antigen hasn't been documented in any clinical trial (235). However, an unexpected cross-reactivity against cardiac tissue in a clinical trial of TCR-engineered T cells resulted in lethalities (236), and as such, the possibility remains a concern with CAR-T cells. *Off-target* toxicities are nearly impossible to predict in advance, and are a major concern any time a new CAR is tested in the clinic (while *in vitro* screening against non-tumor cell lines can be helpful, it is not a perfect system for detecting cross-reactivity).

- *Off-tumor, on-target toxicities*

Off-tumor, on-target toxicities arise when the antigen targeted by the CAR is expressed on non-tumor tissue. These are referred to as autoimmune toxicities (237) as they are triggered by an autologous, albeit CAR-engineered, T cell population.

The B cell aplasia observed in CD19-CAR-T cell trials is a quintessential example of autoimmune CAR-T cell toxicity (238, 239); it can be transient or long lasting and is treatable with intravenous immunoglobulin therapy (240). Off-tumor, on-target responses have also resulted in hepatic toxicity when patients were treated with anti-CAIX CAR-T cells resulting from a response against $CAIX^+$ bile duct epithelial cells (186). More seriously, the aforementioned lethality in a third generation anti-HER2 CAR-T cell trial due to pulmonary toxicity was a result of an off-tumor, on-target response (197).

- *On-tumor, on-target toxicities*

On-tumor, on-target toxicities are those arising as a side effect of the desired anti-tumor CAR-T cell response. These include tumor lysis syndrome (TLS) and cytokine release syndrome (CRS)[19].

TLS can occur naturally or as a result of therapeutic treatment when a massive lysis of tumor cells causes the release of intracellular contents triggering metabolic disturbances (241). Evidence of tumor lysis syndrome has been observed in CAR-T cell trials (242, 243), although it is normally managed through prophylaxis and isn't denoted as a major concern.

The most commonly described CAR-T cell associated toxicity is CRS; an acute (onset within hours to days), systemic inflammation resulting from the activation and expansion of CAR-T cells (244). Patients experiencing CRS present with symptoms ranging from mild fevers and myalgia to severe and (in some cases) life-threatening hypoxia, hypotension, and vascular leakage (among others) (212, 213, 244). The syndrome is characterized by elevated serum levels of several inflammatory cytokines, most commonly IFN-γ, IL-6, and IL-10, although others have been observed (TNF-α, GM-CSF, MCP-1, IL-8, IL-5, IL-2, etc.) (237, 244-247). In CRS, these cytokines are either directly produced by activated CAR-T cells or by other immune cells, such as macrophages, activated as a result of CAR-T cell cytokine production (macrophage activation syndrome). Neurologic toxicity may also be observed, however whether neurologic symptoms are related to CRS (212, 216) or are independent of CRS (244) is unclear. CRS has been observed in the CAR-T cell treatment of both solid (248, 249) and hematological malignancies (212, 213, 215, 226, 250) against a variety of antigenic targets and is a major clinical concern for their implementation; the incidence of CRS has been as high as 100% in some trials (213) and despite advances in monitoring and treatment, severe CRS (sCRS) still carries a risk of mortality (205).

CRS is not uniquely associated with CAR-T cell therapies; CRS is also a concern with BiTEs (251) and has been observed in clinical trials of TCR-engineered T cells (although in this latter scenario CRS is of a lower frequency and severity than has been observed in CAR-T cell trials) (252).

- *Other toxicities*

Many CAR-T cells are targeted using scFv sequences derived from murine antibodies. As such, the development of human anti-mouse antibody (HAMA) responses are a concern as they could contribute to the cellular or humoral rejection of CAR-T cells, thus reducing the efficacy of this therapy (240). In one case, a HAMA response triggered an acute anaphylactic response in a patient being treated with multiple infusions of anti-mesothelin CAR-T cells (232). For this reason, modern CAR-T cells are designed with humanized scFv sequences.

[19] The CRS observed with CD19-CAR-T cells is associated with an on-tumor, on-target response. However, massive increases in systemic cytokine levels (cytokine storms) have also been associated with other types of CAR-T cell toxicities (i.e. off-tumor, on-target responses).

ii) Preventing CAR-T cell associated toxicities

Both *off-tumor/on-target* and *off-target* toxicities are theoretically avoidable, but in practice selection of a truly tumor-specific, CAR-targetable antigen has (thus far) proven elusive. The first level of protection against these toxicities is in CAR-T cell design. Strategies have focused on designing CAR-T cells that are discriminatory between endogenous low level antigen expression and tumor-associated high level expression (e.g. by reducing the affinity of CAR-T cells for their target) (253, 254) and *in vitro* screening against non-tumor/non-target cell lines and proteins to detect possible *off-target* responses before human trials (255). In addition, some next-generation CAR-T cell strategies use a dual CAR system which requires the simultaneous recognition of two tumor antigens to trigger T cell effector functions, increasing the tumor specificity of the CAR-T cell response, even in the absence of a tumor-specific antigen (256). As a secondary level of protection, first-in-man trials are conducted using dose escalation strategies (257).

In contrast, *on-tumor*/*on-target* toxicities are side effects arising from the *desired* anti-tumor activity of CAR-T cells. With respect to CD19-CAR-T cells, efficacy and CRS are tightly linked; the majority of patients demonstrating an objective response will display at least mild CRS (240) and the onset of a fever after CAR-T cell infusion is positively received by both clinicians and patients (176). Preventing *on-tumor/on-target* toxicities is thus a question of whether it is possible to design CAR-T cell treatment regimens that are capable of retaining anti-tumor cytotoxicity while sparing associated toxicities. With current CAR-T cell modalities, this appears to be a challenging goal. Most strategies rely on reducing CRS by limiting the magnitude of the CAR-T cell response by either debulking the tumor prior to ACT or reducing the CAR-T cell dose level. The goal is to find a "Goldilocks zone" or therapeutic window in which it is possible to retain anti-tumor efficacy but spare toxicity. However, one retrospective study found that with current CAR-T cell strategies this window can be narrow or non-existent (258).

iii) Treating CAR-T cell associated toxicities

The treatment of *off-target* or *off-tumor/on-target* toxicities in modern CAR-T cell therapies can be mediated by the elimination of CAR-T cells made possible through the inclusion of suicide genes or other strategies during the T cell engineering process (259-261). However, such strategies are not useful in cases where the toxicity is a by-product of CAR-T cell efficacy (e.g. CRS); CAR-T cell elimination would negate efficacy. In the clinic, mild CRS is managed with supportive care (e.g. fever management, intravenous fluids) (262). Severe CRS, which can be life threatening, is first treated with tocilizumab (an antagonist

antibody specific for IL-6R[20]) (243, 245); patients who fail to respond are escalated to corticosteroid treatments (263) which can reduce therapeutic efficacy (212) and do not always rescue tocilizumab-refractory CRS patients from fatalities (205).

1.3.6 Pre-clinical development of CAR-T cells

The pre-clinical development of CAR-T cells is facilitated by the use of small animal models (reviewed in (264)); murine models can be broadly classified into two categories:

i) Syngeneic models

In syngeneic models both the tumor and engineered T cells are of murine origin; experiments can be conducted in an immunocompetent host. Tumors can arise as a result of genetic engineering (spontaneous tumor models), chemical-induction (e.g. exposure to a carcinogen), or the injection of a transplantable tumor (e.g. a tumor cell line). Syngeneic models are advantageous as they permit the evaluation of engineered T cell therapies in an immune replete microenvironment, as would be seen in the clinical scenario.

ii) Xenograft models

In xenograft models a murine host is engrafted with a human tumor and is treated with human CAR-T cells. In order to prevent the rejection of human cells by the murine host, these models necessitate the use of severely immunocompromised mice (not reflective of the clinical scenario). Tumors originate from the injection of human tumor cell lines or tumor "chunks"[21]. Xenograft models are advantageous as they offer an opportunity to evaluate the actual clinical product, i.e. an engineered human T cell.

1.3.7 Alternative chimeric receptors for engineering anti-tumor T cells

The redirection of T cell specificity against a tumor target via engineered expression of a synthetic receptor is not limited to the use of a traditional CAR. Next-generation targeting approaches are beginning to emerge (265, 266). Alternative synthetic/chimeric receptors retain the modular essence of CARs, being comprised of tumor-targeting and T cell activation domains, but instead eschew the direct incorporation of T cell activation domains in favor of coopting endogenous T cell signaling machinery (primarily the TCR).

[20] Given the association of CRS with high levels of systemic IL-6, antagonism of the IL-6 signaling pathway was evaluated as an anti-CRS therapeutic. Although anti-IL-6R has proven effective at managing CRS, the exact mechanism of action remains unknown.

[21] Small tumor chunks can be prepared from human tumor xenografts or from freshly resected/biopsied human tumors (these latter models are referred to as patient-derived xenografts).

1.4 Thesis scope and content

Herein I describe my doctoral studies which were focused on the pre-clinical development of T cell therapeutics targeted against tumor antigens via the engineered expression of synthetic receptors. This work was undertaken with the ultimate goal of contributing towards next-generation engineered-T cell products capable of systemic function in the absence of toxicity.

1.5 A note to the reader

The content within each of the manuscripts comprising the body of this thesis are unique and there is very little overlap between them – with the exception of the methods sections. The methods from Chapters two and four provide a description of the majority of the methods used for my research. Additionally, the following methods are described only in Chapters three and five:

- Murine DARPin-28z and scFv-28z CAR structure (Chapter 3; "Generation of CAR retroviruses")
- SPICE analysis (Chapter 3; "Functional analysis of CAR-T cells following stimulation with recombinant protein")
- TAC configurations (Chapter 5)
- Luminescence-based cytotoxicity assays (Chapter 5)
- NALM6 xenograft model (Chapter 5; "Adoptive transfer and *in vivo* monitoring")
- SPADE analysis (Chapter 5)

2.0 Chapter Two – T cells engineered with chimeric antigen receptors targeting NKG2D ligands display lethal toxicity in mice

2.1 Introduction

In this manuscript we describe the observation of on-target, off-tumor toxicity when CARs targeted against NKG2D (natural killer group 2, member D) ligands were evaluated in a syngeneic murine model. We identify a mechanism by which chemotherapeutic pre-conditioning drives pulmonary expression of NKG2D ligands, exacerbating the toxicity. Previous pre-clinical models had not denoted any observation of toxicity, and given the continued clinical development of NKG2D-based CAR-T cells dissemination of our findings was particularly pertinent.

2.2 Manuscript status, copyright, and citation

Status: Published manuscript

Citation: VanSeggelen, H, Hammill, JA, Dvorkin-Gheva, A, Tantalo, DGM, Kwiecien, JM, Denisova, GF, Rabinovich, B, Wan, Y, Bramson, JL. (2015). T cells engineered with chimeric antigen receptors targeting NKG2D ligands display lethal toxicity in mice. *Molecular Therapy.* 23(10):1601-1610. doi: 10.1038/mt.2015.119. Available online: http://www.cell.com/molecular-therapy-family/molecular-therapy/fulltext/S1525-0016(16)30291-X.

2.3 Published journal article

To follow beginning on subsequent page.

original article

T Cells Engineered With Chimeric Antigen Receptors Targeting NKG2D Ligands Display Lethal Toxicity in Mice

Heather VanSeggelen[1], Joanne A Hammill[1], Anna Dvorkin-Gheva[1], Daniela GM Tantalo[1], Jacek M Kwiecien[2,3], Galina F Denisova[1], Brian Rabinovich[4], Yonghong Wan[1] and Jonathan L Bramson[1]

[1]Department of Pathology and Molecular Medicine, McMaster Immunology Research Centre, McMaster University, Hamilton, Ontario, Canada; [2]Department of Pathology and Molecular Medicine, Central Animal Facility, McMaster University, Hamilton, Ontario, Canada; [3]Department of Neurosurgery and Pediatric Neurosurgery, Medical University of Lublin, Lublin, Poland; [4]Lion Biotechnologies, Woodland Hills, California, USA

Ligands for the NKG2D receptor are overexpressed on tumors, making them interesting immunotherapy targets. To assess the tumoricidal properties of T cells directed to attack NKG2D ligands, we engineered murine T cells with two distinct NKG2D-based chimeric antigen receptors (CARs): (i) a fusion between the NKG2D receptor and the CD3ζ chain and (ii) a conventional second-generation CAR, where the extracellular domain of NKG2D was fused to CD28 and CD3ζ. To enhance the CAR surface expression, we also engineered T cells to coexpress DAP10. *In vitro* functionality and surface expression levels of all three CARs was greater in BALB/c T cells than C57BL/6 T cells, indicating strain-specific differences. Upon adoptive transfer of NKG2D-CAR-T cells into syngeneic animals, we observed significant clinical toxicity resulting in morbidity and mortality. The severity of these toxicities varied between the CAR configurations and paralleled their *in vitro* NKG2D surface expression. BALB/c mice were more sensitive to these toxicities than C57BL/6 mice, consistent with the higher *in vitro* functionality of BALB/c T cells. Treatment with cyclophosphamide prior to adoptive transfer exacerbated the toxicity. We conclude that while NKG2D ligands may be useful targets for immunotherapy, the pursuit of NKG2D-based CAR-T cell therapies should be undertaken with caution.

Received 14 February 2015; accepted 18 June 2015; advance online publication 21 July 2015. doi:10.1038/mt.2015.119

INTRODUCTION

Treating patients with T cells that are engineered to express tumor-specific receptors has proven to be a clinically efficacious form of immunotherapy. In particular, the use of chimeric antigen receptors (CARs) to direct T cells to attack tumors has shown significant promise in clinical trials.[1–4] These receptors aim to target surface-expressed antigens that are either restricted to, or overexpressed on, tumor cells, eliminating the conventional T cell receptor requirement for antigen presentation on MHC molecules. One method of generating CARs fuses native proteins, which naturally ligate proteins on the surface of tumor cells, with the intracellular signaling domains required to induce T cell activation. Ligands for the natural killer group 2 member D (NKG2D) receptor are numerous and are frequently upregulated on many cancer types.[5–7] Additionally, NKG2D ligand (NKG2DL) expression can be upregulated on tumor cells through the use of already approved drugs such as spironolactone, allowing for further target enhancement.[8]

Using a CAR comprised of NKG2D fused to the CD3ζ TCR signaling domain enables T cells to recognize any of the several natural NKG2DL, and exert their cytolytic functions.[1–4,9–11] While NKG2D is an activating receptor on natural killer (NK) cells, it functions primarily as a costimulatory receptor on activated CD8+ T cells.[5–7,12–15] In both murine and human T cells, signaling through the NKG2D receptor is mediated through an adaptor protein, DAP10 (ref. 8,13). This adaptor protein activates the PI3-K and Grb-2 pathways, much like the T cell costimulatory molecule, CD28 (ref. 14,16). Research has revealed that the inclusion of costimulatory domains in CARs enhances T cell efficacy and persistence postadoptive transfer.[17–20] In that regard, fusion of full-length NKG2D with CD3ζ may provide costimulatory signals via the NKG2D portion of the receptor, in addition to the activation signal delivered through CD3ζ. In this manuscript, we investigated two distinct CARs based on the NKG2D receptor: (i) a fusion of NKG2D with CD3ζ (NKz) and (ii) a fusion of the NKG2D extracellular domain to signaling domains from a conventional second-generation CAR composed of CD28 fused to CD3ζ (NK28z). Since surface expression of full-length NKG2D is dependent upon the DAP10 molecule,[9,21] we also investigated whether coexpression of DAP10 along with the NKz fusion protein (NKz10) could further augment CAR activity.

Our results revealed that the functionality of the CARs was strain-dependent in murine T cells. Further, T cells expressing NKG2D-based CARs displayed *in vivo* toxicity, which was exacerbated when T cell infusion was combined with chemotherapeutic

Correspondence: Jonathan L. Bramson, McMaster Immunology Research Centre, McMaster University, 1200 Main Street West, Hamilton, Ontario L8N 3Z5, Canada. E-mail: bramsonj@mcmaster.ca

lymphodepletion. The NKz-CAR-T cells displayed the lowest toxicity *in vivo*, which suggests that this configuration may be amenable to clinical evaluation. These results revealed that NKG2D-based CAR-T cells can be highly toxic when delivered systemically and indicate that further research is required to better understand how to deploy these CAR-T cells safely in the clinic.

RESULTS

Inclusion of DAP10 in the retrovirus significantly enhances surface expression of NKz

To produce T cells that would be activated by NKG2D-ligands, we engineered murine T cells with one of three different NKG2D-based CAR retrovirus (RV) constructs: full-length NKG2D fused to cytoplasmic CD3ζ (NKz), the same NKz-CAR with the addition of adaptor protein DAP10 to the RV construct (NKz10), or a conventional second-generation CAR that fuses the extracellular domain of NKG2D to a CD8-hinge region, CD28 transmembrane and cytoplasmic domains, and the cytoplasmic domain of CD3ζ (NK28z; Figure 1a). We utilized NKG2D cell surface staining as an indicator of NKG2D-CAR expression, as CAR -ve T cells show very low levels of endogenous NKG2D expression (Figure 1b,c). Engineering T cells with any of the three NKG2D-CAR RVs resulted in over 90% of both CD8+ (Figure 1b) and CD4+ (**Supplementary Figure S1**, top panels) T cells staining positive for NKG2D within three days of transduction with BALB/c-derived T cells. Frequencies of CAR+ T cells

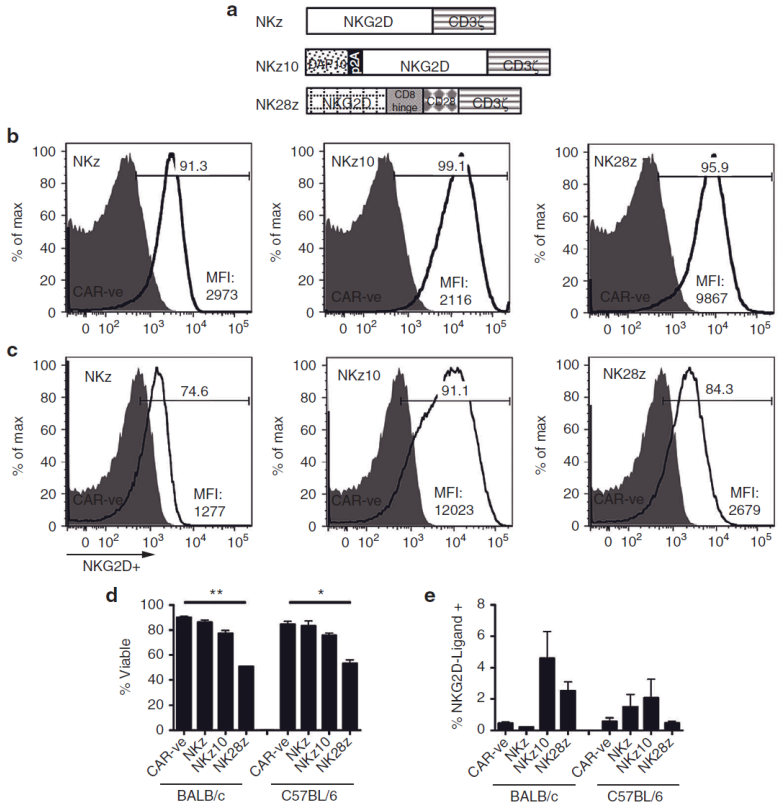

Figure 1 Retrovirus construction and *in vitro* phenotypic profiles of NKG2D-ligand-specific chimeric antigen receptor (CAR)-engineered T cells. (**a**) Schematic diagram of the retrovirus (RV) constructs used to engineer murine T cells. The chimeric NKG2D-CD3ζ (*NKz*) CAR contains the full-length murine NKG2D gene fused to the cytoplasmic portion of CD3ζ. The *NKz10* CAR bears the same CAR as NKz with the addition of adaptor protein DAP10 to the retrovirus, separated by a self-cleaving 2A peptide. The *NK28z* CAR combines the extracellular domain of murine NKG2D, fused to the CD8 hinge region, CD28 transmembrane and endodomains, and cytoplasmic CD3ζ. NKG2D expression on (**b**) BALB/c or (**c**) C57BL/6 CD8+ T cells was evaluated 3 days after transduction with the indicated CAR-containing retroviruses. Surface expression was determined using a fluorescence-minus one control of the anti-NKG2D – APC antibody and compared to basal expression on control CAR -ve T cells (shaded peaks). Mean fluorescence intensity and percentage of NKG2D+ CD8+ cells are shown. Data is representative of at least three independent experiments. (**d**) Viability of NKG2D-CAR-T cells from BALB/c and C57BL/6 mice was determined by flow cytometry using Molecular Probes LIVE/DEAD staining. (**e**) NKG2D-CAR cells were analyzed for NKG2D-ligand expression, as indicated by staining using an NKG2D-IgG-Fc chimeric protein and detected with an anti-human IgG secondary antibody to detect ligand expression.

were generally lower using C57BL/6 T cells for all three CARs tested, with only NKz10 reaching NKG2D+ frequencies above 90% on either CD8+ or CD4+ T cells (**Figure 1c**; **Supplementary Figure S1**, bottom panels) On a per-cell basis, the NKz10-CAR-T cells showed over 7- to 10-fold higher expression of NKG2D compared to the NKz construct, indicating that the endogenous availability of DAP10 can limit surface expression of the NKz-CAR (**Figure 1b,c**). The NK28z-CAR showed an intermediate level of NKG2D surface expression, with twofold lower expression compared to NKz10 in BALB/c T cells (**Figure 1b**) and fivefold lower expression in C57BL/6 T cells (**Figure 1c**).

NKG2D-CARs show strain-specific differences

We evaluated differences in CAR surface expression, T-cell viability, and NKG2DL expression on the NKG2D-CAR-T cells between the three NKG2D-CAR constructs, as well as between two mouse strains. Interestingly, both BALB/c and C57BL/6 T cells showed the same changes in cell viability across NKG2D-CAR constructs; NKz-engineered T cells showed no reduction in viability compared to CAR –'ve T cells, NKz10-CAR-T cells showed a slight reduction in viability, and NK28z-CAR-T cells had a considerably decreased viability (**Figure 1d**; **Supplementary Figure S2a**). We observed variable levels of NKG2DL on CAR-engineered T cells across CAR type and T-cell origin (**Figure 1e**; **Supplementary Figure S2b**). While NKG2DL tended to be higher on NKz10-CAR T cells of either mouse strain, these data did not achieve statistical significance (**Figure 1e**).

Despite the higher per-cell expression, NKz10-CAR did not demonstrate an equivalent enhancement of *in vitro* functionality in BALB/c T cells. In BALB/c T cells, all three NKG2D-CARs were similarly capable of producing the activation cytokines IFNγ and TNFα upon stimulation with recombinant Rae-1β, a well-defined NKG2D ligand (**Figure 2a**; **Supplementary Figure S3**). This was not directly attributed to differences in baseline cytokine production, as only the BALB/c NKz10-CAR T cells showed an increase in cytokine production over their C57BL/6 counterparts without stimulation (**Figure 2a**). The levels of background cytokine were very low in all cases (<2%; **Figure 2a**). In addition, all three NKG2D-CARs were able to induce robust killing of murine breast tumor cells *in vitro*, although NKz10 and NK28z BALB/c-derived NKG2D-CAR-T cells demonstrated moderately increased cytotoxicity compared to NKz counterparts at intermediate effector to target ratios. For example, NKz10 and NK28z were able to kill ~80% of tumor targets compared to only ~50% by NKz after 6 hours of coincubation at a 1:1 T-cell to tumor cell ratio (**Figure 2b**). Most of the tumor targets were killed after coculture of BALB/c NKG2D-CAR-T cells and tumor cells at a 2:1 ratio, illustrating the strong cytotoxic potential of these NKG2D-CAR-T cells (**Figure 2b**).

NKG2D-CAR-engineered C57BL/6 T cells showed slightly reduced cytokine production upon CAR-stimulation compared to BALB/c-derived CAR-T cells (**Figure 2a**; **Supplementary Figure S2**). Interestingly, while NKz10-CAR-T cells had the highest level of CAR expression in C57BL/6-derived cells, the NK28z-CAR-T cells showed the greatest cytokine production (**Figure 2a**). This cytokine production did not translate to killing potential, as the C57BL/6 NK28z-CAR-T cells displayed weak cytotoxicity *in vitro* (**Figure 2c**). Similarly, the C57BL/6-derived NKz-CAR T cells also exhibited weak cytotoxicity (**Figure 2c**). While C57BL/6 NKz10-CAR-T cells were capable of killing tumor targets at higher E:T ratios, their activity was considerably diminished when compared to their BALB/c counterparts (**Figure 2b,c**). Taken together, our data reveal striking strain-dependent differences in the functionality of the various NKG2D-based CARs.

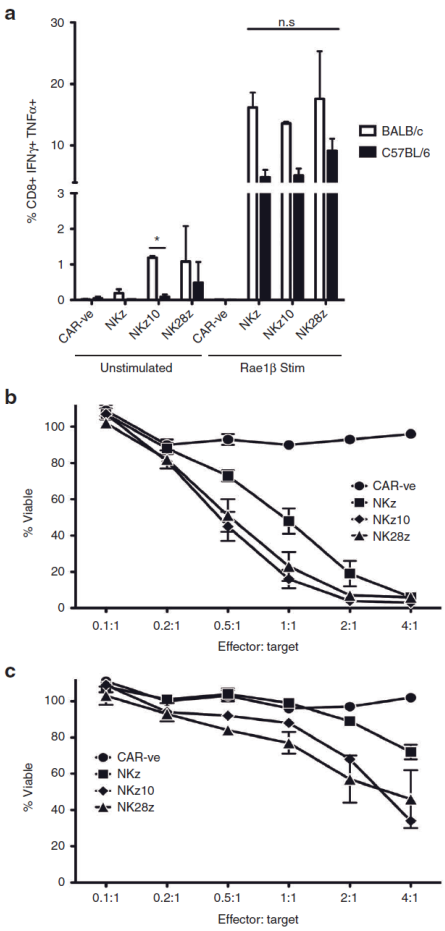

Figure 2 *In vitro* functional profiles of NKG2D-CAR-T cells. (**a**,**b**) BALB/c or (**a**,**c**) C57BL/6 T cells were engineered with the indicated CARs. (**a**) NKG2D-CAR T cells were stimulated with plate-bound recombinant Rae1β-Fc fusion protein and stained for production of IFNγ and TNFα, and analyzed by flow cytometry. Data is expressed as mean frequency ± SEM normalized to background levels from three independent experiments. *In vitro* CAR-T cell-mediated cytotoxicity was assayed using 4T1.2 tumor cells using a 6-hour AlamarBlue assay at the indicated effector: target ratios of BALB/c (**b**) or C57BL/6 (**c**) T cells. Mean frequency of viable tumor cells ± SEM from 3–4 independent experiments of triplicate wells is presented.

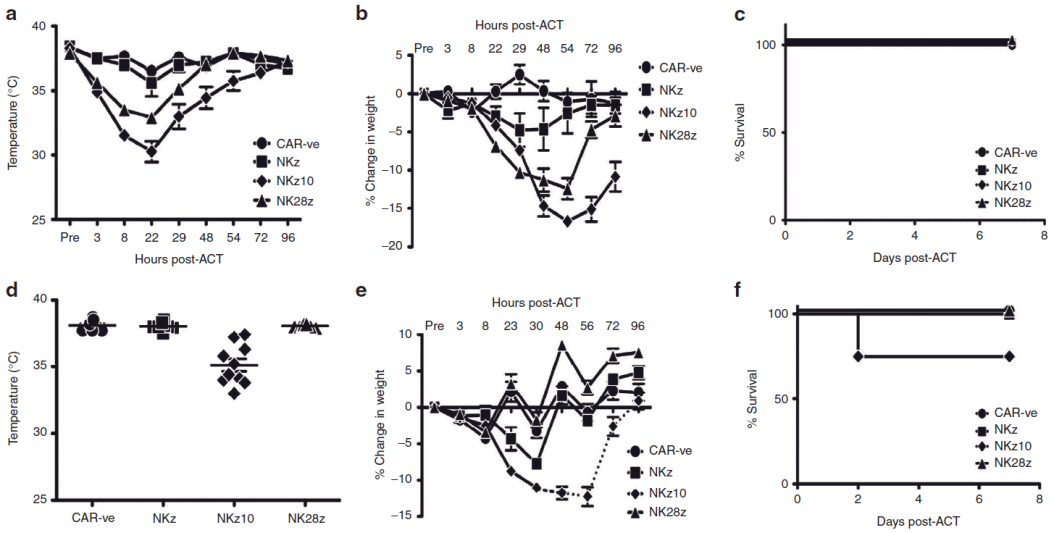

Figure 3 NKG2D-CAR-T cells induce differing levels of toxicity in mice. (**a–c**) Naive BALB/c mice were treated with 10^7 NK-CAR-T cells intravenously as indicated ($n = 6$). (**a**) Temperatures, (**b**) weight loss, and (**c**) survival were monitored over the course of 7 days post-adoptive cell transfer (ACT). (**d–f**) Naive C57BL/6 mice were treated as in **a** ($n = 5–10$). (**d**) Temperatures are shown at the peak drop of 8 hours post ACT. (**e**) Weight loss and (**f**) survival were monitored over 7 days post-ACT. Temperature and weight loss data are presented as mean ± SEM. Dotted lines indicate data from surviving animals.

NKG2D-CAR-T cells can induce significant, acute toxicity upon adoptive transfer

We next investigated the functionality of NKG2D-CAR-T cells *in vivo*. We employed the 4T1.2 breast tumor model in BALB/c mice. Mice bearing established tumors were treated with cyclophosphamide (CTX), followed by infusion of NKG2D-CAR T cells. Strikingly, we observed dramatic clinical toxicity symptoms within just a few hours of adoptive transfer. To understand whether this toxicity was related to an over-exuberant antitumor immune response resulting from the NKG2D–CAR-T cell infusion, we adoptively transferred NKG2D-CAR-T cells into naive, tumor-free animals. Tumor-free mice still exhibited significant clinical symptoms, including lethargy, hunched body posture, ruffled fur, and a lack of grooming, indicating that the NKG2D-CAR-T cells were producing off-tumor toxicities *in vivo*.

To better understand these off-tumor toxicities, naive BALB/c mice were infused with 10^7 NKz, NKz10, or NK28z CAR-T cells, and toxicity was evaluated via changes in core body temperature, body weight, and overall survival (**Figure 3a–c**). Despite similar *in vitro* functionality, the BALB/c-derived NKG2D-CAR-T cells displayed a distinct hierarchy of disease severity between the different CAR-T cells *in vivo*. The NKz10-CAR-T cells elicited the most significant toxicity, with core body temperatures dropping as low as 30°C within 24 hours of adoptive cell transfer (ACT) (**Figure 3a**). Additionally, these mice lost up to 17% of their body weight in less than 3 days post-ACT (**Figure 3b**). The NKz-CAR treated animals conversely showed no significant hypothermia, and only slight weight loss over the course of one week post-ACT (**Figure 3a,b**). The NK28z-CAR-T cells induced an intermediate level of toxicity with respect to both temperature changes and weight loss (**Figure 3a,b**). These toxicities were accompanied by significant clinical symptoms such as lethargy, ruffled fur, hunched posture, and labored breathing that corresponded to the severity of hypothermia and weight loss (**Supplementary Table S1**). Interestingly, these data parallel our observations of the differences in per-cell NKG2D-CAR expression *in vitro* (**Figure 1b**), with the greatest expression and most severe toxicities being observed with NKz10-CAR-T cells. Despite these significant, acute toxicities, all mice survived the treatment, and recovered within 7 days of ACT (**Figure 3c**). We evaluated whether similar toxicities were observed in C57BL/6 mice. Interestingly, C57BL/6 mice did not display any overt physical clinical symptoms such as changes in posture, fur or body condition (**Figure 3d,e**, *data not shown*). In addition, only the NKz10-CAR T cells caused measurable toxicities in the form of hypothermia, weight loss, and morbidity (**Figure 3d–f**). The temperature changes and weight loss in these animals were considerably more modest compared to those observed in BALB/c mice. NKz10-CAR-T cell–treated mice displayed variable temperature changes, with some mice showing only mild hypothermia and others dropping to 33°C within 8 hours of ACT (**Figure 3d**). Weight loss by NKz10-CAR-T cell–treated mice was consistent; over the course of 3 days post-ACT, C57BL/6 mice lost up to 12% of their body mass (**Figure 3e**). Despite the reduced severity of hypothermia and weight loss in C57BL/6 mice, ACT of NKz10-CAR-T cells was lethal in 25% of the treated animals within 48 hours of treatment ($n = 8$; **Figure 3f**). The NKz and NK28z CAR-T cells showed no significant toxicity or lethality in C57BL/6 mice. These data reveal a

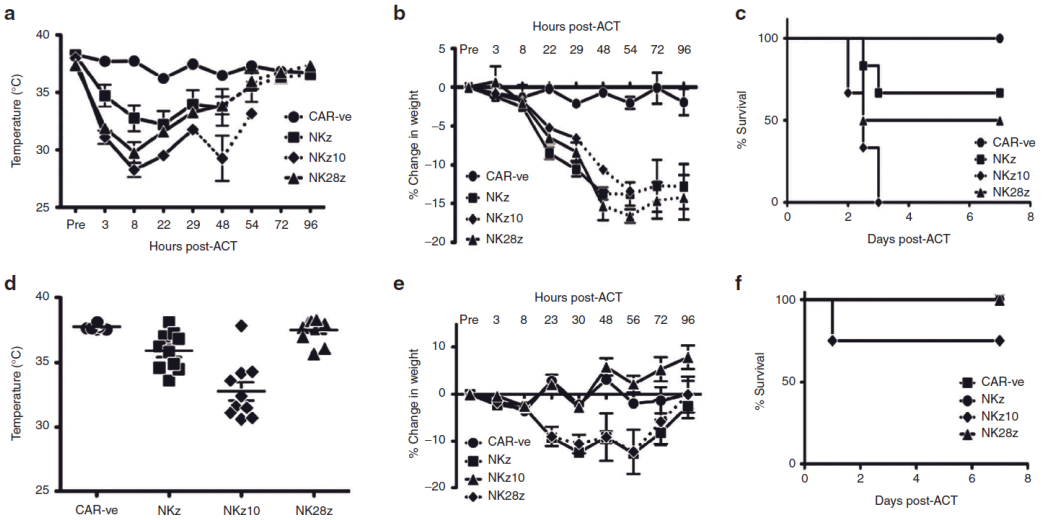

Figure 4 NKG2D-CAR-T cell toxicity is exacerbated by pre-conditioning with chemotherapy. Mice were treated with 150 mg/kg cyclophosphamide (CTX) intraperitoneally 24 hours prior to adoptive transfer. (**a–c**) BALB/c/c mice were treated with 10^7 NK-CAR-T cells intravenously as indicated ($n = 6$). (**a**) Temperatures, (**b**) weight loss, and (**c**) survival were monitored over the course of 7 days post adoptive cell transfer (ACT). (**d–f**) Naive C57BL/6 mice were treated as in **a** ($n = 5–10$). (**d**) Temperatures are shown at the peak drop of 8 hours post ACT. (**e**) Weight loss and (**f**) survival were monitored over 7 days post-ACT. Temperature and weight loss data are presented as mean ± SEM. Dotted lines indicate data from surviving animals.

notable difference in severity of NKG2D-CAR off-tumor toxicity between the two strains of mice tested, with BALB/c mice exhibiting greater toxicity than their C57BL/6 counterparts.

Preconditioning cyclophosphamide exacerbates NKG2D-CAR toxicity

In both preclinical models and clinical trials of CAR-T cells, regimes inducing lymphopenia have proven to enhance the engraftment and persistence of CAR-T cells following adoptive transfer.[22,23] As chemotherapeutic agents cause DNA damage and cell stress, which can upregulate NKG2DL expression, we tested whether pretreatment with CTX would influence toxicity following adoptive transfer of NKG2D-CAR-T cells. Strikingly, CTX pretreatment significantly exacerbated the toxicity induced by all three NKG2D-CARs (**Figure 4**).

In BALB/c mice, the NKz-CAR-T cells, which showed minimal toxicity in naive mice, were highly toxic when combined with CTX, inducing hypothermia and weight loss comparable to those induced by the NKz10-CAR-T cells (**Figure 4a,b**). Further, infusion of NKz-CAR-T cells in CTX pretreated BALB/c mice resulted in 33% mortality (**Figure 4c**). Toxicities produced by NKz10-CAR-T cells were also dramatically exacerbated, with body temperatures dropping below 29°C within as little as 8 hours post-ACT (**Figure 4a**). Other clinical symptoms were likewise exacerbated; mice demonstrated lethargy, a complete lack of grooming and the appearance of an ocular discharge. Most alarmingly, all mice treated with CTX and NKz10-CAR-T cells succumbed to the toxicities within 72 hours of ACT (**Figure 4c**). As observed in naive animals, NK28z-CAR-T cells showed an intermediate level of toxicity that was similarly worsened by CTX; 50% of animals in this treatment group succumbed to T-cell–mediated toxicity (**Figure 4c**).

The preconditioning chemotherapy also enhanced the toxicity of NKG2D-CAR-T cells in C57BL/6 mice (**Figure 4d–f**). Mice treated with NKz-CAR-T cells showed significant weight loss of over 12% of the pretreatment weight (**Figure 4e**), with average core body temperatures dropping below 35 °C within 8 hours of T-cell infusion (**Figure 4d**). In the case of NKz10-CAR-T cells, 25% of the treated animals succumbed to toxicities in less than 24 hours following ACT (**Figure 4f**). Surviving animals varied in their weight loss, with some losing more than 18% of their body weight before recovering (**Figure 4e**). Core body temperatures were also variable, with some of the survivors exhibiting little change, while others dropped below 31°C within 8 hours of ACT (**Figure 4d**). While C57BL/6 mice failed to show any of the physical symptoms of toxicity observed in BALB/c mice, chemotherapeutic pretreatment prior to ACT of NKz10-CAR-T cells resulted in an observable lethargy (noted upon handling the animals) in the C57BL/6 mice (data not shown). The NK28z-CAR-T cells showed no signs of toxicity, even when combined with CTX in C57BL/6 mice. These data reveal that the toxicities are dependent on both the strain and the CAR structure.

Adoptive transfer of NKG2D-CAR-T cells results in an acute cytokine storm *in vivo*

We next sought to investigate possible causes of this *in vivo* toxicity. Using a 32-plex cytokine array, we examined serum cytokine levels in BALB/c mice at 8 hours post-ACT, both with and without preconditioning cyclophosphamide. Strikingly, the majority of the cytokines evaluated were upregulated in the serum of

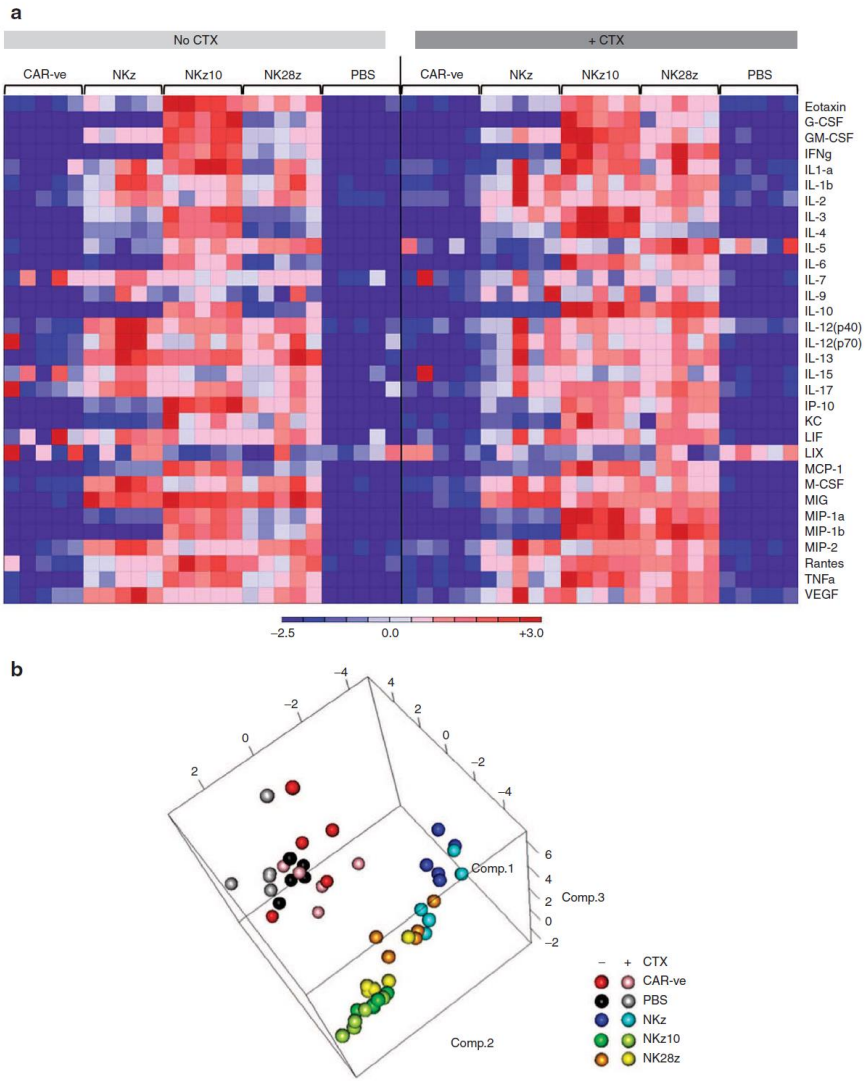

Figure 5 NKz10-CAR-T cells induce severe cytokine storm in BALB/c mice. Mice with or without pre-conditioning CTX were treated with 10^7 engineered T cells as indicated ($n = 5$). Serum was collected at 8 hours post-ACT and sent for Luminex analysis. (**a**) Heat map displaying the relative changes in serum cytokine concentrations from mice treated with CAR -ve, NKz, NKz10 or NK28z CAR-T cells, or PBS control. Data was normalized by row. (**b**) Principal component analysis of serum cytokine concentrations indicating clustering of treatment groups.

mice receiving any of the NKG2D-CAR-T cells (Figure 5a). Mice treated with NKz10-CAR-T cells showed the most dramatic upregulation, with all but four analytes increased compared to CAR -ve controls (Figure 5a; **Supplementary Tables S2 and S3**). These mice showed serum concentrations of over 4 ng/ml of IFNγ, among others, indicating severe immune responses were occurring (Figure 5a; **Supplementary Tables S2 and S3**).

Our previous observations indicated that NKz and NKz10 represented the lowest and highest observed toxicity and CAR-expression, respectively, with NK28z exhibiting an intermediate outcome. This pattern was reinforced through principal component analysis of serum cytokine and chemokine levels. While each NKG2D-CAR-T cell treatment clustered tightly regardless of CTX pretreatment, each NKG2D-CAR-T cell cluster was separate

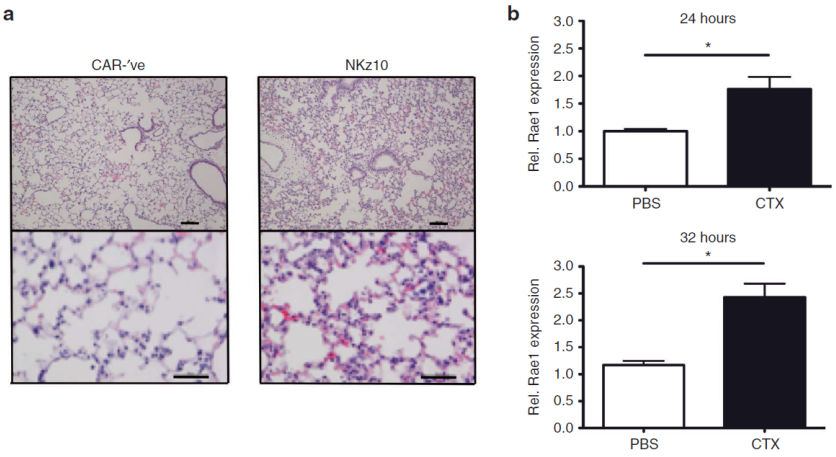

Figure 6 NKG2D-CAR toxicity is mediated via pulmonary inflammation. (**a**) BALB/c mice were treated with 150 mg/kg cyclophosphamide, followed by intravenous injection of 10^7 CAR-'ve or NKz10 CAR-T cells. Animals were sacrificed for complete veterinary necropsy 24 hours later. Hematoxylin and eosin–stained cross-sections of lung tissues from representative mice are shown ($n = 5$). Top panel bars = 100 µm, bottom panel bars =50 µm. (**b**) NKG2D ligand expression was evaluated by qRT-PCR in the lungs of either naive or CTX-treated mice at 24 or 32 hours post-CTX ($n = 5$).

from the others, with NK28z falling between NKz and NKz10 (Figure 5b).

CTX pretreatment enhanced the serum concentration of many cytokines/chemokines (**Supplementary Tables S2 and S3**). The observed serum concentration increases following CTX pretreatment were NKG2D-CAR-T cell specific, as we did not observe any measureable changes between CAR -ve ± CTX or PBS ± CTX control groups (Figure 5a,b). The most dramatic effects of CTX were observed in mice treated with NKz-CAR-T cells and NK28z-CAR-T cells, where the concentrations of many cytokines were more than doubled by CTX pretreatment (**Supplementary Tables S2 and S3**). Overall, our data are indicative of a severe cytokine storm induced by ACT of NKG2D-CAR-T cells that is exacerbated by pre-conditioning with CTX.

NKz10 CAR-T cells induce severe lung immunopathology

Given that the most substantial toxicities were observed in BALB/c mice treated with CTX and NKz10-CAR-T cells, we sought to further investigate the pathology elicited by this treatment. BALB/c mice were treated with CTX followed by adoptive transfer of 10^7 CAR -ve or NKz10-CAR-T cells and subjected to a comprehensive necropsy performed by a veterinary pathologist in a blinded fashion. NKz10-CAR-T cell-treated animals exhibited severe necrotizing pneumonitis, which was deemed to have been likely fatal in these animals (Figure 6a). No tissue pathology was observed in CAR -ve control animals. The lungs of NKz10-CAR-treated mice displayed severe perivascular edema, diffuse thickening of the alveolar septae, as well as heavy infiltration by neutrophils and mononuclear cells (Figure 6a).

Lungs from BALB/c mice treated with either PBS or CTX were harvested at 24 and 36 hours posttreatment and NKG2D ligand expression was measured by qRT-PCR. H60a, H60b, and Mult-1 were detected in all samples, but the expression was not impacted by CTX treatment (**Supplementary Figure S4b–d**). In contrast, CTX treatment resulted in a significant upregulation of Rae1 gene transcription at both time points (Figure 6b). Taken together, our data suggests that NKG2D-CAR toxicity is driven by severe systemic pro-inflammatory changes including pneumonitis.

DISCUSSION

On-target, off-tumor toxicity remains a primary concern for all immunotherapy approaches, especially given that the vast majority of tumor targets are not tumor-restricted in their expression.[24] Here, we examined the preclinical *in vitro* and *in vivo* functionality of three CARs based on the NKG2D receptor. Unexpectedly, we observed severe off-tumor toxicity upon *in vivo* testing of these NKG2D-CARs in multiple mouse strains. We have treated both C57BL/6 and BALB/c mice with CAR-T cells specific for a variety of antigens, including HER-2 and GPNMB, and have never observed toxicity following treatment (unpublished observations). Thus, the toxicity observed with the NKG2D-CARs is not simply reflective of toxicity associated with the infusion of engineered T cells. These previously unreported findings provide insight into considerations that must be taken into account prior to the clinical application of NKG2D-CARs.

The range of homeostatic NKG2DL expression at both the transcriptional and protein levels is currently unclear in both mice and humans. Multiple reports have established NKG2DL expression on various healthy, noncancerous/infected tissues, and these may serve as off-tumor ligand sources for NKG2D-CAR-T cells *in vivo*. At a transcriptional level, several NKG2DL are expressed across diverse tissues such as the spleen, lungs, gut and bronchial epithelia, cardiac and skeletal muscle, and the skin.[25–28] Data from others suggest epithelial, endothelial, and antigen-presenting cells may constitutively express NKG2DL such as UL16-binding

proteins (ULBPs).[29] We have found that systemic treatment with CTX leads to upregulation of NKG2DL in the lungs, which provides an explanation of the enhanced toxicity of NKG2D-CAR-T cells in hosts that were pretreated with CTX and suggests that caution should be employed when combining chemotherapy with cytotoxic therapeutics that target NKG2DLs.

There are known expression differences in the NKG2DLs, H60and Rae-1, between BALB/c and C57BL/6 mice, which may explain observed strain-specific differences in NKG2D-CAR-T cell toxicity.[25,30] In particular, H60a has been shown to be predominantly expressed in BALB/c mice and not in C57BL/6 mice due to a truncated genomic sequence,[31] which results in a lack of functional H60a protein in C57BL/6 mice.[30,32] Conversely, C57BL/6 mice show elevated levels of expression of H60b and H60c when compared to BALB/c mice.[33] Expression of Rae-1 family members also differs across mouse strains; BALB/c mice express Rae-1α, Rae-1β, and Rae1γ, while C57BL/6 mice express Rae-1δ and Rae-1ε.[30,34] Overall, BALB/c mice show elevated levels of expression of Rae-1 proteins and pan-NKG2D-ligands (detected using an NKG2D-Fc fusion protein) on bone marrow isolates compared to C57BL/6 mice,[30] which may explain the heightened toxicity of NKG2D-CAR T cells in BALB/c mice. The diversity of expression patterns of NKG2DL in humans (or mice), coupled with our data indicating the potential for toxicity, cautions strongly against the use of NKG2D-CAR-T cells for therapeutic applications in humans without considerable care and monitoring.

Commensal microbiota may also underpin the strain-specific toxicities of NKG2D-CAR T as C57Bl/6 mice and BALB/c have distinct microbiomes.[35] Commensal microbial composition in the gut has been shown to influence respiratory immune responses,[36] so it is possible that such differences influence the lethal pneumonitis observed following intravenous infusion of NKG2D-CAR-T cells. CTX may further compound the influence of the microbiome as treatment with CTX has been found to alter the microbial composition within the gut and subsequent immune responses.[37] Thus, the differences in toxicity may result from both genetic and microbial differences between the mouse strains.

Endogenous NKG2D receptors recognize NKG2DLs on healthy cells without inducing toxicity. We hypothesize that inherent differences between these receptors and NKG2D-CARs explain our toxicity observations. NKG2D-CARs bind NKG2DL, which induce T-cell activation and cytolytic functions.[9] Similarly, in NK cells, NKG2D acts as a positive signal to induce cytolytic functions.[38] However, in NK cells these positive signals are balanced by inhibitory signals from other NK cell surface receptors that act in concert to determine the fate of the target cell.[38] Under homeostatic conditions, low levels of NKG2DL and concomitant NKG2D signaling would occur in concert with inhibitory signals, such as the presence of MHC-1, preventing NK cell reactivity.[39] Removing the contributions of the inhibitory signals, as in NKG2D-based CARs, effectively takes the brakes off NKG2D-mediated cytotoxicity. Coupling this with a highly expressed, highly activating chimeric NKG2D receptor can therefore have potentially serious consequences, as revealed by the severe toxicity of NKz10-CAR-T cells.

One of our most striking observations was the varied manifestation of toxicity between the two different strains of mice tested. Whereas both NKz10- and NK28z-CAR-T cells were markedly toxic to BALB/c mice, these CAR-T cells manifested little toxicity in C57BL/6 mice. Likewise, although the NKz-CAR-T cells alone were minimally toxic in both strains, when combined with CTX, the NKz-CAR only caused significant morbidity and mortality in BALB/c mice. Our findings are consistent with previous reports describing NKz-CAR-T cells as a tumor therapy in the absence of overt toxicity using C57BL/6 mice, even when combined with CTX.[7,9–11] These data demonstrate that a therapeutic window may exist for treatment with NKz-CAR T cells; however, many factors (as described above) must be taken into consideration prior to treatment to avoid unwanted severe toxicities. The NKz10-CAR, which demonstrated the most severe toxicity in our studies, has only been previously tested on human NK cells using immunodeficient animals, which precludes the ability to assess toxicity due to a lack of cross-reactivity.[40,41] Likewise, CARs composed of the NKG2D extracellular domain fused to a conventional CAR scaffold have thus far only been tested using *in vitro* assays, and so possible toxicities were not yet evaluated.[42,43] The results of this work conclude that NKG2D-CAR-T cells can be highly toxic and that the toxicity is influenced by both the host and the conditioning regimen. As such, our findings suggest that preclinical studies in C57BL/6 mice may underestimate the toxicity associated with NKG2D-CAR-T cells.

While a hierarchy in T-cell surface expression of our NKG2D-CARs (NKz < NK28z < NKz10) was consistent between T cells from BALB/c and C57BL/6 donors, we also observed startling differences when comparing CAR-T cell functionality between mouse strains. While all three NKG2D-CARs exhibited similar *in vitro* functionality in BALB/c T cells, the CARs displayed reduced overall functionality when expressed in C57BL/6 T cells, including capacity to induce both cytokine production and cytotoxicity. In both cases, functional abilities did not appear to correlate with the level of receptor surface expression. However, our data also suggests that measuring CAR-T-cell functionality *in vitro* does not equate to toxicity *in vivo*. Interestingly, the intensity of NKG2D staining on engineered T cells did correspond to the level of toxicity observed, with NKz showing the lowest NK28z an intermediate level, and NKz10 showing the highest in both NKG2D mean fluorescence intensity, as well as toxicity in both BALB/c and C57BL/6 mice. The NKz10-CAR was the only toxic CAR in C57BL/6 mice, consistent with the highest level of surface expression of the three NKG2D-CARs. This hierarchical toxicity was also observed in the magnitude of serum cytokine elevations in BALB/c mice. The high levels of inflammatory cytokines likely contributed to systemic toxicity, similar to those observed in some clinical trials of T-cell therapies.[44] These data suggests that the level of NKG2D-CAR surface expression on each cell may be predictive of their *in vivo* functionality. Together, these studies reveal previously unappreciated strain-specific differences in CAR-T cell functionality following NKG2D-CAR engineering, indicating an important role for the recipient T cells in CAR function.

Overall, our data shows that NKG2D-based CARs have the potential to induce significant toxicities *in vivo*, especially if delivered subsequent to lymphodepletion regimens, like cyclophosphamide. NKz-CAR-T cells revealed similar functionality to the other NKG2D-CAR-T cells *in vitro* while demonstrating the

lowest levels of observed toxicity in both BALB/c and C57BL/6 hosts. Thus, the NKz-CAR-T cells may be suitable for further clinical development. However, given the potential toxicities of these T cells, clinical translation should be undertaken with caution. Our study reveals important new information regarding potential toxicity of therapies targeting NKG2DLs and accentuates the need to identify tumor-restricted antigens, or antigens with limited expression off-tumor (on non-vital organs), for targeting with CAR-T cell therapy to avoid the potential for off-tumor toxicity.

MATERIALS AND METHODS

Mice. Six- to eight-week-old female BALB/c or C57BL/6 mice were purchased from Charles River Breeding Laboratories (Wilmington, MA). All animal studies have received approval by the McMaster University Animal Research Ethics Board.

Generation of CAR retroviral vectors. For cloning CAR retroviruses, the shuttle plasmid pDONR222 oTK-P2A-oFL-T2A-eGFP, and retroviral vectors pRV2011-oFL and pRV100G eGFP were used.[45] The NKz-CAR construct was generated according to previous reports,[9] where the cytoplasmic region of murine CD3ζ was fused to full-length murine NKG2D via DNA synthesis (GenScript, Piscataway, NJ). The NKz-CAR was synthesized and inserted into the shuttle plasmid pDONR222 oTK-P2A-oFL-T2A-eGFP by deleting oTK-P2A and replacing eGFP with NKz, resulting in pDONR222 oFL-T2A-NKz (oFL = firefly luciferase,[45] T2A = Thosea asigna virus self-cleaving 2A peptide [46]). The oFL-T2A-NKz expression cassette was transferred into the retroviral vector pRV100G by LR recombination (Gateway LR Clonase II Enzyme Mix; Life Technologies, Grand Island, NY). Production of the NKz10-CAR construct was similar; pDONR222 oTK-P2A-oFL-T2A-eGFP was modified by replacing oTK with full-length murine DAP10 (accessed from NM_011827.3, codon optimized for murine expression, and synthesized (GenScript)) and eGFP with the synthesized NKz sequence, resulting in pDONR222 DAP10-P2A-oFL-T2A-NKz (P2A = porcine teschovirus-1 self-cleaving 2A peptide[46]). LR recombination transferred DAP10-P2A-oFL-T2A-NKz into pRV100G. The NK28z-CAR was constructed by modifying an existing second generation CAR vector (HER2scFv28z). The extracellular portion of NKG2D was amplified out of the NKz10-CAR (using the primers NKDG2DF: 5′-GTTCAAGGAGACATTTCAGCCTGTG-3′ and NKG2DR: 5′-ACAGCTCTCTTCATACAAATATAGGTATTC-3′) and inserted into the HER2scFv28z vector in place of the scFv and c-myc. The HER2-CAR used as the backbone for the NK28z-CAR was described previously, with the human sequences replaced by murine equivalents.[47] In short, an scFv specific for HER2, a marker epitope from c-myc, the membrane proximal hinge region of murine CD8, the transmembrane and cytoplasmic regions of murine CD28, and the cytoplasmic region of murine CD3ζ were fused together and cloned into the retroviral vector pRV2011 oFL[45] in place of firefly luciferase, leaving the IRES and Thy1.1 sequences intact.

Retroviral supernatants were generated by transient transfection of CAR retroviral vectors (10 µg) and the packaging plasmid pCL-Eco (10 µg) into Platinum-E (PLAT-E) cells[48] using Lipofectamine 2000 (Life Technologies). After 24 hours of culture, media was changed. Retrovirus containing supernatants were collected 48 hours later and concentrated 10-fold using an Amicon Ultra 100K centrifugal filter (EMD Millipore, Billerica, MA).

Murine T-cell transduction. Freshly isolated splenocytes from BALB/C or C57BL/6 mice were cultured in 24-well plates in T-cell growth media (RPMI 1640 supplemented with 10% heat-inactivated fetal bovine serum (FBS), 10 mmol/l HEPES, 2 mmol/l L-glutamine, 0.1 mmol/l nonessential amino acids (Gibco, Life Technologies), 0.1 mg/ml normocin (Invivogen, San Diego, CA), 1 mmol/l sodium pyruvate, and 55 nmol/l β-mercaptoethanol). Splenocytes were activated with 0.1 µg/ml each hamster anti-mouse CD3 (clone 2C11; BD Biosciences, San Jose, CA) and hamster anti-mouse CD28 (clone 37.51; BD Biosciences), and cultured in the presence of 60 IU rhIL-2 (Peprotech, Rocky Hill, NJ). After 24 hours, T cells were transduced via spinfection, whereby 100 µl of concentrated retroviral supernatant was added to 3×10^6 cells in the presence of 1.6 µg/ml Polybrene (Sigma-Aldrich, St. Louis, MO) and 2 µg/ml Lipofectamine 2000. Cultures were centrifuged at 2,000 rpm at 32 °C for 90 minutes. Cells were incubated at 37 °C for 2–4 hours and supplemented with fresh medium and IL-2. Cells were expanded in T-cell growth media supplemented with rhIL-2. Four days after activation, T cells were stained for CAR expression and used for both *in vitro* and *in vivo* experiments.

Intracellular cytokine staining. T cells were stimulated in round-bottom 96-well plates coated with 2,000 ng/ml recombinant mouse Rae1β-Fc chimera (R&D Systems, Minneapolis, MN) or 1,000 ng/ml recombinant human HER2-Fc chimera (R&D Systems). Plates were coated 24–72 hours prior to stimulation at 4 °C. T cells were stimulated for 4 hours at 37 °C in the presence of brefeldin A (BD Pharmingen, San Jose, CA). After stimulation, cells were resuspended in PBS containing 5% FBS and stored at 4 °C overnight. Production of activation cytokines was determined by flow cytometry.

Flow cytometry antibodies and analytical instruments. The following antibodies used for flow cytometry were purchased from BD Biosciences: mouse Fc-Block, anti-CD4-PerCpCy5.5 (clone RM4-5), anti-CD8a-FITC (clone 53–6.7), anti-IFNγ (clone XMG1.2), and anti-TNFα (clone MP6-XT22). The following antibodies were purchased from eBiosciences (San Diego, CA): anti-CD8a-AlexaFluor 700 (clone 53–6.7) and anti-NKG2D-APC (clone CX5). Recombinant murine NKG2D-Fc (R&D Systems) was used to stain for NKG2D ligands, and detected with goat-anti-human IgG PE (Jackson ImmunoResearch). Viability staining was performed using the Molecular Probes LIVE/DEAD Fixable Near-IR kit (Life Technologies). For intracellular cytokine staining, CAR-T cells were fixed and permeabilized according to Cytofix/Cytoperm Fixation/Permeabilization protocol (BD Biosciences). Data were acquired on a FACSCanto or LSRII (BD Biosciences) and analyzed using FlowJo software (FlowJo LLC, Ashland, OR).

In vitro *cytotoxicity assay.* The NKG2DL$^+$ murine 4T1.2 breast tumor line was used for *in vitro* cytotoxicity assays. We confirmed NKG2DL expression by flow cytometry following expansion from recently thawed vials. Varying ratios of transduced T cells were cocultured with 1.25×10^4 target cells (adhered overnight) per well in triplicate in 96-well flat-bottom plates in a 200 µl volume. After 6 hours of coculture, plates were washed three times with PBS, and 100 µl of a 10% alamarBlue (Life Technologies) in T-cell media was added. Three hours later, fluorescence was measured with excitation at 530 nm and emission at 590 nm using a Safire plate reader (Tecan, Maennedorf, Switzerland). Viability was calculated as the loss of fluorescence between experimental wells compared to untreated target cells.

Adoptive transfer and* in vivo *monitoring. For ACT studies, 10^7 viable CAR-T cells were administered i.v. in 200 µl of sterile PBS. In experiments using preconditioning CTX treatment, CTX (Sigma-Aldrich) was reconstituted in sterile PBS and administered i.p. at 150 mg/kg 24 hours prior to ACT. Temperatures were assessed by rectal probe at the indicated time points.

Multiplex cytokine analysis. We quantified 32 murine chemokines and cytokines using the Mouse Discovery Assay (Eve Technologies, Calgary, Canada). The 32-plex panel included: Eotaxin, G-CSF, GM-CSF, IFNγ, IL-1α, IL-1β, IL-2, IL-3, IL-4, IL-5, IL-6, IL-7, IL-9, IL-10, IL-12 (p40), IL-12 (p70), IL-13, IL-15, IL-17, IP-10, KC, LIF, LIX, MCP-1, M-CSF, MIG, MIP-1α, MIP-1β, MIP-2, RANTES, TNFα, and VEGF. The assay sensitivities of these markers range from 0.3–33.3 pg/ml. Individual analyte values can be found in the Milliplex protocol. Serum samples were

derived from terminal retro-orbital blood samples processed as per Eve Technologies recommendations. The multiplex assay was performed by Eve Technologies using the Bio-Plex 200 system and the Milliplex Mouse Cytokine/Chemokine Magnetic Bead Panel Kit according to their protocol. Heat maps were created using the HeatMapImage (version 6) module available on Gene Pattern (http://genepattern.broadinstitute.org/gp/pages/index.jsf). Luminex data were preprocessed using the "affy" package in R, with RMA background adjustment and quantile normalization procedures.[49] Resulting cytokine expression values were transformed to the $\log_2$ scale. Linear models were fit for each cytokine using the "limma" package in R to test for differential expression for pre-specified contrasts.[50] *P* values for each contrast were obtained for each cytokine and adjusted for multiple comparisons using the Benjamini–Hochberg procedure.[51] After preprocessing, we confirmed that samples were separated into homogeneous groups matching experimental groups and performed principal component analysis (princomp function from "stats" package R) with all 32 cytokines.

Immunohistochemistry. Tissues were prepared for veterinary necropsy via whole body formalin perfusion as described previously.[52] After fixation in 10% neutral buffered formalin, tissues were paraffin embedded, sectioned, and stained using hematoxylin and eosin at the Core Histology Facility, McMaster Immunology Research Centre.

RNA extraction from lungs and quantitative real-time PCR. Lungs were perfused with PBS, excised, and snap-frozen in liquid nitrogen prior to storage at −80 °C. Tissues were homogenized in Trizol (Life Technologies) using a Polytron PT1200c (Kinematica, Bohemia, NY), with total RNA extracted as per the manufacturer's specifications. RNA samples were then treated with the DNA-Free kit (Ambion, Austin, TX), followed by reverse transcription using Superscript III First-Strand (Invitrogen, Life Technologies) according to the manufacturer's directions. Quantitative PCR was performed on a StepOnePlus Real-Time PCR System (Applied Biosystems, Foster City, CA) using Perfecta SYBR Green SuperMix with ROX (Quanta Biosciences, Gaithersburg, MD). Data for the indicated target genes (primer sequences found in Table 1) were analyzed via $\Delta\Delta C_T$ method using GAPDH as the endogenous control. Analysis was performed using the StepOne Software.

Statistical analysis. Student's *t*-tests were used to compare data between two groups. One and two-way ANOVA were used for analysis of more than two groups, with Bonferroni posttests used to evaluate significance between groups. Results were prepared using GraphPad Prism 5. Significant differences between means were defined as: $^{*}P < 0.05$; $^{**}P < 0.01$; $^{***}P < 0.001$.

SUPPLEMENTARY MATERIAL

Figure S1. NKG2DCARs are well expressed on murine CD4+ T cells.
Figure S2. Phenotypic profile of NKG2DCAR T cells *in vitro*.
Figure S3. *In vitro* cytokine production from CAR-T cells.
Figure S4. NKG2D ligand expression in the lungs of BALB/c mice.
Table S1. Clinical observations following ACT into naive BALB/c mice.
Table S2. Serum cytokine concentrations 8h post ACT.
Table S3. Serum cytokine concentrations 8h post ACT into CTX-pretreated mice.

Table 1 Primer sequences used for gene detection

Gene	Primer sequence
GAPDH[53]	Fwd: AGGAGCGAGACCCCACTAAC
	Rev: GGTTCACACCCATCACAAAC
H60a[33]	Fwd: TGCCTGATTCTGAGCCTTTTCA
	Rev: ATTCACTGAGCACTGTCCATGTAGAT
H60b[33]	Fwd: AGCCTTTTGGTCCTGCTGAAT
	Rev: ATGTTTTTTATCACCAAAATCAAGGAGT
panRae-1[54]	Fwd: CCCCAGTATCACCCAGCTTACAT
	Rev: CCCTCCTCTGGCCTCTCCTT
Mult-1[55]	Fwd: AGCAGCTATGGAGCTGACTGCCA
	Rev: AGCCTGCAGAGTGAGGGGCTTT

ACKNOWLEDGMENTS

This work was supported by funds from the Terry Fox Foundation and the Canadian Institutes for Health Research. H.V. and J.A.H. were supported by scholarships from the Canadian Institutes for Health Research, the Government of Ontario and the Canadian Breast Cancer Foundation. J.L.B. holds the Canada Research Chair in Translational Cancer Immunology and the John Bienenstock Chair in Molecular Medicine. John Stagg (Institut du Cancer de Montreal, Montreal, QC) kindly provided the murine 4T1.2 breast tumor line.

REFERENCES

1. Grupp, SA, Kalos, M, Barrett, D, Aplenc, R, Porter, DL, Rheingold, SR *et al.* (2013). Chimeric antigen receptor-modified T cells for acute lymphoid leukemia. *N Engl J Med* **368**: 1509–1518.
2. Brentjens, RJ, Davila, ML, Riviere, I, Park, J, Wang, X, Cowell, LG *et al.* (2013). CD19-targeted T cells rapidly induce molecular remissions in adults with chemotherapy-refractory acute lymphoblastic leukemia. *Sci Transl Med* **5**: 177ra38.
3. Maus, MV, Grupp, SA, Porter, DL and June, CH (2014). Antibody-modified T cells: CARs take the front seat for hematologic malignancies. *Blood* **123**: 2625–2635.
4. Aranda, F, Vacchelli, E, Obrist, F, Eggermont, A, Galon, J, Hervé Fridman, W *et al.* (2014). Trial watch: adoptive cell transfer for anticancer immunotherapy. *Oncoimmunology* **3**: e28344.
5. Spear, P, Barber, A, Rynda-Apple, A and Sentman, CL (2013). NKG2D CAR T-cell therapy inhibits the growth of NKG2D ligand heterogeneous tumors. *Immunol Cell Biol* **91**: 435–440.
6. Nausch, N and Cerwenka, A (2008). NKG2D ligands in tumor immunity. *Oncogene* **27**: 5944–5958.
7. Barber, A, Meehan, KR and Sentman, CL (2011). Treatment of multiple myeloma with adoptively transferred chimeric NKG2D receptor-expressing T cells. *Gene Ther* **18**: 509–516.
8. Leung, WH, Vong, QP, Lin, W, Janke, L, Chen, T and Leung, W (2013). Modulation of NKG2D ligand expression and metastasis in tumors by spironolactone via RXRγ activation. *J Exp Med* **210**: 2675–2692.
9. Zhang, T, Lemoi, BA and Sentman, CL (2005). Chimeric NK-receptor-bearing T cells mediate antitumor immunotherapy. *Blood* **106**: 1544–1551.
10. Zhang, T and Sentman, CL (2013). Mouse tumor vasculature expresses NKG2D ligands and can be targeted by chimeric NKG2D-modified T cells. *J Immunol* **190**: 2455–2463.
11. Barber, A, Zhang, T, DeMars, LR, Conejo-Garcia, J, Roby, KF and Sentman, CL (2007). Chimeric NKG2D receptor-bearing T cells as immunotherapy for ovarian cancer. *Cancer Res* **67**: 5003–5008.
12. Jamieson, AM, Diefenbach, A, McMahon, CW, Xiong, N, Carlyle, JR and Raulet, DH (2002). The role of the NKG2D immunoreceptor in immune cell activation and natural killing. *Immunity* **17**: 19–29.
13. Long, EO (2002). Versatile signaling through NKG2D. *Nat Immunol* **3**: 1119–1120.
14. Groh, V, Rhinehart, R, Randolph-Habecker, J, Topp, MS, Riddell, SR and Spies, T (2001). Costimulation of CD8alphabeta T cells by NKG2D via engagement by MIC induced on virus-infected cells. *Nat Immunol* **2**: 255–260.
15. Verneris, MR, Karimi, M, Karami, M, Baker, J, Jayaswal, A and Negrin, RS (2004). Role of NKG2D signaling in the cytotoxicity of activated and expanded CD8+ T cells. *Blood* **103**: 3065–3072.
16. Upshaw, JL and Leibson, PJ (2006). NKG2D-mediated activation of cytotoxic lymphocytes: unique signaling pathways and distinct functional outcomes. *Semin Immunol* **18**: 167–175.
17. Savoldo, B, Ramos, CA, Liu, E, Mims, MP, Keating, MJ, Carrum, G *et al.* (2011). CD28 costimulation improves expansion and persistence of chimeric antigen receptor-modified T cells in lymphoma patients. *J Clin Invest* **121**: 1822–1826.
18. Song, DG, Ye, Q, Carpenito, C, Poussin, M, Wang, LP, Ji, C *et al.* (2011). *In vivo* persistence, tumor localization, and antitumor activity of CAR-engineered T cells is enhanced by costimulatory signaling through CD137 (4-1BB). *Cancer Res* **71**: 4617–4627.
19. Milone, MC, Fish, JD, Carpenito, C, Carroll, RG, Binder, GK, Teachey, D *et al.* (2009). Chimeric receptors containing CD137 signal transduction domains mediate enhanced survival of T cells and increased antileukemic efficacy in vivo. *Mol Ther* **17**: 1453–1464.
20. Till, BG, Jensen, MC, Wang, J, Qian, X, Gopal, AK, Maloney, DG *et al.* (2012). CD20-specific adoptive immunotherapy for lymphoma using a chimeric antigen receptor with both CD28 and 4-1BB domains: pilot clinical trial results. *Blood* **119**: 3940–3950.
21. Wu, J, Song, Y, Bakker, AB, Bauer, S, Spies, T, Lanier, LL *et al.* (1999). An activating immunoreceptor complex formed by NKG2D and DAP10. *Science* **285**: 730–732.
22. Brentjens, RJ, Rivière, I, Park, JH, Davila, ML, Wang, X, Stefanski, J *et al.* (2011). Safety and persistence of adoptively transferred autologous CD19-targeted T cells in patients with relapsed or chemotherapy refractory B-cell leukemias. *Blood* **118**: 4817–4828.
23. Cheadle, EJ, Gilham, DE and Hawkins, RE (2008). The combination of cyclophosphamide and human T cells genetically engineered to target CD19 can eradicate established B-cell lymphoma. *Br J Haematol* **142**: 65–68.

24. Dotti, G, Gottschalk, S, Savoldo, B and Brenner, MK (2014). Design and development of therapies using chimeric antigen receptor-expressing T cells. *Immunol Rev* **257**: 107–126.
25. Champsaur, M and Lanier, LL (2010). Effect of NKG2D ligand expression on host immune responses. *Immunol Rev* **235**: 267–285.
26. Eagle, RA, Jafferji, I and Barrow, AD (2009). Beyond stressed self: evidence for NKG2D ligand expression on healthy cells. *Curr Immunol Rev* **5**: 22–34.
27. Borchers, MT, Harris, NL, Wesselkamper, SC, Vitucci, M and Cosman, D (2006). NKG2D ligands are expressed on stressed human airway epithelial cells. *Am J Physiol Lung Cell Mol Physiol* **291**: L222–L231.
28. Kraetzel, K, Stoelcker, B, Eissner, G, Multhoff, G, Pfeifer, M, Holler, E *et al.* (2008). NKG2D-dependent effector function of bronchial epithelium-activated alloreactive T-cells. *Eur Respir J* **32**: 563–570.
29. González, S, López-Soto, A, Suarez-Alvarez, B, López-Vázquez, A and López-Larrea, C (2008). NKG2D ligands: key targets of the immune response. *Trends Immunol* **29**: 397–403.
30. Ogasawara, K, Benjamin, J, Takaki, R, Phillips, JH and Lanier, LL (2005). Function of NKG2D in natural killer cell-mediated rejection of mouse bone marrow grafts. *Nat Immunol* **6**: 938–945.
31. Zhang, H, Hardamon, C, Sagoe, B, Ngolab, J and Bui, JD (2011). Studies of the H60a locus in C57BL/6 and 129/Sv mouse strains identify the H60a 3′UTR as a regulator of H60a expression. *Mol Immunol* **48**: 539–545.
32. Malarkannan, S, Shih, PP, Eden, PA, Horng, T, Zuberi, AR, Christianson, G *et al.* (1998). The molecular and functional characterization of a dominant minor H antigen, H60. *J Immunol* **161**: 3501–3509.
33. Takada, A, Yoshida, S, Kajikawa, M, Miyatake, Y, Tomaru, U, Sakai, M *et al.* (2008). Two novel NKG2D ligands of the mouse H60 family with differential expression patterns and binding affinities to NKG2D. *J Immunol* **180**: 1678–1685.
34. Cerwenka, A and Lanier, LL (2003). NKG2D ligands: unconventional MHC class I-like molecules exploited by viruses and cancer. *Tissue Antigens* **61**: 335–343.
35. Ericsson, AC, Davis, JW, Spollen, W, Bivens, N, Givan, S, Hagan, CE *et al.* (2015). Effects of vendor and genetic background on the composition of the fecal microbiota of inbred mice. *PLoS One* **10**: e0116704.
36. Ichinohe, T, Pang, IK, Kumamoto, Y, Peaper, DR, Ho, JH, Murray, TS *et al.* (2011). Microbiota regulates immune defense against respiratory tract influenza A virus infection. *Proc Natl Acad Sci USA* **108**: 5354–5359.
37. Viaud, S, Saccheri, F, Mignot, G, Yamazaki, T, Daillère, R, Hannani, D *et al.* (2013). The intestinal microbiota modulates the anticancer immune effects of cyclophosphamide. *Science* **342**: 971–976.
38. Moretta, L and Moretta, A (2004). Unravelling natural killer cell function: triggering and inhibitory human NK receptors. *EMBO J* **23**: 255–259.
39. Long, EO, Kim, HS, Liu, D, Peterson, ME and Rajagopalan, S (2013). Controlling natural killer cell responses: integration of signals for activation and inhibition. *Annu Rev Immunol* **31**: 227–258.
40. Chang, YH, Connolly, J, Shimasaki, N, Mimura, K, Kono, K and Campana, D (2013). A chimeric receptor with NKG2D specificity enhances natural killer cell activation and killing of tumor cells. *Cancer Res* **73**: 1777–1786.
41. Zhang, T and Sentman, CL (2011). Cancer immunotherapy using a bispecific NK receptor fusion protein that engages both T cells and tumor cells. *Cancer Res* **71**: 2066–2076.
42. Lehner, M, Götz, G, Proff, J, Schaft, N, Dörrie, J, Full, F *et al.* (2012). Redirecting T cells to Ewing's sarcoma family of tumors by a chimeric NKG2D receptor expressed by lentiviral transduction or mRNA transfection. *PLoS One* **7**: e31210.
43. Song, DG, Ye, Q, Santoro, S, Fang, C, Best, A and Powell, DJ Jr (2013). Chimeric NKG2D CAR-expressing T cell-mediated attack of human ovarian cancer is enhanced by histone deacetylase inhibition. *Hum Gene Ther* **24**: 295–305.
44. Stauss, HJ and Morris, EC (2013). Immunotherapy with gene-modified T cells: limiting side effects provides new challenges. *Gene Ther* **20**: 1029–1032.
45. Rabinovich, BA, Ye, Y, Etto, T, Chen, JQ, Levitsky, HI, Overwijk, WW *et al.* (2008). Visualizing fewer than 10 mouse T cells with an enhanced firefly luciferase in immunocompetent mouse models of cancer. *Proc Natl Acad Sci USA* **105**: 14342–14346.
46. Szymczak, AL, Workman, CJ, Wang, Y, Vignali, KM, Dilioglou, S, Vanin, EF *et al.* (2004). Correction of multi-gene deficiency *in vivo* using a single 'self-cleaving' 2A peptide-based retroviral vector. *Nat Biotechnol* **22**: 589–594.
47. Haynes, NM, Trapani, JA, Teng, MW, Jackson, JT, Cerruti, L, Jane, SM *et al.* (2002). Single-chain antigen recognition receptors that costimulate potent rejection of established experimental tumors. *Blood* **100**: 3155–3163.
48. Morita, S, Kojima, T and Kitamura, T (2000). Plat-E: an efficient and stable system for transient packaging of retroviruses. *Gene Ther* **7**: 1063–1066.
49. Irizarry, RA, Hobbs, B, Collin, F, Beazer-Barclay, YD, Antonellis, KJ, Scherf, U *et al.* (2003). Exploration, normalization, and summaries of high density oligonucleotide array probe level data. *Biostatistics* **4**: 249–264.
50. Smyth, GK (2005). limma: Linear Models for Microarray Data. In: Gentleman, R, Carey, V, Dudoit, R, Irizarry, RA and Huber, W (eds.) Bioinformatics and Computational Biology Solutions Using R and Bioconductor, Chapter 23. Springer-Verlag: New York. pp. 397–420. <http://link.springer.com>.
51. Benjamini, Y (1995). Controlling the false discovery rate: a practical and powerful approach to multiple testing. *J R Statist Soc B* **57**: 289–300.
52. Kwiecien, JM, Blanco, M, Fox, JG, Delaney, KH and Fletch, AL (2000). Neuropathology of bouncer Long Evans, a novel dysmyelinated rat. *Comp Med* **50**: 503–510.
53. McGray, AJ, Hallett, R, Bernard, D, Swift, SL, Zhu, Z, Teoderascu, F *et al.* (2014). Immunotherapy-induced CD8+ T cells instigate immune suppression in the tumor. *Mol Ther* **22**: 206–218.
54. Popa, N, Cedile, O, Pollet-Villard, X, Bagnis, C, Durbec, P and Boucraut, J (2011). RAE-1 is expressed in the adult subventricular zone and controls cell proliferation of neurospheres. *Glia* **59**: 35–44.
55. Hansen, CH, Holm, TL, Krych, Ł, Andresen, L, Nielsen, DS, Rune, I *et al.* (2013). Gut microbiota regulates NKG2D ligand expression on intestinal epithelial cells. *Eur J Immunol* **43**: 447–457.

Supplemental Material

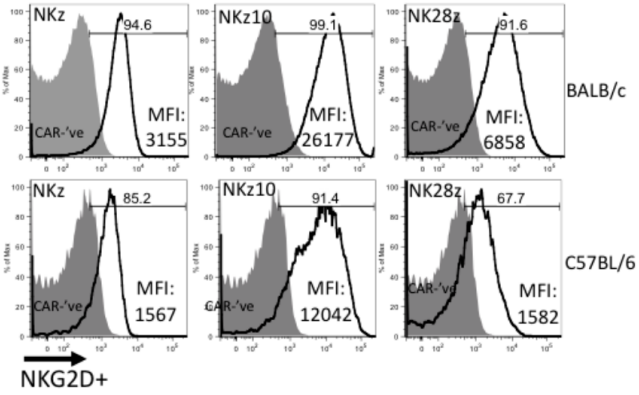

Supplemental Figure 1: NKG2D-CARs are well expressed on murine CD4+ T cells. Expression of NKG2D on CD4+ T cells was evaluated 3 days post retroviral transduction using the indicated NKG2D-CAR retroviruses, with surface expression detected using an anti-NKG2D-APC antibody. Shaded peaks represent CAR-'ve T cell staining. Mean fluorescence intensity and percentage of NKG2D+ CD4+ cells are shown. Data is representative of at least three independent experiments.

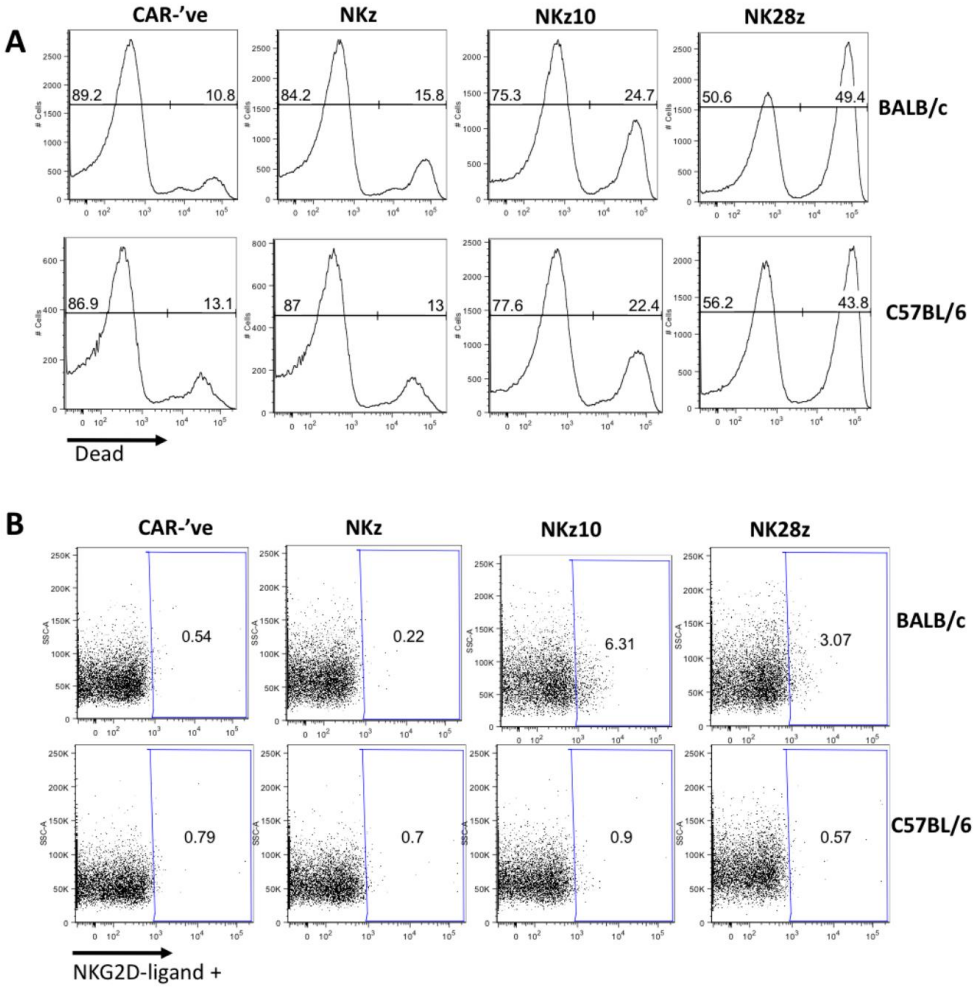

Supplemental Figure 2: Phenotypic profile of NKG2D-CAR T cells *in vitro*. (a) Viability of T cells engineered with the indicated retroviruses was evaluated 3 days post transduction using the Molecular Probes LIVE/DEAD Fixable kit, gating on all cells. Viability gates were set using acid-killed and unstained controls. (b) Expression of NKG2D-ligands was evaluated 3 days post transduction using an NKG2D-Fc chimeric protein, detected with an anti-human IgG-PE by flow cytometry. Data is representative of at least three independent experiments.

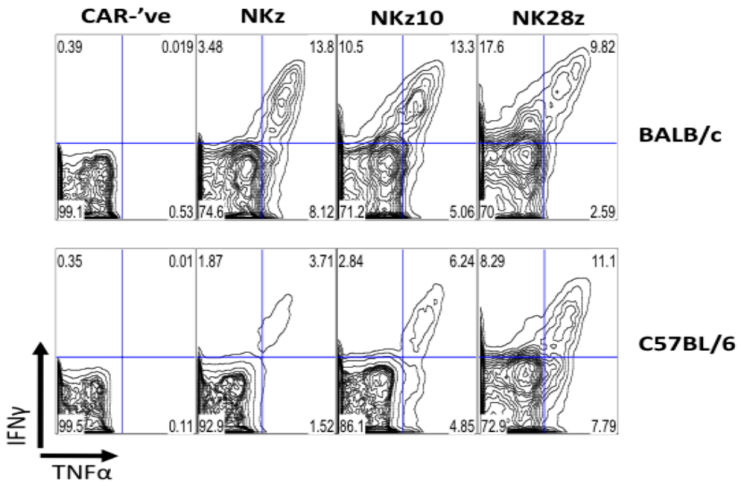

Supplemental Figure 3: *In vitro* cytokine production from CAR-T cells. T cells from BALB/c or C57BL/6 mice engineered with the indicated CARs were stimulated with plate-bound Rae1β-Fc in the presence of brefeldin A and stained for intracellular cytokine production. Gates are set on unstimulated cells.

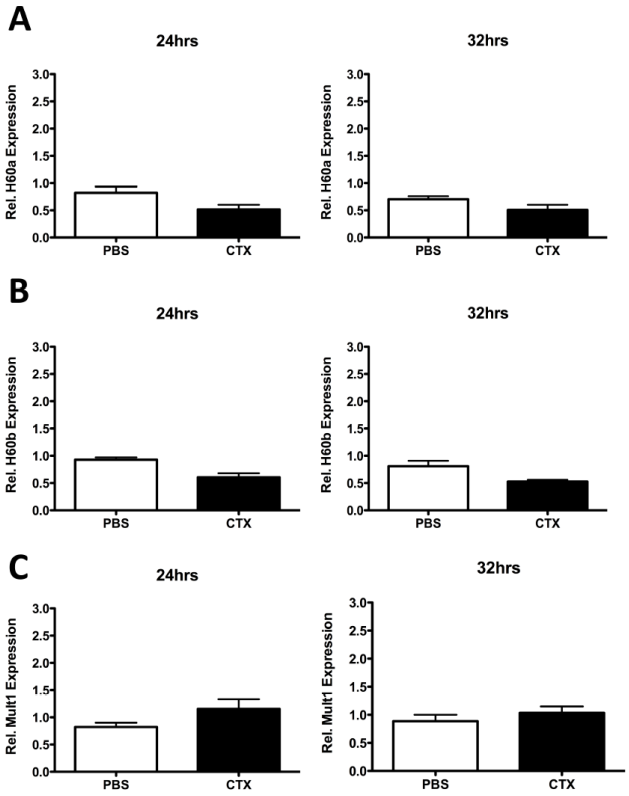

Supplemental Figure 4: NKG2D ligand expression in the lungs of BALB/c mice. NKG2D ligand expression was evaluated using qRT-PCR within the lungs of naïve or CTX-pre-treated BALB/c mice at either 24 or 32 hours post CTX administration (n=5). Expression of (a) H60a, (b) H60b, and (c) Mult1 were evaluated using GAPDH as an internal reference, with relative expression calculated via the delta/delta Ct method.

Tables

Supplemental Table 1: Clinical observations following ACT into naïve BALB/c mice

	CAR-'ve	NKz	NKz10	NK28z
Ruffled	-	++	+++	++
Hunched	-	+	+++	+
Ocular Discharge	-	++	+++	+
Lack of grooming	-	+	+++	++
Labored breathing	-	++	++	++
Decreased activity	-	+	++	++

Supplemental Table 2: Serum cytokine concentrations 8h post ACT. Luminex analysis was performed on BALB/c serum samples collected 8 hours post ACT. Concentrations are presented as mean ± SEM of N=5 run in duplicate. Fold change was calculated relative to PBS-treated controls.

	No CTX							
	CAR-'ve		NKz		NKz10		NK28z	
CYTOKINE	[pg/ml]	Fold Change	[pg/ml]	Fold Change	[pg/ml]	Fold Change	[pg/ml]	Fold Change
Eotaxin	434.19 ± 28.17	1.38	757.31 ± 54.79	2.40	2365.86 ± 137.71	7.49	1405.26 ± 91.03	4.45
G-CSF	182.81 ± 32.73	2.01	463.54 ± 18.18	5.10	18355.48 ± 1493.15	201.93	2800.72 ± 464.96	30.81
GM-CSF	3.16 ± 3.16	3.16	75.93 ± 5.76	75.93	196.41 ± 10.12	196.41	67.20 ± 5.93	67.20
IFNγ	0.06 ± 0.06	0.06	97.51 ± 8.49	97.51	4040.56 ± 236.12	4040.56	1285.92 ± 146.14	1285.92
IL-1α	44.63 ± 14.78	2.24	132.58 ± 21.16	6.66	237.15 ± 15.23	11.92	105.25 ± 17.17	5.29
IL-1β	5.46 ± 2.14	1.56	60.66 ± 10.23	17.37	41.16 ± 4.52	11.78	48.42 ± 8.14	13.86
IL-2	10.41 ± 2.11	1.50	51.13 ± 5.16	7.36	37.43 ± 4.10	5.39	44.40 ± 5.50	6.40
IL-3	6.93 ± 2.80	2.06	286.96 ± 16.38	85.48	1021.21 ± 56.54	304.20	205.14 ± 20.17	61.11
IL-4	1.76 ± 0.80	2.76	21.26 ± 0.49	33.32	123.03 ± 4.72	192.84	16.55 ± 2.19	25.94
IL-5	9.44 ± 1.34	1.61	41.04 ± 5.30	6.97	104.61 ± 7.17	17.78	144.79 ± 12.54	24.61
IL-6	5.24 ± 1.37	4.20	22.65 ± 1.50	18.15	514.19 ± 48.20	412.01	79.64 ± 8.62	63.81
IL-7	22.44 ± 7.49	4.33	28.03 ± 3.13	5.40	18.10 ± 1.16	3.49	19.47 ± 1.44	3.76
IL-9	0.16 ± 0.13	0.63	22.20 ± 9.70	86.71	22.41 ± 10.51	87.55	18.32 ± 8.75	71.58
IL-10	16.69 ± 7.06	2.82	123.38 ± 5.90	20.86	2583.26 ± 220.78	436.80	588.91 ± 141.58	99.58
IL-12 (p40)	17.76 ± 2.29	1.33	93.08 ± 9.34	6.98	66.70 ± 4.23	5.01	63.34 ± 5.62	4.75
IL-12 (p70)	60.46 ± 30.07	5.54	147.74 ± 24.55	13.53	76.20 ± 9.52	6.98	108.17 ± 18.12	9.90
IL-13	54.23 ± 9.02	1.36	404.71 ± 26.21	10.14	382.07 ± 13.20	9.57	361.50 ± 39.98	9.06
IL-15	196.75 ± 60.61	10.94	220.40 ± 34.94	12.26	128.80 ±19.05	7.16	158.34 ± 23.14	8.81
IL-17	3.50 ± 0.99	2.98	5.37 ± 0.46	4.58	4.73 ± 0.42	4.04	4.05 ± 0.38	3.46
IP-10	119.58 ± 12.82	2.82	1191.45 ± 48.79	28.08	8763.98 ± 522.19	206.55	3422.32 ± 240.86	80.66
KC	30.48 ± 4.78	1.16	113.71 ± 7.29	4.34	1162.94 ± 315.50	44.42	422.39 ± 78.25	16.13
LIF	5.47 ± 1.72	4.51	7.29 ± 0.81	6.02	6.00 ± 0.50	4.96	7.00 ± 0.65	5.78
LIX	1755.92 ± 505.48	1.91	1066.31 ± 235.15	1.16	505.08 ± 45.30	0.55	805.97 ± 305.34	0.88
MCP-1	23.86 ± 4.47	1.18	290.99 ±20.67	14.39	2006.50 ± 134.65	99.26	385.33 ± 29.06	19.06
M-CSF	7.12 ± 1.65	1.47	70.55 ± 7.90	14.59	38.71 ± 3.88	8.00	50.89 ± 7.28	10.52
MIG	184.72 ± 35.25	8.72	3299.98 ± 145.92	155.74	3323.12 ± 93.95	156.83	3247.80 ± 154.06	153.28
MIP-1α	29.18 ± 6.10	1.39	121.60 ± 5.33	5.81	796.61 ± 45.80	38.08	267.13 ± 22.02	12.77
MIP-1β	19.04 ± 5.58	2.68	183.45 ± 3.88	25.79	4183.29 ± 296.51	588.04	1627.44 ± 202.10	228.77
MIP-2	33.22 ± 9.97	1.73	231.21 ± 19.43	12.07	133.15 ± 10.34	6.95	191.16 ±16.12	9.98
RANTES	29.73 ± 9.11	2.57	81.47 ± 4.42	7.04	161.05 ± 13.13	13.92	108.18 ± 10.28	9.35
TNFα	3.01 ± 1.15	6.80	24.07 ± 2.75	54.34	56.42 ± 2.81	127.35	29.22 ± 3.32	65.96
VEGF	0.55 ± 0.10	2.14	2.61 ± 0.27	10.10	1.62 ± 0.05	6.29	1.85 ± 0.19	7.16

Supplemental Table 3: Serum cytokine concentrations 8h post ACT into CTX-pretreated mice. Luminex analysis was performed on BALB/c serum samples collected 8 hours post ACT. Concentrations are presented as mean ± SEM of N=5 run in duplicate. Fold change was calculated relative to PBS-treated controls.

	+ CTX							
	CAR-'ve		NKz		NKz10		NK28z	
CYTOKINE	[pg/ml]	Fold Change	[pg/ml]	Fold Change	[pg/ml]	Fold Change	[pg/ml]	Fold Change
Eotaxin	344.78 ± 26.65	0.93	742.30 ± 34.12	2.01	1523.53 ± 107.80	4.12	1154.83 ± 73.99	3.12
G-CSF	164.07 ± 16.00	1.77	523.85 ± 25.55	5.64	15625.04 ± 1681.74	168.21	4578.15 ± 548.72	49.29
GM-CSF	3.70 ± 2.49	0.64	81.86 ± 9.07	14.08	214.62 ± 11.23	36.91	96.58 ± 7.83	16.61
IFNγ	1.08 ± 0.72	2.88	361.31 ± 26.98	960.92	4802.61 ± 341.31	12772.90	4037.89 ± 429.08	10739.07
IL-1α	33.61 ± 5.37	1.01	109.46 ± 28.35	3.29	219.73 ± 20.74	6.60	151.47 ± 26.76	4.55
IL-1β	8.37 ± 1.32	1.13	56.53 ± 11.99	7.67	47.69 ± 5.41	6.47	51.48 ± 4.26	6.98
IL-2	13.07 ± 2.05	1.22	56.77 ± 11.26	5.30	43.91 ±2.69	4.10	54.67 ± 4.40	5.10
IL-3	4.11 ± 0.52	1.25	429.66 ± 34.59	130.87	1165.46 ± 82.10	355.00	418.17 ± 36.20	127.38
IL-4	0.62 ± 0.06	1.76	27.75 ± 1.71	78.40	183.40 ± 6.32	518.09	27.60 ± 1.77	77.95
IL-5	53.65 ± 18.93	0.51	37.67 ± 4.59	0.36	69.52 ± 6.37	0.67	211.56 ± 16.72	2.03
IL-6	1.93 ± 0.29	1.39	44.35 ± 5.76	31.93	751.15 ± 97.43	540.79	331.95 ± 34.36	238.98
IL-7	18.25 ± 8.77	5.36	21.21 ± 4.74	6.23	15.19 ± 2.25	4.46	19.93 ± 1.61	5.85
IL-9	2.23 ± 1.37	9.96	40.99 ± 14.18	183.00	30.58 ± 10.72	136.53	27.17 ± 10.15	121.31
IL-10	8.89 ± 1.48	1.91	266.35 ± 16.15	57.19	4185.06 ± 266.87	898.66	3189.75 ± 253.54	684.94
IL-12 (p40)	17.42 ± 2.88	0.80	63.02 ± 14.01	2.88	53.65 ± 3.50	2.45	64.58 ± 6.10	2.95
IL-12 (p70)	10.18 ± 1.84	1.47	101.99 ± 23.42	14.77	77.87 ± 8.95	11.28	99.18 ± 8.83	14.37
IL-13	26.91 ± 3.37	1.26	262.93 ± 58.43	12.27	290.18 ± 25.29	13.55	297.78 ± 24.10	13.90
IL-15	140.78 ± 87.42	8.03	156.52 ± 35.16	8.93	128.46 ± 18.07	7.33	160.92 ± 21.04	9.18
IL-17	1.35 ± 0.15	1.41	4.48 ± 0.66	4.68	5.66 ± 0.31	5.91	5.15 ± 0.41	5.38
IP-10	126.21 ± 8.31	2.73	1532.65 ± 127.84	33.15	4907.29 ± 397.68	106.13	3871.74 ± 406.00	83.73
KC	61.05 ± 9.63	2.57	132.36 ± 13.63	5.57	1180.65 ± 247.97	49.69	802.26 ± 162.40	33.77
LIF	1.25 ± 0.31	2.21	7.33 ± 1.17	12.98	6.87 ± 0.51	12.15	7.99 ± 0.61	14.13
LIX	944.88 ± 204.04	0.63	703.14 ± 100.35	0.47	623.66 ± 39.59	0.41	811.58 ± 175.70	0.54
MCP-1	36.27 ± 5.29	1.99	278.37 ± 23.55	15.24	2191.20 ± 246.48	120.00	1076.61 ± 122.42	58.96
M-CSF	10.82 ± 1.45	3.54	55.61 ± 7.37	18.21	37.11 ± 3.37	12.15	45.02 ± 3.79	14.74
MIG	374.52 ± 67.19	19.51	3019.26 ± 165.12	157.32	2416.97 ± 100.74	125.94	2416.42 ± 73.57	125.91
MIP-1α	38.13 ± 3.50	1.80	164.71 ± 4.50	7.76	1182.53 ± 86.41	55.73	802.65 ± 77.03	37.83
MIP-1β	32.78 ± 4.33	6.97	480.86 ± 24.25	102.22	6349.63 ± 281.83	1349.84	5302.19 ± 427.62	1127.17
MIP-2	46.54 ± 8.76	2.05	205.27 ± 33.37	9.03	147.62 ± 15.25	6.49	166.75 ± 9.29	7.33
RANTES	12.28 ± 3.10	3.04	83.80 ± 5.10	20.76	145.06 ± 3.58	35.94	118.60 ± 6.39	29.38
TNFα	3.17 ± 1.32	1.08	19.63 ± 3.64	6.70	67.25 ± 5.03	22.94	43.45 ± 4.06	14.82
VEGF	0.66 ± 0.09	1.14	2.22 ±0.37	3.82	1.79 ± 0.22	3.09	2.30 ± 0.18	3.96

3.0 Chapter Three – Designed ankyrin repeat proteins are effective targeting elements for chimeric antigen receptors

3.1 Introduction

Given the toxicities associated with NKG2D-based CAR-T cells, we ceased our work developing these agents. As a consequence, we began to pursue other chimeric antigen receptor strategies.

This manuscript describes a proof-of-concept study which was the first to demonstrate that designed ankryin repeat proteins (DARPins) could be used as the antigen-binding domains in chimeric antigen receptors. Human and murine variants of a DARPin-targeted CAR, with specificity for the tumor associated antigen HER2, were generated to permit the future evaluation of DARPin-targeted CAR-T cells in syngeneic or xenograft models. This manuscript only describes the *in vitro* evaluation of anti-HER2 DARPin-targeted CAR-T cells because the engineered human T cells unexpectedly proved to be toxic *in vivo*.

3.2 Manuscript status, copyright, and citation

Status: Published manuscript

Citation: Hammill, JA, VanSeggelen, H, Helsen, CW, Denisova, GF, Evelegh, C, Tantalo, DGM, Bassett, JD, Bramson, JL. (2015). Designed ankyrin repeat proteins are effective targeting elements for chimeric antigen receptors. *Journal for ImmunoTherapy of Cancer*. 3:55. doi: 10.1186/s40425-015-0099-4. Available online: https://jitc.biomedcentral.com/articles/10.1186/s40425-015-0099-4.

3.3 Published journal article

To follow beginning on subsequent page.

Hammill *et al. Journal for ImmunoTherapy of Cancer* (2015) 3:55
DOI 10.1186/s40425-015-0099-4

Journal for ImmunoTherapy of Cancer

RESEARCH ARTICLE Open Access

Designed ankyrin repeat proteins are effective targeting elements for chimeric antigen receptors

Joanne A. Hammill, Heather VanSeggelen, Christopher W. Helsen, Galina F. Denisova, Carole Evelegh, Daniela G. M. Tantalo, Jennifer D. Bassett and Jonathan L. Bramson*

Abstract

Background: Adoptive cell transfer of tumor-specific T lymphocytes (T cells) is proving to be an effective strategy for treating established tumors in cancer patients. One method of generating these cells is accomplished through engineering bulk T cell populations to express chimeric antigen receptors (CARs), which are specific for tumor antigens. Traditionally, these CARs are targeted against tumor antigens using single-chain antibodies (scFv). Here we describe the use of a designed ankyrin repeat protein (DARPin) as the tumor-antigen targeting domain.

Methods: We prepared second generation anti-HER2 CARs that were targeted to the tumor antigen by either a DARPin or scFv. The CARs were engineered into human and murine T cells. We then compared the ability of CARs to trigger cytokine production, degranulation and cytotoxicity.

Results: The DARPin CARs displayed reduced surface expression relative to scFv CARs in murine cells but both CARs were expressed equally well on human T cells, suggesting that there may be a processing issue with the murine variants. In both the murine and human systems, the DARPin CARs were found to be highly functional, triggering cytokine and cytotoxic responses that were similar to those triggered by the scFv CARs.

Conclusions: These findings demonstrate the utility of DARPins as CAR-targeting agents and open up an avenue for the generation of CARs with novel antigen binding attributes.

Keywords: Cancer, Immunotherapy, Chimeric antigen receptor, CAR, Designed ankyrin repeat protein, DARPin

Background

Cancer immunotherapy aims to treat tumors by engaging the patient's immune system. One form of immunotherapy, called adoptive cell transfer, infuses cancer patients with a bolus of tumor-specific T lymphocytes (T cells), and is proving to be an effective treatment for a variety of malignancies [1–3]. In adoptive cell transfer, T cells isolated from a tumor-bearing patient are grown to large numbers *ex vivo* and are administered back into the patient to induce a robust anti-tumor immune response. Tumor specificity can be achieved by either i) isolating naturally occurring tumor-specific T cells from the patient, or ii) engineering bulk T cells from the peripheral blood to express tumor-specific receptors on their surface. Naturally-occurring tumor-specific T cells are rare and expanding them from a cancer patient is typically a laborious procedure. In contrast, it is becoming relatively easy to engineer readily-available peripheral T cells with tumor-specific receptors through genetic manipulation. Techniques have been developed for this engineering process which are clinically-viable and multiple clinical trials have demonstrated feasibility and efficacy of genetically-engineered T cells for the treatment of cancer [1, 3–9].

Chimeric antigen receptors (CARs), recombinant proteins designed for expression on the surface of T cells, offer one way to engineer T cells with anti-tumor functionality. CARs are composed of an extracellular antigen recognition domain linked to intracellular signaling domains derived from the T cell receptor and co-receptors (including combinations of the signaling regions of

* Correspondence: bramsonj@mcmaster.ca
Department Pathology and Molecular Medicine, McMaster Immunology Research Centre, McMaster University, Hamilton, ON, Canada

CD3ζ, CD28, and/or 4-1BB, for example) such that the T cells become activated following binding of tumor antigen by the CAR. Depending upon the nature of the intracellular signaling domains, this activation event can lead to cytokine production, cytotoxic attack of the tumor, and proliferation of the T cells.

Most CARs developed to date, including those specific for the tumor associated antigens human epidermal growth factor receptor 2 (HER2) [4, 10] and CD19 [3, 7, 8], utilize a single-chain variable fragment (scFv), derived from an antibody, to enable antigen recognition. However, scFvs do not represent the sole or, necessarily, the optimal option for antigen targeting of CARs.

Ankyrin repeats (ARs), one of the most common protein motifs found in nature, are 33 amino acid long sequences composed of a β-turn followed by two anti-parallel α-helices and a loop [11, 12]. Various numbers of these individual ARs stack together to form ankyrin repeat proteins which function as protein binders [11, 13]. Recognizing the potential of these natural ankyrin repeat proteins as alternative target-binding domains, libraries of artificial stacked ARs, called designed ankyrin repeat proteins (DARPins) were developed to allow for the generation of repeat protein binders against a defined target of interest [14, 15]. Each DARPin in these libraries typically consists of between 2 and 6 repeating units; 2–4 repeats containing both fixed (framework sites required for correct AR folding) and variable (randomized sites leading to a diversity of target-binding capacity within the library) amino acid positions sandwiched between non-variable N-terminal and C-terminal capping repeats (essential for correct DARPin folding) [16, 17]. Expression of these genetic DARPin libraries using ribosome or phage display systems allows for the selection of DARPins with the capacity to bind a defined target of interest as well as refine binding affinity for that target [18].

DARPins offer a number of features which make them attractive for use in the CAR field: 1) they are more compact than scFvs and, thus, take up less space in the genetic transfer vectors typically used for engineering T cells (ex. retrovirus and lentivirus), 2) they are very thermodynamically stable, and 3) they do not require pairing of separate binding domains (e.g. V_H and V_L of the scFv), allowing the facile linkage of multiple DARPins, with different specificities, which could be used to create a multi-specific CAR.

We tested the utility of DARPins to target CARs using a DARPin specific for the tumor associated antigen HER2 [19]. As a gold standard, we employed an scFv against HER2 [20]. Both targeting elements were incorporated into murine and human CAR scaffolds to rigorously test the suitability of DARPins. Our results demonstrated that targeting CARs with DARPins is as efficacious as targeting CARs with scFvs and supports the further investigation of DARPin CARs.

Results and discussion

Expression of DARPin28z on murine and human T lymphocytes

To generate a chimeric antigen receptor which uses a DARPin for its antigen recognition domain, we exchanged the scFv domain of a second generation CAR with specificity against HER2 [20] (herein referred to as scFv28z) with a HER2-specific DARPin [19] (herein referred to as DARPin28z) (Fig. 1a, b). We created both a murine and a human version of both CARs to allow for testing of the DARPin antigen-binding domain in T cells from both species. We noted that the DARPin28z CAR displayed reduced surface expression on T cells from both C57BL/6 and BALB/c mice relative to the scFv28z CAR (Fig. 1c, d). While we do not know the reason for the reduced surface expression, the effect appeared to be related to the murine system because the human DARPin28z receptors were expressed at high levels on T cells from two different donors and displayed surface expression levels equivalent to the scFv28z CAR in the human T cells (Fig. 1c, e). Together these data indicate that DARPin28z is successfully expressed on the surface of both murine and human T lymphocytes.

DARPin28z induces cytokine production by CAR-T cells upon antigen binding

To test the functionality of the DARPin28z CARs, we stimulated the engineered murine and human T cells with recombinant HER2 or an unrelated control protein (recombinant kinase insert domain receptor (KDR), also known as vascular endothelial growth factor receptor 2 (VEGFR-2)) and measured the production of cytokines using flow cytometry. Murine T lymphocytes expressing the scFv28z CAR produced both IFN-γ and TNF-α upon stimulation with HER2, as did the same cells expressing the DARPin28z CAR (Fig. 2a). Both scFv28z and DARPin28z were able to trigger IFN-γ and TNF-α production in a similar proportion of retrovirally engineered T cells (those expressing the transduction marker Thy1.1) (Fig. 2b). However, the level of CAR expression by retrovirally transduced (Thy1.1 positive) cells varied significantly between scFv28z and DARPin 28z CAR-T cells (Fig. 1d), and when cytokine production data was normalized for CAR-expression, DARPin28z was more effective at inducing IFN-γ and TNF-α double-producing T cells on a per-CAR-T cell basis (Fig. 2c). Indeed, similar results were observed for human T cells; DARPin28z was able to trigger production of both IFN-γ and TNF-α by human T cells (Fig. 3a). In fact, in human T lymphocytes, DARPin28z proved more efficient than scFv28z at inducing cells producing IFN-γ and TNF-α among NGFR-positive

Hammill *et al. Journal for ImmunoTherapy of Cancer* (2015) 3:55

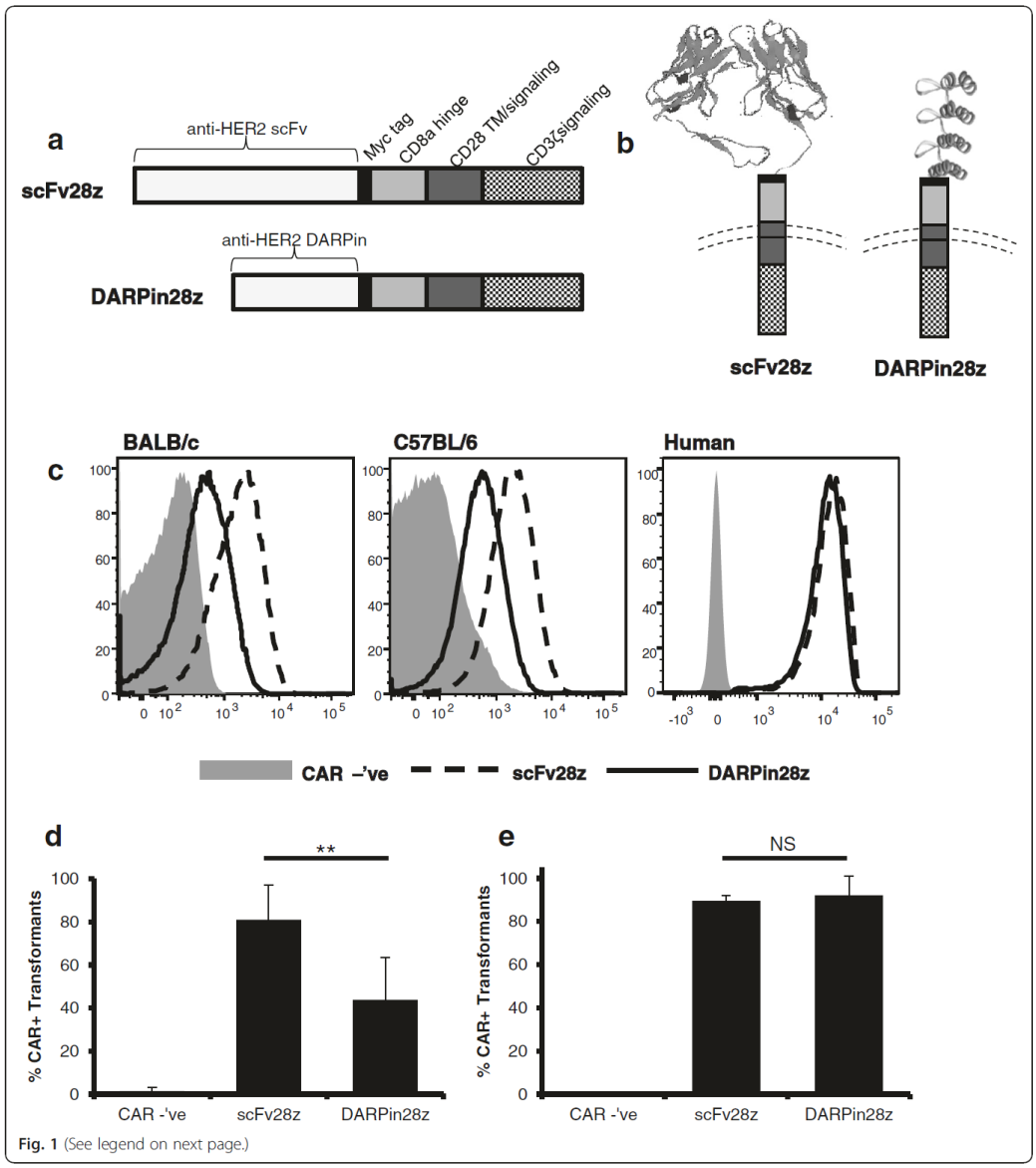

Fig. 1 (See legend on next page.)

(See figure on previous page.)
Fig. 1 Expression of scFv28z and DARPin28z on the surface of murine and human T lymphocytes. **a** Schematic representation of CAR structures. Each construct was composed of an antigen recognition domain (either scFv or DARPin), specific for HER2, fused to a myc tag, CD8α hinge, CD28 transmembrane and signaling domains, and the signaling portion of CD3ζ. Identical constructs were generated for expression in murine or human T cells, using species specific sequences for CAR components. **b** Schematic showing orientation of CAR structures in relation to the T cell surface. Ribbon diagrams for the scFv and DARPin domains illustrate differences in tertiary structure and size. **c**-**e** CAR expression on the surface of murine (BALB/c or C57BL/6) or human T cells was analyzed by flow cytometry. All plots show virally transduced $CD8^+$ lymphocytes (CAR-expressing viruses also expressed transduction markers; Thy1.1 for murine constructs and NGFR for human constructs). CAR negative cells were used as controls; T cells were transduced with constructs expressing transduction markers in the absence of a CAR. CAR expression was measured by staining with an α-myc tag antibody, or a HER2Fc fusion protein, followed by a secondary detection antibody. **c.** Representative plots are shown. **d**-**e** Level of CAR expression by transduced cells; calculated for murine ((**d**) % CAR^+/% $Thy1.1^+$) and human ((**e**) % CAR^+/$NGFR^+$) CAR-T cell cultures. Data representative of multiple experiments ((**d**) murine: CAR –'ve $n = 3$, scFv28z $n = 6$, DARPin28z $n = 6$) ((**e**) human: two donors, $n = 3$ each for CAR –'ve, scFv28z, DARPin28z). Error bars = standard deviation (SD). * = $p < 0.05$ ** = $p < 0.005$ *** = $p < 0.001$

cells (lentivirally engineered T cells); IFN-γ^+ TNF-α^-: 11.7 ± 2.6 vs 17.0 ± 5.2 ($p < 0.05$), IFN-γ^+ TNF-α^+: 12.2 ± 2.2 vs 28.8 ± 7.5 ($p < 0.001$), IFN-γ^- TNF-α^+: 6.7 ± 1.2 vs 11.7 ± 3.1 ($p < 0.05$). Furthermore, DARPin28z was also more efficient at inducing production of IL-2 by human CAR-T cell cultures (Fig. 3b), although showed no enhanced capacity to induce degranulation of HER2 stimulated CAR-T cells, as determined by CD107a release (Fig. 3c). Since the T cell populations are comprised of a constellation of cells with distinct functional phenotypes, we also employed SPICE analysis to determine whether the two CARs selectively activated a particular subpopulation of cells, but this analysis revealed no preferential activation of a particular subpopulation by either CAR (Fig. 3d).

Observed differences in the magnitudes of response may be explained by variances in target binding by the anti-HER2 DARPin vs anti-HER2 scFv. For example, the anti-HER2 DARPin utilized here has an affinity for HER2 of 0.070nM [21] while the scFv has an affinity of 7.2nM [22]. In addition, the scFv used to generate our scFv28z CAR (FRP5 [20, 22]) binds to the distal-most extracellular loops of HER2 [23], whereas the anti-HER2 DARPin used to generate our DARPin28z CAR binds HER2 proximal to the cell membrane [24], which may influence epitope availability. While these differences negate any direct comparisons between DARPin28z and scFv28z efficacy, the above data reveals that the DARPin28z CAR demonstrates an equivalent capacity to activate T cell effector functions, specifically cytokine production, as the scFv28z CAR.

DARPin28z induces CAR-T cell cytotoxicity against HER2-positive tumor cells

To test the capacity of our DARPin28z CAR-T cells to induce cytotoxicity against HER2-positive tumor cell targets, engineered murine and human CAR-T cells were incubated with a variety of HER2-positive and HER2-negative tumor cell lines; viability of the cell lines was measured 6 h later. HER2-positive cell lines included murine D2F2/E2, a murine breast carcinoma engineered to express human HER2, as well as SKBR3 and HCC1954, human breast carcinomas which naturally overexpress HER2. HER2-negative cell lines included D2F2, a murine breast carcinoma (the parental line of D2F2/E2), and LOX-IMVI, a human melanoma cell line. HER2 expression status on tumor cells was verified via flow cytometry (Fig. 4a). Murine DARPin28z CAR-T cells showed minimal killing of HER2-negative tumor cells (Fig. 4b) but were able to kill HER2-positive tumor cells at effector(E):target(T) ratios of as low as 0.6 T cells per tumor cell (D2F2/E2 and HCC1954, Fig. 4c, e) and 1 T cell per tumor cell (SKBR3, Fig. 4d). Levels of tumor cell killing were similar between scFv28z and DARPin28z CAR-T cells, with the exception of SKBR3 tumor cells, against which DARPin28z CAR-T cells showed increased cytotoxicity compared to scFv28z (Fig. 4d). Human DARPin28z CAR-T cells behaved similarly; HER2-negative tumor cells showed minimal cell death after incubation with CAR-T cells at all E:T ratios tested (Fig. 4f, j) while HER2-positive tumor cells showed evidence of cytotoxicity starting at E:T ratios of 0.1 CAR-T cells per tumor cell (D2F2/E2, Fig. 4g) and 2 CAR-T cells per tumor cell (SKBR3, HCC1954, Fig. 4h, i). Human DARPin28z CAR-T cells were equally as cytotoxic as their scFv28z counterparts against SKBR3 targets (Fig. 4f), but showed superior induction of cytotoxicity against D2F2/E2 targets at all E:T ratios tested (Fig. 4g) and HCC1954 targets at a 2:1 E:T ratio (Fig. 4i). As such, we can conclude that the DARPin28z CAR is capable of activating T cells to induce cytotoxicity against a HER2-positive tumor target while sparing target-negative cells. These data, similar to the results generated following stimulation with recombinant HER-2, confirm that the DARPin28z receptors demonstrate biological activity that is similar to the scFv28z receptor.

Conclusions

These experiments position DARPin-targeted CARs as a suitable alternative to their scFv-targeted counterparts and strongly support the further investigation of DARPins for use targeting CARs; by all measures investigated, DARPin28z performed similarly to scFv28z as a

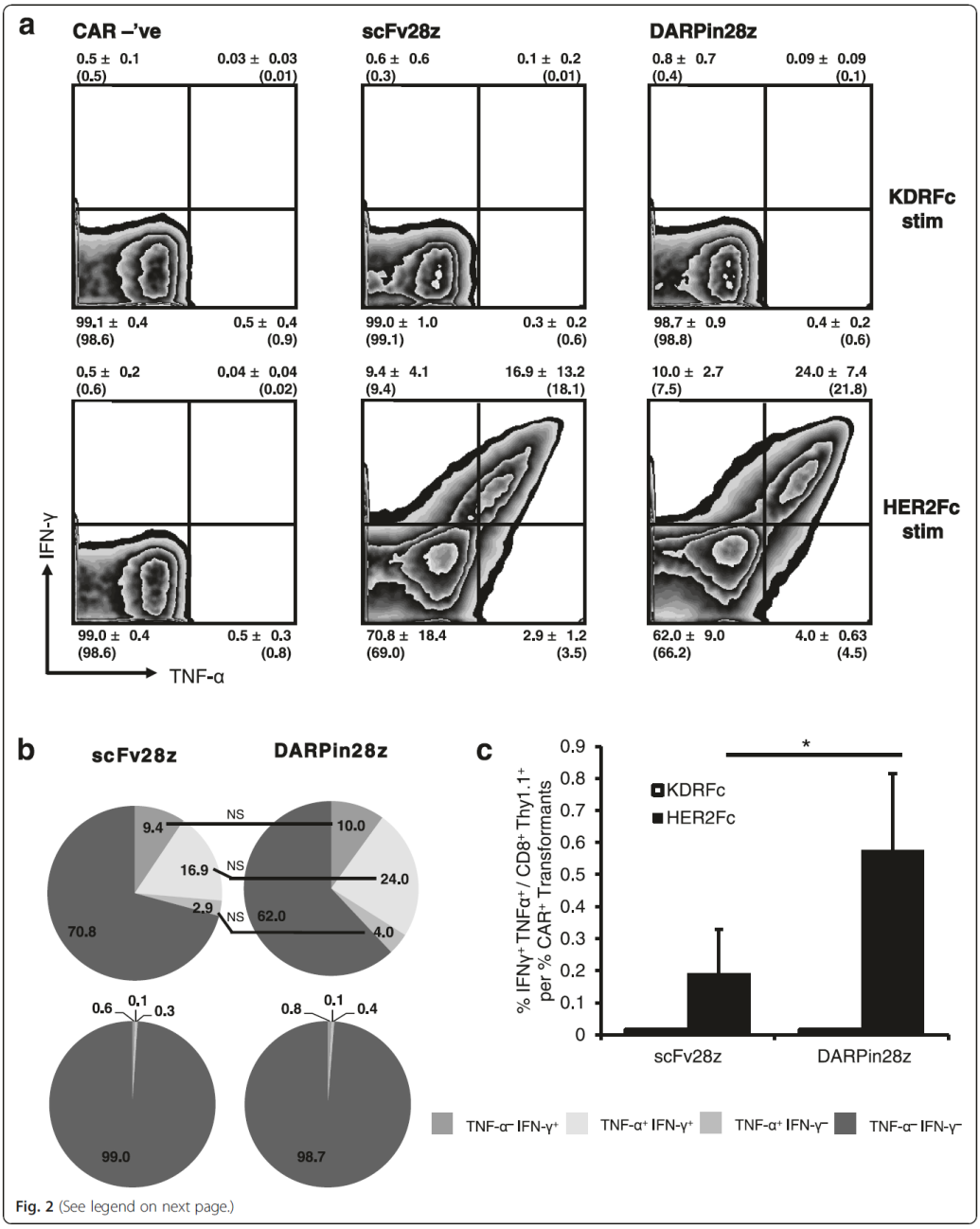

Fig. 2 (See legend on next page.)

(See figure on previous page.)
Fig. 2 DARPin28z induces murine CAR-T cell cytokine production upon HER2 stimulation. **a** 10^6 scFv28z, DARPin28z, or CAR –'ve transduced murine T cells were stimulated with HER2 (HER2Fc fusion protein) or an unrelated target (KDRFc fusion protein) for four hours at 37 °C in a 96-well plate. Production of IFN-γ and TNF-α was measured by intracellular cytokine staining (ICS) and subsequent flow cytometry. Data from $CD8^+$ $Thy1.1^+$ T cells is presented as mean of $n = 3$ experiments (CAR –'ve) and $n = 5$ experiments (scFv28z and DARPin28z) ± SD. Bracketed numbers are quantitative of the representative plots shown. **b** Visual comparison of cytokine production data from a. **c** Cytokine expression data expressed relative to CAR-positivity of transduced cells where CAR^+ transformant = % CAR^+/% $Thy1.1^+$. Error bars = SD. * = $p < 0.05$ ** = $p < 0.005$ *** = $p < 0.001$

mechanism for targeting T cells against a HER2-positive target.

In our opinion, DARPins offer a number of attractive features as an antigen-targeting domain. First, DARPins are smaller than scFvs; our anti-HER2 scFv is 739 bp [20] compared to 408 bp for the anti-HER2 DARPin [19]. Since lentivirus titers are often inversely correlated with the size of the lentiviral insert [25, 26], the ability to conserve coding sequence in the lentivirus insert is a desirable feature afforded by using DARPins. Second, it has been argued that DARPins are poorly immunogenic [16, 17], a useful property for the safety and longevity of DARPin-based CAR-T cell therapies. Finally, ARs are amenable to stacking; the number of ARs stacked consecutively in a single protein ranges from one to 33 [11]. As such, we postulate that several DARPin molecules, each with unique antigen-binding properties, could be stacked consecutively to generate a single CAR with the capacity to identify multiple tumor-targets.

Methods

Cell lines

Parental D2F2 and human HER2 expressing D2F2/E2 murine mammary tumor cell lines (provided by Dr. Wei-Zen Wei, Barbara Ann Karmanos Cancer Institute, Detroit, MI) were cultured in hi-glucose DMEM supplemented with 5 % FBS (Gibco; Life Technologies, Grand Island, NY), 5 % cosmic calf serum (Fisher Scientific, Waltham, MA), 2.4 mM L-glutamine (BioShop Canada Inc., Burlington, ON), 0.12 mM non-essential amino acids (Gibco), 120U/mL penicillin (Gibco), 120 μg/mL streptomycin (Gibco), 55 μM β-mercaptoethanol (Gibco), and 0.6 mM sodium pyruvate (Sigma-Aldrich Canada Co., Oakville, ON). D2F2/E2 media contained 800 μg/mL geneticin (Gibco). The human tumor cell lines SKBR3, HCC1954, and LOX-IMVI (provided by Dr. Karen Mossman, McMaster University, Hamilton, ON) were cultured in RPMI 1640 supplemented with 10 % FBS, 2 mM L-glutamine, 10 mM HEPES (Roche Diagnostics, Laval, QC), 100U/mL penicillin, 100 μg/mL streptomycin, and 55 μM β-mercaptoethanol. All cell lines were grown at 5 % CO_2, 95 % air, and 37 °C.

Generation of CAR retroviruses

A murine anti-HER2 scFv CAR (murine scFv28z) was synthesized at Genscript using the FRP5 scFv sequence (kindly provided by Dr. Phillip K Darcy (University of Melbourne, Parkville, Victoria, Australia) [27]; the scFv [20], was linked to a marker epitope from human *c-myc*, the membrane proximal hinge region of murine CD8, the transmembrane and cytoplasmic regions of murine CD28, and the cytoplasmic region of murine CD3ζ (Table 1). The murine scFv28z was cloned into the retroviral vector pRV2011 oFL (used for the generation of CAR –'ve transduced murine T cells) [28] (kindly provided by Dr. Brian Rabinovich, MD Anderson, Houston, TX, USA) which also encodes that Thy1.1 marker gene. To generate DARPin28z, the FRP5 sequence in murine scFv28z was replaced with the sequence for the G3 anti-HER2 DARPin [19] [RCSB Protein Data Bank: 2jab]. The G3 DARPin sequence was synthesized at Genscript (Piscataway, NJ, USA). Retroviral supernatants were generated by transient transfection of a packaging cell line with pRV2011 CAR vectors. CAR retroviral vectors (10 μg) and the packaging plasmid pCL-Eco (10 μg) were co-transfected into PLAT-E cells using Lipofectamine 2000 (Invitrogen; Life Technologies). Retrovirus containing supernatants were collected 48 h later and concentrated 40-fold using an Amicon Ultra 100 K centrifugal filter (Millipore (Canada) Ltd., Etobicoke, ON); this process was repeated at 72 h.

Generation of CAR lentiviruses

Human variants of scFv28z and DARPin28z were constructed in which the membrane proximal CD8 hinge region, the transmembrane and cytoplasmic regions of CD28, and the cytoplasmic region of CD3ζ of the murine CARs were replaced with the corresponding regions of their human counterparts (Table 1) (again, the cDNA sequence was synthesized at Genscript). Human scFv28z and DARPin28z CAR sequences were cloned into the lentiviral vector pCCL ΔNGFR (used for the generation of CAR –'ve transduced human T cells) [29] (kindly provided by Dr. Megan Levings, University of British Columbia, Vancouver, BC). CARs were cloned downstream of the human EF1α promoter leaving ΔNGFR intact downstream of the minimal cytomegalovirus promoter in a bicistronic vector, pCCL. Third generation lentiviruses were made for

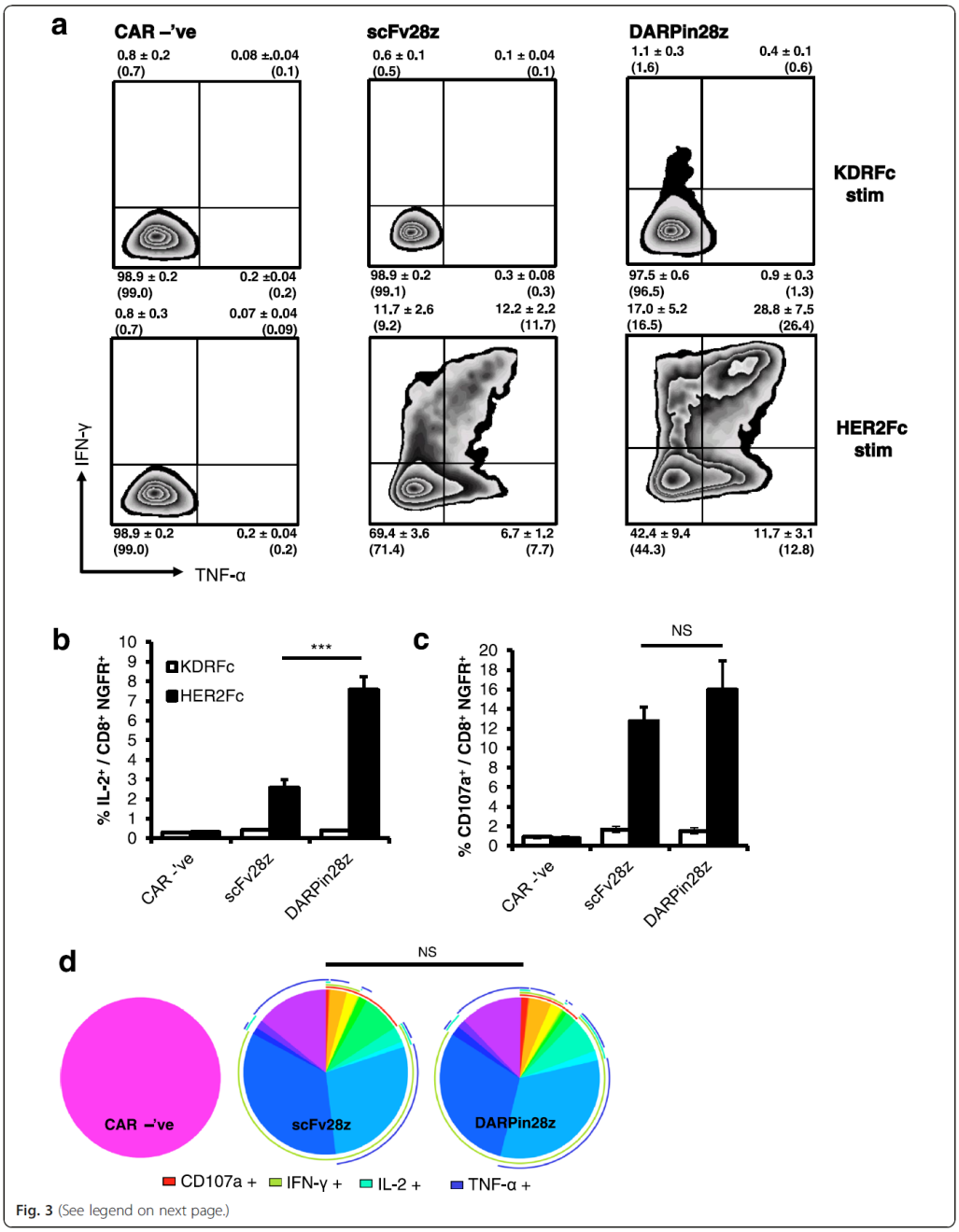

Fig. 3 (See legend on next page.)

(See figure on previous page.)
Fig. 3 DARPin28z induces human CAR-T cell cytokine production upon HER2 stimulation. 10^6 scFv28z, DARPin28z, or CAR –'ve transduced human T cells were stimulated with HER2 (HER2Fc fusion protein) or an unrelated target (KDRFc fusion protein) for four hours at 37 °C in a 96-well plate. **a** Production of IFN-γ and TNF-α was measured by ICS and subsequent flow cytometry. Data from $CD8^+$ $NGFR^+$ T cells is presented as mean ± SD. Bracketed numbers are quantitative of the representative plots shown. **b** Production of IL-2 by $CD8^+$ $NGFR^+$ T cells as measured by ICS. **c** Production of CD107a by $CD8^+$ $NGFR^+$ T cells as measured by ICS. **d** Pie graphs capturing the distribution of single and multi-functional CAR-T cells as produced with SPICE software. Pie arcs indicate functional populations represented by pie wedges. Error bars = SD. * = $p < 0.05$ ** = $p < 0.005$ *** = $p < 0.001$. All data from $n = 3$ experiments repeated with T cells from two donors

each CAR construct; 8×10^6 HEK 293 T cells in 15 cm tissue culture treated dishes (NUNC) (cultured in DMEM supplemented with 10 mM HEPES, 2 mM L-glutamine, 10 % FBS, and 0.1 mg/mL normocin (Invivogen, San Diego, CA)) were transfected with plasmids pRSV-Rev (6.25 μg), pMDLg-pRRE (12.5 μg), pMD2.G (9 μg), and CAR-encoding pCCL (30 μg) (kindly provided by Dr. Megan Levings, University of British Columbia, Vancouver, BC) using Lipofectamine 2000. After overnight incubation, media was replaced and supplemented with 1 mM sodium butyrate (Sigma-Aldrich). 30 h later, supernatants were harvested, filtered (0.45 μm), and concentrated (4 °C, 1 hr 40 min, 1.3×10^5rcf). Viral stocks were resuspended in PBS and stored at −80 °C. Thawed virus aliquots were titrated by serial dilution and transduction of HEK 293 T cells to determine transduction units per milliliter.

Transduction of murine T cells

Female BALB/c and C57BL/6 mice were purchased from Charles River Breeding Laboratory (Wilmington, MA). All of our investigations have been approved by the McMaster Animal Research Ethics Board. To generate murine T lymphoctes for retroviral transduction, 3×10^6 freshly isolated splenocytes were cultured in 1 mL T cell media (RPMI supplemented with 10 % FBS, 2 mM L-glutamine, 10 mM HEPES, 0.5 mM sodium pyruvate, 0.1 mM non-essential amino acids, 55 μM β-mercaptoethanol, and 0.1 mg/mL normocin *or* 100U/mL penicillin + 100 μg/mL streptomycin) supplemented with 0.3 μg/mL α-CD3e (clone 145-2C11, Cat No. 553057, BD Pharmingen, San Diego, CA) and 400U/mL rhIL-2 (Cat No. 200–02, Peprotech, Rocky Hill, NJ). Twenty-four hours after activation, 600 μL of media were removed from T cell cultures and 100 μL of the concentrated retroviral supernatant was added, along with 2 μg/mL Lipofectamine 2000 and 1.6 μg/mL Polybrene (Sigma-Aldrich). Cultures were spun at 2000 rpm, 32 °C for 90 min, allowed to rest for 1–4 h, and were supplemented with 0.5 mL T cell media + 400U/mL rhIL-2. This process was repeated at 48 h after activation with the 72 h retroviral concentrates. Seventy-two hours after activation, retrovirally transduced T cell cultures were expanded into 30 mL of DC media + 400U/mL rhIL-2. Six to eight days after activation, resultant CAR-T cells were enumerated for use *in vitro*.

Transduction of human T cells

Peripheral blood mononuclear cells from healthy donors were obtained using Ficoll-Paque-Plus (GE Healthcare, Baie d'Urfe, QC) separation. This research was approved by the McMaster Health Sciences Research Ethics Board that operates in compliance with the ICH Good Clinical Practice Guidelines, the Tri-Council Policy Statement: Ethical Conduct for Research Involving Humans, Division 5 Health Canada Food and Drug Regulations, and the Helsinki Declaration. All donors in this study provided informed written consent. 1×10^5 cells were activated with anti-CD3/CD28 beads at a 1:1 ratio (Dynabeads, Cat No. 11131D, Life Technologies) in a 96-well round bottom plate (cultured in T cell media) with 100U/mL rhIL-2 and 10 ng/mL rhIL-7. Twenty-four hours after activation, T cells were transduced with lentivirus at an MOI of 1:1. CAR-T cell cultures were expanded into fresh media (T cell media supplemented with 100U/mL rhIL-2 and 10 ng/mL rhIL-7) as required for a period of 10–15 days prior to enumeration and use *in vitro*.

Flow cytometry

Detection of CAR constructs on the surfaces of murine or human T lymphocytes was determined by indirect immunofluorescence with HER2Fc chimeric protein (Cat No. 1129-ER-050, R&D Systems, Minneapolis, MN) followed by a phycoerythrin (PE)-conjugated goat anti-human IgG (Cat No. 109-115-098, Jackson ImmunoResearch, West Grove, PA) *or* anti-myc-tag (clone 9B11, Cell Signaling Technology, Danvers, MA) followed by a PE-conjugated goat anti-mouse IgG (Cat No. 115-116-146, Jackson ImmunoResearch). Cell surface phenotyping of murine CAR-T cells was determined by direct staining with AlexaFluor(AF)700-conjugated anti-CD8a (clone 53–6.7, eBioscience Inc., San Diego, CA), PerCP-Cy5.5-conjugated anti-CD8a (clone 53–6.7, BD Pharmingen), PE-conjugated anti-CD8b (clone H35-17.2, BD Pharmingen), PE-conjugated anti-CD90.1 (Thy1.1, clone OX-7, BD Pharmingen), and/or fluorescein isothiocyanate (FITC)-conjugated anti-CD90.1 (clone HIS51, eBioscience Inc.). Cell surface phenotyping of human CAR-T cells was determined by indirect staining with HER2Fc chimeric protein (as for murine T cells) and direct staining with PE-CF594-conjugated

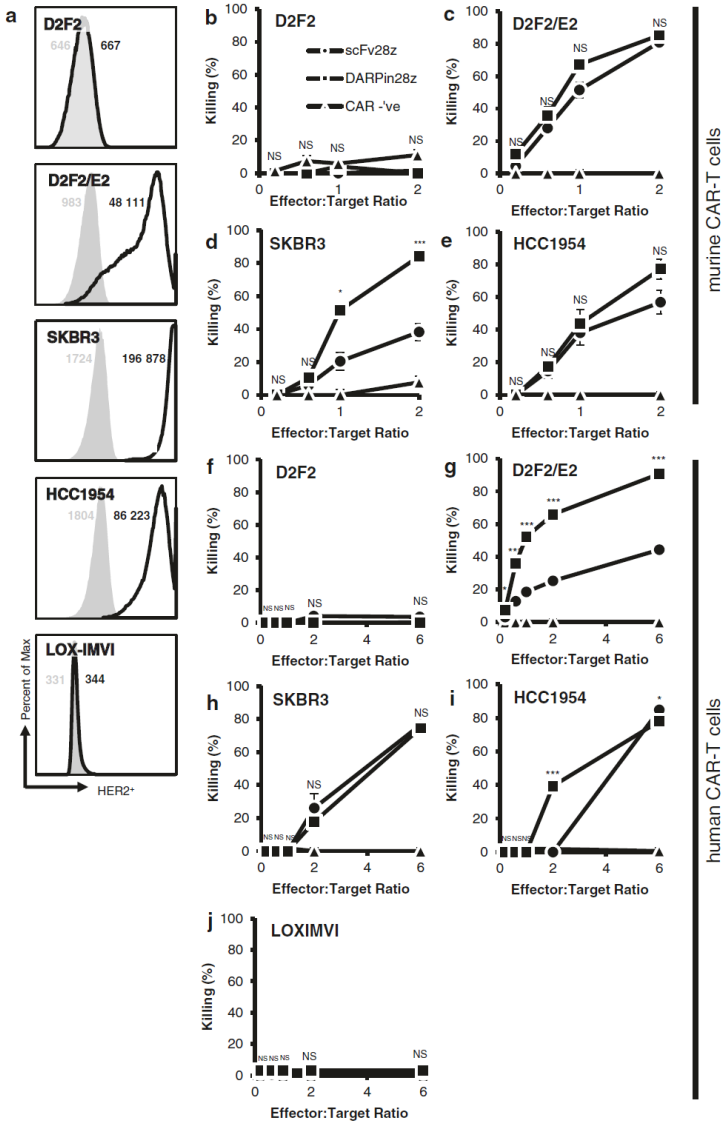

Fig. 4 DARPin28z murine and human CAR-T cells are capable of killing HER2$^+$ tumor cells. **a** Expression of HER2 on a panel of five tumor cell lines was verified by flow cytometry using a primary anti-HER2 antibody followed by a secondary detection antibody (thick lines). Shaded histograms indicate secondary only controls and numbers indicate mean fluorescence intensity. **b**-**e** Transduced murine T cells (effectors) were incubated together with tumor cells (targets) at various E:T ratios for 6 h in a 96-well plate. Each E:T was tested in triplicate. Error bars = standard error (SE). **f**-**j** Human CAR-T cells were incubated together with tumor cells at various E:T ratios for 6 h. Each E:T was tested in triplicate, data shown is the mean from $n = 3$ experiments repeated with T cells from two donors. Error bars = SE. Statistics compare scFv28z vs DARPin28z (* = $p < 0.05$ ** = $p < 0.005$ *** = $p < 0.001$)

Table 1 Amino acid sequences of CAR domains. The ten n-terminal and ten c-terminal amino acids which flank the protein regions utilized as CAR domains (with the exception of c-myc for which the sequence is listed in its entirety)

Murine CAR sequences:		
Domain	N-terminus	C-terminus
c-myc tag	EQKLISEEDL	
CD8 hinge	VISNSVMYFS	SVKGTGLDFA
CD28 transmembrane and cytoplasmic	ALVVVAGVLF	PARDFAAYRP
CD3ζ cytoplasmic	LRAKFSRSAE	ALHMQTLAPR
Human CAR sequences:		
Domain	N-terminus	C-terminus
CD8 hinge	SALSNSIMYF	GGAVHTRGLD
CD28 transmembrane and cytoplasmic	FWVLVVVGGV	PPRDFAAYRS
CD3ζ cytoplasmic	RVKFSRSADA	ALHMQALPPR

anti-CD271 (NGFR, clone C40-1457, BD Biosciences), and AF700-conjugated anti-CD8a (clone OKT8, eBioscience Inc.). All flow cytometry was conducted on a BD FACSCanto or BD LSRII cytometer (BD Bioscience) and analyzed using FlowJo vX.0.7 software (FlowJo, LLC, Ashland, OR, USA).

Functional analysis of CAR-T cells following stimulation with recombinant protein

10^6 murine or human CAR-T cells were stimulated in round bottom tissue culture treated 96-well plates coated with 200 ng HER2Fc chimeric protein (Cat No. 1129-ER-050, R&D Systems) or 200 ng KDRFc chimeric protein (Cat No. 443-KD, R&D Systems) for 4 h at 37 °C. Protein transport was inhibited according to the BD Golgi Plug protocol (Cat No. 555029 BD Biosciences, San Diego, CA). Production of activation cytokines was determined by flow cytometry. Cells were stained for surface phenotype markers as above. To permit intracellular cytokine staining (ICS), CAR-T cells were fixed and permeabilized according to BD Cytofix/Cytoperm Fixation/Permeabilization Kit protocol (Cat No. 554714, BD Biosciences). ICS of murine CAR-T cells was conducted by direct staining with allophycocyanin (APC)-conjugated anti-IFN-γ (clone XMG1.2, BD Pharmingen) and PE-cyanine(Cy)7-conjugated anti-TNF (clone MP6-XT22, BD Pharmingen). ICS of human CAR-T cells was conducted by direct staining with APC-conjugated anti-IFN-γ (clone B27, BD Pharmingen), FITC-conjugated anti-TNF (clone MAb11, BD Pharmingen), PE-conjugated anti-IL-2 (clone MQ1-17H12, BD Biosciences), and FITC-conjugated anti-CD107a (clone H4A3, BD Pharmingen). Analysis and presentation of distributions was performed using SPICE version 5.1, downloaded from [30]. Comparison of distributions was performed using a Student's T test and a partial permutation test as described [31], with a threshold of 0.09.

In vitro cytotoxicity assay

Adherent tumor cell lines were plated at 1.25×10^4 cells/well (D2F2, D2F2/E2, HCC1954, or LOX-IMVI) or 1.25×10^4 (human CAR-T cell cytotoxicity assay) *or* 2.5×10^4 cells/well (murine CAR-T cell cytotoxicity assay) (SKBR3) overnight in 96-well flat bottom tissue culture treated plates. Transformed murine or human T cell cultures were added to wells of tumor cells at various E:T ratios (from 0.1:1 to 6:1) and co-incubated together at 37 °C for 6 h. Murine T cells were added based on effectors defined as cells from day 6 to 8 transduced murine T cell cultures. Human T cells were added based on effectors defined as CAR-positive cells from day 15 transduced human T cell cultures. Wells were washed 3× with warmed PBS to remove any non-adherent cells. 100 μL of a 10 % solution of AlamarBlue cell viability reagent (Life Technologies) in T cell media was added and wells were incubated at 37 °C overnight. Colour change, indicative of live cells, was measured by fluorescence (excitation 530 nm, emission 595 nm) on a Safire plate reader (Tecan, Maennendorf, Switzerland). Tumor cell viability was calculated as the loss of fluorescence in experimental wells compared to untreated target cells. Each condition was tested in triplicate.

Statistical analysis

Student's *t* tests, two-tailed, type two, were used to compare data between two groups. Results were prepared using Microsoft Excel 2010. Significant differences were defined as: * = $p < 0.05$, ** = $p < 0.01$, *** = $p < 0.001$; NS = not significant.

Abbreviations

AR: ankyrin repeat; CAR: chimeric antigen receptor; CAR-T cell: chimeric antigen receptor transduced T cell; DARPin: designed ankyrin repeat protein; E: effector; scFv: single-chain variable fragment; SD: standard deviation; SE: standard error; T: target.

Competing interests

The authors declare that they have no competing interests.

Authors' contributions

JAH helped to coordinate and plan the study, was involved in all aspects of its execution (murine/human CAR-T cell studies, CAR retrovirus design and preparation, CAR lentivirus preparation, and cytotoxicity assays), and drafted/revised the manuscript. HV executed CAR retrovirus preparation, murine CAR-T cell studies, and helped to revise the manuscript. CWH designed CAR lentiviruses and executed human CAR-T cell studies, and helped to revise the manuscript. GFD designed CAR retroviruses and helped to revise the manuscript. CE executed CAR lentivirus generation and helped to revise the manuscript. DGMT executed CAR lentivirus generation, cytotoxicity assays, and helped to revise the manuscript. JDB executed CAR retrovirus preparation, murine CAR-T cell studies, and helped to revise the manuscript. JLB conceived of the study, participated in its coordination and planning, and contributed to the drafting/revision of the manuscript. All authors read and approved the final manuscript.

Authors' information
JLB holds the Canada Research Chair in Translational Cancer Immunology and the John Bienenstock Chair in Molecular Medicine.

Acknowledgements
This work was supported by funds from the Terry Fox Foundation and the Canadian Institutes for Health Research. JAH and HV were supported by scholarships from the Canadian Institutes for Health Research and the Government of Ontario. JAH was also supported by a scholarship from the Canadian Breast Cancer Foundation - Ontario Region.

Received: 29 May 2015 Accepted: 23 October 2015
Published online: 15 December 2015

References

1. Aranda F, Vacchelli E, Obrist F, Eggermont A, Galon J, Fridman WH, et al. Trial Watch: Adoptive cell transfer for anticancer immunotherapy. Oncoimmunology. 2014;3:e28344.
2. Rosenberg SA, Yang JC, Sherry RM, Kammula US, Hughes MS, Phan GQ, et al. Durable complete responses in heavily pretreated patients with metastatic melanoma using T-cell transfer immunotherapy. Clin Cancer Res. 2011;17:4550–7.
3. Kalos M, Levine BL, Porter DL, Katz S, Grupp SA, Bagg A, et al. T cells with chimeric antigen receptors have potent antitumor effects and can establish memory in patients with advanced leukemia. Sci Transl Med. 2011;3:95ra73.
4. Zhao Y, Wang QJ, Yang S, Kochenderfer JN, Zheng Z, Zhong X, et al. A herceptin-based chimeric antigen receptor with modified signaling domains leads to enhanced survival of transduced T lymphocytes and antitumor activity. J Immunol. 2009;183:5563–74.
5. Kershaw MH, Westwood JA, Slaney CY, Darcy PK. Clinical application of genetically modified T cells in cancer therapy. Clin Transl Immunol. 2014;3:e16.
6. Louis CU, Savoldo B, Dotti G, Pule M, Yvon E, Myers GD, et al. Antitumor activity and long-term fate of chimeric antigen receptor-positive T cells in patients with neuroblastoma. Blood. 2011;118:6050–6.
7. Kochenderfer JN, Dudley ME, Feldman SA, Wilson WH, Spaner DE, Maric I, et al. B-cell depletion and remissions of malignancy along with cytokine-associated toxicity in a clinical trial of anti-CD19 chimeric-antigen-receptor-transduced T cells. Blood. 2011;119:2709–20.
8. Grupp SA, Kalos M, Barrett D, Aplenc R, Porter DL, Rheingold SR, et al. Chimeric antigen receptor-modified T cells for acute lymphoid leukemia. N Engl J Med. 2013;368:1509–18.
9. Kershaw MH, Slaney CY, Darcy PK. Cancer immunotherapy utilizing gene-modified T cells: from the bench to the clinic. Mol Immunol. 2015;67:46-57.
10. Morgan RA, Yang JC, Kitano M, Dudley ME, Laurencot CM, Rosenberg SA. Case report of a serious adverse event following the administration of T cells transduced with a chimeric antigen receptor recognizing ERBB2. Mol Ther. 2010;18:843–51.
11. Mosavi LK, Cammett TJ, Desrosiers DC, Peng Z. The ankyrin repeat as molecular architecture for protein recognition. Protein Sci. 2004;13:1435–48.
12. Sedgwick SG, Smerdon SJ. The ankyrin repeat: a diversity of interactions on a common structural framework. Trends Biochem Sci. 1999;24:311–6.
13. Li J, Mahajan A, Tsai M. Ankyrin repeat: a unique motif mediating protein-protein interactions. Biochemistry. 2006;45:15168–78.
14. Binz HK, Stumpp MT, Forrer P, Amstutz P, Plückthun A. Designing repeat proteins: well-expressed, soluble and stable proteins from combinatorial libraries of consensus ankyrin repeat proteins. J Mol Biol. 2003;332:489–503.
15. Binz HK, Amstutz P, Kohl A, Stumpp MT, Briand C, Forrer P, et al. High-affinity binders selected from designed ankyrin repeat protein libraries. Nat Biotechnol. 2004;22:575–82.
16. Plückthun A. Designed ankyrin repeat proteins (DARPins): binding proteins for research, diagnostics, and therapy. Annu Rev Pharmacol Toxicol. 2015;55:489–511.
17. Stumpp MT, Binz HK, Amstutz P. DARPins: a new generation of protein therapeutics. Drug Discov Today. 2008;13:695–701.
18. Tamaskovic R, Simon M, Stefan N, Schwill M, Plückthun A. Designed ankyrin repeat proteins (DARPins) from research to therapy. Meth Enzymol. 2012;503:101–34.
19. Zahnd C, Wyler E, Schwenk JM, Steiner D, Lawrence MC, McKern NM, et al. A designed ankyrin repeat protein evolved to picomolar affinity to Her2. J Mol Biol. 2007;369:1015–28.
20. Wels W, Harwerth IM, Mueller M, Groner B, Hynes NE. Selective inhibition of tumor cell growth by a recombinant single-chain antibody-toxin specific for the erbB-2 receptor. Cancer Res. 1992;52:6310–7.
21. Zahnd C, Kawe M, Stumpp MT, de Pasquale C, Tamaskovic R, Nagy-Davidescu G, et al. Efficient tumor targeting with high-affinity designed ankyrin repeat proteins: effects of affinity and molecular size. Cancer Res. 2010;70:1595–605.
22. Wels W, Harwerth IM, Zwickl M, Hardman N, Groner B, Hynes NE. Construction, bacterial expression and characterization of a bifunctional single-chain antibody-phosphatase fusion protein targeted to the human erbB-2 receptor. Biotechnology (NY). 1992;10:1128–32.
23. Grada Z, Hegde M, Byrd T, Shaffer DR, Ghazi A, Brawley VS, et al. TanCAR: a novel bispecific chimeric antigen receptor for cancer immunotherapy. Mol Ther Nucleic Acids. 2013;2:e105.
24. Epa VC, Dolezal O, Doughty L, Xiao X, Jost C, Plückthun A, et al. Structural model for the interaction of a designed Ankyrin Repeat Protein with the human epidermal growth factor receptor 2. PLoS ONE. 2013;8:e59163.
25. Kumar M, Keller B, Makalou N, Sutton RE. Systematic determination of the packaging limit of lentiviral vectors. Hum Gene Ther. 2001;12:1893–905.
26. Yacoub al N, Romanowska M, Haritonova N, Foerster J. Optimized production and concentration of lentiviral vectors containing large inserts. J Gene Med. 2007;9:579–84.
27. Haynes NM, Trapani JA, Teng MWL, Jackson JT, Cerruti L, Jane SM, et al. Single-chain antigen recognition receptors that costimulate potent rejection of established experimental tumors. Blood. 2002;100:3155–63.
28. Rabinovich BA, Ye Y, Etto T, Chen JQ, Levitsky HI, Overwijk WW, et al. Visualizing fewer than 10 mouse T cells with an enhanced firefly luciferase in immunocompetent mouse models of cancer. Proc Natl Acad Sci U S A. 2008;105:14342–6.
29. Allan SE, Alstad AN, Merindol N, Crellin NK, Amendola M, Bacchetta R, et al. Generation of potent and stable human CD4+ T regulatory cells by activation-independent expression of FOXP3. Mol Ther. 2007;16:194.
30. SPICE data mining & visualization software for multicolor flow cytometry. http://exon.niaid.nih.gov/spice/. Accessed 15 Oct 2014.
31. Roederer M, Nozzi JL, Nason MC. SPICE: Exploration and analysis of post-cytometric complex multivariate datasets. Cytometry Part A. 2011;79:167–74.

4.0 Chapter Four – Chimeric antigen receptor driven toxicity is mediated by co-stimulation of $CD4^+$ T cells in a donor-specific manner

4.1 Introduction

When anti-HER2 DARPin-targeted human CAR-T cells were evaluated in a solid tumor xenograft model, mice displayed clinical symptoms of toxicity within days of adoptive transfer. This manuscript describes the characterization of those toxicities and our use of the model to probe whether factors intrinsic to a human CAR-T cell product may be contributing to CAR-T cell-associated toxicities, a previously unappreciated facet of the pathogenesis of CAR-T cell toxicity. The human DAPRin28z CAR evaluated in Chapter Three is identical to the DARPin-28z CAR utilized in this study.

4.2 Manuscript status, copyright, and citation

Status: Submitted to The Journal of Clinical Investigation

Copyright: The Journal of Clinical Investigation's editorial policy states "The JCI does not consider doctoral theses or dissertations to be prior publications." (https://www.jci.org/kiosks/authors#Editorial_Policies). To safeguard against the possibility of ineligibility for submission to other publications with alternatively defined prior publication bans, a temporary hold on the electronic publication of the thesis will be requested.

Citation: Hammill, JA, Kwiecien, JM, Dvorkin-Gheva, A, Bezverbnaya, K, Aarts, C, Helsen, CW, Denisova, GF, Derocher, H, Milne, K, Nelson, BH, Bramson, JL (2018). Chimeric antigen receptor driven toxicity is mediated by co-stimulation of $CD4^+$ T cells in a donor-specific manner. In submission: *The Journal of Clinical Investigation*.

4.3 Preprint of journal article

To follow beginning on subsequent page**.**

Chimeric antigen receptor driven toxicity is mediated by co-stimulation of CD4$^+$ T cells in a donor-specific manner

Joanne A. Hammill[1], Jacek M. Kwiecien[1,2], Anna Dvorkin-Gheva[1], Ksenia Bezverbnaya[1], Craig Aarts[1], Christopher W. Heslen[1], Galina F. Denisova[1], Heather Derocher[3], Katy Milne[3], Brad H. Nelson[3], and Jonathan L. Bramson[1]

[1] Department of Pathology and Molecular Medicine, McMaster University, Hamilton, ON, Canada

[2] Department of Clinical Pathomorphology, Medical University of Lublin, Lublin, Poland

[3] Trev and Joyce Deeley Research Centre, British Columbia Cancer Agency, Victoria, BC, Canada

Address correspondence to: Jonathan L. Bramson, Office of the Associate Dean, Health Sciences, Research, McMaster University, HSC 2E17, 1280 Main St West, Hamilton, ON, Canada, L8S 4K1. Phone: (905)525-9140 X73884; Email: bramsonj@mcmaster.ca.

Conflict of interest: CW Helsen holds equity in and receives income from Triumvira Immunologics Inc. CW Helsen is a co-inventor on patent WO2015117229 A1. BH Nelson is a paid consultant for Symvivo Corporation and Immunovaccine Inc. JL Bramson holds equity in, receives income from, and receives research funding from Triumvira Immunologics Inc. JL Bramson is a co-inventor on several patents related to chimeric receptors and oncolytic viruses.

Abstract:

Tumor-targeted chimeric antigen receptor (CAR)-engineered T cells (CAR-T cells) have demonstrated a great deal of clinical success. However, the administration of CAR-T cells is associated with a constellation of toxicities. Currently, the pathogenesis of CAR-T cell-associated toxicities are incompletely understood and elucidation of contributing factors is required to develop CAR-T cell therapies with an enhanced safety profile. Herein we use a novel xenograft model of CAR-T cell-associated toxicity, which permits simultaneous monitoring of anti-tumor efficacy, to determine whether donor-specific attributes contribute to CAR-T cell toxicity. In this model, human CAR-T cells targeted against the tumor associated antigen HER2 were capable of driving acute, often lethal, toxicities. The severity of toxicity correlated with the degree of therapeutic efficacy. Both toxicity and efficacy were dependent upon CAR-T cell dose, the composition of intracellular signaling domains, and the PBMC-donor used as a T cell source. The inclusion of CD28 or 4-1BB co-stimulatory domains within the CAR structure were central to the activity of the CAR T cells; the CD28 domain yielded a more potent T cell product which was associated with superior expansion *in vivo* and exacerbated toxicities. Donor-dependent differences in the severity of toxicity paralleled the $CD4^+$ to $CD8^+$ T cell ratio in the adoptive transfer product, which was not a result of the starting ratios but rather reflected an inherent biological property of the donor. $CD4^+$ CAR-T cells were determined to be the primary contributors to CAR-T cell-associated toxicity. Differences in the severity of toxicity across donors persisted even after the CAR-T cell products were normalized for $CD4^+$ cells, underpinned by differences in expansion and/or cytokine production, which were unique amongst donors. We conclude that donor-specific attributes of the CAR T cell product may be contributing to the clinical variation observed in the severity of CAR-T cell-associated toxicity.

Introduction:

The adoptive transfer of chimeric antigen receptor (CAR)-engineered T lymphocytes (CAR-T cells) for the treatment of cancer has been generating a great deal of clinical success, particularly in the realm of hematological malignancies (1-7). An unfortunate outcome of this success has been a constellation of CAR-T cell associated toxicities, ranging in severity from mild to life threatening, of which the pathogenesis is incompletely understood (8-10). A more comprehensive understanding of the factors contributing to CAR-T cell toxicities is critical to facilitate the development of therapeutics with an improved safety profile.

Chimeric antigen receptors (reviewed in (11-13)) are recombinant proteins which, when engineered for expression on the surface of T lymphocytes, are capable of redirecting those T cells against a tumor target. CARs are composed of an extracellular antigen recognition domain, specific for a tumor target, and intracellular T cell activation domains, which trigger T cell effector functions and cytotoxicity upon target ligation. Second generation CARs, which dominate clinical trials, pair an intracellular T cell activation signal (primarily CD3ζ) with a co-stimulatory domain (typically either CD28 or 4-1BB). Currently, most CAR-T cells are prepared as an autologous product where the patient's own T cells are extracted, engineered to express the CAR, and infused into the patient as a cellular drug.

The excitement generated by the remarkable clinical efficacy of CAR-T cells in hematological malignancies has been tempered by a profound toxicity profile. CAR-T cell associated toxicities can be broadly classified into two categories: cytokine associated and autoimmune (14).

The most commonly described CAR-T cell associated toxicity is cytokine release syndrome (CRS) (8). CRS is an acute (onset within hours to days), systemic inflammation resulting from the activation and expansion of CAR-T cells. Patients experiencing CRS present with symptoms ranging from mild fevers and myalgia to severe and (in some cases) life-threatening hypoxia, hypotension, and vascular leakage (among others) (4, 8, 15). The syndrome is characterized by elevated serum levels of several inflammatory cytokines, most commonly IFN-γ, IL-6, and IL-10, although others have been observed (TNF-α, GM-CSF, MCP-1, IL-8, IL-5, IL-2, etc.) (8, 10, 14, 16, 17). In CRS, these cytokines are either directly produced by activated CAR-T cells or by other immune cells, such as macrophages, activated as a result of CAR-T cell cytokine production (macrophage activation syndrome). Neurologic toxicity may also be observed, however whether neurologic symptoms are related to CRS (6, 15), or are an independent observation (8), is unclear. CRS has been observed in the treatment of both solid (18, 19) and hematological malignancies (1, 2, 4, 7, 15) with CAR-T cells and is a major clinical concern for their implementation; the incidence of CRS has been as high as 100% in some trials (4), and despite advances in monitoring and treatment, severe CRS (sCRS) still carries a risk of mortality (20). While several studies have identified pre-treatment tumor burden as a strong predictor of the occurrence or severity of CAR-T cell associated CRS (4, 6, 15, 20, 21), disease burden alone is unable to predict patients

at risk for developing CRS/sCRS (17) (see patients 4 and 16 in (5), for example), suggesting that additional, unidentified factors contribute to its pathogenesis.

Autoimmune toxicities arise when CAR-T cells respond against healthy, non-tumor tissues. This can occur when CAR-T cells respond against expression of their target antigen on non-tumor tissue, so-called "on-target, off-tumor" toxicity. Clinical use of CAR-T cell therapies for hematological tumors have been associated with the destruction of non-tumor tissues, as tumor-associated targets like CD19 and BCMA are also expressed on healthy B cells and plasma cells (2, 22, 23). However, these antibody producing tissues are considered non-essential as their loss can be managed by intravenous immunoglobulin therapy (IVIG). Other cases of on-target, off-tumor toxicities have been graver. Patients treated with anti-carbonic anhydrase IX (CAIX) CAR-T cells experienced hepatic toxicity resulting from a response against $CAIX^+$ bile duct epithelial cells (24). More seriously, on-target, off-tumor toxicity was lethal in one patient when CAR-T cells targeted against HER2 responded against $HER2^+$ lung epithelial cells (25). Alternatively, cross-reactivity of CAR-T cells against a non-target antigen, "off-target, off-tumor" responses, could also theoretically damage healthy tissues (10). Indeed, in related clinical studies TCR-engineered T cells targeted against MAGE-A3 caused lethal toxicities due to unexpected cross-reactivity against an antigen expressed on healthy tissue (26). Autoimmune toxicities can be managed during the development of the CAR-T cell by selecting for targets that are unique to the tumor and performing in-depth cross-reactivity analysis to ensure the CAR is antigen-specific. However, as CAR-T cell therapy expands into the realm of solid tumors, where many of the currently identified CAR-targetable tumor antigens are also expressed at low levels on healthy tissues, on-target, off-tumor toxicities are likely to become more prevalent. Therefore, it is imperative that we better understand the features of CAR-T cell products that influence autoimmune toxicities.

A better understanding of the biological underpinnings of these toxicities may aid the development of safer engineered T cell therapeutics. In particular, little is known about if and how the CAR-T cell product itself contributes to toxicity. Elucidation of any CAR-T cell intrinsic properties contributing to differences in toxicity is occluded in clinical data by other sources of patient-to-patient variability (such as pre-treatment regime, pre-treatment tumor-burden, and CAR-T cell dose).

We have developed a pre-clinical xenograft model where the efficacy of the CAR-T cell therapy is associated with severe, often lethal, toxicities. Here, we use this model as a standardized system to characterize toxic properties intrinsic to human CAR-T cell products. We observed differences in toxicity onset and severity dependent upon the T cell donor used to generate the CAR-T cell product and attributed these differences, in part, to the frequency of $CD4^+$ T cells in the cell product. However, even when normalized for $CD4^+$ CAR-T cell dose, donor-specific differences in CAR-T cell toxicity persisted and mirrored donor-specific differences in *in vivo* expansion and cytokine production. These data shed new light on the factors that contribute to the clinical variation observed in the severity of CAR-T cell-associated toxicity. Moreover, these results have important

implications for the selection of donors to be used for the production of allogeneic off-the-shelf CAR-T cell products.

Results:

Second-generation DARPin-targeted anti-HER2 CAR-T cells were toxic *in vivo*

We previously described a second-generation CAR targeted against the tumor-associated antigen HER2 using a designed ankyrin repeat protein (DARPin) and containing the intracellular signaling domains from CD3ζ and CD28 (27) (herein referred to as DARPin-28z; **Fig. 1A**). For this report, we also generated two other anti-HER2 DARPin-targeted CARs: a second generation CAR containing the 4-1BB co-stimulatory domain (DARPin-BBz) and a first generation CAR containing CD3ζ alone (DARPin-z). As a negative control for these studies, T cells were engineered with a lentivirus encoding truncated NGFR alone (NGFR-T cells) (**Fig. 1A**). All three CARs were similarly well expressed on the surface of lentiviral-transduced primary human T cells (**Fig. 1B**). Upon stimulation with a HER2-positive tumor cell line (OVCAR-3), DARPin-28z-, DARPin-BBz-, and DARPin-z-T cells all showed a similar capacity to produce the activation cytokines IFN-γ (**Fig. 1C**) and TNF-α (**Fig. 1D**). All three DARPin-targeted CAR-T cells were similarly cytotoxic against OVCAR-3 tumor cells, whilst sparing HER2-negative LOX-IMVI tumor cells (**Fig. 1E-F**). NGFR-T cells were functionally unresponsive against either tumor cell line.

To evaluate whether differences in efficacy would manifest *in vivo*, NRG mice bearing subcutaneous OVCAR-3 tumors were treated with 2.0×10^6 CAR-T cells. Despite having demonstrated similar functionality *in vitro*, only DARPin-28z-T cells demonstrated anti-tumor efficacy *in vivo*; tumor growth in DARPin-BBz- and DARPin-z-T cell-treated mice was no different than NGFR-T cell-treated controls (**Fig. 1G**).

We observed lethal toxicity associated with DARPin-28z-T cell treatment. Symptoms of toxicity included decreased body condition, hunched posture, ruffled coat, and labored breathing (*data not shown*); simultaneous decreases in core body temperature (**Fig. 1H**) and weight loss (**Fig. 1I**) were used as quantifiable measures of toxicity onset and severity. Importantly, mice treated with DARPin-BBz-, DARPin-z-, or NGFR-T cells showed no evidence of toxicity, indicating that the toxicity was a consequence of the CD28 co-stimulatory domain. Toxicity was lethal in 7 of 8 mice within 42d of DARPin-28z-T cell treatment (**Fig. 1J**).

When DARPin-28z- and DARPin-BBz-T cells were administered at a higher dose, we observed comparable toxicity and noted that the onset was much more rapid, demonstrating a dose-dependence to the magnitude and rate of the toxicity. Even at this elevated dose, first-generation CAR- and NGFR-T cells remained non-toxic (**Fig. 1K-L**), confirming the contribution of the co-stimulatory domains to the toxicity. Due to the rapidity of demise, we were unable to evaluate anti-tumor efficacy. A subsequent dose titration experiment confirmed the dose-dependency of DARPin-28z-T cell toxicity (**Supplemental Fig. 1**); while reducing the dose to 0.66×10^6 DARPin-28z-T cells was able to abate toxicities, the anti-

tumor efficacy was also tempered (**Supplemental Fig. 1D**), suggesting the two events were linked.

DARPin-28z-T cells became activated in pulmonary and cardiac tissues, driving a systemic cytokine storm

DARPin-28z-T cells also produced toxicity in tumor-free mice (**Supplemental Fig. 2A-C**), indicating that the toxicity was due to CAR-T cell attack against healthy tissues. To uncover the anatomical site or sites of the CAR-T cell attack, total body necropsy was performed on DARPin-28z-T cell-treated mice. Aberrant masses of immune cell infiltrate were observed in pulmonary and cardiac tissues of DARPin-28z-T cell treated mice, but not in matched NGFR-T cell treated counterparts.

Pulmonary masses of immune cells, as observed by H&E, began forming at subpleural areas (*data not shown*) and as perivascular cuffs as early as one day post-adoptive cell transfer dose 1 (ACT1). Pulmonary masses worsened over time and were present throughout the tissue by three days post-ACT1 (**Fig. 2A**). The masses contained scattered neutrophils and IHC for human CD3 confirmed the concentrated presence of human T cells; in contrast, NGFR-T cell treated mice exhibited only scattered T cells throughout the lungs (**Fig. 2B**). Upon closer inspection, there was also a striking difference in the size of $CD3^+$ cells; DAPRin-28z-T cells were much larger than matched NGFR-T cells, suggesting that DARPin-28z-T cells were activated at pulmonary sites.

In comparison to lung, the formation of T cell-containing immune deposits at cardiac sites in DARPin-28z-T cell treated mice was delayed. Moderate immune deposits formed in a papillary muscle or the right heart wall, starting at three days post-ACT1 and reaching ubiquity (3/3 mice) by five days post-ACT1. Again, NGFR-T cells were smaller and showed only a scattered presence in cardiac tissue (**Fig. 2C**).

Both DARPin-28z- and NGFR-T cell treated mice showed only a scattered intratumoral infiltrate of $CD3^+$ cells at day 5, consistent with the limited anti-tumor efficacy observed at this time (**Fig. 2D**).

Multiplex immunofluorescence was performed to characterize the T cells within these tissues. Lung slides were stained concurrently for $CD4^+$, $CD8^+$, and the proliferative marker Ki-67. The pulmonary infiltrate in DARPin-28z-T cell treated mice was almost entirely composed of Ki-67^+ $CD4^+$ cells, indicating local proliferation of $CD4^+$ CAR-T cells (**Fig. 2E,F**).

Multiplex analysis of human cytokines in the serum of the treated mice revealed a marked cytokine storm resulting from the activation of the DARPin-28z-T cells, which exacerbated over time. (**Fig. 2G, Supplemental Fig. 3, Supplemental Table 1,2**). The profile of the cytokines reflected an unbiased activation of $CD4^+$ T cells, with evidence of Th1 cytokines (GM-CSF, IFN-γ), Th2 cytokines (IL-5, IL-13) and regulatory cytokines (IL-10).

DARPin-28z-T cell toxicity was donor-dependent

The relationship between toxicity and efficacy observed in our model parallels the clinical experience where therapeutic doses of CAR-T cells are often associated with toxicities. However, toxicities are not apparent in all patients with good responses to CAR-T cell therapies, suggesting that the donor may influence the toxic profile of the T cell product. To address this hypothesis, DARPin-28z-T cells were generated from three PBMC donors: MAC014, LEUK001, and MAC026. The CAR was equally well expressed on the surface of T cells from all donors (**Fig. 3A**) and resultant CAR-T cells were equally capable of producing the T cell activation cytokines IFN-γ (**Fig. 3B**) and TNF-α (**Fig. 3C**) upon exposure to a $HER2^+$ tumor cell line (with the exception of LEUK001 $CD4^+$ cells, which showed an ~2-fold increase in IFN-γ production over $CD4^+$ DARPin-28z-T cells of MAC026 origin). MAC014-derived DAPRin-28z-T cells demonstrated superior cytotoxicity against $HER2^+$ tumor cell targets as compared to MAC026- or LEUK001-derived counterparts (**Fig. 3D,E**), which was likely a result of the higher frequency of $CD8^+$ T cells in the MAC014 CAR product (**Fig. 3F**) ($CD8^+$ CAR-T cells outperform $CD4^+$ CAR-T cells during *in vitro* cytotoxicity assays (*data not shown*)).

NRG mice bearing OVCAR-3 tumors were treated with 6.0×10^6 (**Fig. 3G-I**) or 2.0×10^6 (**Fig. 3J-L**) CAR-T cells from each donor, or a matched number of NGFR-T cells. While the *in vitro* comparisons revealed little difference between the various T cell products, the DARPin-28z-T cells displayed dramatically different properties *in vivo*. MAC014-derived DARPin-28z-T cells showed only a mild, transient toxicity at the 6.0×10^6 dose (**Fig. 3G**), and were completely non-toxic at the 2.0×10^6 dose (**Fig. 3J**). In contrast, both MAC026- and LEUK001-derived DARPin-28z-T cells were highly toxic; at the 6.0×10^6 dose, CAR-T cells derived from either donor were universally toxic within seven days of ACT (**Fig. 3I**). At the 2.0×10^6 dose, despite an equivalent onset of toxicity (**Fig. 3J**), mice treated with MAC026-derived DAPRin-28z-T cells were ultimately more toxic than the product generated from LEUK001 (**Fig. 3L**). Again, we observed a link between efficacy and toxicity. The minimally toxic DARPin-28z-T cell product derived from MAC014 PBMCs did not demonstrate any significant anti-tumor efficacy (**Fig. 3H,K**). In contrast, toxic LEUK001-derived DARPin-28z-T cells were capable of mediating tumor regressions (**Fig. 3K**) (the rapidity of demise in MAC026-derived DARPin-28z-T cell treated mice negated an evaluation of long-term anti-tumor efficacy).

In summation, these data indicate that factors endogenous to the CAR-T cell product itself, particularly differences arising as a result of donor-to-donor (analogous to patient-to-patient in the clinical setting) variation, contribute to differences in CAR-T cell associated toxicities.

Both T cell subset composition and donor background influenced toxicities

We next aimed to understand the factors underpinning the donor-to-donor differences in toxicity and efficacy. We noted that the donor hierarchy of DAPRin-

28z-T cell-associated toxicity severity (MAC014 < LEUK001 < MAC026) paralleled the $CD4^+$ T cell fraction of the CAR-T cell products generated from those donors (**Fig. 3F**). Given that the pulmonary immune pathology in DAPRin-28z-T cell treated mice was largely composed of $CD4^+$ T cells, we hypothesized that $CD4^+$ T cells were the critical drivers of toxicity.

To address this possibility, we generated T cell products from the least toxic donor, MAC014, using either unselected, $CD4^+$ T cell purified, or $CD8^+$ T cell purified MAC014 PBMCs (**Fig. 4A**). The T cell products were used to treat OVCAR-3 tumor-bearing or tumor-free mice. Consistent with our previous results, MAC014 DARPin-28z-T cells generated from unselected PBMCs remained non-lethal. The product generated from $CD8^+$ purified T cells was also non-toxic. In contrast, mice treated with $CD4^+$ purified MAC014 DAPRin-28z-T cells experienced weight loss of up to 20% (**Fig. 4B**), and universal lethality (**Fig. 4C**), pinpointing $CD4^+$ DARPin-28z-T cells as the toxic culprits. Although the $CD8^+$ purified DARPin-28z-T cells were associated with lessened toxicity, they were also less efficacious against a $HER2^+$ tumor challenge compared to DARPin-28z-T cells comprised of a mixed population of $CD4^+$ and $CD8^+$ T cells (**Fig. 4D**).

Together these data implicate $CD4^+$ T cells as the main contributors to DARPin-28z-T cell toxicity and, thus, a critical factor in donor-to-donor differences in CAR-T cell associated toxicity as the $CD4^+$:$CD8^+$ T cell ratio in a CAR-T cell product can vary significantly between donors.

Interestingly, the disparity observed in the ratio of $CD4^+$:$CD8^+$ T cells between MAC014 and MAC026 DARPin-28z-T cell products (**Fig. 3F**) was not reflective of intrinsic differences present in PBMCs. Rather, our data suggests that the ratio of $CD4^+$:$CD8^+$ cells changes during the *ex vivo* culture period in a donor-specific manner. Unlike other donors, DARPin-28z-T cells generated from MAC026 PBMCs demonstrated an increase in their $CD4^+$:$CD8^+$ ratio over time (**Supplemental Fig. 4A**). Expansion data for DARPin-28z-T cell cultures generated from purified $CD4^+$ or $CD8^+$ T cells revealed that while both MAC014 and MAC026 donors showed a similar proliferative capacity in their $CD4^+$ T cells, $CD8^+$ T cells from MAC026 had a diminished proliferative capacity (**Supplemental Fig. 4B**). While DARPin-28z-T cells showed a trend towards a $CD4^+$-biased T cell expansion compared to other CAR scaffolds, this was not statistically significant (**Supplemental Fig. 4C**).

If variability in the $CD4^+$:$CD8^+$ T cell ratio is the sole source of donor-to-donor differences in severity of toxicity, then normalization of the dose of $CD4^+$ CAR-T cells should eliminate this variation. However, upon adoptive transfer of equal numbers of $CD4^+$ purified DARPin-28z-T cells generated from either MAC014 or MAC026 PBMCs, differences in the severity of toxicity between donors were still observed, becoming increasingly apparent (particularly in survival differences) at lower doses (**Fig. 4E**), indicating additional donor-intrinsic properties exist that influence toxicity beyond simply the ratio of $CD8^+$ and $CD4^+$ T cells.

CAR-T cell cytokine production and *in vivo* expansion contributed to donor differences in toxicity

To better understand additional factors (secondary to the $CD4^+$:$CD8^+$ T cell ratio) contributing to donor-to-donor variations in toxicity, purified $CD4^+$ DARPin-28z-T cells were generated from a panel of five different PBMC donors and used at equal doses to treat tumor-bearing NRG mice.

While doses of 6.0×10^6 $CD4^+$ DARPin-28z-T cells resulted in very similar toxicities regardless of donor (**Supplemental Fig. 5**), donor-specific differences in the toxicity of $CD4^+$ T cells were most apparent at lower doses (2.0×10^6 CAR-T cells) (**Fig. 5A-C**). MAC002-derived $CD4^+$ DARPin-28z-T cells induced the most rapid toxicity and were uniformly lethal within eight days of treatment. MAC003, MAC014, and MAC026 treated mice all showed similar onsets in toxicity (all were experiencing weight loss by 10 days post-ACT1; the average percent change in weights being -16.0 ± 3.6%, -16.2 ± 9.3%, and -16.3 ± 5.8%, respectively at that point in time), however, MAC014-treated mice showed better overall survival. In contrast, LEUK001-derived $CD4^+$ DARPin-28z-T cells showed a delay in toxicity onset (average percent change in weight of 1.0 ± 4.9% at 10 days post-ACT1, reaching -16.9 ± 4.6% at 13 days post-ACT1).

To determine whether the expansion or survival of $CD4^+$ DARPin-28z-T cells could explain these donor differences, $CD4^+$ DARPin-28z-T cells derived from the same five donors were co-transduced with *firefly* luciferase to permit bioluminescent imaging of CAR-T cells *in vivo* (**Supplemental Fig. 6**). At early time points, MAC002-derived $CD4^+$ DARPin-28z-T cells showed an increased expansion when compared to CAR-T cells derived from other donors (**Fig. 5D**), which likely contributed to the more rapid onset of toxicities. No other significant differences were observed in the *in vivo* CAR-T cell expansion between donors at any time point tested, suggesting that MAC003-, MAC014-, MAC026-, and LEUK001-derived $CD4^+$ DAPRin-28z-T cells all had similar expansion and survival *in vivo*.

We next asked whether there were inter-donor differences in the intensity or patterning of cytokine release in the ensuing cytokine storm. Mice were bled one day or seven days post-ACT and multiplex analysis was used to quantify serum levels of a panel of 13 different human cytokines. At each of one and seven days post-ACT, principal component analysis (PCA) of the serum cytokine data showed tight clustering based on the source PBMC donor, supporting that differences in the serum cytokine levels were donor-dependent (**Fig. 5E**). Hierarchical clustering of the serum cytokine data also supports donor-dependency; interestingly, at each time point tested, mice treated with $CD4^+$ DARPin-28z-T cells from the most rapidly toxic donor, MAC002, experienced the most severe cytokine storms and those from the delayed toxicity donor, LEUK001, experienced the lowest levels (**Supplemental Fig. 7**). Serum levels of four different human cytokines (IFN-γ, GM-CSF, IL-6, and MCP-1), across all CAR-T cell doses and donors, showed strong positive correlations between concentration in the serum and severity of toxicity as determined by Pearson's coefficient of correlation (**Fig. 5F**;

Supplemental Fig. 8), consistent with the cytokine patterns associated with CAR toxicity in humans.

In summation, these data further support that inter-donor differences in the CAR-T cell product itself, primarily the ability to expand and the magnitude of cytokines released *in vivo*, contribute to donor-dependent differences in the severity of toxicity.

Co-stimulation of CD4$^+$ anti-HER2 DARPin-targeted CAR-T cells drove toxicity through improved expansion and persistence

To determine if the relationship between severity of toxicity and CAR co-stimulation persisted with a CD4+ purified population, tumor-bearing NRG mice were treated with equal doses of CD4$^+$ purified DARPin-28z-, DARPin-BBz-, or DARPin-z-T cells. At a dose of 2.0×10^6 CAR-T cells/mouse, mice treated with first generation CAR-T cells showed no evidence of toxicity *in vivo* (**Fig. 6A,B**). In contrast, both DARPin-28z- and DARPin-BBz-T cells resulted in comparable acute toxicities (**Fig. 6A**), indicating that CAR-T cell toxicity resulted from the co-stimulatory signals delivered to the T cell via the CAR; however, only the DARPin-28z-T cells were ultimately lethal (**Fig. 6B**). Mice were also treated with lower doses of the CAR T cells (0.66×10^6 CAR-T cells/mouse; **Fig. 6D,E**). Under these circumstances, the DARPin-28z-T cells were clearly more toxic than DARPin-BBz-T cells and, again, resulted in lethality. This hierarchy of toxic potential (28z > BBz > z) is consistent with findings using CAR-T cells derived from whole (non-purified) PBMCs (**Fig. 1**).

The anti-tumor efficacy observed with these co-stimulatory variants (**Fig. 6C,F**), particularly in the case of DARPin-28z-T cells, reinforces the casual observation that increased toxicity is paralleled by increased efficacy. This phenomenon was quantified in those mice surviving to experimental endpoint; regardless of dose or CAR scaffold, a positive correlation was found between the overall severity of toxicity and anti-tumor efficacy (measured as the area under the change in weight or tumor volume over time curves, respectively) (**Fig. 6G**).

To determine whether the differences in toxicity of our co-stimulatory CAR variants were related to expansion or persistence *in vivo*, DARPin-28z-, DARPin-BBz-, and DARPin-z-T cells were co-transduced to express *firefly* luciferase; expansion and persistence of the cells *in vivo* was monitored via bioluminescent imaging (**Fig. 6H**; **Supplemental Fig. 9**) and the resultant cytokine storm was compared (**Fig. 6I**).

Mice treated with first generation CAR-T cells showed no evidence of *in vivo* expansion post-adoptive transfer, nor did we measure any elevation in serum cytokines (as compared to NGFR-T cell treated mice) (**Fig. 6H,I**), consistent with an absence of toxicity. It should be noted that DARPin-z-T cells are capable of causing a transient toxicity if doses are escalated (**Supplemental Fig. 10**), indicating that the toxicity is a function of the total number of CAR-T cells in the host.

At a dose of 2.0×10^6 CAR-T cells/mouse, DAPRin-BBz-T cells initially expanded at the same rate as DARPin-28z-T cells (**Fig. 6H**), and accordingly both were experiencing a systemic cytokine storm (**Fig. 6I**). However, about 3 weeks post-adoptive transfer, the DARPin-BBz-T cells began to contract, whereas the DARPin-28z-T continued to expand (**Fig. 6H**). This likely accounts for the similar acute toxicity (**Fig. 6A**) but differential lethality (**Fig. 6B**) observed between CD28 and 4-1BB co-stimulated second generation CARs at this dose. The differential capacity for expansion was more notable when lower doses of CAR-T cells were infused (0.66×10^6 CAR-T cells/mouse); the expansion of the DARPin-28z-T cells was an order of magnitude greater than the expansion of the DARPin-BBz-T cells (**Fig. 6H**). While most serum cytokine levels were similar between DARPin-28z- and DARPin-BBz-T cell treated mice, only the mice receiving DARPin-28z T cells exhibited IL-10 in their serum (**Fig. 6I**).

Together, these data indicate that anti-HER2 DARPin CARs co-stimulated by CD28 are more toxic than those co-stimulated by 4-1BB, as a result of the increased expansion afforded by the CD28 domain.

Discussion:

We have developed a xenograft model that permits simultaneous characterization of anti-tumor efficacy and off-tumor toxicity arising from CAR-T cell treatment, a situation that will increasingly be encountered as CAR-T cell therapies expand for use against solid tumors. While current clinical reports of off-tumor CAR-T cell toxicity have identified the targeted healthy tissues, they have not addressed the fundamental features of the CAR-T cell product responsible for driving toxicity (24, 25, 28). In one clinical report, CAR-T cells with specificity for CAIX responded to target antigen expression on bile duct epithelial cells driving hepatic toxicity. A liver biopsy permitted immunohistochemical analysis of the hepatic T cell infiltrate; bile duct adjacent inflammation was heavily biased towards $CD4^+$ T cells (only scattered $CD8^+$ T cells were present), seemingly inexplicable given the patient's CAR-T cell infusion product was $CD8^+$ T cell-biased (28). Unlike previous pre-clinical models (29-34), ours has allowed a deep characterization of the CAR-T cell intrinsic factors within a human cell product that contribute to severe off-tumor CAR-T cell toxicity. We demonstrated that $CD4^+$ T cells are the key drivers of the toxicity, in support of the clinical evidence observed in the CAIX-CAR-T cell study and consistent with the findings of previous reports using murine CAR-T cell products (35). Moreover, we found the choice of co-stimulatory domain (CD28 vs 4-1BB) profoundly affected the toxicity of the product and, by extension, the therapeutic efficacy. Similar to clinical results observed with CD19 CAR-T cell therapy (36), toxic attributes of the CAR-T cell product were directly linked to efficacy in this model, resulting in a narrow therapeutic window. Our study also suggests that additional, as-of-yet unidentified, genetic or environmental factors may contribute to donor source influences on toxicities, as different toxicities were observed even when the CAR-T cell product was generated from purified $CD4^+$ T cells.

We noted that the toxicity of CAR-T cells generated from bulk PBMCs correlated with the frequency of $CD4^+$ T cells in the final T cell product (**Fig. 3**). Interestingly, the ratio of $CD4^+$:$CD8^+$ T cells in the final CAR-T cell product was not reflective of the $CD4^+$:$CD8^+$ ratio of the starting T cell population; instead the final ratio emerged during the manufacturing process such that some donors yielded products with elevated frequencies of $CD4^+$ T cells. The outgrowth of $CD4^+$ T cells appeared to be exacerbated by the CD28 co-stimulatory domain, but this difference did not prove to be significant (**Supplemental Fig. 4C**). Products with disproportionate frequencies of $CD4^+$ T cells seem to be related to poor expansion of the $CD8^+$ T cell population, rather than enhanced growth of the $CD4^+$ T cell population (**Supplemental Fig. 4**); the biological mechanisms accounting for this phenomenon remain to be determined but appear donor-specific. When purified $CD4^+$ T cells were used as the substrate for initiating the CAR-T cell product, we noted severe toxicity across all T cell products (**Fig. 4**). While our data implicated $CD4^+$ T cells as the key contributors to toxicity, we have also observed that high doses of $CD8^+$ DARPin-28z-T cells are capable of causing acute toxicities (*data*

not shown). These findings are consistent with correlative data from CAR-T cell clinical trials in which peak levels of $CD4^+$ or $CD8^+$ CAR-T cells were higher in patients with CRS (6), or sCRS (7), than those without; such clinical correlates have yet to emerge from cases of off-tumor toxicities as CAR-T cells have not been as extensively studied in the solid tumor arena. Clinical CAR-T cell products are often manufactured from PBMCs or bulk isolated T cells (5, 15, 37), resulting in CAR-T cell products with varying $CD4^+$ and $CD8^+$ T cell compositions from patient-to-patient (see Table S1 in (15), or Table 1 in (22), for example). Our results provide concrete evidence that, as suggested by others (38), patient-to-patient differences in the $CD4^+$:$CD8^+$ ratio of a CAR-T cell product contribute to differences in toxicity and argue in favor of defined composition CAR-T cell products (6, 7, 20).

Curiously, the relative toxicity of $CD4^+$ purified DARPin-28z-T cells differed between donors, indicating that, in addition to the composition of T cell subsets in the CAR-T cell product, toxicity and efficacy are influenced by donor background. Correlative data from clinical trials has also pointed to a relationship between CAR-T cell expansion and increased toxicity (4, 17, 37), although this is typically in reference to peak expansion rather than rate of expansion. $CD4^+$ T cells derived from the most toxic donor, MAC002, also displayed the greatest proliferative capacity, suggesting a possible link between proliferative capacity and toxicity; however, proliferation alone did not appear to be the key distinguishing factor between the most and least toxic donors.

Our observations of donor-to-donor differences in the severity of toxicity attributed to the CAR-T cell product itself suggest that for universal CAR-T cell strategies, in which modified T cells from an allogeneic donor are utilized to generate an "off-the-shelf" CAR-T cell product (39-41), donor selection will be critical. A clinical trial of universal CAR-T cells targeted against CD123 was put on hold due to severe toxicities arising at the initial T cell dose level (42). Based on previous experiences, this dose level was not expected to be toxic. It is possible that the toxicity was driven by the donor selected for the universal CAR-T cells. The model described in this manuscript may provide a useful tool for screening donors with a low likelihood of toxicity.

The deep clinical experience with CD19-targeted CAR-T cell therapies has enabled extensive evaluation of toxicities, which arise as a combination of on-tumor (pre-treatment tumor burden has been correlated to severity of CRS) and off-tumor (B cell aplasia) effects, both of which presumably contribute to CAR-T cell activation. In the context of solid tumors, severe off-tumor toxicities have been noted with CAR-T cells directed against HER-2 (25) and CAIX (24, 28). In all cases, toxicity was associated with high levels of circulating cytokines arising from activation of the CAR-T cells. In some cases, this cytokine storm manifests as cytokine release syndrome (CRS), a specific pathology associated with endothelial activation and vascular leakage. In other cases, the cytokine storm is linked to other pathologies (ex. macrophage activation syndrome). The cytokines circulating following CAR-T cell therapy originate from a combination of activated CAR-T cells and other immune cells which become activated in response (8). In the model

described herein, CAR-T cell therapy leads to high levels of serum cytokines that have also been linked to toxicities in humans, including IFN-γ (4-6, 15, 23, 43), GM-CSF (5, 15), TNFα (22), IL-5 (15), IL-2 (43), and IL-10 (5, 6, 15, 23) (**Fig. 2, Supplemental Table 1**). Although we could measure human IL-6 in our studies, the circulating levels were quite low; this is not surprising as the human IL-6 produced following CAR-T cell therapy is believed to result from innate immune cell activation (44). Consistent with the non-T cell source of the IL-6, we do measure murine IL-6 in the serum (**Supplemental Fig. 3, Supplemental Table 2**), as has been observed with another pre-clinical xenograft model of a CAR-T cell driven cytokine storm (30).

Interestingly, although mice were treated with equal number of $CD4^+$ CAR-T cells, we observed cytokine profiles that were donor specific. The cytokine profile was independent of expansion rate, as $CD4^+$ DARPin-28z-T cells from all donors, with the exception of MAC002, expanded equally. The magnitude of serum cytokines correlated with the degree of toxicity, confirming that toxicity was directly related to the magnitude of T cell activation. We suspect that the differences in cytokine profile reflect the complexity of $CD4^+$ T cell differentiation. Indeed, a broad collection of $CD4^+$ T cell subtypes have been identified (ex. Th1, Th2, Th17, etc.) and the composition of these distinct $CD4^+$ T cells in a CAR-T cell product will undoubtedly differ between donors. Understanding the relative contribution of the various $CD4^+$ T cell subtypes to anti-tumor immunity and off-tumor toxicity may prove useful to mitigate unwanted toxicity while retaining robust anti-tumor immunity.

The two most common CAR scaffolds under clinical investigation are second generation variants using either CD28 (2, 3, 5, 15) or 4-1BB (4, 6, 7, 18, 20, 37) as the co-stimulatory domain. Clinical toxicities have been observed following treatment with CAR-T cells carrying either domain. However, differences between clinical trials (patient populations, dosing, pre-treatment, antigen-binding domain, etc.) have made it difficult to conclude whether CAR-T cells carrying CD28 or 4-1BB are equally effective and equally toxic. Consistent with the clinical data, we found that both CD28- and 4-1BB-based CAR-T cells could produce severe toxicities. The CD28-based CARs, however, yielded CAR-T cell products that were more potent on a per-cell basis. Notably, the greater toxicity of the CD28-based CAR-T cells was also linked directly to enhance therapeutic efficacy. The toxicity of the various CARs correlated strongly with the proliferative capacity of the T cell product. We noted a marked hierarchy in proliferative capacity *in vivo* where CD28-CAR-T cells > CD137-CAR-T cells >>> first-generation CAR-T cells. The first-generation CARs revealed no capacity to expand *in vivo*, confirming the importance of the co-stimulatory domain in CAR-T cell expansion. The lack of toxicity with a first generation CAR was not unexpected, as clinical trials of first generation CAR-T cells rarely report CAR-T cell associated toxicities (39, 45, 46). It should be noted that upon escalating the dose of DARPin-z-T-cells we were able to resolve transient toxicities (**Supplemental Fig. 10** and *data not shown*), consistent with clinical outcomes in which first generation CAR-T cells have demonstrated toxicities under

the right conditions (increased dose, an intensified pre-treatment regimen, etc.) (19). Consistent with our results, other pre-clinical murine models have revealed an increased efficacy of CD28-co-stimulated CAR-T cells over their 4-1BB counterparts (47, 48). Interestingly, in one of these models, differences were also found to be more apparent at lower doses (47), akin to our data. 4-1BB and CD28 co-stimulatory domains activate different signaling pathways (49), which have been shown to differentially impact on CAR-T cell memory formation (50) and exhaustion (51), likely contributing to observations of longer persistence of CAR-T cells in clinical trials utilizing 4-1BB (4, 37) as opposed to CD28 (5, 21) as their source of co-stimulation.

Whether or not toxicity is required for CAR-T cell efficacy in the clinical scenario is a matter of debate. While the severity of CRS is not predictive of disease response, the vast majority of clinical responders will experience some degree of CRS (5, 9, 10, 15, 37). A recent retrospective analysis of CD19 CAR-T cell trials at the Fred Hutchinson Cancer Research Center determined that toxicity is closely linked to efficacy and suggested the therapeutic window for CAR-T cells is narrow (36). Developing a better understanding of CAR-T cell associated toxicities, with the goal of producing safer CAR-T cell products in the future, could serve to reduce fatalities and increase the number of patients who benefit from CAR-T cell therapies. Despite the identification of tocilizumab (an antagonist antibody specific for IL-6R) as a treatment for CRS (16, 23), some patients fail to respond. While such patients can be escalated to corticosteroid treatments (52), these likely reduce therapeutic efficacy (15), and fatalities in corticosteroid treated, tocilizumab-refractory CRS patients still occur (20). Our study is the first to definitively demonstrate that differences intrinsic to the CAR-T cells themselves can contribute to toxicity, helping to shed light on the underlying pathogenic mechanisms.

Methods:

Cell lines: Human tumor cell lines OVCAR-3 and LOX-IMVI, originating from the NCI-60 panel (kind gift from Dr. Karen Mossman, McMaster University, Hamilton, ON), were cultured in RPMI 1640 (Gibco; Thermo Fisher Scientific) supplemented with 10% heat-inactivated fetal bovine serum (FBS; Gibco), 2mM L-glutamine (BioShop, Burlington, ON), 10mM HEPES (Roche Diagnostics, Laval, QC), 100U/mL penicillin + 100μg/mL streptomycin (Gibco), and 55μM β-mercaptoethanol (Gibco). Prior to their use, parental OVCAR-3 cells were subjected to an *in vivo* passage. In short, OVCAR-3 cells were injected *s*.c. into the hind flank of an NRG mouse and allowed to grow for 72 days prior to harvest, digestion (incubation with a mixture of collagenase type I (Gibco), DNase I (Roche), and hyaluronidase (MP Biomedicals LLC, Solon, OH)), and *ex vivo* expansion. All cell lines were grown at 5% CO_2, 95% air, and 37°C. All cell lines tested negative for mycoplasma contamination (LookOut Mycoplasma PCR Detection Kit, Sigma-Aldrich Canada Co., Oakville, ON).

Generation of lentiviral/CAR vectors: Generation of the DARPin-28z-CAR (consisting of the IgGκ leader, anti-HER2 H10-2-G3 DARPin, human myc tag, BamHI site, CD8α hinge, CD28 TM and cytoplasmic domains, CD3ζ cytoplasmic tail, and NheI site), was previously described (27). The DARPin-BBz-CAR (consisting of the IgGκ leader, anti-HER2 H10-2-G3 DARPin, human myc tag, BamHI site, CD8α hinge and TM, 4-1BB cytoplasmic domain, CD3ζ cytoplasmic tail, and NheI site) was generated by cloning the CD8α hinge and TM, 4-1BB cytoplasmic domain, and CD3ζ cytoplasmic tail portions from an anti-CD19 CAR (prepared according to (53)) between the BamHI and NheI sites of the DARPin-28z-CAR. To generate the DARPin-z-CAR, overlap extension PCR was used to delete the 4-1BB sequence from the DAPRin-BBz-CAR. To facilitate the production of third-generation lentiviruses, the transfer plasmid pCCL was used (54) (kind gift from Dr. Megan Levings, University of British Columbia, Vancouver, BC). The parental pCCL vector consists of a bi-directional promoter system; tNGFR (truncated NGFR; used as a transduction control) is expressed under control of the minimal cytomegalovirus promoter (mCMV) and the human EF-1α promoter lacks a transgene (the parental pCCL vector was used to generate receptor negative control T cells). CARs were cloned into pCCL under the control of the EF-1α promoter. Luciferase expression was achieved using a variant of the pCCL plasmid in which puromycin resistance was encoded under the mCMV promoter and an enhanced firefly luciferase (55) was encoded under the EF-1α promoter.

Lentivirus production: Self-inactivating, non-replicative lentivirus produced using a third-generation system has been previously discussed (56, 57). Briefly, 8×10^6 HEK293T cells cultured on 15 cm diameter tissue culture-treated dishes (NUNC; Thermo Fisher Scientific) were transfected with the packaging plasmids pRSV-Rev

(6.25 μg), pMD2.G (9 μg), pMDLg-pRRE (12.5 μg), and the desired pCCL transfer plasmid (see above; 32 μg), using Opti-MEM (Gibco; Thermo Fisher Scientific) and Lipofectamine 2000 (Thermo Fisher Scientific). Twelve to sixteen hours after transfection, media was replaced; fresh medium was supplemented with sodium butyrate (1 mM; Sigma-Aldrich). Cell culture supernatant, containing lentiviral particles, was collected after 36-48 hours and lentivirus was isolated by ultracentrifugation. Lentiviruses were stored at -80°C. Viral titer in transduction units (TU)/mL was determined by serial dilution and transduction of HEK293T cells with virus (transduction after ~72hrs was measured as %tNGFR$^+$ via flow cytometry using an anti-NGFR-VioBrightFITC antibody (ME20.4-1.H7, Cat No. 130-104-847, Miltenyi Biotec, Bergisch Gladbach, Germany)).

Transduction of human T cells: Lentivirus-engineered human T cells were generated as previously described (57). Human peripheral blood mononuclear cells (PBMC) from healthy donors (McMaster Adult Cohort (MAC) donor) or commercial leukapheresis products (LEUK donor) (HemaCare, Van Nuys, CA) were isolated by Ficoll-Paque-Plus gradient centrifugation (GE Healthcare, Baie d'Urfe, QC) and cryopreserved in inactivated human AB serum (Corning, Corning, NY) containing 10% DMSO (Sigma-Aldrich Canada Co.). T cells were activated from PBMCs with anti-CD3/28 Dynabeads at a 0.8:1 bead-to-cell ratio (Gibco) following manufacturer's guidelines, and were cultured in T cell media (RPMI 1640 (Gibco) supplemented with 10% heat-inactivated FBS (Gibco), 2mM L-glutamine, 10mM HEPES, 1mM sodium pyruvate (Sigma-Aldrich Canada Co.), 1x non-essential amino acids (Gibco), 55μM β-mercaptoethanol, 100U/mL penicillin + 100μg/mL streptomycin, 660 I.U. rhL-2 and 10 ng/mL rhIL-7 (PeproTech, Rocky Hill, NJ)). After 18-24hrs, cells were transduced with lentivirus at a multiplicity of infection (MOI) of 2-5. In cases of co-transduction for luciferase expression, a second lentivirus was added 6-12 hours later at an MOI of 2. Cells were monitored daily and fed T cell media according to cell counts every 2-3 days to maintain a concentration of 1×10^6cells/mL for a period of 11-14 days prior to use *in vitro* and/or *in vivo*. Purified CD4$^+$ or CD8$^+$ T cells were generated using the same protocol, except that CD4$^+$ or CD8$^+$ T cells were isolated from PBMCs, prior to activation, using magnetic negative selection (Cat No. 19052 and Cat No. 19053, STEMCELL Technologies, Vancouver, BC, Canada), according to the manufacturer's instructions.

Phenotypic analysis by flow cytometry: Cell surface phenotyping of CAR- or control-T cells was evaluated by direct staining with AlexaFluor700-conjugated anti-CD4 (clone: OKT4, Cat No. 56-0048-82, eBioscience; Thermo Fisher Scientific), PerCP-Cyanine5.5-conjugated anti-CD8 (clone: RPA-T8, Cat No. 45-0088-42, eBioscience), and BV421-conjugated anti-tNGFR (clone:C40-1457 , Cat No. 562562, BD Biosciences). Detection of CAR expression was determined in a two-step stain by indirect immunofluorescence; incubation with rhHER2-Fc chimeric protein (Cat No. 1129-ER-050, R&D Systems, Minneapolis, MN) was

followed by a phycoerythrin (PE)-conjugated goat anti-human IgG secondary antibody (Cat No. 109-115-098, Jackson ImmunoResearch, West Grove, PA). Detection of cytosolic luciferase was determined via intracellular cytokine staining (ICS); in brief, cells were fixed and permeabilized according to BD Cytofix/Cytoperm Fixation and Permeabilization Kit (Cat No. 554714, BD Biosciences) and luciferase expression was determined in a two-step stain by indirect immunofluorescence (incubation with anti-Luc (clone: Luci17, Cat No. ab16466, Abcam) was followed by a PE-conjugated goat anti-mouse IgG secondary antibody (Cat No. 115-116-146, Jackson ImmunoResearch)). All stains were conducted at room temperature for 30 minutes unless otherwise stated. All flow cytometry was conducted on a BD LSRFortessa or BD LSRII cytometer (BD Bioscience) and analyzed using FlowJo vX software (FlowJo, LLC, Ashland, OR, USA).

Functional analysis of CAR-T cells following stimulation with tumor cell lines: 5×10^5 CAR-T cells were stimulated with 5×10^4 $HER2^+$ (OVCAR-3) or $HER2^-$ (LOX-IMVI) tumor cells for 4 hours at 37°C in a round-bottom 96-well plate. Brefeldin A (BD GolgiPlug protein transport inhibitor (Cat No. 555029, BD Biosciences)) was added at the start of stimulation following manufacturer's instructions. After stimulation, cells were stained for desired surface markers as above. BD Cytofix/Cytoperm (as above) was used to permit intracellular cytokine staining and cells were stained directly for fluorescein isothiocyanate (FITC)-conjugated anti-TNFα (clone: MAb11, Cat No. 554512, BD Biosciences), and APC-conjugated anti-IFN-γ (clone: B27, Cat No. 554702, BD Biosciences) expression. Flow cytometry and analysis was conducted as above.

In vitro cytotoxicity assay: Adherent tumor cell lines were plated at 1.25×10^4 cells/well (OVCAR-3) or 2.5×10^4cells/well (LOX-IMVI) in a 96-well flat bottom tissue culture-treated plate and allowed to rest overnight. CAR-T cell cultures (a mix of $NGFR^+$ and non-transduced T cells) were added at various E:T ratios (from 0.25:1 to 8:1) in triplicate and co-cultures were incubated for 6 hours at 37°C. To resolve cytotoxicity, wells were washed 3X with warmed PBS to remove any non-adherent cells and 100µL of a 10% solution of AlamarBlue cell viability reagent (Life Technologies) in T cell media was added. After a 3-4hr incubation at 37°C colour change was measured by fluorescence (excitation 530nm, emission 595nm) on a Synergy plate reader (BioTek, Winooski, VT, USA). Tumor cell viability was calculated as the loss of fluorescence in experimental wells compared to untreated target cells.

Mice: 5-week-old female NOD.Cg-Rag1^{tm1Mom}Il2rg^{tm1Wjl}/SzJ (NRG) mice were purchased from The Jackson Laboratory (Stock No. 007799, Bar Harbor, ME, USA), or bred in-house.

Adoptive transfer and in vivo monitoring: Mice (6-12-weeks-old) were implanted with 2.5×10^6 OVCAR-3 cells subcutaneously (s.c.) on the right hind flank. After 35-56d of tumor growth mice were optimized into treatment groups based on tumor volume (58); average tumor volume at time of treatment was $155mm^3$. CAR-T cells were infused intravenously (i.v.) (deemed adoptive cell transfer (ACT)) through the tail vein as two doses delivered 48hrs apart in 200µL of sterile PBS (T cells were d14 and d16 in culture on respective treatment days; doses as specified in text and figure legends represent the total sum of effective ($NGFR^+$) T cells received/mouse). Tumor volume was measured by caliper (Cat No. 500-196-30, Mitutoyo Canada Inc., Toronto, ON, Cat No. 500-196-30) every 2-3 days post-ACT and calculated as L×W×H; % change in tumor volume was calculated as ((current volume (mm^3) – pre-ACT volume (mm^3))/pre-ACT volume (mm^3))*100. Core body temperature (via rectal probe; Cat No. 23609-230, VWR) and weight (Cat No. 01922406, OHAUS Corporation, Parsippany, NJ) were measured every 1-3 days post-ACT; % change in weight was calculated as ((current weight (g) – pre-ACT weight (g))/pre-ACT weight (g))*100. Luciferase-engineered T cells were monitored through bioluminescent imaging every 1-9 days post-ACT1. In short, mice received an intraperitoneal injection of 150mg/kg D-Luciferin (Perkin Elmer; Waltham, MA, USA) and ventral images were collected 14 minutes later using an IVIS Spectrum (Caliper Life Sciences; Waltham, MA). Images were analyzed using Living Image Software v4.2 for MacOSX (Perkin Elmer). Fold change in whole body total flux (p/s; photons/second) relative to one day post-ACT1 was calculated as ((current flux (p/s) – 1d flux (p/s))/1d flux (p/s)). Measurements of overall toxicity and efficacy encompassing the duration of the experiment were calculated as net area under the curve (using GraphPad Prism, version 6.01) for percent weight loss over time or percent change in tumor volume over time graphs, respectively (baseline at y = 0, peaks below baseline included).

Serum cytokine analysis: Whole blood was collected via a terminal or non-terminal retro-orbital bleed. Serum was isolated using CapiJect capillary blood collection serum tubes according to manufacturer instructions (Terumo Medical Corporation, Somerset, NJ, Cat No. T-MG). Quantification of 13 human cytokines and chemokines (Cat No. HDF13) or 31 murine cytokines and chemokines (Cat No. MD31) was performed in a multiplex assay by Eve Technologies (Eve Technologies Corporation, Calgary, AB) using the Bio-Plex 200 system and MILLIPLEX assay kits from Millipore. The assay sensitivities of these markers ranged from 0.1-9.5pg/mL (human) and 0.1-33.3pg/mL (murine); individual analyte values can be found through the Eve Technologies website. Prior to downstream analysis, fluorescence intensity values were transformed to the log2 scale (59). Heat maps (**Fig. 2** and **Supplemental Fig. 3**) were created using HeatMapViewer version 13.9 available on GenePattern (https://genepattern.broadinstitute.org/). After preprocessing, we confirmed that samples were separated into homogeneous groups matching experimental groups and performed principal component analysis (princomp function from "stats" and

"rgl"(60) packages R) with all 13 human cytokines. Heat maps (**Supplemental Fig. 7**) were generated using "gplots" package (61) in R. Linear models were fit for each cytokine using the "limma" package in R to test for differential expression for pre-specified contrasts (62). P values for each contrast were obtained for each cytokine and adjusted for multiple comparisons using the Benjamini–Hochberg procedure (63).

Histology: Tissues were prepared for veterinary necropsy via whole body formalin perfusion as described previously (64). After fixation in 10% neutral buffered formalin, tissues were paraffin-embedded, sectioned and stained using hematoxylin and eosin (H&E) or immunohistochemistry (IHC) for expression of human CD3 (Abcam Inc., Toronto, ON, Cat No. ab16669) (conducted using the Leica BOND RX (Leica Biosystems Inc., Concord, ON)). Aforementioned histology services were performed by the Core Histology Facility at the McMaster Immunology Research Centre. Opal multiplex immunofluorescence was performed by the Molecular and Cellular Immunology Core at the British Columbia Cancer Agency's Deeley Research Centre. In short, formalin-fixed paraffin embedded tissue sections were stained with anti-CD4 (ab133616, Abcam, Cat No. EPR6855) detected with Opal 520 (PerkinElmer, NEL797001KT), anti-CD8 (SP16, Spring Biosciences, Cat No. M3162) detected with Opal 650 (PerkinElmer, NEL797001KT), anti-HER2 (polyclonal, Cell Signaling Technology, Cat No. 2242) detected with Opal 570 (PerkinElmer, NEL797001KT), anti-pan-CK (PCK-26, Sigma Aldrich, Cat No. C1801) detected with Opal 690 (PerkinElmer, NEL797001KT) anti-Ki-67 (SP6, Spring Biosciences, Cat No. M3062) detected with Opal 620 (PerkinElmer, NEL797001KT), and DAPI (PerkinElmer, NEL797001KT). Multispectral images (20X magnification, 3 fields per tumor and 3 fields containing perivascular sites per lung) were collected using the PerkinElmer Vectra system. Quantification was performed using inForm Advanced Image Analysis Software (PerkinElmer). Blinded pathologic assessment of H&E and CD3 IHC slides was performed by a veterinary pathologist (Dr. Jacek Kwiecein, McMaster University).

Statistics: One-way ANOVA was used to determine whether any statistically significant differences existed in the means of three or more groups (alpha = 0.05). Student's *t* tests, two-tailed, type two or three (depending on variance), were used to compare data between two groups and as a post hoc test for ANOVA results. Strength of linear correlation was determined using the Pearson correlation coefficient. Results were prepared using Microsoft Excel 2010. Log-rank tests were used to compare survival using GraphPad Prism version 6.01 for Windows (GraphPad Software, La Jolla, California, USA). Significant differences were defined as: * = $p < 0.05$, ** = $p < 0.01$, *** = $p < 0.001$; N.S. = not significant.

Study approval: This research was approved by the Hamilton Integrated Research Ethics Board and all PBMC donors provided informed written consent. All animal studies were approved by the McMaster University Animal Research Ethics Board.

Author contributions:

JAH and JLB conceived of these studies, designed experiments, and wrote the manuscript. JAH acquired and analyzed all data (unless otherwise stated). JMK performed pathological analysis of murine tissues. ADG performed PCA and hierarchical clustering. KB and CA assisted with *in vivo* experiments. CWH and GFD made contributions to receptor design. HD and KM performed and analyzed multiplex immunofluorescence as designed by BHN, KM, and JLB. All authors reviewed the final manuscript prior to submission.

Acknowledgements:

This research is funded by the Canadian Cancer Society (grant # 313397). JAH was supported by a doctoral fellowship funded by the Canadian Cancer Society (grant # 313416). JLB is supported by a Canadian Research Chair in Translational Immunology and the John Bienenstock Chair in Molecular Medicine.

References:

1. Park JH, Geyer MB, Brentjens RJ. CD19-targeted CAR T-cell therapeutics for hematologic malignancies: interpreting clinical outcomes to date. *Blood*. 2016;127(26):3312–3320.

2. Ali SA et al. T cells expressing an anti-B-cell maturation antigen chimeric antigen receptor cause remissions of multiple myeloma. *Blood*. 2016;128(13):1688–1700.

3. Locke FL et al. Phase 1 Results of ZUMA-1: A Multicenter Study of KTE-C19 Anti-CD19 CAR T Cell Therapy in Refractory Aggressive Lymphoma. *Mol Ther*. 2017;25(1):285–295.

4. Maude SL et al. Chimeric Antigen Receptor T Cells for Sustained Remissions in Leukemia. *New England Journal of Medicine*. 2014;371(16):1507–1517.

5. Lee DW et al. T cells expressing CD19 chimeric antigen receptors for acute lymphoblastic leukaemia in children and young adults: a phase 1 dose-escalation trial. *Lancet*. 2014;385(9967):517–528.

6. Turtle CJ et al. Durable Molecular Remissions in Chronic Lymphocytic Leukemia Treated With CD19-Specific Chimeric Antigen Receptor-Modified T Cells After Failure of Ibrutinib. *J Clin Oncol*. 2017;35(26):3010–3020.

7. Turtle CJ et al. Immunotherapy of non-Hodgkins lymphoma with a defined ratio of CD8+ and CD4+ CD19-specific chimeric antigen receptor-modified T cells. *Sci Transl Med*. 2016;8(355):355ra116.

8. Brudno JN, Kochenderfer JN. Toxicities of chimeric antigen receptor T cells: recognition and management. *Blood*. 2016;127(26):3321–3330.

9. Bonifant CL, Jackson HJ, Brentjens RJ, Curran KJ. Toxicity and management in CAR T-cell therapy. *Mol Ther Oncolytics*. 2016;3:16011.

10. Bedoya F, Frigault MJ, Maus MV. The Flipside of the Power of Engineered T Cells: Observed and Potential Toxicities of Genetically Modified T Cells as Therapy. *Mol Ther*. 2017;25(2):314–320.

11. Jackson HJ, Rafiq S, Brentjens RJ. Driving CAR T-cells forward. *Nature reviews Clinical oncology*. 2016;13(6):370–383.

12. Gill S, Maus MV, Porter DL. Chimeric antigen receptor T cell therapy: 25years in the making. *Blood Reviews*. 2015;30(3):157–167.

13. Dotti G, Gottschalk S, Savoldo B, Brenner MK. Design and development of therapies using chimeric antigen receptor-expressing T cells. *Immunol Rev*. 2013;257(1):107–126.

14. Lee DW et al. Current concepts in the diagnosis and management of cytokine release syndrome. *Blood*. 2014;124(2):188–195.

15. Davila ML et al. Efficacy and toxicity management of 19-28z CAR T cell therapy in B cell acute lymphoblastic leukemia. *Sci Transl Med*. 2014;6(224):224ra25.

16. Maude SL, Barrett D, Teachey DT, Grupp SA. Managing cytokine release syndrome associated with novel T cell-engaging therapies. *Cancer J*. 2014;20(2):119–122.

17. Teachey DT et al. Identification of Predictive Biomarkers for Cytokine Release Syndrome after Chimeric Antigen Receptor T-cell Therapy for Acute Lymphoblastic Leukemia. *Cancer Discov*. 2016;6(6):664–679.

18. Feng K et al. Phase I study of chimeric antigen receptor modified T cells in treating HER2-positive advanced biliary tract cancers and pancreatic cancers. *Protein Cell*. [published online ahead of print: July 14, 2017]; doi:10.1007/s13238-017-0440-4

19. Thistlethwaite FC et al. The clinical efficacy of first-generation carcinoembryonic antigen (CEACAM5)-specific CAR T cells is limited by poor persistence and transient pre-conditioning-dependent respiratory toxicity. *Cancer Immunol Immunother*. 2017;66(11):1425–1436.

20. Turtle CJ et al. CD19 CAR–T cells of defined CD4+:CD8+ composition in adult B cell ALL patients. *Journal of Clinical Investigation*. 2016;126(6):2123–2138.

21. Brentjens RJ et al. CD19-targeted T cells rapidly induce molecular remissions in adults with chemotherapy-refractory acute lymphoblastic leukemia. *Sci Transl Med*. 2013;5(177):177ra38.

22. Kochenderfer JN et al. B-cell depletion and remissions of malignancy along with cytokine-associated toxicity in a clinical trial of anti-CD19 chimeric-antigen-receptor-transduced T cells. *Blood*. 2011;119(12):2709–2720.

23. Grupp SA et al. Chimeric antigen receptor-modified T cells for acute lymphoid leukemia. *N Engl J Med*. 2013;368(16):1509–1518.

24. Lamers CHJ et al. Treatment of metastatic renal cell carcinoma with autologous T-lymphocytes genetically retargeted against carbonic anhydrase IX: first clinical experience. *J Clin Oncol*. 2006;24(13):e20–e22.

25. Morgan RA et al. Case report of a serious adverse event following the administration of T cells transduced with a chimeric antigen receptor recognizing ERBB2. *Mol Ther*. 2010;18(4):843–851.

26. Linette GP et al. Cardiovascular toxicity and titin cross-reactivity of affinity-enhanced T cells in myeloma and melanoma. *Blood*. 2013;122(6):863–871.

27. Hammill JA et al. Designed ankyrin repeat proteins are effective targeting elements for chimeric antigen receptors. *Journal for ImmunoTherapy of Cancer*. 2015;3(55). doi:10.1186/s40425-015-0099-4

28. Lamers CH et al. Treatment of metastatic renal cell carcinoma with CAIX CAR-engineered T cells: clinical evaluation and management of on-target toxicity. *Mol Ther*. 2013;21(4):904–912.

29. Smith JB et al. Tumor Regression and Delayed Onset Toxicity Following B7-H4 CAR T Cell Therapy. *Mol Ther*. 2016;24(11):1987–1999.

30. van der Stegen SJC et al. a Window of Therapeutic Opportunity? ErbB-Retargeted Human T Cells: Identifying Release Syndrome Induced by Preclinical In Vivo Modeling of Cytokine. *The Journal of Immunology*. 2013;191(9):4589–4598.

31. Globerson-Levin A, Waks T, Eshhar Z. Elimination of progressive mammary cancer by repeated administrations of chimeric antigen receptor-modified T cells. *Mol Ther*. 2014;22(5):1029–1038.

32. VanSeggelen H et al. T Cells Engineered With Chimeric Antigen Receptors Targeting NKG2D Ligands Display Lethal Toxicity in Mice. *Mol Ther*. 2015;23(10):1600–1610.

33. Tran E et al. Immune targeting of fibroblast activation protein triggers recognition of multipotent bone marrow stromal cells and cachexia. *J Exp Med*. 2013;210(6):1125–1135.

34. Cheadle EJ et al. Differential role of Th1 and Th2 cytokines in autotoxicity driven by CD19-specific second-generation chimeric antigen receptor T cells in a mouse model. *J Immunol*. 2014;192(8):3654–3665.

35. Chinnasamy D et al. Gene therapy using genetically modified lymphocytes targeting VEGFR-2 inhibits the growth of vascularized syngenic tumors in mice. *J Clin Invest*. 2010;120(11):3953–3968.

36. Hay KA et al. Kinetics and biomarkers of severe cytokine release syndrome after CD19 chimeric antigen receptor-modified T-cell therapy. *Blood*. 2017;130(21):2295–2306.

37. Porter DL et al. Chimeric antigen receptor T cells persist and induce sustained remissions in relapsed refractory chronic lymphocytic leukemia. *Sci Transl Med*. 2015;7(303):303ra139.

38. Sommermeyer D et al. Chimeric antigen receptor-modified T cells derived from defined CD8+ and CD4+ subsets confer superior antitumor reactivity in vivo. *Leukemia*. 2015;30(2):492–500.

39. Torikai H et al. A foundation for universal T-cell based immunotherapy: T cells engineered to express a CD19-specific chimeric-antigen-receptor and eliminate expression of endogenous TCR. *Blood*. 2012;119(24):5697–5705.

40. Ren J et al. A versatile system for rapid multiplex genome-edited CAR T cell generation. *Oncotarget*. 2017;8(10):17002–17011.

41. Qasim W et al. Molecular remission of infant B-ALL after infusion of universal TALEN gene-edited CAR T cells. *Sci Transl Med*. 2017;9(374):eaaj2013.

42. Cellectis. Press Release: Cellectis Reports Clinical Hold of UCART123 Studies. *http://wwwcellectiscom/en/press/cellectis-reports-clinical-hold-of-ucart123-studies*. 2017;

43. Brentjens RJ et al. CD19-targeted T cells rapidly induce molecular remissions in adults with chemotherapy-refractory acute lymphoblastic leukemia. *Sci Transl Med*. 2013;5(177):177ra38.

44. Singh N et al. Monocyte lineage-derived IL-6 does not affect chimeric antigen receptor T-cell function. *Cytotherapy*. 2017;19(7):867–880.

45. Till BG et al. Adoptive immunotherapy for indolent non-Hodgkin lymphoma and mantle cell lymphoma using genetically modified autologous CD20-specific T cells. *Blood*. 2008;112(6):2261–2271.

46. Pule MA et al. Virus-specific T cells engineered to coexpress tumor-specific receptors: persistence and antitumor activity in individuals with neuroblastoma. *Nat Med*. 2008;14(11):1264–1270.

47. Zhao Z et al. Structural Design of Engineered Costimulation Determines Tumor Rejection Kinetics and Persistence of CAR T Cells. *Cancer Cell*. 2015;28(4):415–428.

48. Carpenito C et al. Control of large, established tumor xenografts with genetically retargeted human T cells containing CD28 and CD137 domains. *Proc Natl Acad Sci USA*. 2009;106(9):3360–3365.

49. Chen L, Flies DB. Molecular mechanisms of T cell co-stimulation and co-inhibition. *Nat Rev Immunol*. 2013;13(4):227–242.

50. Kawalekar OU et al. Distinct Signaling of Coreceptors Regulates Specific Metabolism Pathways and Impacts Memory Development in CAR T Cells. *Immunity*. 2016;44(2):380–390.

51. Long AH et al. 4-1BB costimulation ameliorates T cell exhaustion induced by tonic signaling of chimeric antigen receptors. *Nat Med*. 2015;21(6):581–590.

52. Fitzgerald JC et al. Cytokine Release Syndrome After Chimeric Antigen Receptor T Cell Therapy for Acute Lymphoblastic Leukemia. *Critical Care Medicine*. 2017;45(2):e124.

53. Brogdon J, June CH, Loew A, Maus MV, Scholler J. Treatment of cancer using humanized anti-cd19 chimeric antigen receptor 2014; (US20140271635 A1).

54. Allan SE et al. Generation of Potent and Stable Human CD4+ T Regulatory Cells by Activation-independent Expression of FOXP3. *Molecular Therapy*. 2007;16(1):194–202.

55. Rabinovich BA et al. Visualizing fewer than 10 mouse T cells with an enhanced firefly luciferase in immunocompetent mouse models of cancer. *Proc Natl Acad Sci USA*. 2008;105(38):14342–14346.

56. Dull T et al. A third-generation lentivirus vector with a conditional packaging system. *J Virol*. 1998;72(11):8463–8471.

57. Hammill JA, Afsahi A, Bramson JL, Helsen CW. Viral Engineering of Chimeric Antigen Receptor Expression on Murine and Human T Lymphocytes. In: Ursini-Siegel J, Beauchemin N eds. *The Tumor Microenvironment. Methods in Molecular Biology*. Humana Press, New York, NY; 2016:137–157

58. Bertsimas D, Kallus N. The Power of Optimization Over Randomization in Designing Experiments Involving Small Samples. *Operations Research*. 2015;63(4):868–876.

59. Breen EJ, Tan W, Khan A. The Statistical Value of Raw Fluorescence Signal in Luminex xMAP Based Multiplex Immunoassays. *Sci Rep*. 2016;6:26996.
60. Adler D, Murdoch D. rgl: 3D Visualization Using OpenGL. *https://cranr-projectorg/web/packages/rgl/indexhtml*.

61. Warnes GR et al. gplots: Various R Programming Tools for Plotting Data. *https://cranr-projectorg/web/packages/gplots/indexhtml*.

62. Smyth GK. limma: Linear Models for Microarray Data. In: Gentleman R, Carey V, Huber W, Irizarry R, Dudoit S eds. *Bioinformatics and Computational Biology Solutions Using R and Bioconductor. Statistics for Biology and Health.* New York: Springer; 2005:397–420

63. Benjamini Y, Hochberg Y. Controlling the false discovery rate: a practical and powerful approach to multiple testing. *Journal of the Royal Statistical Society Series B (Methodological)*. 1995;57(1):289–300.

64. Kwiecien JM, Blanco M, Fox JG, Delaney KH, Fletch AL. Neuropathology of bouncer Long Evans, a novel dysmyelinated rat. *Comp Med*. 2000;50(5):503–510.

Figure Legends:

Figure 1. A comparison between anti-HER2 DARPin-targeted first- and second-generation CAR-T cells *in vitro* and *in vivo*. (**A**) Schematics of the dual-promoter lentiviral (LV) gene cassettes used to generate anti-HER2 DARPin-targeted first- or second-generation CAR-T cells (structural details as shown; TM = transmembrane, IC = intracellular, myc = Myc tag), or CAR-negative NGFR-T cells; in all cases truncated NGFR (tNGFR) is included as a transduction marker. (**B**) Expression of CARs on the surface of engineered ($NGFR^+$) T cells as determined by flow cytometry (upstream gating strategy: lymphocytes → singlets → $NGFR^+$). Mean fluorescence intensity (MFI) for CAR expression is shown in brackets. Representative results have been replicated in 2-4 additional independent experiments (*data not shown*). (**C**-**D**) Production of IFN-γ (**C**) and TNF-α (**D**) upon CAR-T cell stimulation with $HER2^+$ (OVCAR-3; dark grey squares) or $HER2^-$ (LOX-IMVI; light grey circles) human tumor cell lines was measured by intracellular cytokine staining (ICS) and subsequent flow cytometry (upstream gating strategy: lymphocytes → singlets → $CD4^+$ *or* $CD8^+$ T cells). Percent cytokine production was normalized for transduction (transduction ranges observed: DARPin-28z = 39-60%, DARPin-BBz = 33-52%, DARPin-z = 25-63%, NGFR = 63-86%). Each point shows data from a single independent experiment (n = 3-5 per LV construct); black lines indicate mean values. (**E**-**F**) Cytotoxicity across various effector:target (E:T) ratios with LOX-IMVI (**E**) or OVCAR-3 (**F**) tumor cell targets; ratios are based on total T cell numbers and have not been normalized for transduction. Error bars = standard error of the mean (SEM). Data from n = *x* independent experiments; DARPin-z = 4, DARPin-28z = 5, DARPin-BBz = 4, NGFR = 3. (**G**-**J**) OVCAR-3 tumor-bearing NRG mice were treated with 2.0×10^6 engineered-T cells (DARPin-28z (black circles), DARPin-BBz (blue squares), or DARPin-z (red triangles) as indicated) or an equal or greater number of NGFR-T cells (grey diamonds). Mice were monitored over time for (**G**) tumor volume, (**H**) core body temperature, (**I**) weight, and (**J**) survival. Data are pooled from two independent experiments, n = 8 for CAR groups, n = 7 for NGFR group. Lines become dashed after the first mouse in the group succumbs to toxicity. Error bars = standard deviation (SD). (**K**-**L**) OVCAR-3 tumor-bearing NRG mice were treated with 6.0×10^6 CAR-engineered-T cells or an equal or greater number of NGFR-T cells. Mice were monitored over time for (**K**) weight and (**L**) survival. Data are pooled from one to two independent experiments with n = *x* mice/treatment; DARPin-28z = 7, DARPin-BBz = 3, DARPin-z = 4, NGFR = 4. Error bars = standard deviation (SD). A one-way ANOVA followed by post hoc two-tailed t-tests (as needed) or log-rank tests were used for statistical analyses. P-values as indicated or N.S. = not significant, * = $p < 0.05$.

Figure 2. DARPin-28z-T cells activated in the lungs and heart, resulting in a systemic cytokine storm. OVCAR-3 tumor-bearing NRG mice were treated with 6×10^6 effective DARPin-28z- or a matched number of NGFR-T cells. (**A**-**F**) Mice were sacrificed at 1, 3, 5 or 7d post-ACT1 for total body perfusion, fixation, necropsy, and histological analysis. (**A**) Hematoxylin and eosin (H&E) staining of the lungs at 20X magnification (scale bars = 100μm); **V** indicates vasculature. (**B**) Immunohistochemistry (IHC) for human CD3 in the lungs at 20X magnification (scale bars = 100μm) or 60X magnification (zoom-in; scale bars = 50μm). (**C**) H&E or CD3 IHC staining of the heart at 20X magnification (scale bars = 100μm); arrow indicates aberrant region of inflammation along the right heart wall. (**D**) CD3 IHC staining of the tumor at 20X magnification (scale bars = 100μm). Representative images from n = 2-3 mice are shown. Findings have been recapitulated in 1-2 additional independent experiments. (**E**) Multiplex immunofluorescence (IF) was performed on lung tissue at 7d post-ACT; tissues were stained for CD8 (cyan), CD4 (yellow), DNA (DAPI, blue) and a proliferation marker (Ki-67, magenta). Data are representative of 3 mice, n = 3 images/mouse (scale bars = 100μm). (**F**) Quantification of pulmonary multiplex IF images. Error bars = standard deviation. Two-tailed t-tests were used for statistical analysis: * = $p < 0.05$, *** = $p < 0.001$. (**G**) Mice were bled at 1, 3, 5, or 7d post-ACT1 for multiplex analysis of human serum cytokine content; a globally normalized heat map of log2-transformed human cytokine fluorescence readings is shown. Each square is data from one mouse. Colorimetric scale bar indicates minimum, average, and maximum values on map. Results are consistent with those observed in an additional two independent experiments.

Figure 3. DARPin-28z-T cells were differentially toxic *in vivo*, dependent upon the PBMC donor used for CAR-T cell generation. (**A**) Expression of DARPin-28z on the surface of transduced T cells (upstream gating strategy: lymphocytes → singlets → $NGFR^+$) generated from three different PBMC sources (donors: MAC026 (gold/triangles), MAC014 (pink/circles), or LEUK001 (teal/squares)) as determined by flow cytometry and compared to a secondary only staining control (dashed histogram). Results were replicated in an additional independent experiment (*data not shown*). (**B**-**C**) Production of IFN-γ (**B**) and TNF-α (**C**) by $CD4^+$ or $CD8^+$ DARPin-28z-T cells after exposure to $HER2^+$ (OVCAR-3; dark grey squares) or $HER2^-$ (LOX-IMVI; light grey circles) tumor cell lines. Each data point shows data from a single independent experiment (n = 4-6 per donor); black lines indicate mean values. (**D**-**E**) Cytotoxicity against $HER2^-$ (**D**) or $HER2^+$ (**E**) tumor cell lines. Error bars = SEM. Data from n = *x* independent experiments; MAC014 = 4, LEUK001 = 5, MAC026 = 6. (**F**) Composition of $CD4^+$ or $CD8^+$ cells in DARPin-28z-T cell cultures (d13-14) determined using flow cytometry (upstream gating strategy: lymphocytes → singlets → $NGFR^+$). Error bars = SD. Data from n

= *x* independent experiments; MAC014 = 5 (2 unique PBMC preparations), LEUK001 = 6 (1 PBMC preparation), MAC026 = 12 (5 unique PBMC preparations). (**G-L**) OVCAR-3 tumor-bearing NRG mice were treated with 6.0×10^6 (**G-I**) or 1.7-2.0×10^6 (**J-L**) DARPin-28z-T cells produced from MAC014, LEUK001, or MAC026 PBMCs or an equal or greater number of NGFR-T cells (grey/diamonds; donor: MAC026 (**G-I**) or LEUK001 (**J-L**)). Mice were monitored over time for changes in weight (**G**,**J**), tumor volume (**H**,**K**), and survival (**I**,**L**). Data pooled from *x* independent experiments (n = *y* mice total); (**G-I**) MAC014 = 2 (n = 10), LEUK001 = 3 (n = 13), MAC026 = 4 (n = 16), NGFR = 1 (n = 4), (**J-L**) MAC014 = 1 (n = 5), LEUK001 = 2 (n = 8; this data is also displayed in Fig. 1G-I), MAC026 = 1 (n = 3), NGFR = 1 (n = 3). Lines become dashed after the first mouse in the group succumbs to toxicity. Error bars = SD. A one-way ANOVA followed by post hoc two-tailed t-tests (as needed) or log-rank tests were used for statistical analyses. P-values as indicated or N.S. = not significant, * = $p < 0.05$, *** = $p < 0.001$.

Figure 4. $CD4^+$ DARPin-28z-T cells were the drivers of toxicity, but did not wholly account for donor-to-donor variability. DARPin-28z-T cells were generated from MAC014 PBMCs that were unselected or enriched for $CD4^+$ or $CD8^+$ T cells via negative magnetic selection. (**A**) Purity of $CD4^+$ and $CD8^+$ cells on day 0 (post-sort, pre-activation/engineering) and after 14 days in culture (post-activation/engineering) was assessed by flow cytometry; representative data is shown (upstream gating strategy: lymphocytes → singlets). Results are representative of n = 4-8 independent experiments. (**B-D**) OVCAR-3 tumor-bearing or tumor-free NRG mice were treated with DARPin-28z-T cells generated from $CD4^+$ purified (black open circles), $CD8^+$ purified (grey open circles), or unselected (grey filled circles) MAC014 PBMCs (3.2×10^6 – 6.0×10^6 DARPin-28z-T cells/mouse). Mice were followed for changes in (**B**) weight (up to 14d post-ACT1 shown; each line shows data from one mouse, curves end when mice succumbed to toxicity), (**C**) survival, and (**D**) tumor volume (tumors receiving no T cells (PBS carrier solution only) are shown for comparison (black filled circles)). Lines become dashed after the first mouse in the group succumbs to toxicity. Error bars = SD. n = *x*, as indicated; bulk product and $CD8^+$ purified results have been validated in an additional independent experiment (n = 5, *data not shown*). Results have been replicated with a second PBMC donor (*data not shown*). (**E**) $CD4^+$ purified DARPin-28z-T cells were generated from MAC014 (grey lines) or MAC026 (black lines) PBMCs and used to treat tumor-bearing NRG mice at 5.0×10^6 or 1.0×10^6 engineered cells/mouse. Mice were followed for changes in weight, core body temperature (each line shows data from one mouse), and survival. Two-tailed t-tests were used for statistical analysis: * = $p < 0.05$.

Figure 5. Donor-to-donor differences in CD4$^+$ DARPin-28z-T cell associated toxicity were associated with differences in expansion and cytokine production. Purified CD4$^+$ DARPin-28z-CAR-T cells were generated from a panel of five different PBMC donors (MAC002 (orange/diamonds), MAC003 (blue/crosses), MAC014 (pink/circles), MAC026 (gold/triangles), and LEUK001 (teal/squares)); cells were co-transduced with a *firefly* luciferase-expressing lentivirus. Tumor-bearing NRG mice were treated with 2.0×10^6 DARPin-28z-T cells. Mice were followed for changes in (**A**) weight, (**B**) tumor volume (each line shows data from one mouse; n = 3 per donor), and (**C**) survival. (**D**) Bioluminescent imaging was used to follow T cell persistence and expansion; fold change in total body flux (p/s), relative to total body flux at one day post-ACT1, is presented. Per donor, data shown are average values ± SD. Unless otherwise stated, differences between donors are not significant (determined by two-tailed t-tests: N.S. = not significant, * = $p < 0.05$, ** = $p < 0.01$). (**E**) Mice were bled at one and seven days post-ACT1. Serum levels for a 13-plex panel of human cytokines were determined by multiplex analysis. Log2-transformed fluorescence intensity values were analyzed via principal component analysis. Each sphere shows data from one mouse. Grey spheres indicate data from no T cell control mice (PBS carrier treatment only). (**F**) Out of the 13 serum cytokines tested, four (GM-CSF, IFN-γ, IL-6, and MCP-1) had a strong (> 0.7) Pearson's coefficient of correlation (r) between serum cytokine level (luminex fluorescence intensity) and severity of toxicity (measured as percent weight loss at time of bleed) across all donors and doses tested; each point is data from a single mouse treated with 2.0×10^6 or 6.0×10^6 DARPin-28z-T cells from one of the five donors.

Figure 6. CAR-derived co-stimulation of CD4$^+$ engineered T cells drove toxicity via improved expansion and persistence. OVCAR-3 tumor-bearing NRG mice were treated with 2.0×10^6 (**A-C, I**) or 0.66×10^6 (**D-F**) CD4$^+$ purified CAR-T cells (DARPin-28z (black/circles), DARPin-BBz (blue/squares), or DARPin-z (red/triangles), as indicated) which had been co-transduced with *firefly* luciferase (donor: LEUK001). Mice were followed for weight (**A**,**D**), survival (**B**,**E**), and tumor volume (**C**,**F**). Data are from a single experiment; each line shows data from one mouse (n = 3 per treatment). (**G**) The relationship between toxicity (overall severity was measured as net area under the change in weight (%) over time curve, y = 0 baseline) and efficacy (overall efficacy was measured as net area under the change in tumor volume (%) over time curve, y = 0 baseline) for mice reaching experimental endpoint (59d post-ACT1). *r* = Pearson correlation coefficient. (**H**) Bioluminescent imaging data; each line shows data from one mouse. Two-tailed t-tests were used for statistical analysis: N.S. = not significant, * = $p < 0.05$. (**I**) Mice were bled eight days post-ACT for multiplex analysis of human serum cytokine content (13-plex panel). Values presented as average of n =

3 mice in pg/mL (error bars = SD). Cytokine concentrations below the range of the standard conversion curve were excluded. Statistics were calculated using log2-transformed fluorescence intensity data using a one-way ANOVA followed by post hoc two-tailed t-tests as needed.

Supplemental Figure Legends:

Supplemental Figure 1. DARPin-28z-T cell toxicity was dose-dependent. OVCAR-3 tumor-bearing NRG mice were treated with 0.66×10^6, 2.0×10^6, or 6.0×10^6 DARPin-28z-T cells or a matched number or NGFR-T cells (donor: MAC026). Mice were followed for changes in (**A**) weight, (**B**) core body temperature, (**C**) survival, and (**D**) tumor volume. Each curve indicates data from one mouse; data from 1 experiment (dose dependency results have been replicated in a second independent experiment (*data not shown*)).

Supplemental Figure 2. DARPin-28z-T cell toxicity was off-tumor. (**A**-**C**) Tumor-free NRG mice were treated with 6×10^6 effective ($NGFR^+CAR^+$) DARPin-28z- or a matched number of NGFR-T cells intravenously over two doses, 48hrs apart. Mice were followed for changes in (**A**) core body temperature, (**B**) weight, and (**C**) survival over a fourteen day period. Each curve indicates data from one mouse; representative data from 1 experiment shown (conclusions are supported by n = 7 additional independent experiments, encompassing n = 6 PBMC donors, and n = 53 total mice where DARPin-28z toxicity was observed in tumor-free mice).

Supplemental Figure 3. Murine serum cytokine levels after DARPin-28z-T cell treatment. OVCAR-3 tumor-bearing NRG mice were treated with 6×10^6 effective DARPin-28z-T cells (or an excess number of donor-matched NGFR-T cells). Mice (n = 3) were bled at 1, 3, 5, or 7d post-ACT1 for multiplex analysis of murine serum cytokine content. A globally normalized heat map of log2-transformed fluorescence readings was generated. Each square displays data from one mouse and is the average value of n = 2 technical replicates. Colorimetric scale bar indicates minimum, average, and maximum values on map.

Supplemental Figure 4. The *ex vivo* expansion of DARPin-28z-T cell cultures from PBMCs caused a donor-specific shift in the $CD4^+$:$CD8^+$ T cell ratio and may be related to a differential proliferative capacity of $CD8^+$ T cells. DARPin-28z-T cells were engineered from thawed PBMCs (various donors, as indicated (pink circles = MAC014, teal squares = LEUK001, blue crosses = MAC003, gold triangles = MAC026, grey diamonds = MAC016)) and evaluated after 14d in culture. (**A**) Freshly thawed PBMCs or the 14d DARPin-28z-T cell products they generated were stained for $CD4^+$ and $CD8^+$ and detected by flow cytometry (gating strategy: lymphocytes → singlets → $CD4^+$ vs $CD8^+$). The ratio of single-positive $CD4^+$:$CD8^+$ cells are presented. Each line indicates a single PBMC → DARPin-28z-T cell culture. (**B**) Purified $CD8^+$ or $CD4^+$ T cells were generated from thawed PBMCs via negative magnetic selection and engineered to become DARPin-28z-T cells. Fold expansion in the absolute number of $CD8^+$ or $CD4^+$ T cells in culture at d14 vs d0 are shown. Each point indicates expansion data from a single DARPin-28z-T cell culture (each from an independent experiment). Black lines indicate

mean values. (**C**) After 14d in culture, first- or second-generation-CAR-T-cells, or NGFR controls (generated from unpurified PBMCs), were evaluated for composition of $CD4^+$ single-positive T-cells using flow cytometry (gating strategy: lymphocytes → singlets → NGFR+ → $CD4^+$ vs $CD8^+$). Each point is data from one experiment. Black lines indicate mean values. Statistical significance evaluated via one-way ANOVA.

Supplemental Figure 5. $CD4^+$ purified DARPin-28z-T cells generated from a variety of PBMC donors caused similar toxicity at increased doses. Tumor-bearing NRG mice were treated with 6.0×10^6 $CD4^+$ purified DARPin-28z-T cells generated from a panel of five different PBMC donors (as indicated, orange diamonds = MAC002, blue crosses = MAC003, pink circles = MAC003, gold triangles = MAC026, teal squares = LEUK001). Mice were followed for changes in (**A**) weight (each line shows data from one mouse; n = 3-4 per donor) and (**B**) survival.

Supplemental Figure 6. DAPRin-28z-CAR-T cells generated from a five PBMC-donor panel were co-transduced with a *firefly* luciferase-expressing lentivirus to permit *in vivo* bioluminescent imaging. Purified $CD4^+$ DARPin-28z-CAR-T cells were generated from a panel of five different PBMC donors (MAC002, MAC003, MAC014, MAC026, and LEUK001); cells were co-transduced with a *firefly* luciferase-expressing lentivirus. (**A**) Expression of luciferase was determined by flow cytometry (gating strategy: lymphocytes → singlets → Luc histogram). Percent Luc^+ is indicated. Dotted histogram shows a secondary only staining control. (**B**) OVCAR-3 tumor-bearing NRG mice (n = 3 per treatment) received 2.0×10^6 $CD4^+$ purified DARPin-28z-CAR-T cells. After injection of D-luciferin substrate, mice were subjected to bioluminescent imaging at various time points post-ACT1 (as indicated). Images were acquired with aperture: f4, exposure: 1s. A white "X" indicates the mouse had succumbed to toxicity prior to the measurement.

Supplemental Figure 7. Hierarchical clustering of human serum cytokine levels. Tumor-bearing NRG mice were treated with 2.0×10^6 $CD4^+$ purified DARPin-28z-T cells generated from a panel of five different PBMC donors (MAC002 (orange), MAC003 (blue), MAC014 (pink), MAC026 (gold), and LEUK001 (teal)) or no T cells (grey). At one (**A**) or seven (**B**) days post-ACT1 mice were bled for multiplex analysis of human serum cytokine content (using a 13-plex panel). Log2-transformed fluorescence intensity values from the multiplex results (each being the average of n = 2 technical replicates) were analyzed through hierarchical clustering; heat maps were globally normalized, legends as shown. Change in weight (percent versus ACT1) and core body temperature (°C) at time of bleed for each mouse has been overlaid on the clustering data. Each column

displays data from a single mouse; n = 3 per treatment (d1), n = 1-3 per treatment (d7).

Supplemental Figure 8. Strong linear correlations between toxicity and serum cytokine concentration broken down by dose and donor. Tumor-bearing NRG mice were treated with 2.0×10^6 or 6.0×10^6 $CD4^+$ purified DARPin-28z-T cells generated from a panel of five different PBMC donors (MAC002, MAC003, MAC014, MAC026, and LEUK001). At five (6.0×10^6) or seven (2.0×10^6) days post-ACT1 mice were bled for multiplex analysis of human serum cytokine content (using a 13-plex panel). Across all donors and both doses, the level of serum cytokine (raw fluorescence intensity value; an average of n = 2 technical replicates) was compared to severity of toxicity (as measured by weight loss or core body temperature at time of bleed) using Pearson's coefficient of correlation (r). (**A**) Correlation coefficients between toxicity (weight loss *or* temperature) and serum cytokine levels are presented. For those cytokines achieving a correlation coefficient of > 0.7, data is presented graphically: (**B**) GM-CSF, (**C**) IFN-γ, (**D**) IL-6, and (**E**) MCP-1. Inset graphs display the same data broken down by dose (upper inset panel, as indicated: light purple = 2.0×10^6, dark purple = 6.0×10^6) or donor (lower inset panel, as indicated: orange diamonds = MAC002, blue crosses = MAC003, pink circles = MAC003, gold triangles = MAC026, teal squares = LEUK001). This experimental data matches that presented elsewhere in Fig. 5 and Supplemental Fig. 6, 7.

Supplemental Figure 9. Bioluminescent images of first- and second-generation anti-HER2 DARPin CAR- versus NGFR-T cell expansion *in vivo*. OVCAR-3 tumor-bearing NRG mice were treated with 2.0×10^6 or 0.66×10^6 $CD4^+$ purified CAR-T cells (DARPin-28z, DARPin-BBz, or DARPin-z) or NGFR-T cells, as indicated, which had been co-transduced with *firefly* luciferase (donor: LEUK001). Alternatively, mice were treated with carrier only (PBS; no T cells). After injection of D-luciferin substrate, mice were subjected to bioluminescent imaging at various time points post-ACT1 (as indicated). (**A**) Images acquired with aperture: f4, exposure: 1s. (**B**) Images acquired with aperture: f1, exposure: 30s; scale adjusted to enable visualization of low level signal. A white "X" indicates the mouse had succumbed to toxicity prior to the measurement.

Supplemental Figure 10. DARPin-z-T cells were toxic at increased doses. OVCAR-3 tumor-bearing NRG mice were treated with 12.0×10^6 DARPin-z-T cells, or an equal number of NGFR-T cells (donor: MAC026). Mice were monitored over time for changes in (**A**) core body temperature and (**B**) weight. Data are from a single experiment; each line shows data from one mouse (n = 4, DARPin-z; n = 3, NGFR). DARPin-z-T cell toxicity has been recapitulated in a second independent experiment (*data not shown*).

Supplemental Table Legends:

Supplemental Table 1. Human serum cytokine concentrations of DARPin-28z- or NGFR-T cell treated mice. OVCAR-3 tumor-bearing NRG mice were treated with 6×10^6 DARPin-28z-T cells (or an excess number of donor-matched NGFR-T cells). Mice were bled at 1, 3, 5, or 7d post-ACT1 for multiplex analysis of human serum cytokine content. Values presented are average serum cytokine concentrations (n = 3 mice, with n = 2 technical replicates/mouse) in pg/mL ± SEM.

Supplemental Table 2. Murine serum cytokine concentrations of DARPin-28z- or NGFR-T cell treated mice. OVCAR-3 tumor-bearing NRG mice were treated with 6×10^6 DARPin-28z-T cells (or an excess number of donor-matched NGFR-T cells). Mice were bled at 1, 3, 5, or 7d post-ACT1 for Multiplex analysis of murine serum cytokine content. Values presented are average serum cytokine concentrations (n = 3) in pg/mL ± SEM.

Figure 1.

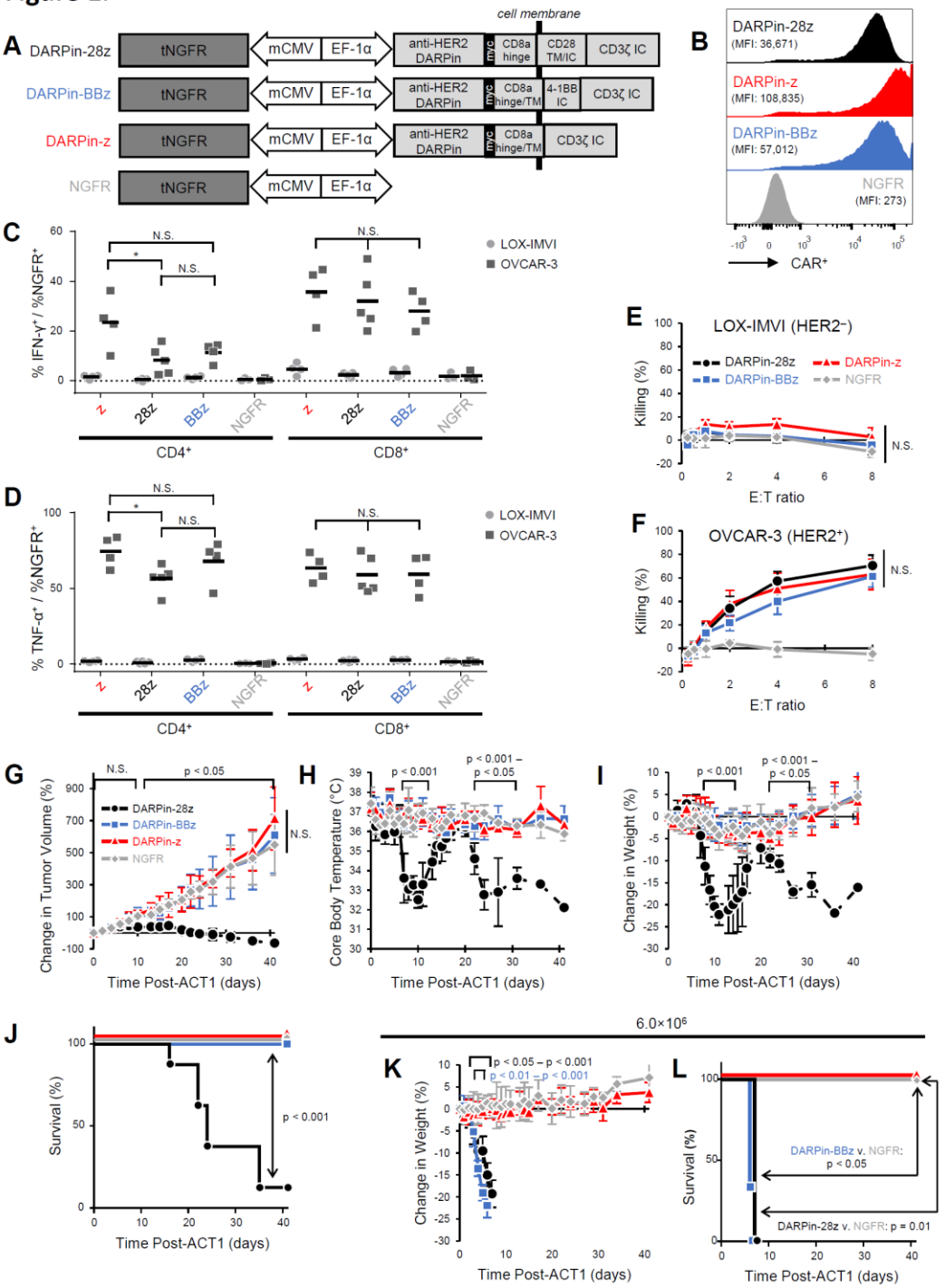
A
DARPin-28z
DARPin-BBz
DARPin-z
NGFR
tNGFR
mCMV
EF-1α
anti-HER2 DARPin
myc
CD8a hinge
CD28 TM/IC
4-1BB IC
CD3ζ IC
cell membrane
B
DARPin-28z (MFI: 36,671)
DARPin-z (MFI: 108,835)
DARPin-BBz (MFI: 57,012)
NGFR (MFI: 273)
CAR+
C
% IFN-γ+ / %NGFR+
LOX-IMVI
OVCAR-3
N.S.
CD4+
CD8+
D
% TNF-α+ / %NGFR+
E
LOX-IMVI (HER2−)
Killing (%)
E:T ratio
F
OVCAR-3 (HER2+)
G
Change in Tumor Volume (%)
Time Post-ACT1 (days)
H
Core Body Temperature (°C)
I
Change in Weight (%)
J
Survival (%)
p < 0.001
6.0×10⁶
K
L
DARPin-BBz v. NGFR: p < 0.05
DARPin-28z v. NGFR: p = 0.01

Figure 2.

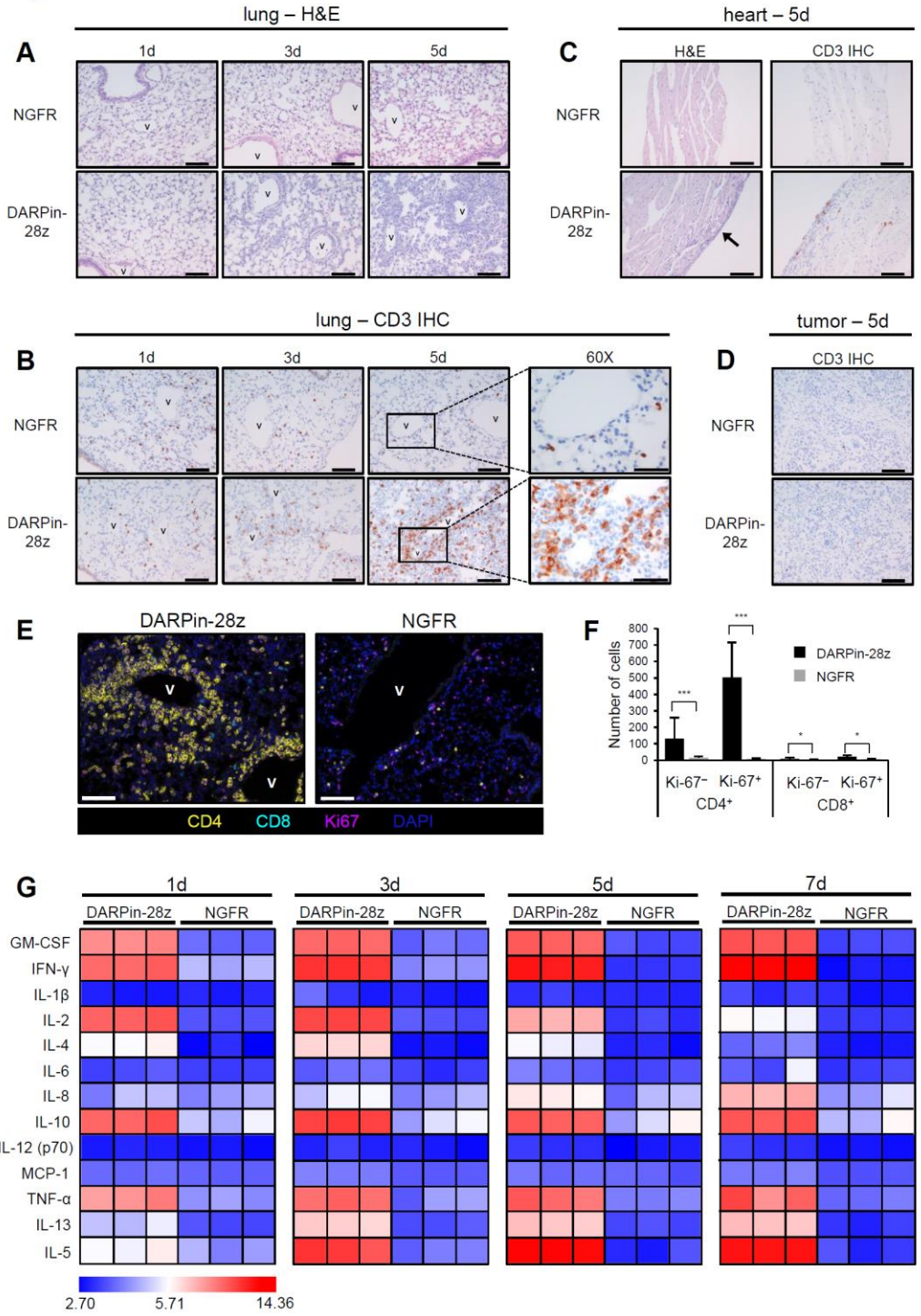
lung – H&E
A
1d
3d
5d
NGFR
DARPin-28z
heart – 5d
C
H&E
CD3 IHC
lung – CD3 IHC
B
60X
tumor – 5d
D
E
DARPin-28z
NGFR
CD4
CD8
Ki67
DAPI
F
Number of cells
Ki-67⁻ CD4⁺
Ki-67⁺ CD4⁺
Ki-67⁻ CD8⁺
Ki-67⁺ CD8⁺
G
GM-CSF
IFN-γ
IL-1β
IL-2
IL-4
IL-6
IL-8
IL-10
IL-12 (p70)
MCP-1
TNF-α
IL-13
IL-5
2.70
5.71
14.36

Figure 3.

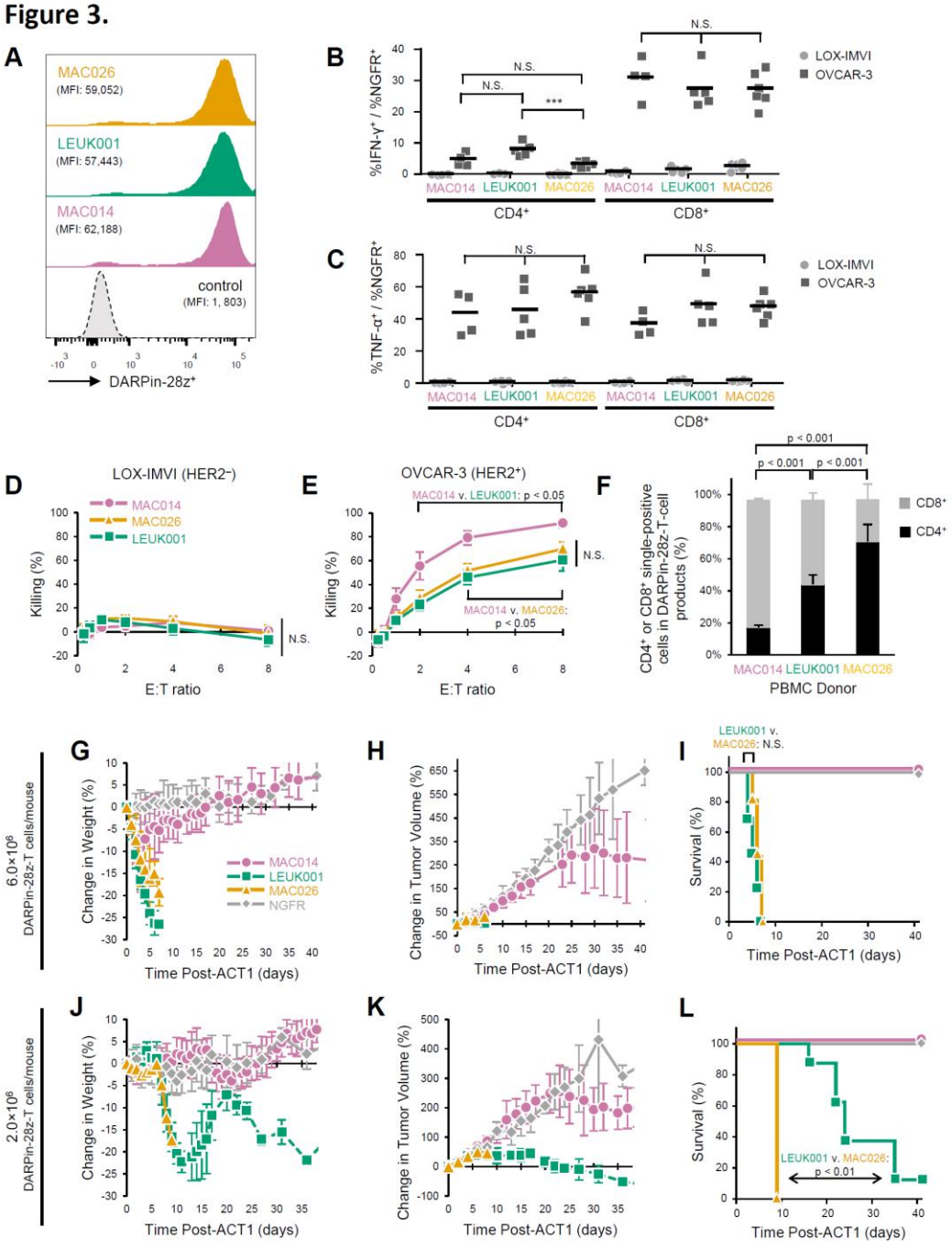
A
MAC026
(MFI: 59,052)
LEUK001
(MFI: 57,443)
MAC014
(MFI: 62,188)
control
(MFI: 1, 803)
DARPin-28z+
B
%IFN-γ+ / %NGFR+
N.S.
N.S.
***
LOX-IMVI
OVCAR-3
MAC014 LEUK001 MAC026 MAC014 LEUK001 MAC026
CD4+
CD8+
C
%TNF-α+ / %NGFR+
N.S.
N.S.
LOX-IMVI
OVCAR-3
MAC014 LEUK001 MAC026 MAC014 LEUK001 MAC026
CD4+
CD8+
D
LOX-IMVI (HER2−)
MAC014
MAC026
LEUK001
Killing (%)
N.S.
E:T ratio
E
OVCAR-3 (HER2+)
MAC014 v. LEUK001: p < 0.05
N.S.
MAC014 v. MAC026:
p < 0.05
Killing (%)
E:T ratio
F
p < 0.001
p < 0.001
p < 0.001
CD4+ or CD8+ single-positive cells in DARPin-28z-T-cell products (%)
CD8+
CD4+
MAC014 LEUK001 MAC026
PBMC Donor
G
6.0×10^6 DARPin-28z-T cells/mouse
Change in Weight (%)
MAC014
LEUK001
MAC026
NGFR
Time Post-ACT1 (days)
H
Change in Tumor Volume (%)
Time Post-ACT1 (days)
I
LEUK001 v. MAC026: N.S.
Survival (%)
Time Post-ACT1 (days)
J
2.0×10^6 DARPin-28z-T cells/mouse
Change in Weight (%)
Time Post-ACT1 (days)
K
Change in Tumor Volume (%)
Time Post-ACT1 (days)
L
Survival (%)
LEUK001 v. MAC026:
p < 0.01
Time Post-ACT1 (days)

Figure 4.

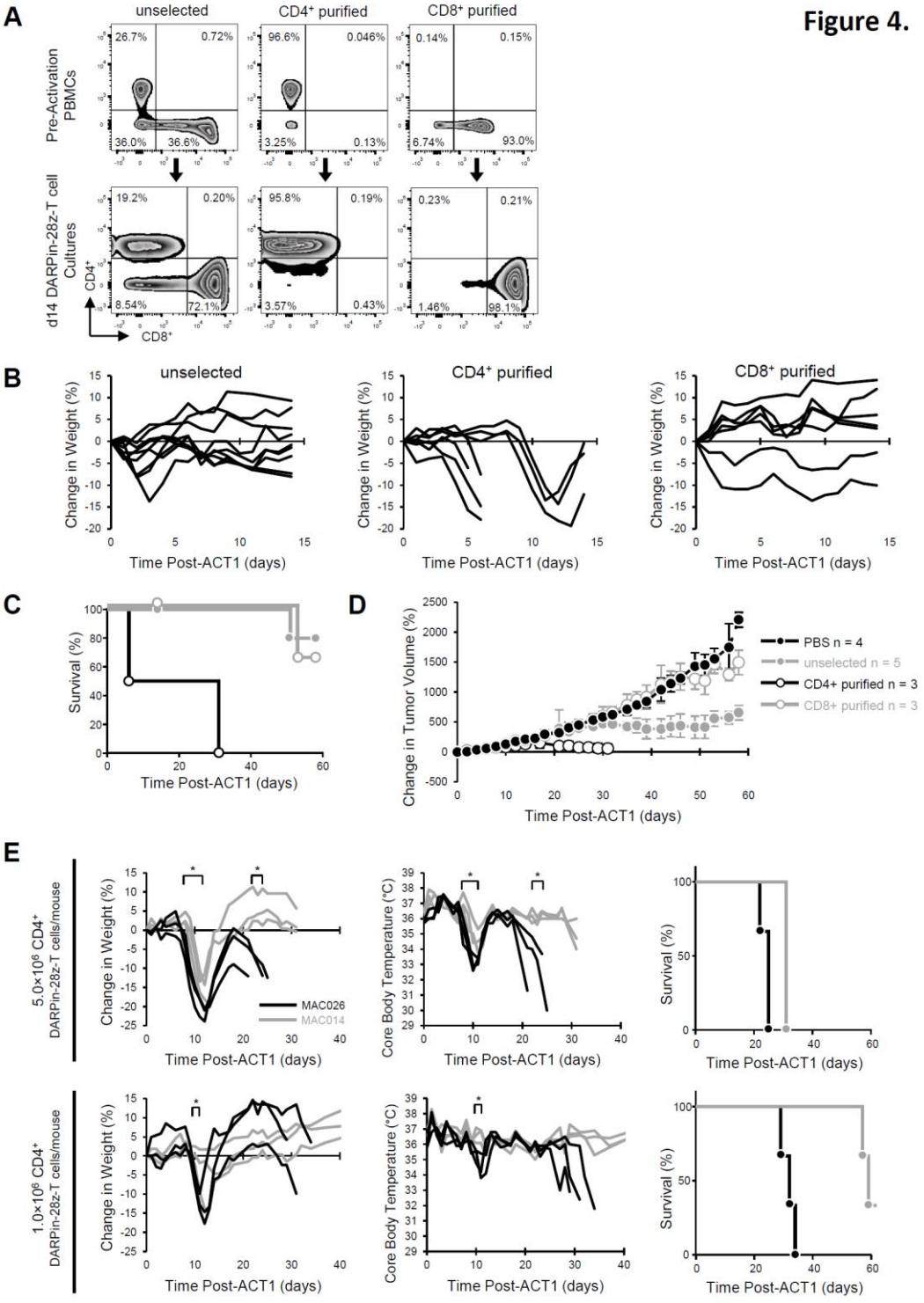
A
unselected
CD4+ purified
CD8+ purified
Pre-Activation PBMCs
d14 DARPin-28z-T cell Cultures
CD4+
CD8+
26.7%
0.72%
36.0%
36.6%
96.6%
0.046%
3.25%
0.13%
0.14%
0.15%
6.74%
93.0%
19.2%
0.20%
8.54%
72.1%
95.8%
0.19%
3.57%
0.43%
0.23%
0.21%
1.46%
98.1%
B
unselected
CD4+ purified
CD8+ purified
Change in Weight (%)
Time Post-ACT1 (days)
C
Survival (%)
Time Post-ACT1 (days)
D
Change in Tumor Volume (%)
Time Post-ACT1 (days)
PBS n = 4
unselected n = 5
CD4+ purified n = 3
CD8+ purified n = 3
E
5.0×10⁶ CD4+ DARPin-28z-T cells/mouse
1.0×10⁶ CD4+ DARPin-28z-T cells/mouse
Change in Weight (%)
Core Body Temperature (°C)
Survival (%)
Time Post-ACT1 (days)
MAC026
MAC014

Figure 5.

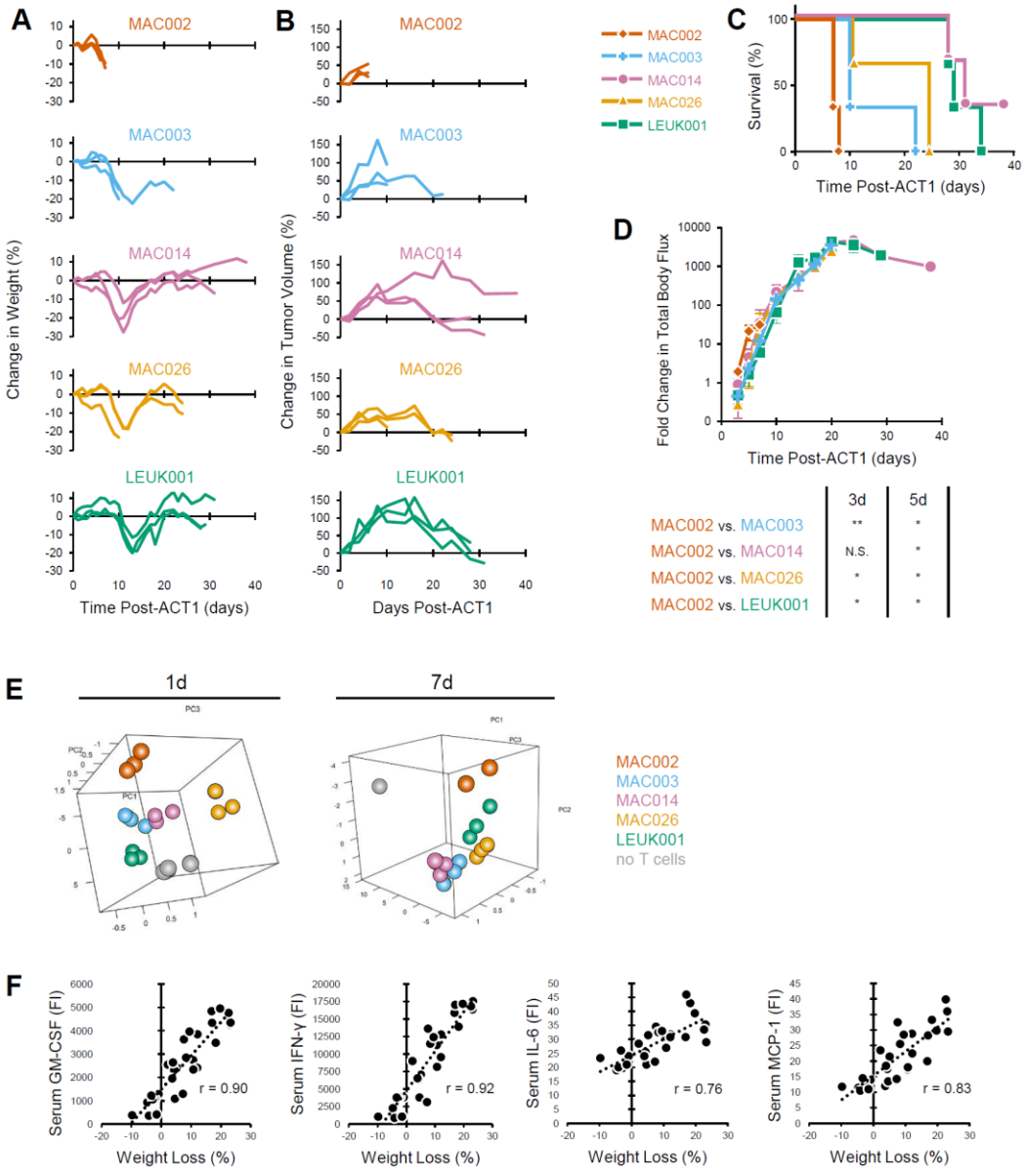
A
MAC002
MAC003
MAC014
MAC026
LEUK001
Change in Weight (%)
Time Post-ACT1 (days)
B
Change in Tumor Volume (%)
Days Post-ACT1
C
Survival (%)
Time Post-ACT1 (days)
D
Fold Change in Total Body Flux
Time Post-ACT1 (days)
3d
5d
MAC002 vs. MAC003 ** *
MAC002 vs. MAC014 N.S. *
MAC002 vs. MAC026 * *
MAC002 vs. LEUK001 * *
E
1d
7d
MAC002
MAC003
MAC014
MAC026
LEUK001
no T cells
F
Serum GM-CSF (FI)
r = 0.90
Weight Loss (%)
Serum IFN-γ (FI)
r = 0.92
Weight Loss (%)
Serum IL-6 (FI)
r = 0.76
Weight Loss (%)
Serum MCP-1 (FI)
r = 0.83
Weight Loss (%)

Figure 6.

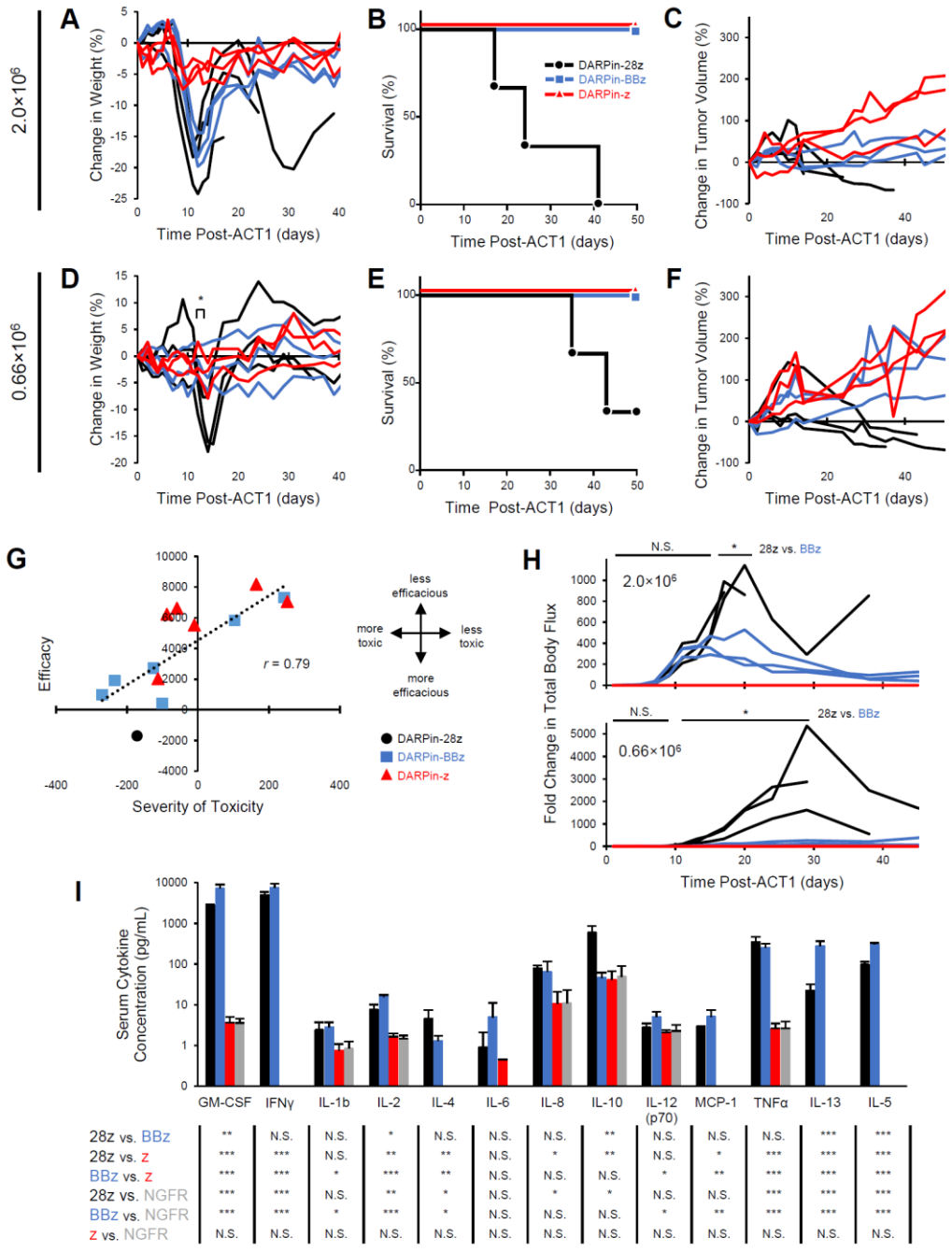
A
B
C
D
E
F
G
H
I
2.0×10⁶
0.66×10⁶
Change in Weight (%)
Survival (%)
Change in Tumor Volume (%)
Time Post-ACT1 (days)
DARPin-28z
DARPin-BBz
DARPin-z
Efficacy
Severity of Toxicity
r = 0.79
less efficacious
more toxic
less toxic
more efficacious
Fold Change in Total Body Flux
N.S.
*
28z vs. BBz
Serum Cytokine Concentration (pg/mL)
GM-CSF
IFNγ
IL-1b
IL-2
IL-4
IL-6
IL-8
IL-10
IL-12 (p70)
MCP-1
TNFα
IL-13
IL-5
28z vs. BBz ** N.S. N.S. * N.S. N.S. N.S. ** N.S. N.S. N.S. *** ***
28z vs. z *** *** N.S. ** ** N.S. * ** N.S. * *** *** ***
BBz vs. z *** *** * *** ** N.S. N.S. N.S. * ** *** *** ***
28z vs. NGFR *** *** N.S. ** * N.S. * * N.S. N.S. *** *** ***
BBz vs. NGFR *** *** * *** * N.S. N.S. N.S. * ** *** *** ***
z vs. NGFR N.S. N.S. N.S. N.S. N.S. N.S. N.S. N.S. N.S. N.S. N.S. N.S. N.S.

Supplemental Figure 1.

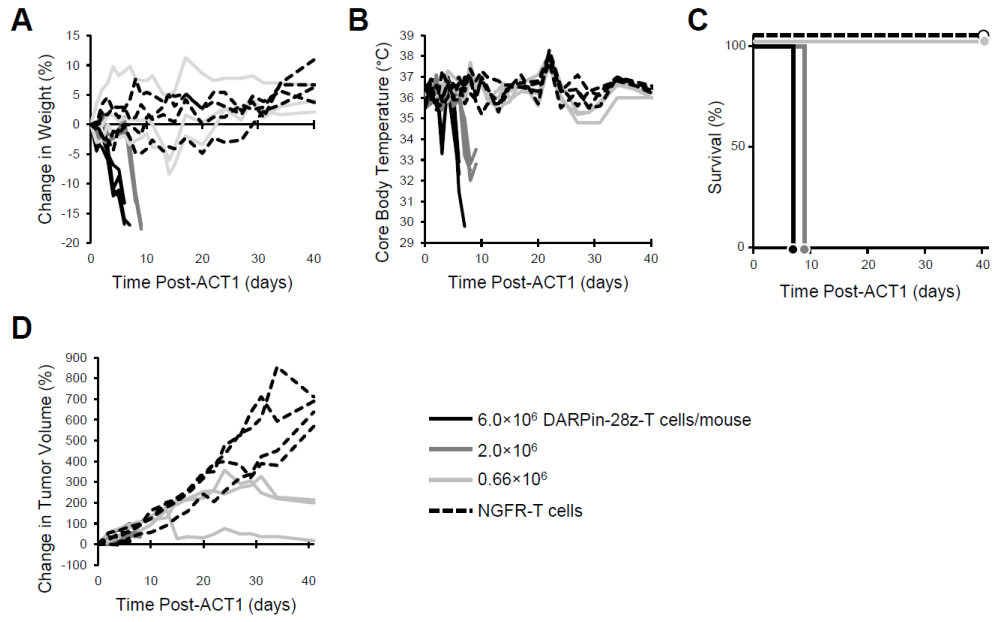

Supplemental Figure 2.

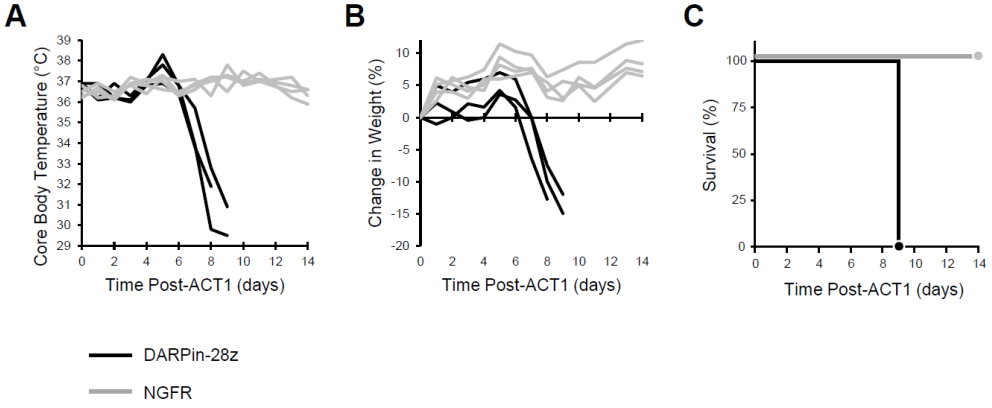

Supplemental Figure 2.

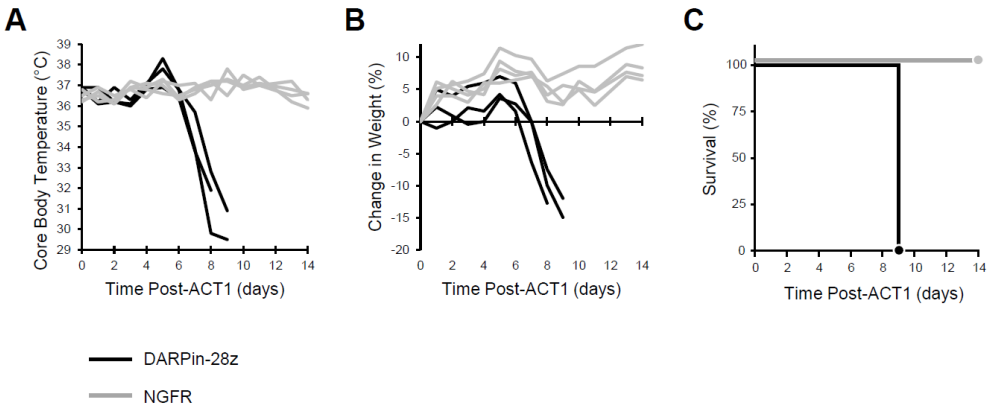

Supplemental Figure 3.

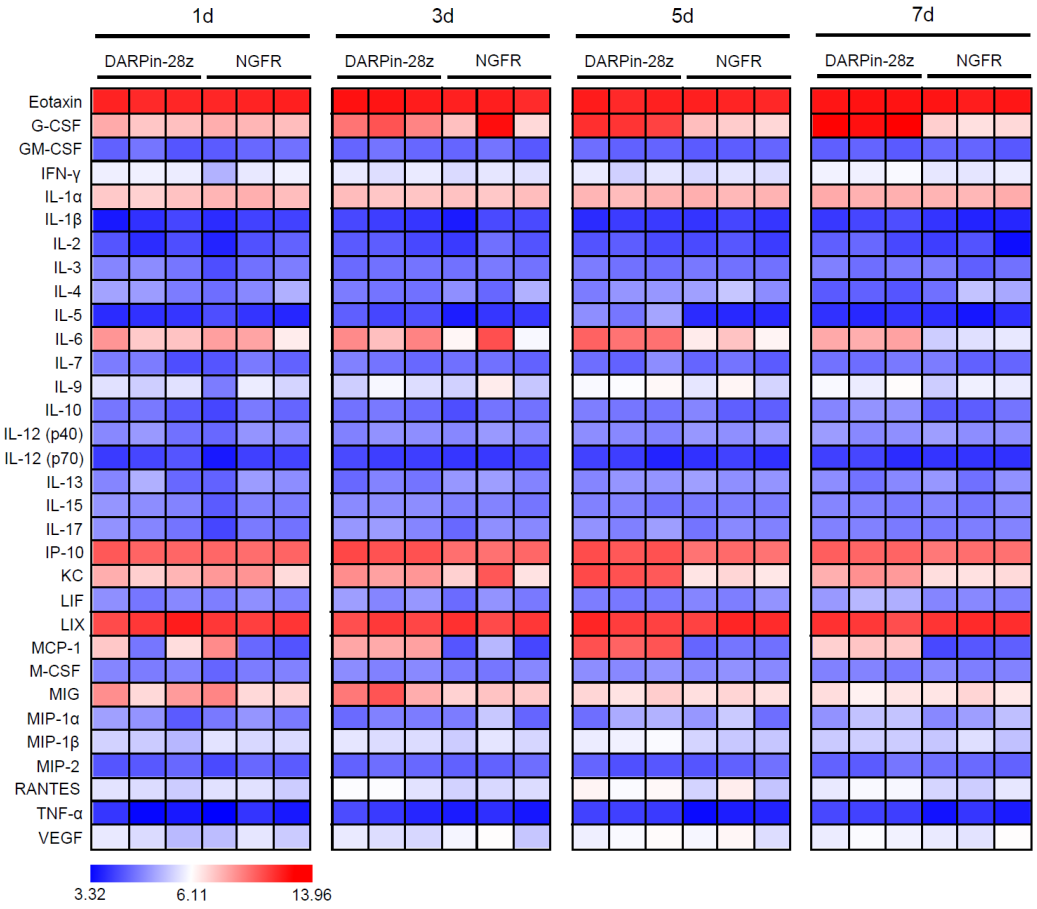

Supplemental Figure 4.

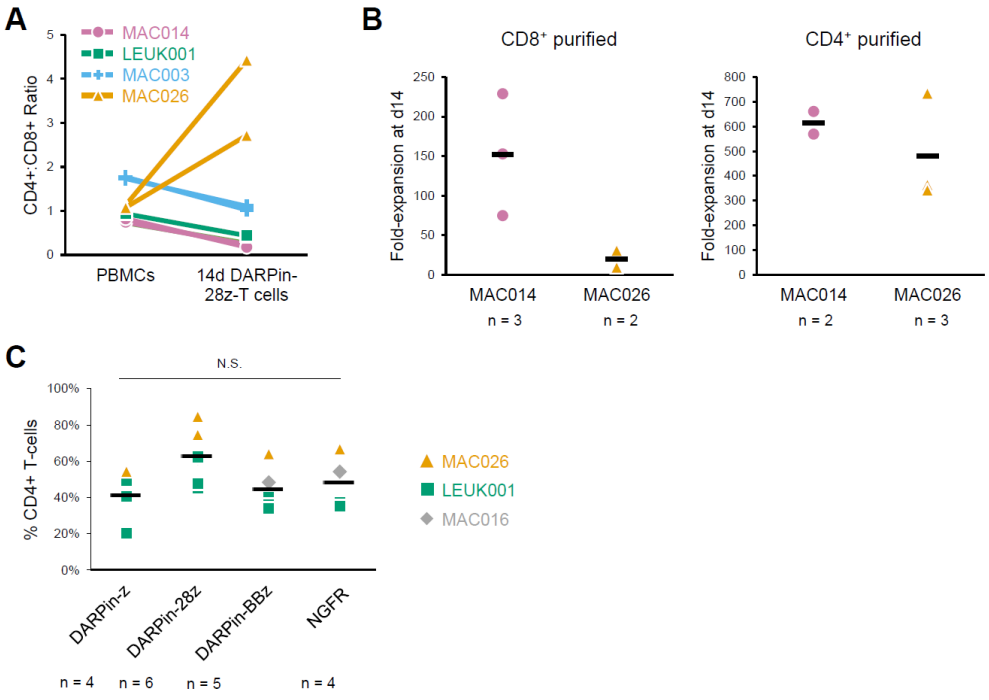

Supplemental Figure 5.

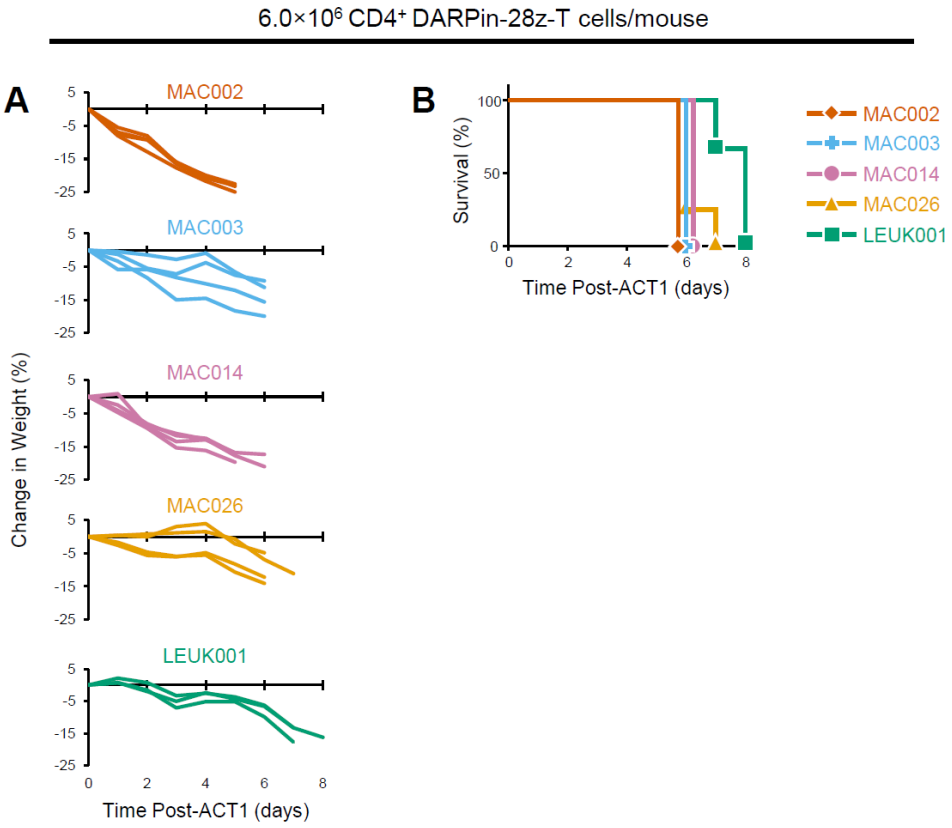

Supplemental Figure 6.

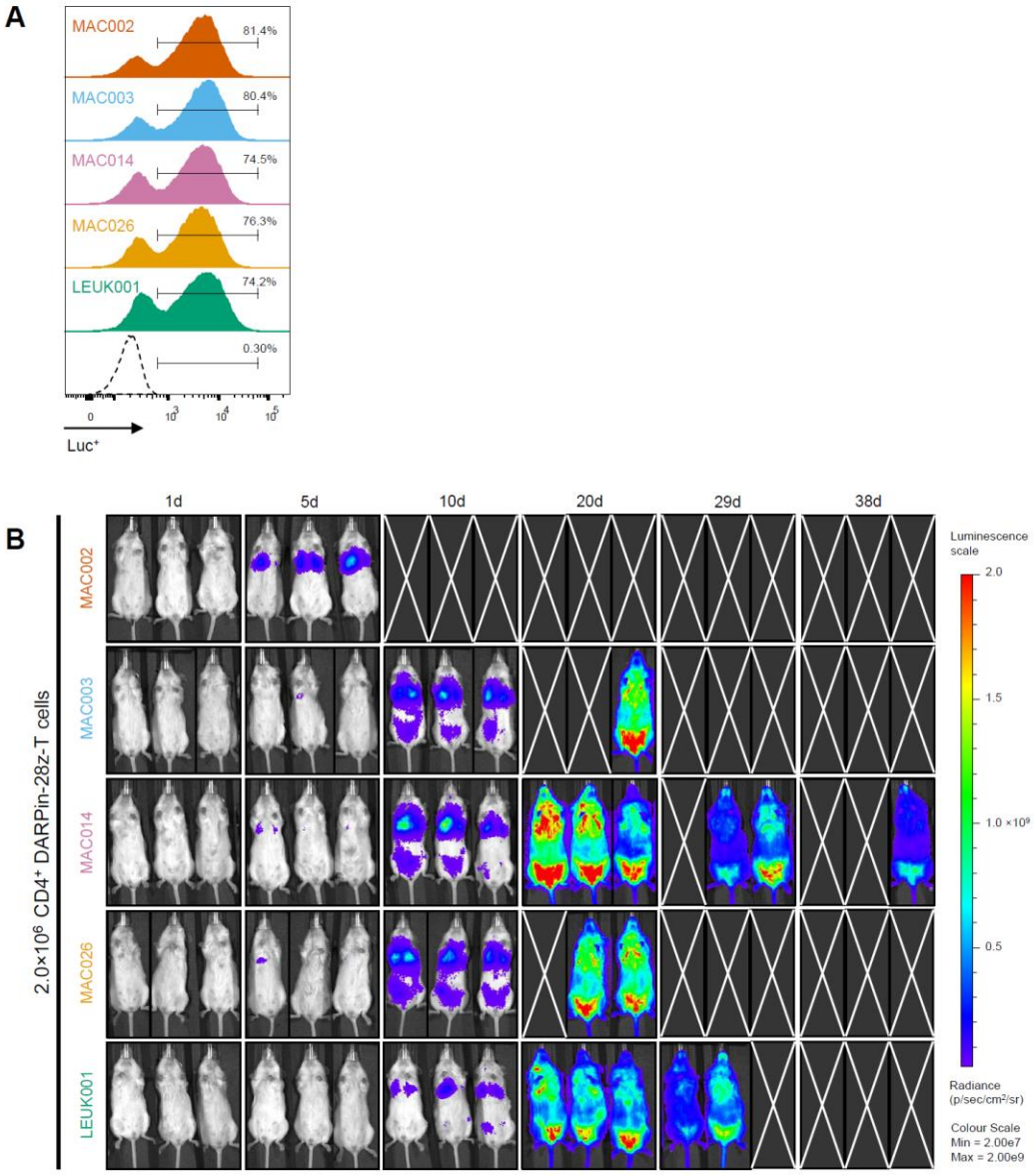

Supplemental Figure 7.

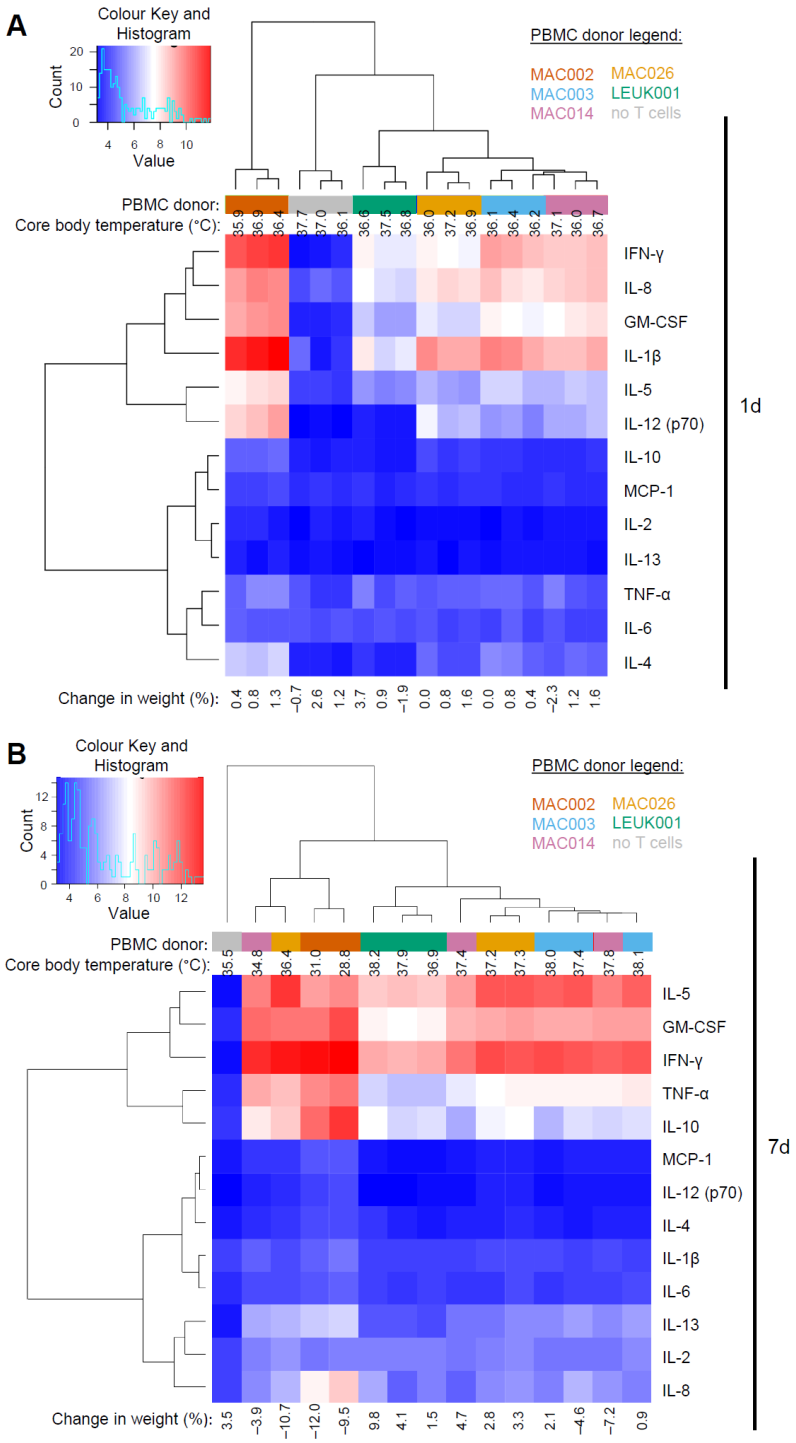

Supplemental Figure 8.

A

	Weight Loss	Core Body Temperature
GM-CSF	0.90	-0.83
IFN-γ	0.92	-0.86
IL-1b	0.64	-0.39
IL-2	-0.03	0.07
IL-4	0.64	-0.41
IL-6	0.76	-0.78
IL-8	0.42	-0.73
IL-10	0.32	-0.48
IL-12 (p70)	0.58	-0.40
MCP-1	0.83	-0.81
TNF-α	0.48	-0.64
IL-13	0.35	-0.40
IL-5	0.30	-0.27

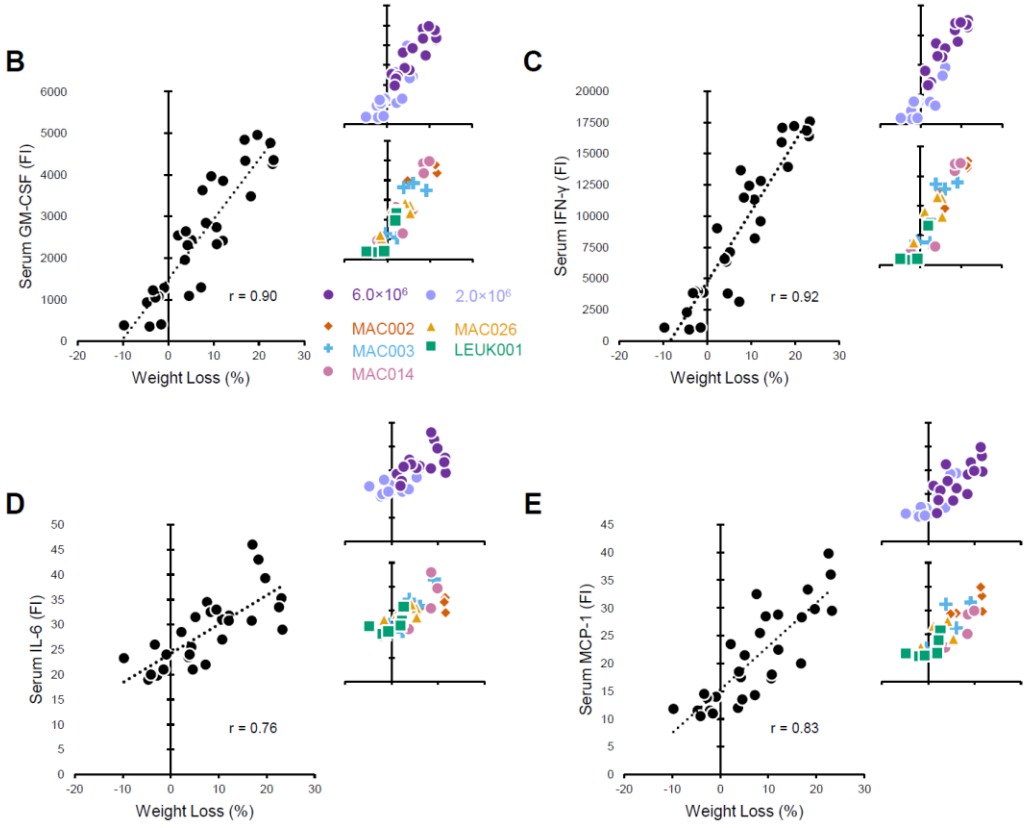

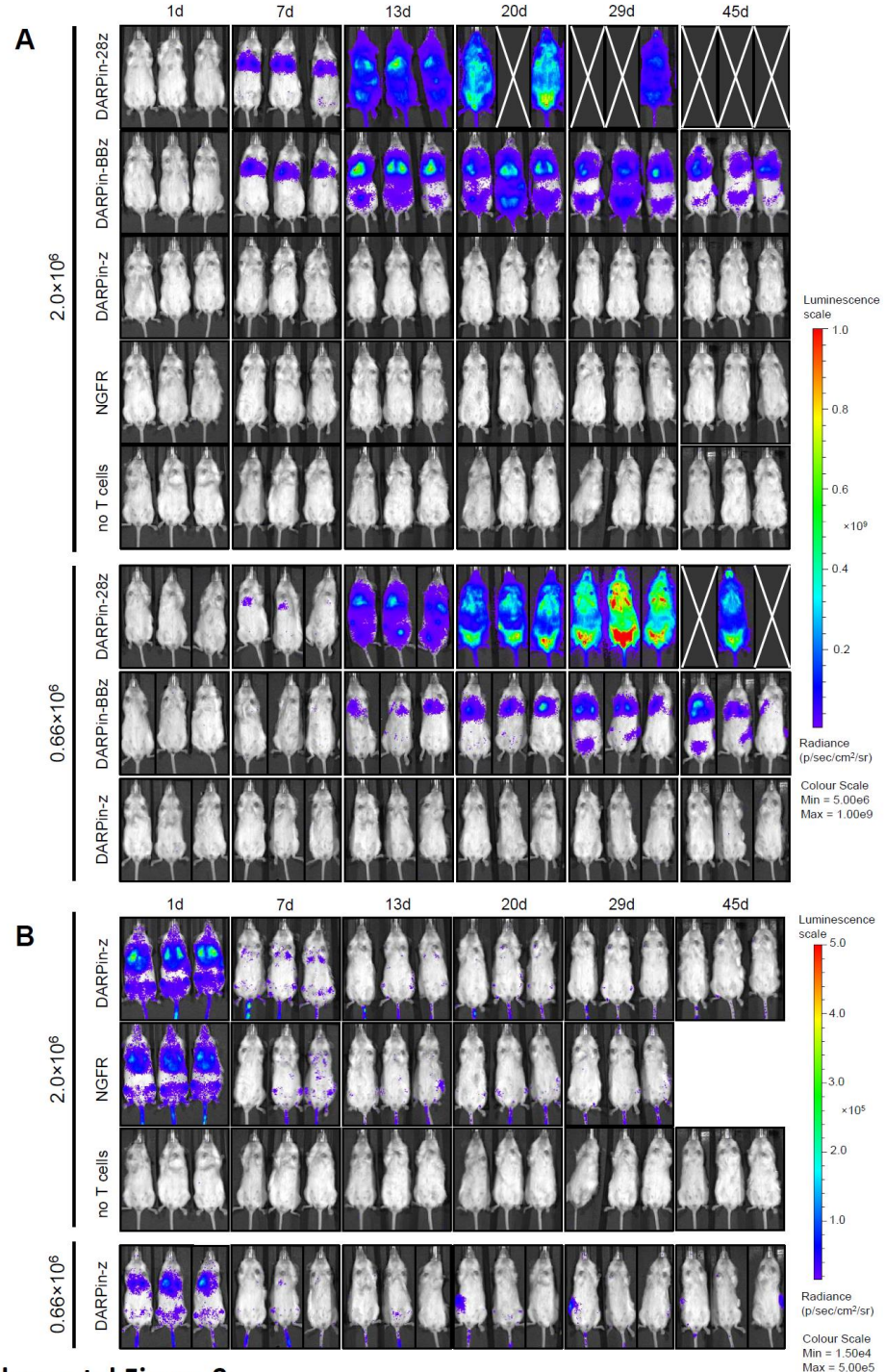

Supplemental Figure 9.

Supplemental Figure 10.

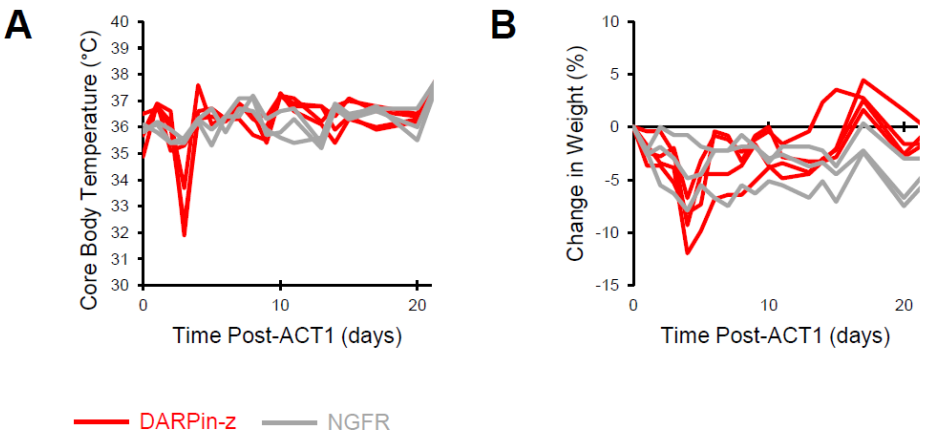

Supplemental Table 1.

	1d		3d		5d		7d	
	DARPin-28z	NGFR	DARPin-28z	NGFR	DARPin-28z	NGFR	DARPin-28z	NGFR
GM-CSF	803.0 (± 76.1)	3.9 (± 0.4)	1759.4 (± 120.2)	4.5 (± 0.9)	2023.1 (± 209.6)	2.0 (± 0.4)	2885.4 (± 172.0)	1.8 (± 0.3)
IFN-γ	445.4 (± 56.3)	4.7 (± 0.4)	1643.9 (± 128.0)	3.1 (± 0.2)	3587.5 (± 410.6)	0.6 (± 0.0)	9845.2 (± 873.0)	0.2 (± 0.1)
IL-1β	0.0 (± 0.0)	0.0 (± 0.0)	0.2 (± 0.2)	0.0 (± 0.0)	0.0 (± 0.0)	0.0 (± 0.0)	0.0 (± 0.0)	0.0 (± 0.0)
IL-2	487.8 (± 58.6)	0.5 (± 0.0)	860.2 (± 36.2)	0.5 (± 0.2)	80.7 (± 7.4)	0.1 (± 0.1)	10.1 (± 0.9)	0.0 (± 0.0)
IL-4	34.5 (± 4.5)	0.2 (± 0.2)	86.0 (± 2.1)	0.0 (± 0.0)	26.5 (± 1.5)	0.2 (± 0.2)	5.6 (± 1.0)	0.0 (± 0.0)
IL-6	0.0 (± 0.0)	0.0 (± 0.0)	0.1 (± 0.0)	0.0 (± 0.0)	0.1 (± 0.1)	0.0 (± 0.0)	0.5 (± 0.5)	0.0 (± 0.0)
IL-8	0.3 (± 0.1)	0.1 (± 0.1)	1.0 (± 0.3)	0.1 (± 0.1)	3.1 (± 0.4)	0.2 (± 0.1)	17.9 (± 2.8)	0.3 (± 0.3)
IL-10	361.9 (± 83.6)	3.2 (± 0.8)	842.4 (± 94.9)	3.4 (± 1.0)	352.6 (± 37.1)	4.1 (± 1.7)	445.6 (± 45.5)	3.6 (± 1.4)
IL-12 (p70)	0.4 (± 0.1)	0.1 (± 0.1)	0.8 (± 0.3)	0.3 (± 0.2)	1.0 (± 0.1)	0.2 (± 0.1)	1.0 (± 0.2)	0.1 (± 0.0)
MCP-1	0.0 (± 0.0)	0.0 (± 0.0)	0.0 (± 0.0)	0.0 (± 0.0)	0.0 (± 0.0)	0.0 (± 0.0)	0.2 (± 0.2)	0.0 (± 0.0)
TNF-α	51.2 (± 14.3)	0.7 (± 0.1)	114.0 (± 16.8)	0.6 (± 0.3)	126.1 (± 28.4)	0.4 (± 0.1)	159.1 (± 69.8)	0.2 (± 0.1)
IL-13	5.1 (± 1.2)	0.0 (± 0.0)	34.0 (± 3.3)	0.1 (± 0.1)	41.6 (± 4.2)	0.0 (± 0.0)	47.0 (± 3.8)	0.0 (± 0.0)
IL-5	1.2 (± 0.3)	0.3 (± 0.1)	173.4 (± 43.7)	0.1 (± 0.0)	1707.1 (± 248.5)	0.0 (± 0.0)	734.5 (± 17.6)	0.0 (± 0.0)

Supplemental Table 2.

	1d		3d		5d		7d	
	DARPin-28z	NGFR	DARPin-28z	NGFR	DARPin-28z	NGFR	DARPin-28z	NGFR
Eotaxin	751.1 (± 19.1)	769.1 (± 41.8)	1056.3 (± 83.5)	783.3 (± 60.1)	812.4 (± 62.7)	773.6 (± 37.9)	1106.3 (± 31.8)	1002.8 (± 65.1)
G-CSF	701.8 (± 87.2)	561.2 (± 49.7)	3115.7 (± 1026.4)	9509.8 (± 9079.4)	10077.9 (± 1291.0)	437.3 (± 64.6)	32231.1 (± 3202.8)	332.3 (± 35.6)
GM-CSF	11.8 (± 2.0)	21.6 (± 1.6)	19.5 (± 2.0)	17.0 (± 3.8)	17.5 (± 1.9)	14.3 (± 1.5)	14.0 (± 1.5)	15.4 (± 2.5)
IFN-γ	6.1 (± 3.0)	9.0 (± 0.6)	7.3 (± 0.8)	6.1 (± 0.8)	6.0 (± 1.6)	5.4 (± 0.7)	10.5 (± 0.7)	7.8 (± 0.5)
IL-1a	1191.4 (± 118.3)	1237.5 (± 192.7)	1141.7 (± 60.3)	1138.9 (± 59.2)	1378.4 (± 54.4)	1459.1 (± 59.5)	1572.7 (± 51.8)	1478.2 (± 80.9)
IL-1b	12.9 (± 7.0)	20.1 (± 3.2)	21.3 (± 3.2)	19.8 (± 8.5)	16.0 (± 3.0)	18.9 (± 3.5)	24.6 (± 3.9)	9.6 (± 2.6)
IL-2	6.5 (± 2.0)	8.0 (± 2.4)	9.3 (± 1.2)	10.0 (± 3.2)	8.9 (± 1.0)	7.3 (± 1.2)	10.6 (± 1.9)	5.1 (± 2.3)
IL-3	1.8 (± 0.9)	2.6 (± 0.5)	1.7 (± 0.2)	2.0 (± 0.2)	2.0 (± 0.3)	1.9 (± 0.1)	2.2 (± 0.3)	1.7 (± 0.5)
IL-4	1.3 (± 0.3)	1.7 (± 0.3)	1.0 (± 0.1)	1.5 (± 0.4)	1.4 (± 0.2)	2.0 (± 0.4)	0.5 (± 0.0)	1.8 (± 0.5)
IL-5	0.2 (± 0.2)	0.0 (± 0.0)	0.8 (± 0.2)	0.0 (± 0.0)	2.7 (± 0.5)	0.0 (± 0.0)	0.0 (± 0.0)	0.0 (± 0.0)
IL-6	144.5 (± 32.6)	80.7 (± 35.2)	200.5 (± 57.0)	297.3 (± 284.0)	448.4 (± 56.7)	41.8 (± 19.9)	135.1 (± 8.2)	7.8 (± 0.7)
IL-7	1.5 (± 1.2)	3.0 (± 0.7)	3.2 (± 0.7)	2.3 (± 0.4)	3.3 (± 1.3)	2.0 (± 0.6)	3.0 (± 0.3)	2.3 (± 0.8)
IL-9	190.3 (± 59.8)	236.1 (± 18.9)	250.1 (± 25.2)	286.1 (± 79.1)	322.7 (± 18.6)	288.7 (± 47.7)	303.0 (± 17.4)	253.3 (± 22.3)
IL-10	7.2 (± 3.3)	12.3 (± 1.8)	12.0 (± 1.1)	9.3 (± 2.9)	13.6 (± 0.9)	10.5 (± 3.4)	20.3 (± 1.5)	8.5 (± 1.9)
IL-12 (p40)	35.7 (± 5.2)	54.1 (± 2.8)	48.0 (± 3.5)	49.9 (± 4.4)	45.4 (± 2.2)	56.0 (± 2.9)	52.3 (± 4.3)	53.6 (± 4.2)
IL-12 (p70)	16.1 (± 5.7)	19.3 (± 0.6)	18.8 (± 1.4)	16.7 (± 1.8)	15.1 (± 3.0)	15.1 (± 1.9)	16.7 (± 2.5)	13.7 (± 0.2)
IL-13	30.3 (± 3.9)	50.2 (± 5.9)	31.9 (± 2.8)	44.3 (± 3.8)	42.7 (± 2.3)	45.7 (± 2.4)	36.9 (± 3.2)	39.6 (± 5.0)
IL-15	29.1 (± 18.1)	26.3 (± 7.3)	38.7 (± 1.4)	17.7 (± 5.1)	17.2 (± 6.2)	15.5 (± 1.8)	21.3 (± 4.2)	22.8 (± 7.2)
IL-17	1.4 (± 0.8)	1.8 (± 0.2)	2.9 (± 0.3)	2.0 (± 0.5)	2.8 (± 0.4)	2.0 (± 0.3)	1.9 (± 0.1)	1.9 (± 0.1)
IP-10	227.7 (± 27.3)	198.9 (± 13.5)	372.7 (± 36.6)	173.5 (± 12.0)	337.6 (± 30.1)	162.3 (± 11.8)	221.7 (± 12.0)	153.0 (± 9.9)
KC	546.9 (± 93.3)	419.1 (± 182.8)	761.1 (± 82.8)	998.2 (± 780.1)	2894.3 (± 264.1)	191.2 (± 18.9)	674.6 (± 106.0)	200.2 (± 7.2)
LIF	0.5 (± 0.2)	0.4 (± 0.2)	1.0 (± 0.3)	0.3 (± 0.3)	0.1 (± 0.0)	0.5 (± 0.2)	2.0 (± 0.4)	0.4 (± 0.1)
LIX	14009.6 (± 4093.7)	11728.1 (± 742.5)	9272.5 (± 1223.8)	11515.6 (± 1769.9)	12795.5 (± 2570.3)	14538.9 (± 2533.6)	11172.8 (± 1869.1)	14823.7 (± 951.5)
MCP-1	791.6 (± 299.3)	57.1 (± 7.2)	950.6 (± 31.8)	71.5 (± 30.8)	2860.3 (± 222.0)	62.6 (± 3.5)	564.6 (± 26.8)	45.1 (± 4.1)
M-CSF	18.7 (± 6.1)	20.5 (± 1.1)	27.2 (± 2.3)	20.5 (± 3.3)	31.7 (± 2.5)	30.0 (± 2.3)	21.6 (± 2.0)	24.4 (± 2.2)
MIG	223.6 (± 21.4)	73.6 (± 2.1)	345.3 (± 127.0)	90.4 (± 6.0)	74.1 (± 7.4)	68.6 (± 3.8)	58.1 (± 5.6)	63.7 (± 6.2)
MIP-1a	125.6 (± 14.5)	137.1 (± 6.5)	121.9 (± 5.1)	139.3 (± 23.0)	147.3 (± 16.2)	148.9 (± 20.6)	167.1 (± 12.8)	153.7 (± 12.5)
MIP-1b	113.4 (± 13.0)	118.9 (± 4.8)	130.1 (± 3.3)	122.7 (± 7.3)	149.8 (± 4.4)	110.2 (± 4.4)	110.8 (± 1.2)	111.4 (± 9.4)
MIP-2	143.4 (± 58.0)	197.4 (± 23.4)	242.1 (± 15.1)	230.4 (± 18.8)	164.1 (± 35.7)	210.8 (± 38.8)	233.4 (± 35.1)	246.2 (± 16.9)
RANTES	84.3 (± 3.1)	83.3 (± 2.6)	94.8 (± 3.7)	82.7 (± 1.2)	106.6 (± 4.8)	93.4 (± 15.6)	94.6 (± 2.1)	83.2 (± 3.2)
TNF-α	0.8 (± 0.8)	0.3 (± 0.3)	4.7 (± 2.9)	0.0 (± 0.0)	5.9 (± 0.9)	0.0 (± 0.0)	7.2 (± 0.9)	0.8 (± 0.8)
VEGF	2.3 (± 0.3)	2.6 (± 0.2)	2.7 (± 0.1)	3.0 (± 0.4)	3.4 (± 0.2)	3.4 (± 0.5)	3.2 (± 0.1)	3.1 (± 0.3)

5.0 Chapter Five – A novel chimeric T cell receptor that delivers robust anti-tumor activity and low off-tumor toxicity

5.1 Introduction

Given the pattern of CAR-T cell-associated toxicity that was beginning to emerge within our own pre-clinical data, and in reports from CAR-T cell clinical trials, we began to question whether toxicities were a consequence of the chimeric antigen receptor design.

In this manuscript we describe the T cell antigen coupler (TAC), a novel synthetic receptor capable of redirecting T cell effector functionality against a tumor target; we use model TACs targeting CD19 and HER2. Targeting of the TAC against HER2 was achieved using the same anti-HER2 DARPin used in the DARPin-28z CAR detailed in Chapters three and four. In the same solid tumor xenograft model in which DARPin-28z-T cells proved lethal in Chapter Four, anti-HER2 DARPin-targeted TAC T cells were efficacious and non-toxic. A detailed head-to-head comparison between DARPin-28z-T cells (referred to as HER2-CAR-T cells in this manuscript) and anti-HER2 DARPin-targeted TAC T cells is presented.

5.2 Manuscript status, copyright, and citation

Status: In review at Nature Communications

Copyright: Nature Communications is an open access journal which publishes its articles under the terms of the Creative Commons Attribution 4.0 International License (https://creativecommons.org/licenses/by/4.0/). Their author licence policy states: "Authors grant Nature Research an exclusive licence to publish, in return for which they can reuse their papers in their future printed work without first requiring permission from the publisher of the journal." Their self-archiving policy states: "Preprint posting is not considered prior publication and will not jeopardize consideration at Nature Research journals." (http://www.nature.com/authors/policies/license.html).

Citation: Helsen, CW, Hammill, JA, Mwawasi, KA, Lau, VWC, Afsahi, A, Bezverbnaya, K, Newhook, L, Hayes, DL, Aarts, C, Bojovic, B, Denisova, GF, Kwiecien, JM, Brain, I, Derocher, H, Milne, K, Nelson, BH, Bramson, JL. (2017). A novel chimeric T cell receptor that delivers robust anti-tumor activity and low off-tumor toxicity. In submission, under review: *Nature Communications*.

5.3 Preprint of journal article

To follow beginning on subsequent page**.**

A novel chimeric T cell receptor that delivers robust anti-tumor activity and low off-tumor toxicity

Christopher W. Helsen[1], Joanne A. Hammill[1], Kenneth A. Mwawasi[1], Vivian W.C. Lau[1], Arya Afsahi[1], Ksenia Bezverbnaya[1], Lisa Newhook[1], Danielle L. Hayes[1], Craig Aarts[1], Bojana Bojovic[1], Galina F. Denisova[1], Jacek M. Kwiecien[1,2], Ian Brain[1], Heather Derocher[3], Katy Milne[3], Brad H. Nelson[3] and Jonathan L. Bramson[1]

[1] Department of Pathology and Molecular Medicine, McMaster University, Hamilton, ON, Canada
[2] Department of Clinical Pathomorphology, Medical University of Lublin, Lublin, Poland
[3] Trev and Joyce Deeley Research Centre, British Columbia Cancer Agency, Victoria, BC, Canada

Address correspondence to: Jonathan L. Bramson, Phone: (905)525-9140 X73884; Email: bramsonj@mcmaster.ca.

Abstract

Engineering T cells with chimeric antigen receptors (CARs) is an effective method for directing T cells to attack tumors in an MHC-independent manner. CARs aim to recapitulate T cell signaling by incorporating functional components of the TCR and costimulatory molecules into a single receptor. We designed an alternate chimeric receptor, the T cell antigen coupler (TAC), that retains MHC-independent antigen recognition but signals through the native TCR. TACs are membrane-anchored chimeric receptors that co-opt the TCR in the presence of tumor antigen. Human T cells engineered with TAC receptors (TAC-T cells) directed against multiple antigens demonstrated robust and antigen-specific cytokine production and cytotoxicity *in vitro* and strong anti-tumor activity in a variety of xenograft models, including solid and liquid tumors. Comparative studies in a solid tumor model demonstrated that TAC-T cells outperformed CD28-based CAR-T cells, revealing both increased anti-tumor efficacy and reduced toxicity. Histological analysis revealed that HER2-TAC-T cells rapidly infiltrated tumors within days, whereas HER2-CAR-T cells displayed limited tumor penetration, even at 7 days post-administration. The TAC-T cell infiltrate was dominated by Ki-67+ CD8+ T cells, confirming local expansion. In contrast, CAR-T cells expanded in non-tumor tissues, such as heart and lung. Notably, CAR-T cell expansion in non-tumor tissue was dominated by Ki-67+ CD4+ cells and associated with overexuberant cytokine production and severe toxicity, including death. No toxicities were observed in mice treated with TAC-T cells, even at doses that produced complete tumor regression. These differences in functional characteristics, anti-tumor efficacy, and toxicity highlight the biological differences of TAC and CAR receptors and indicate that TAC-T cells may have a superior therapeutic index relative to CAR-T cells.

Introduction

Adoptive T cell transfer (ACT) involves the *ex vivo* expansion of a patient's T cells followed by infusion of the cell product into the patient. ACT with T cells engineered to express chimeric antigen receptors (CARs) has proven to be a highly effective strategy for the treatment of CD19-positive and BCMA-positive malignancies[1–3]. First-generation CARs aimed to mimic T cell activation by linking the intracellular signaling domain of CD3ζ to a single chain antibody (scFv)[4]. Next generation CARs have included one or more costimulatory molecules, such as CD28 or 4-1BB, upstream of CD3ζ[4,5]. These signaling components appear to successfully recapitulate signals 1 and 2 of T cell activation, although it is unclear whether these signals are subject to the same regulation as the native T cell receptor (TCR) and costimulatory receptors[6].

Synonymous with the clinical success of CAR-T cells in hematological malignancies[1,7–9] have been serious, and potentially lethal, toxicities including cytokine release syndrome, macrophage activation syndrome, hemophagocytic lymphohistiocytosis, and neurotoxicity[10–12]. Toxicities related to CAR-T cells are complex, multi-factorial, and manifest in a variety of ways[13–15]. Management of these toxicities has been a major concern for clinical implementation[12]. In contrast, ACT with T cell products (e.g. tumor-infiltrating lymphocytes (TIL) or TCR-engineered T cells) that rely on TCR signalling have reported low rates of adverse events relative to CAR-T cells [16]. Thus, the serious toxicities observed in the CD19 CAR-T cell clinical trials may be a specific feature of second-generation CAR-T cells, rather than T cell therapies in general.

We hypothesized that CAR toxicity is linked to the synthetic nature of the receptor design. As a strategy to redirect T cells in a TCR-dependent, MHC-independent manner, we created an alternative receptor, the T cell antigen coupler (TAC), which has three components: (1) an antigen-binding domain, (2) a TCR-recruitment domain, and (3) a co-receptor domain (hinge, transmembrane, and cytosolic regions). Since TAC receptors operate through the native TCR, we hypothesized they would induce a more controlled T cell response.

Here, we describe the modular design (Fig. 1) and functional characterization of TAC receptors. We present experimental evidence for the compatibility of the TAC platform with different classes of functional domains. Furthermore, we demonstrate the efficacy and unique biology of TAC-engineered human T cells in preclinical models of solid and hematological tumors. Notably, using a solid tumor model, we observed that TAC-engineered T cells displayed both enhanced *in vivo* anti-tumor efficacy and decreased off-tumor toxicity compared to first- and second-generation CARs.

Results

Selection of the TCR recruitment domain

The TAC receptor was designed to trigger aggregation of the native TCR following binding of tumor antigens by co-opting the native TCR via the CD3 binding domain (Fig. 1). To evaluate the influence of CD3 binding on TAC receptor function, multiple anti-CD3 single-chain antibodies (scFvs) were evaluated, including UCHT1[17], huUCHT1[18,19], OKT3[20], L2K[21] and F6A[22]. These scFvs, which differ in their recognition of the ε chain[17,22–24], were assessed in the context of a TAC containing the CD4 co-receptor domain and various tumor-targeting moieties (Fig. 2A,E).

OKT3 and UCHT1 were evaluated in a HER2-specific TAC using a designed ankyrin repeat protein (H10-2-G3 DARPin[25]) as an antigen-binding domain. TACs employing OKT3 and UCHT1 displayed comparable levels of surface expression (Fig. 2B). Despite high surface expression, stimulation via the OKT3-TAC elicited low level cytokine production and poor cytotoxicity (Fig. 2C,D). In contrast, antigen stimulation via the UCHT1-TAC triggered robust cytokine production and cytotoxicity (Fig. 2 C,D). Using a TAC directed against CD19 via the FMC63 scFv[26], we also evaluated a humanized version of UCHT1 (huUCHT1)[18,19] and two other scFvs, L2K[21] and F6A[22] (Fig. 2E). The huUCHT1-TAC displayed the highest surface expression (Fig. 2F). The F6A-TAC was not detected on the T cell surface (Fig. 2F), despite successful detection on the surface of 293T cells (Supplementary Fig. 1A). Following stimulation with CD19-positive targets, we observed that significantly higher frequencies of CD4+ T cells engineered with huUCHT1-TAC produced cytokines (IFN-γ, TNF-α, IL-2), compared to CD4+ T cells engineered with F6A- or L2K-TACs (Fig. 2G). CD8+ T cells engineered with huUCHT1- and F6A-TAC produced comparable amounts of cytokine whereas stimulation via L2K-TACs elicited low levels of cytokine production (Fig. 2G). T cells engineered with the huUCHT1-TAC displayed markedly increased cytotoxicity relative to T cells engineered with either the F6A- and L2K-TAC (Fig. 2H). The ability of F6A-TAC to trigger cytokine production and cytotoxicity in an antigen-specific manner suggests that it was expressed on the T cell surface (Supplementary Fig. 1B), but was below the limit of detection. Compared to L2K, OKT3, and F6A, UCHT1 demonstrated preferred properties in the TAC platform and was employed in all subsequent TAC designs.

The CD3 binding domain was absolutely required for TAC activation (Supplementary Fig. 2A-D). Importantly, in the absence of antigen, we did not observe auto-activation of TAC-T cells (Supplementary Fig. 3A-C). To determine whether the CD8 co-receptor could be swapped in to replace the CD4 transmembrane and cytosolic domain, a TAC variant was generated using the CD8α co-receptor. To limit dimerization potential, we mutated two CD8α cysteine residues (C164S/C181S) creating the CD8-TAC. Direct comparisons of TAC receptors employing UCHT1 and either the CD4 or CD8 co-receptor revealed no functional differences (Supplementary Fig. 4A-D).

The phenotype of TAC-T cells is consistent with lack of auto-activation

Auto-activation has been noted in the CAR literature causing expression of checkpoint receptors in the absence of antigenic stimulation[27,28]. T cells were engineered with a TAC targeted via an anti-HER2 DARPin (HER2-TAC) or a second-generation CD28-based chimeric antigen receptor (CAR) carrying the same targeting element (HER2-CAR). Consistent with previous reports, HER2-CAR-T cells showed evidence of tonic signaling through increased expression of PD-1 and LAG-3 receptors in CD4+ and CD8+ subpopulations, respectively. In contrast, HER2-TAC-T cells did not upregulate any checkpoint receptors (Fig. 3A,B). Auto-activation would be expected to promote T cell differentiation. Multi-parameter flow cytometry SPADE analysis[29] were used to visualize clustering patterns of phenotypic markers associated with T cell differentiation (Fig. 3C). HER2-TAC-T cells maintained a phenotypic profile most similar to vector control T cells, with higher expression of lymphoid homing markers (CCR7, CD62L) and co-stimulatory receptors (CD27, CD28) whereas HER2-CAR-T cells, exhibited a more differentiated, effector-like phenotype. Thus, consistent with our functional data (Supplementary Fig. 3), phenotypic profiling of memory markers and checkpoint receptors revealed no evidence of auto-activation of TAC-T cells.

TAC- T cells show efficacy in both solid and liquid xenograft tumor models

We first evaluated the efficacy of TAC-T cells against OVCAR-3, a solid tumor xenograft that expresses HER2[30] (Fig. 4A). Tumor-bearing mice treated with HER2-TAC-T cells experienced rapid tumor regressions within 4-5 days following ACT, compared to mice treated with either CD19-TAC-T cells or T cells engineered with vector only (Fig. 4B). In all cases (n=11), long-term tumor control was observed, with mice surviving to the experimental endpoint (~60 days post-ACT; data not shown).

TAC-T cells were also tested against NALM-6 tumors, an acute lymphoblastic leukemia xenograft that expresses CD19[31] (Fig. 4C). Mice were treated with CD19-TAC-T cells or a variety of control T cell products, including T cells engineered with vector only and T cells engineered with a TAC lacking an antigen-binding domain. Like the OVCAR-3 model, NALM-6 tumors regressed rapidly following treatment with CD19-TAC-T cells (Fig. 4D).

TAC-T cells show enhanced *in vivo* activity compared to CAR-T cells in a solid tumor model

We compared HER2-TAC-T cells to T cells engineered with either a first-generation or a CD28-based, second-generation HER2-CAR[32]; all chimeric receptors were targeted against HER2 with the same DARPin. All engineered T cells displayed comparable *in vitro* cytotoxicity and cytokine production (Supplementary Fig. 5A-F). These *in vitro* similarities notwithstanding, we observed marked differences in the anti-tumor activity of HER2-TAC- and HER2-CAR-engineered T cells *in vivo* (Fig. 5A-D). Consistent with the earlier data, tumors treated with HER2-TAC-T cells regressed within a few days following T

cell infusion (Fig. 5A). In striking contrast, first-generation HER2-CAR-T cells showed no anti-tumor activity in this model (Fig. 5B), and second-generation HER2-CAR-T cells displayed only moderate, delayed anti-tumor efficacy which manifested around 3 weeks post-ACT (Fig. 5C).

In addition to efficacy, we compared the toxicities associated with TAC versus CAR engineered T cells. HER2-CAR-T cells elicited a profound toxicity that manifested as a ruffled coat, laboured breathing and decreased body condition (manuscript in preparation). We employed weight loss as a quantitative measure of toxicity. Mice treated with first-generation HER2-CAR-T cells did not exhibit signs of toxicity, consistent with the lack of anti-tumor efficacy (Fig. 5B). In contrast, we noted toxicities emerging following treatment with second-generation HER2-CAR-T cells were quite severe and all mice became moribund within 40 days of ACT (Fig. 5C, X marks the endpoint). Conversely, HER2-TAC-T cells clearly distinguish themselves from HER2-CAR-T cells as the HER2-TAC-T cells did not trigger any observable toxicities while demonstrating robust anti-tumor efficacy (Fig. 5A).

TAC-engineered T cells penetrate tumors to a higher degree than CAR-engineered T cells

To elucidate the differential effects of HER2-targeted TAC- and CAR-T cells *in vivo*, mice treated with equal doses of HER2-TAC- or second-generation HER2-CAR-T cells were subjected to pathologic and serum cytokine analysis at 1, 3, 5, and 7 days post-adoptive transfer (Fig. 6 and Supplementary Fig. 6,7,8). Mice receiving HER2-CAR-T cells developed severe pulmonary pathology. Masses of infiltrating leukocytes formed at perivascular (Supplementary Fig. 6A) and sub-pleural (data not shown) sites, becoming progressively larger over time. Immunohistochemistry (IHC) showed that the pulmonary deposits were largely composed of CD3+ T cells (Supplementary Fig. 6B). A patchy leukocytic infiltrate containing CD3+ cells was also present in the cardiac tissue (Supplementary Fig. 6C). In contrast, HER2-TAC- or vector control T cells showed only scattered pulmonary infiltrates (Supplementary Fig. 6A,B) and were undetectable in cardiac tissue (data not shown). Instead, HER2-TAC-T cells accumulated primarily within tumor tissue, whereas little accumulation of HER2-CAR-T cells or vector control T cells was observed within the experimental time frame (Supplementary Fig. 6D,E), consistent with the delayed tumor control exhibited by the HER2-CAR-T cells.

To further define the nature of the T cell infiltrate within tissues, we employed multiparametric IHC. Lung sections from mice treated with HER2-CAR-T cells revealed a dominant infiltration of Ki-67+CD4+ T cells, suggesting localized expansion (Fig. 6A, Supplementary Fig. 6F). In contrast, the few CD4+ and CD8+ T cells observed in the lungs of mice treated with HER2-TAC-T cells or vector control T cells were quiescent based on their small size (Supplementary Fig. 6B) and relative lack of Ki-67 staining (Fig. 6A). Similar observations were made in cardiac tissue (Supplementary Fig. 6C, 8). In tumors, the HER2-TAC-T cell

population was dominated by CD8+ T cells, although CD4+ T cells were also evident. Further, intra-tumoral HER2-TAC-T cells were Ki-67+, indicating localized proliferation (Fig. 6A). Tumor tissue infiltrated by HER2-TAC-T cells also contained necrotic tumor cells indicative of cytotoxicity (Supplementary Fig. 6E). Findings regarding tissue-specific CD3+ T cell infiltration were quantified by blinded scoring of IHC slides (Supplementary Fig. 6F).

Examination of circulating human cytokines in the serum of treated mice demonstrated a striking discordance in the quantity and chronology of inflammatory cytokine production between HER2-TAC- and HER2-CAR-T cells. HER2-CAR-T cell-treated mice exhibited the highest levels of circulating cytokines when compared to receptor-negative or TAC-T cell-treated mice (Fig. 6B). Moreover, while serum cytokine levels in HER2-TAC-T cell-treated mice remained low throughout treatment, serum cytokine levels in HER2-CAR-T cell-treated mice became progressively higher over the course of treatment (Fig. 6B).

We were unable to determine what antigen was triggering CAR-T cells, but can exclude murine HER2 (data not shown). Thus, cells were responding against an unknown antigen in the lungs and heart driving a lethal systemic inflammatory reaction. In contrast, HER2-TAC-T cells, which carry the same antigen recognition domain, show improved penetration and expansion within the tumor and did not show evidence of activation or pathology within the lung and heart.

Discussion

Novel strategies, such as splitting of activation and co-stimulation signals[33], and Boolean-gated receptors[34], seek to improve the toxicity profile of CAR-T cells. Rather than modifying the CAR design, we opted to design a major histocompatibility complex (MHC)-independent receptor that recapitulates the architecture of a TCR-CD3/co-receptor complex to engage natural cellular pathways and achieve a more nuanced T cell response.

Our data show that engagement of the TCR-CD3 complex is crucial for the function of TAC-engineered T cells. The activity of the TAC receptor was critically dependent upon the choice of CD3-binding domain, with UCHT1 demonstrating the strongest combination of phenotypic and functional characteristics *in vitro*. Curiously, the scFv derived from OKT3, one of the most commonly used agonistic anti-CD3 antibodies, performed poorly in the TAC platform. Despite the overlapping epitopes of OKT3 and UCHT1[17], our findings, and those of previous studies[23], indicate that small differences in binding to the CD3 complex can result in substantially different functional outcomes.

Regardless of whether the anti-CD3 scFv binds a complex structural epitope (UCHT1[35–37], OKT3[23,35,38] and L2K[21]) or a simple amino acid sequence (F6A binds to a linear N-terminal CD3ε epitope, AA 22-26 "QDGNE" [22]), all CD3-recruiting scFvs displayed some level of functionality within the TAC framework. The varying functionalities of the TAC receptors carrying different CD3-binding moieties suggest that these variabilities could be used to fine-tune T cell responses by altering the various modules of the TAC to create an appropriate indication-specific receptor.

Since the use of murine-derived scFvs in chimeric receptors has been associated with the generation of human anti-mouse antibodies that eliminate engineered T cells[39,40], we have validated the use of humanized UCHT1 in the TAC receptor and all future iterations of the TAC will employ the human scaffold. Our proof-of-concept studies have focused on TAC receptors directed at either CD19 or HER2, but in principle, any cell surface target should be amenable to TAC recognition.

Our *in vitro* comparison of TAC- and first- or second-generation CAR-T cells revealed no functional differences in cytotoxicity or cytokine production. We noted that second-generation CARs, but not TAC receptors, delivered tonic signals to T cells, which manifested in elevated expression of checkpoint receptors and diminished expression of CCR7 and CD62L. Given recent reports that indicate tonic signaling can impair CAR T cell function[27,28], the lack of tonic signaling may be an advantage to TAC receptors. Tonic signaling in CARs can be exacerbated by the choice of scFv[27,41]. We have employed multiple scFvs with the TAC platform and failed to observe evidence of tonic signaling (data not shown). We believe that the lack of tonic signaling may be due to the lack of immunoreceptor tyrosine-based activation motifs (ITAMs) in the TAC receptor. It has been suggested that less differentiated T cells are preferable to terminally-differentiated effector cells for

adoptive therapy, as they retain greater proliferative ability and improved *in vivo* persistence[42]. Data reveal that T cells engineered with TAC receptors retain a less differentiated phenotype, which may translate to a more potent T cell product.

Based on the 2-signal hypothesis of T cell activation[43], one could expect TAC-T cells to perform similarly to a first-generation CAR. However, TAC-T cells showed superior outcomes *in vivo* compared to both first- and second-generation CARs. Pathological analysis revealed two important features of TAC-T cells: 1) greater infiltration of solid tumors post-adoptive transfer and 2) reduced expansion in healthy tissues that express antigens that trigger the HER2-CAR. Intratumorally, both CD4+ and CD8+ TAC-T cells expanded, demonstrating a balanced anti-tumor attack. Importantly, TAC-T cells did not show evidence of activation or expansion within the lungs, heart or any other tissue and did not cause any other toxicities.
Looking at CAR-T cell mediated toxicities, the incidence and severity of clinical adverse events vary widely across CAR-T cell trials. In some trials, 100% of treated patients experienced toxicities, including fever, nausea, general malaise, and in rare cases, lethality[44,45]. The solid tumor model we employed enables simultaneous monitoring of CAR-T cell-mediated efficacy and toxicity. Therefore, it is intriguing that, in addition to superior solid tumor control, TAC-T cells also displayed less toxicity than CAR-T cells. In contrast, HER2-CAR-T cells infiltrated normal lung and heart tissues, resulting in robust expansion of CD4+ CAR-T cells, which are responsible for toxicity (manuscript in preparation). Examination of serum cytokines following infusion of the second-generation CAR-T cells revealed exuberant production of a range of cytokines, indicating the expansion was not reflective of a specific CD4+ T cell subset [46]. In contrast, circulating cytokines following infusion of TAC-T cells were markedly lower and biased towards a Th1 cytokine profile, suggesting a more controlled response.

It is curious that TAC-, but not CAR-, T cells infiltrated the tumor tissue at early time points post-ACT and, conversely, that CAR-, but not TAC-, T cells expanded greatly within the lungs and heart. The lungs, as the first-pass organ, could be expected to be more susceptible to off-tumor reactivity of engineered T cells; however, CAR-T cell expansion within the heart argues that the infiltration/pathology is not simply a first-pass effect. We observed some CD8+ and CD4+ T cells in the lung following infusion of TAC-T cells. However, their small size and lack of Ki-67 expression indicated that they were quiescent. It remains to be determined why TAC-T cells did not react to these healthy tissues as exuberantly as the CAR-T cells. Regardless, these results demonstrate that while TACs can engage and eliminate antigen-bearing tumor cells, they are also sufficiently selective to bypass healthy cells bearing low levels of antigen. This ability to differentiate between antigen in healthy and cancerous tissues could, if generalizable, allow TAC-T cells to be used with solid tumor antigens that are expressed at low levels on healthy cells.

Our observations with HER2-TAC-T cells demonstrate that the efficacy of engineered T cells can be uncoupled from toxicity. Importantly, we predict that this profile will significantly reduce risk and improve tolerability in patients – including

those with significant comorbidities. Furthermore, the improved safety profile would make TAC therapy accessible to a much larger pool of patients, as it would no longer be limited to academic centres capable of handling the complex toxicities currently encountered with CAR therapies. For these reasons, the use of TAC in clinical applications is highly anticipated.

Acknowledgments

We gratefully acknowledge research support from the Terry Fox Foundation, Samuel Family Foundation and Triumvira Immunologics. J.A.H. was supported by a fellowship from the Canadian Cancer Society.

Competing Financial Interests

Christopher W. Helsen, Joanne A. Hammill, Kenneth A. Mwawasi, Arya Afsahi, Galina F. Denisova, Jonathan L. Bramson all hold shares in Triumvira Immunologics. Christopher W. Helsen and Jonathan L. Bramson are founding scientists of Triumvira Immunologics.

References

1. Ali, S. A. *et al.* T cells expressing an anti-B-cell-maturation-antigen chimeric antigen receptor cause remissions of multiple myeloma Running title: Anti-B-cell maturation CAR T cells. (2016). doi:10.1182/blood-2016-04-711903

2. Kochenderfer, J. N., Yu, Z., Frasheri, D., Restifo, N. P. & Rosenberg, S. A. Adoptive transfer of syngeneic T cells transduced with a chimeric antigen receptor that recognizes murine CD19 can eradicate lymphoma and normal B cells. *Blood* **116,** 3875–3886 (2010).

3. Ramos, C. a, Savoldo, B. & Dotti, G. CD19-CAR trials. *Cancer J.* **20,** 112–8 (2015).

4. Gross, G., Waks, T. & Eshhar, Z. Expression of immunoglobulin-T-cell receptor chimeric molecules as functional receptors with antibody-type specificity. *Proc. Natl. Acad. Sci. U. S. A.* **86,** 10024–8 (1989).

5. Finney, H. M., Lawson, A. D., Bebbington, C. R. & Weir, A. N. Chimeric receptors providing both primary and costimulatory signaling in T cells from a single gene product. *J. Immunol.* **161,** 2791–7 (1998).

6. Fesnak, A. D., June, C. H. & Levine, B. L. Engineered T cells: the promise and challenges of cancer immunotherapy. *Nat. Rev. Cancer* **16,** 566–81 (2016).

7. Locke, F. L. *et al.* Phase 1 Results of ZUMA-1: A Multicenter Study of KTE-C19 Anti-CD19 CAR T Cell Therapy in Refractory Aggressive Lymphoma. *Mol. Ther.* **25,** 285–295 (2017).

8. Porter, D. L. *et al.* Chimeric antigen receptor T cells persist and induce sustained remissions in relapsed refractory chronic lymphocytic leukemia. *Sci. Transl. Med.* **7,** 303ra139 (2015).

9. Shah, N. N. *et al.* Minimal Residual Disease Negative Complete Remissions Following Anti-CD22 Chimeric Antigen Receptor (CAR) in Children and Young Adults with Relapsed/Refractory Acute Lymphoblastic Leukemia (ALL). *Blood* **128,** 650 LP-650 (2016).

10. Abate-Daga, D. & Davila, M. L. CAR models: next-generation CAR modifications for enhanced T-cell function. *Mol. Ther. Oncolytics* **3,** 16014 (2016).

11. Fitzgerald, J. C. *et al.* Cytokine Release Syndrome After Chimeric Antigen Receptor T Cell Therapy for Acute Lymphoblastic Leukemia. *Crit. Care Med.* **45,** e124–e131 (2017).

12. Barrett, D. M., Teachey, D. T. & Grupp, S. A. Toxicity management for patients receiving novel T-cell engaging therapies. *Curr. Opin. Pediatr.* **26,** 43–9 (2014).

13. Maude, S. L., Barrett, D., Teachey, D. T. & Grupp, S. A. Managing cytokine release syndrome associated with novel T cell-engaging therapies. *Cancer J.* **20,** 119–22 (2014).

14. Maude, S. & Barrett, D. M. Current status of chimeric antigen receptor therapy for haematological malignancies. *Br. J. Haematol.* **172,** 11–22 (2016).

15. Hinrichs, C. S. & Rosenberg, S. A. Exploiting the curative potential of adoptive T-cell therapy for cancer. *Immunol. Rev.* **257,** 56–71 (2014).

16. Mackall, C. *et al.* Cytokine release syndrome (CRS) in patients treated with NY-ESO-1c259 TCR. *J. Clin. Oncol.* **34,** 3040 (2016).

17. Arnett, K. L., Harrison, S. C. & Wiley, D. C. Crystal structure of a human CD3-ε/δ dimer in complex with a UCHT1 single-chain antibody fragment. *Proc. Natl. Acad. Sci. U. S. A.* **101,** 16268–16273 (2004).

18. Shalaby, M. R. *et al.* Development of humanized bispecific antibodies reactive with cytotoxic lymphocytes and tumor cells overexpressing the HER2 protooncogene. *J. Exp. Med.* **175,** 217–225 (1992).

19. Zhu, Z. & Carter, P. Identification of heavy chain residues in a humanized anti-CD3 antibody important for efficient antigen binding and T cell activation. *J. Immunol.* **155,** 1903–10 (1995).

20. Kipriyanov, S. M., Moldenhauer, G., Martin, a C., Kupriyanova, O. a & Little, M. Two amino acid mutations in an anti-human CD3 single chain Fv antibody fragment that affect the yield on bacterial secretion but not the affinity. *Protein Eng.* **10,** 445–453 (1997).

21. Kufer, P., Lutterbüse, R., Kohleisen, B., Zeman, S. & BÄUERLE, P. Pharmaceutical compositions comprising bispecific anti-cd3, anti-cd19 antibody constructs for the treatment of b-cell related disorders. (2004). at <http://www.google.com/patents/WO2004106381A1?cl=en>

22. Klinger, M. *et al.* Cross-species-specific bispecific binders. (2012). at <http://www.google.com/patents/EP2155788B1?cl=en>

23. Van Wauwe, J. P., Goossens, J. G. & Beverley, P. C. Human T lymphocyte activation by monoclonal antibodies; OKT3, but not UCHT1, triggers mitogenesis via an interleukin 2-dependent mechanism. *J. Immunol.* **133,** 129–32 (1984).

24. Salmerón, a, Sánchez-Madrid, F., Ursa, M. a, Fresno, M. & Alarcón, B. A conformational epitope expressed upon association of CD3-epsilon with either CD3-delta or CD3-gamma is the main target for recognition by anti-CD3 monoclonal antibodies. *J. Immunol.* **147,** 3047–3052 (1991).

25. Zahnd, C. *et al.* A designed ankyrin repeat protein evolved to picomolar affinity to Her2. *J. Mol. Biol.* **369,** 1015–28 (2007).

26. Nicholson, I. C. *et al.* Construction and characterisation of a functional CD19 specific single chain Fv fragment for immunotherapy of B lineage leukaemia and lymphoma. *Mol. Immunol.* **34,** 1157–1165 (1997).

27. Long, A. H. *et al.* 4-1BB costimulation ameliorates T cell exhaustion induced by tonic signaling of chimeric antigen receptors. *Nat. Med.* **21,** 581–90 (2015).

28. Eyquem, J. *et al.* Targeting a CAR to the TRAC locus with CRISPR/Cas9 enhances tumour rejection. *Nature* **543,** 113–117 (2017).

29. Qiu, P. *et al.* Extracting a cellular hierarchy from high-dimensional cytometry data with SPADE. *Nat. Biotechnol.* **29,** 886–91 (2011).

30. Lanitis, E. *et al.* Primary human ovarian epithelial cancer cells broadly express HER2 at immunologically-detectable levels. *PLoS One* **7,** e49829 (2012).

31. Brentjens, R. J. *et al.* Genetically targeted T cells eradicate systemic acute lymphoblastic leukemia xenografts. *Clin. Cancer Res.* **13,** 5426–5435 (2007).

32. Hammill, J. A. *et al.* Designed ankyrin repeat proteins are effective targeting elements for chimeric antigen receptors. *J. Immunother. cancer* **3,** 55 (2015).

33. Kloss, C. C., Condomines, M., Cartellieri, M., Bachmann, M. & Sadelain, M. Combinatorial antigen recognition with balanced signaling promotes selective tumor eradication by engineered T cells. *Nat. Biotechnol.* **31,** 71–5 (2013).

34. Roybal, K. T. *et al.* Precision Tumor Recognition by T Cells With Combinatorial Antigen-Sensing Circuits. *Cell* **164,** 770–9 (2016).

35. Burns, G. F., Boyd, a W. & Beverley, P. C. Two monoclonal anti-human T lymphocyte antibodies have similar biologic effects and recognize the same cell surface antigen. *J. Immunol.* **129,** 1451–7 (1982).

36. Beverley, P. C. L. & Callard, R. E. Distinctive functional characteristics of human 'T' lymphocytes defined by E rosetting or a monoclonal anti-T cell antibody. *Eur. J. Immunol.* **11,** 329–334 (1981).

37. Ma, S., Thompson, J., Hu, H. & Neville, D. M. Expression and characterization of a divalent chimeric anti-human CD3 single chain antibody. *Scand. J. Immunol.* **43,** 134–139 (1996).

38. Law, C.-L. *et al.* Expression and characterization of recombinant soluble human CD3 molecules: presentation of antigenic epitopes defined on the native TCR-CD3 complex. *Int. Immunol.* **14,** 389–400 (2002).

39. Maude, S. L. *et al.* Efficacy and Safety of Humanized Chimeric Antigen Receptor (CAR)-Modified T Cells Targeting CD19 in Children with Relapsed/Refractory ALL. *Blood* **126,** 683 LP-683 (2015).

40. Maus, M. V *et al.* T cells expressing chimeric antigen receptors can cause anaphylaxis in humans. *Cancer Immunol. Res.* **1,** 26–31 (2013).

41. Frigault, M. J. *et al.* Identification of chimeric antigen receptors that mediate constitutive or inducible proliferation of T cells. *Cancer Immunol. Res.* **3,** (2015).

42. Gattinoni, L. *et al.* A human memory T cell subset with stem cell-like properties. *Nat. Med.* **17,** 1290–7 (2011).

43. Chen, L. & Flies, D. B. Molecular mechanisms of T cell co-stimulation and co-inhibition. *Nat. Rev. Immunol.* **13,** 227–42 (2013).

44. Park, J. H., Geyer, M. B. & Brentjens, R. J. CD19-targeted CAR T-cell therapeutics for hematologic malignancies: interpreting clinical outcomes to date. *Blood* **127,** 3312–20 (2016).

45. Lee, D. W. *et al.* Current concepts in the diagnosis and management of cytokine release syndrome. *Blood* **124,** 188–95 (2014).

46. DuPage, M. & Bluestone, J. A. Harnessing the plasticity of CD4(+) T cells to treat immune-mediated disease. *Nat. Rev. Immunol.* **16,** 149–63 (2016).

Figure Legends

Figure 1:
TAC design mimics the TCR-CD3:co-receptor complex. **A**. Left: Naturally occurring TCR-CD3 complex interacts directly with the antigen presented by MHC. Meanwhile, the CD8/CD4 co-receptor interacts with MHC I/II in an antigen-independent manner. Together, these interactions comprise the first step in T cell activation. Right: The TAC receptor re-directs the TCR-CD3 complex towards an antigen of choice using an interchangeable antigen binding moiety (here depicted with an scFv, purple). An scFv is used to recruit the TCR-CD3 complex (blue). Co-receptor properties are incorporated by including the CD4 hinge, TM region, and cytosolic tail (green). **B.** The TAC is incorporated into the pCCL DNA backbone containing a truncated NGFR (tNGFR), which lacks cytosolic signalling domains, as a transduction control. The vector features a bi-directional promoter system with tNGFR under control of the mCMV promoter and TAC expression being driven by the EF-1α promoter. TAC is comprised of an antigen binding domain, a CD3-binding domain and a co-receptor domain. A variety of proteins can be used for each of these three TAC domains allowing the TAC to be modified to best respond to numerous different antigens. The specific domain combinations tested are described below.

Figure 2:
Evaluation of multiple anti-CD3 scFv domains for recruitment of TAC to the TCR-CD3 complex. **A, E** Schematic representation of evaluated TAC constructs. TAC receptors utilizing the (**A**) anti-HER2 DARPin are paired with either the UCHT1 or OKT3 anti-CD3 scFv. TAC receptors (**E**) using the anti-CD19 scFv are paired with either the huUCHT1, F6A, or L2K anti-CD3 scFv. **B, F** Relative TAC surface expression is measured by flow cytometry. Cells are stained for CD4, CD8, tNGFR and TAC, and gated on either $CD4^+NGFR^+$ or $CD8^+NGFR^+$. Representative data of 3 independent experiments are presented as histogram analysis of (**B**) HER2-TAC or (**F**) CD19-TAC. Surface expression of OKT3 relative to UCHT1 was significantly higher in CD4 cells ($p=0.0007$) but not in CD8 cells. huUCHT1 expression is significantly higher compared to either L2K ($p=0.005$ (CD4)/0.0002 (CD8)) or F6A ($p=>0.0001$ (CD4)/ >0.0001 (CD8)). **C, G** HER2- and CD19-specific TAC-T cells are stimulated with antigen-positive (**C**) SK-OV-3 and (**G**) Raji tumor cells, respectively. Data are presented as percent of CD4 or CD8 T cells producing cytokine. Cytokine producing cells are compared from (**C**) TAC-T cells bearing UCHT1 (square) or OKT3 (inverted triangle), or (**G**) TAC-T cells bearing huUCHT1 (square), F6A (triangle), or L2K (diamond). Lines represent the mean. **D, H** HER2- and CD19-TAC and vector control (vector only carrying tNGFR) T cells are co-cultured with (**D**) SK-OV-3 and (**H**) NALM-6 tumor cells, respectively, to measure TAC-T cell-mediated cytotoxicity. Vector control T cells (circles) are compared against (**D**) HER2-specific TAC-T cells bearing UCHT1 (square) or OKT3 (triangle), or (**H**) CD19-specific TAC-T cells

bearing huUCHT1 (square), F6A (triangle), or L2K (diamond). Data are from 3 independent experiments with 3 different donors, error bars are standard deviation.

Figure 3:
Relative expression of memory-associated markers and checkpoint receptors in CAR- and TAC-engineered T cells. T cells are transduced with HER2-DARPin-CD4 TAC and stained for surface marker expression and analyzed by flow cytometry for: **A.** Expression of checkpoint receptors PD-1, LAG-3 and TIM-3. Populations are gated for tNGFR and CD4 or CD8 positivity. **B.** Cell population positive for the specified receptors/ relative to experimental controls are shown. The bar indicates the median of three independent experiments. **C.** SPADE tree visualization of memory-associated marker expression in CD8+ T cells. Populations are pre-gated for transduction marker tNGFR positivity. Nodes represent populations of phenotypically similar single-cell events based on all markers (CD45RA, CCR7, CD62L, CD27, CD28, and CD127), with node size indicating number of cells represented. Initial assignment of node clusters is based on CD45RA and CCR7 expression. Color of nodes represents fold expression of a given marker compared to vector control T cells, as indicated by the color scale. All data are derived from 2 independent experiments with 3 different donors.

Figure 4:
TAC-T cells demonstrate *in vivo* efficacy against solid and liquid tumors. A. Treatment schema for OVCAR-3 tumor-bearing mice. In short, NRG mice receive 2.5 million OVCAR-3 cells subcutaneously. Tumors grew for 35-42 days until an average size of ~100mm^3 is achieved. T cells are delivered over two doses, 48 hours apart. **B.** Tumor-bearing mice receive intravenous delivery of 4-6×10^6 HER2-TAC engineered T cells (black lines) or equivalent dose of vector control T cells (grey lines). Tumor growth is followed over time; volume is calculated as $l \times w \times h$ and % change vs tumor volume at ACT1 (first T cell dose) is calculated. Curves each represent a single treated tumor. Data are from 3 donors, from 2 independent experiments, n = 11 for each of HER2-TAC and vector control groups; CD19-TAC data generated from 1 donor, 1 experiment, n=4. **C.** Treatment schema for NALM-6 tumor-bearing mice. In short, 0.5 million NALM-6 cells are administered intravenously and allowed to establish for 5 days. Mice were treated with a total dose of 4×10^6 CD19-TAC-T cells. T cells were delivered over two doses, 7 days apart. **D.** Mice are treated with either vector control, TAC-ΔAntigen binding domain or CD19-TAC-T cells. Curves each represent a single treated tumor. Data are from 1 donor, 1 experiment, n = 5 for each of CD19-TAC and control groups. Data has been replicated in independent experiments, n=10. Tumor progression is followed weekly via luminescence.

Figure 5:
HER2-TAC-T cells demonstrate an enhanced safety profile and improved efficacy over first and second generation HER2-CAR-T cells *in vivo*. OVCAR-

3 tumor-bearing mice are treated with 2.0×10^6 HER2-TAC-T cells (**A.**), first generation HER2-CAR (**B.**), second generation HER2-CAR (**C.**), or a matched total number of vector control T cells (**D.**). Mice are followed for change in body weight and tumor volume; each curve represents a single treated mouse relative to pre-treatment weight/volume. When mice reach endpoint, this is indicated via X in Figure C. Data has been replicated in an independent experiment.

Figure 6:
Engineered T cell distribution and cytokine release *in vivo*. OVCAR-3 tumor-bearing mice were treated with 6.0×10^6 HER2-CAR -or HER2-TAC-T cells, or a matched total number of vector control cells. Mice are sacrificed at 1, 3, 5 and 7 days post-ACT1 for multiplex serum cytokine analysis or perfusion and fixation of tissues for subsequent histology. **A.** Multicolour IHC is performed on tumor and lung tissue 7d post-ACT1. Tissues is stained for CD8 (cyan), CD4 (yellow), DNA (blue) and a proliferation marker (Ki-67, purple). Data are representative of 3 mice. **B.** Multiplex analysis of human cytokines in mouse serum on day 3 and 7. Measurements that fall below 0.2 pg/ml are below the calibration range and are therefore defined as 0. 0 values are depicted on the graph's x axis. Statistical analysis is provided in supplemental figure 9. Individual data points are shown, bars indicated standard deviation and center bars indicate the median.

Material and Methods

CAR and TAC vector generation

TAC receptor transgenes were designed by linking tumor-directing moiety to a CD3-TCR complex-targeting single chain variable fragment (scFv), and the hinge, transmembrane (TM), and cytoplasmic domains of a T cell co-receptor.

The TAC sequence using UCHT1, CD4 hinge, transmembrane, and cytoplasmic domains was synthesized from GeneArt (Invitrogen; Thermo Fisher Scientific, Waltham, MA) in the pUC57 vector. The HER2-specific H10-2-G3 DARPin[1] targeting domain (using a IgGκ leader sequence) was PCR amplified (fwd 5' GGCGCGCCATGGATTTCCAGGTCCAGATTTTC 3', rev 5' CCCGGGGTTCAGGTCTTCTTCGCTAATC 3') and cloned into the pUC57 TAC vector using *AscI* and *XmaI* cut sites. The resulting TAC was then cloned into the pCCL vector, containing bi-directional minimal CMV (mCMV) and EF-1α promoters[2] (kindly provided by Dr. Megan Levings, University of British Columbia, Vancouver, BC), using *AscI* and *NheI* cut sites. To generate the OKT3 TAC the V_L-V_H configuration of the OKT3 Q/S variant[3] was ordered from GeneArt and cloned into pUC57 using *BamHI* and *SpeI*. The resulting TAC construct was then sub-cloned into pCCL as above.

The TAC encoding the humanized version of UCHT1 (huUCHT1)[4,5] was ordered from GeneArt and sub-cloned by the manufacturer into the pCCL TAC backbone we provided. The sequence for the scFv derived from FMC63, a CD19-specific monoclonal antibody[6] was synthesized with a N-terminal CD8α leader sequence and a Whitlow linker sequence between the heavy and light variable fragments[7] (Integrated DNA Technologies Inc., Coralville, AI). The FMC63 scFv was amplified via the TOPO cloning kit (Invitrogen), then subcloned into the huUCHT1 TAC pCCL backbone using *AscI* and *BamHI*. TAC constructs using the F6A[8] or L2K[9] CD3-binding domain in place of the huUCHT1 were ordered from GeneArt.

The CD8α TAC was cloned as follows: the CD8α sequence was obtained from the UniProtKB/Swiss-Prot database (entry: P01732) and ordered from GeneArt containing C164S and C181S mutations within the hinge domain. The sequence was cloned into the pUC57 UCHT1 TAC vector using *XhoI* and *NheI*. The resulting CD8α -TAC was then sub-cloned into the pCCL vector using *AscI* and *NheI*.

Generation of the second-generation HER2-28ζ CAR consisting of the IgGκ leader, anti-HER2 H10-2-G3 DARPin, human myc tag, CD8α hinge, CD28 TM and cytoplasmic domains, and CD3ζ cytoplasmic tail was previously described[1]. The first-generation HER2-ζ CAR was constructed by removing the 4-1BB portion of a HER2-4-1BBζ CAR containing a CD8α hinge and transmembrane (HER2-4-1BBζ CAR based off the design of a CD19 second-generation CAR[6,10].

All restriction enzymes were purchased from New England BioLabs (NEB, Whitby, ON). All sequences were codon-optimized for expression in human cells and verified. All TAC and CAR constructs are under the control of the human EF-

1α promoter through 5' *AscI* and 3' *NheI* cut sites. Truncated LNGFR (tNGFR) under control of a minimal human cytomegalovirus (mCMV) promoter was utilized as a transduction marker. The receptor-negative control vector codes only for the tNGFR transgene under the mCMV promoter.

Lentivirus production

Self-inactivating, non-replicative lentivirus produced using a third-generation system has been previously discussed[2,11]. Briefly, 8×10^6 HEK293T cells cultured on 15 cm diameter tissue culture-treated dishes (NUNC; Thermo Fisher Scientific) were transfected with the packaging plasmids pRSV-Rev (6.25 μg), pMD2.G (9 μg), pMDLg-pRRE (12.5 μg) and the transfer plasmid pCCL containing the transgene (32 μg) using Opti-MEM (Gibco; Thermo Fisher Scientific) and Lipofectamine 2000 (Thermo Fisher Scientific). Twelve to sixteen hours after transfection, media was replenished with new medium supplemented with sodium butyrate (1 mM; Sigma-Aldrich Canada Co., Oakville, ON). Media containing lentivirus particles was collected after 36-48 hours and concentrated by ultracentrifugation. Viral titer in TU/mL was determined by serial dilution and transduction of HEK293T cells, and subsequently determining %tNGFR$^+$ via flow cytometry using an anti-NGFR-VioBrightFITC antibody (Miltenyi Biotec, Bergisch Gladbach, Germany).

Transduction of human T cells

This research was approved by the McMaster Health Sciences Research Ethics Board and all donors in this study provided informed written consent. Receptor-engineered human T cells were generated as previously described[11]. Human peripheral blood mononuclear cells (PBMC) from healthy donors (McMaster Adult Cohort (MAC) donor) or commercial leukapheresis products (LEUK donor) (HemaCare, Van Nuys, CA) were isolated by Ficoll-Paque-Plus gradient centrifugation (GE Healthcare, Baie d'Urfe, QC) and cryopreserved in inactivated human AB serum (Corning, Corning, NY) containing 10% DMSO (Sigma-Aldrich Canada Co.).

Bulk T cells were activated from PBMCs with anti-CD3/28 Dynabeads at a 0.8:1 bead-to-cell ratio (Gibco) following manufacturer's guidelines, and were cultured in RPMI 1640 (Gibco) supplemented with 8.7% heat-inactivated fetal bovine serum (Gibco), 1.75 mM L-glutamine, 8.7 mM HEPES, 0.87 mM sodium pyruvate (Sigma-Aldrich Canada Co.), 0.87x non-essential amino acids (Gibco), 48 μM β-mercaptoethanol, 87 U/mL penicillin + 87 μg/mL streptomycin, 660 I.U. rhIL-2 and 10 ng/mL rhIL-7 (PeproTech, Rocky Hill, NJ) . After 18-24 hrs, cells were transduced with lentivirus at an MOI between 2-5 (CAR or tNGFR) or 10 (TAC). Cells were monitored daily and fed according to cell counts every 2-3 days for a period of 11-14 days prior to use *in vitro* and/or *in vivo*.

Phenotypic analysis by flow cytometry

Engineered T cell surface expression of CD4, CD8, and tNGFR was evaluated through direct staining with conjugated antibodies. All stains were carried at room temperature for 30 minutes. HER2-specific CAR- or TAC-T cells were first stained with rhHER2-Fc chimera protein (R&D Systems, Minneapolis, MN), followed by conjugated antibodies against CD4, CD8, NGFR (BD Biosciences, San Jose, CA; eBioscience, Thermo Fisher Scientific) and human IgG (Jackson ImmunoResearch, West Grove, PA). CD19-specific TAC-T cells were first stained with biotinylated Protein L (Thermo Fisher Scientific), followed by streptavidin-APC (BD Biosciences), and finally conjugated antibodies against CD4, CD8, and NGFR (BD Biosciences). All flow cytometry was conducted on a BD LSRFortessa or BD LSRII cytometer (BD Bioscience) and analyzed using FlowJo vX software (FlowJo, LLC, Ashland, OR).

Functional analysis of CAR-T cells following stimulation with cell lines

5×10^5 or 4×10^5 engineered T cells were stimulated with 5×10^4 antigen-positive or -negative tumor cells for 4 hours at 37°C in a round- or flat-bottom 96-well plate. Raji ($CD19^+$) and K562 ($CD19^-$) tumor cell lines were used to stimulate CD19-specific TAC-T cells, whereas OVCAR-3 ($HER2^+$) and LOX-IMVI ($HER2^-$) cell lines were used for HER2-specific TAC- and CAR-T cells.

BD GolgiPlug protein transport inhibitor (BD Biosciences) was added at the start of stimulation per manufacturer's instruction. FITC- or APC-H7-conjugated anti-CD107a antibody (BD Biosciences) was incorporated in the stimulation to assess degranulation. After stimulation, cells were stained for surface markers as above. BD Cytofix/Cytoperm fixation and permeabilization kit (BD Biosciences) was used to permit intracellular cytokine staining and cells were stained directly for TNFα, IFNγ, and IL-2 expression. Flow cytometry was conducted as above and data was analyzed using FlowJo (FlowJo, LLC), and SPICE 5.1 as described[12] (National Institute of Allergy and Infectious Disease). Data of cytokine positive T-cell percent is calculated as: cytokine TAC/CAR [%] - vector control T-cell [%].

***In vitro* cytotoxicity assay - Luminescence**

To evaluate cytotoxicity, $5x10^4$ luciferase engineered cells (NALM-6, SK-OV-3, LOX-IMVI, OVCAR-3) were co-cultured with T cells in a white flat bottom 96-well plate (Corning) at indicated effector:target for 6 or 24 hrs at 37°C. After co-culture, 0.15 mg/mL D-Luciferin (Perkin Elmer, Waltham, MA) was added per well and luminescence was measured using a i3 SpectraMax (Molecular Devices, Sunnyvale, CA) across all wavelengths. Tumor cell viability was calculated as: ((Emission – Background)/(Tumor cell alone – Background)) * 100%. Each condition was tested in duplicate or triplicate.

***In vitro* cytotoxicity assay - Colorimetric**

Adherent tumor cell lines LOX-IMVI and OVCAR-3 were used to evaluate cytotoxicity of HER2-CAR- and TAC-T cells. Tumor cells were plated at 1.25×10^4

(LOX-IMVI) or 2.5×10^4 (OVCAR-3) cells/well overnight in a flat-bottom 96-well plate. T cells were evaluated at effector:target ratios of 0.25:1 to 8:1 and co-cultured for 6 hrs at 37°C. After co-culture, T cells were washed off and tumor cell viability was determined using a 10% solution of AlamarBlue cell viability reagent (Life Technologies) per manufacturer's instructions. Colour change, indicative of live cells, was measured by fluorescence ($\lambda_{excitation}$ 530 nm, $\lambda_{emission}$ 595 nm) on a Safire plate reader (Tecan, Maennendorf, Switzerland). Tumor cell viability was calculated as: ((Emission – Background)/(Tumor cell alone – Background)) * 100%. Each condition was tested in triplicate.

Adoptive transfer and *in vivo* monitoring

The McMaster Animal Research Ethics Board approved all murine experiments. 5-week-old female NOD.Cg-Rag1^{tm1Mom}Il2rg^{tm1Wjl}/SzJ (NRG) mice were purchased from The Jackson Laboratory (Bar Harbor, ME) (Stock #007799), or bred in-house. Mice (6-12-weeks-old) were implanted with 2.5×10^6 OVCAR-3 cells subcutaneously (s.c.) into the right hind flank. After 35-42d of tumor growth mice were optimized into treatment groups based on tumor volume[13]. Engineered T cells were infused intravenously (i.v.) (deemed adoptive cell transfer (ACT)) through the tail vein as two doses delivered 48hrs apart (T cells were d14 and d16 in culture on respective treatment days; doses as specified in figure legends represent the total sum of effective (transduced receptor positive) T cells received/mouse). Tumor volume was measured by caliper (Mitutoyo Canada Inc., Toronto, ON) every 2-3 days post-ACT and calculated as L×W×H; % change in tumor volume was calculated as ((current volume (mm^3) – pre-ACT volume (mm^3))/pre-ACT volume (mm^3))*100. Mice were weighed (OHAUS Corporation, Parsippany, NJ) every 1-3 days post-ACT; % change in weight was calculated as ((current weight (g) – pre-ACT weight (g))/pre-ACT weight (g))*100. ***Or*** 7-11-week-old male NRG mice were injected with 0.5×10^6 NALM6-effLuc cells intravenously. Two doses of engineered T cells were administered as above after 3d of tumor growth. Tumor burden was monitored through bioluminescent imaging. Briefly, 10 µL/g of a 15 mg/mL D-Luciferin solution (Perkin Elmer; Waltham, MA) is injected intraperitoneally 14 minutes prior to dorsal and ventral imaging using an IVIS Spectrum (Caliper Life Sciences; Waltham, MA). Images were analyzed using Living Image Software v4.2 for MacOSX (Perkin Elmer) and dorsal and ventral radiance was summed.

Histology

Tissues were prepared for veterinary necropsy via whole body formalin perfusion as described previously[14]. After fixation in 10% neutral buffered formalin, tissues were paraffin-embedded, sectioned and stained using hematoxylin and eosin (H&E) or immunohistochemistry (IHC) for expression of human CD3 (Abcam Inc., Toronto, ON, cat#: ab16669) (conducted using the Leica BOND RX (Leica Biosystems Inc., Concord, ON)). Aforementioned histology services were performed by the Core Histology Facility at the McMaster Immunology Research

Centre. Opal multiplex IHC was performed by the Molecular and Cellular Immunology Core at the British Columbia Cancer Agency's Deeley Research Centre. In short, formalin-fixed paraffin embedded tissue sections were stained with anti-CD4 (Abcam, cat#: ab133616) detected with Opal 520 (PerkinElmer), anti-CD8 (Spring Biosciences, cat# M3162) detected with Opal 650 (PerkinElmer), anti-HER2 (polyclonal, Cell Signaling Technology, ca#: 2242) detected with Opal 570 (PerkinElmer), anti-pan-CK Sigma Aldrich, cat#: C1801) detected with Opal 690 (PerkinElmer,) anti-Ki67 (Spring Biosciences, cat#: M3062) detected with Opal 620 (PerkinElmer), and DAPI (PerkinElmer). Multispectral images (20X magnification, 3 fields per tumor and 3 fields containing perivascular sites per lung) were collected using the PerkinElmer Vectra system. Quantification was performed using inform Advanced Image Analysis Software (PerkinElmer). Blinded pathologic assessment of H&E and CD3 IHC slides was performed by a veterinary pathologist (Dr. Jacek Kwiecein, McMaster University). Blinded CD3 IHC scoring was performed by a pathology resident (Dr. Ian Brain, McMaster University)[15].

Serum cytokine analysis

Prior to necropsy, mice were underwent a non-terminal retro-orbital bleed. Serum was isolated using CapiJect capillary blood collection serum tubes according to manufacturer instructions (Terumo Medical Corporation, Somerset, NJ, Cat No. T-MG). Quantification of 13 human cytokines and chemokines (cat#: HDF13) or 31 murine cytokines and chemokines (cat#: MD31) was performed in a multiplex assay by Eve Technologies (Eve Technologies Corporation, Calgary, AB) using the Bio-Plex 200 system and MILLIPLEX assay kits from Millipore. The assay sensitivities of these markers ranged from 0.1-9.5pg/mL (human) and 0.1-33.3pg/mL (murine); individual analyte values can be found through the Eve Technologies website.

Cell Lines

Human tumor cell lines SK-OV-3, LOX-IMVI, and OVCAR-3 originating from the NCI-60 panel (kind gift from Dr. Karen Mossman, McMaster University, Hamilton, ON) were cultured in RPMI 1640 (Gibco) supplemented with 8.7% heat-inactivated fetal bovine serum (Gibco) 1.75 mM L-glutamine (BioShop, Burlington, ON), 8.7 mM HEPES (Roche Diagnostics, Laval, QC), 87 U/mL penicillin + 87 μg/mL streptomycin (Gibco), and 48 nM β-mercaptoethanol (Gibco). Prior to use OVCAR-3 cells, were passaged *in vivo*. In brief, OVCAR-3 cells were injected *s*.c. into the hind flank of an NRG mouse and allowed to grow for 72 days prior to harvest, digested with a mixture of collagenase type I (Gibco), DNase I (Roche), and hyaluronidase (MP Biomedicals LLC, Solon, OH), and the resulting cell product was expanded *ex vivo*. The Raji, NALM-6, and K562 cell lines were obtained from the American Type Culture Collection (ATCC, Manassas, VA), Deutsche Sammlung von Mikroorganismen und Zellkulturen GmbH (Braunschweig, Germany), and kindly provided by Dr. Carl June (University of Pennsylvania, Philadelphia, PA), respectively, and were cultured in RPMI 1640

(Gibco) supplemented with 8.7% heat-inactivated fetal bovine serum (FBS), 1.75 mM L-glutamine, 8.7 mM HEPES, 0.87 mM sodium pyruvate (Sigma-Aldrich Canada Co.), 0.87x non-essential amino acids (Gibco), 48 μM β-mercaptoethanol, and 87 U/mL penicillin + 87 μg/mL streptomycin. NALM6-effLuc, SK-OV-03-effLuc, K562-effLuc, and LOX-IMVI-effLuc cells were generated by transducing tumor cells by lentivirus encoding enhanced firefly luciferase[16] and a puromycin selection marker. effLuc$^+$ cells were selected for by supplementing culture medium with 2-8 μg/mL puromycin (InvivoGen, San Diego, CA). HEK293T cells were cultured in DMEM (Gibco) with 8.7% heat-inactivated FBS, 8.7 mM HEPES, 1.75 mM L-glutamine, 87 U/mL penicillin + 87 μg/mL streptomycin or 0.1 mg/mL normocin (InvivoGen, San Diego, CA). All cell lines were cultured under ambient atmosphere adjusted to 5 % CO_2 and 37 °C, and confirmed mycoplasma-negative by MycoAlert mycoplasma detection kit (Lonza Inc, Basel, Switzerland).

Statistical analysis

Multiple *t* tests, using the Holm-Sidak method, were used to compare data between two groups. Results were prepared using Prism 6 Software (GraphPad, La Jolla, CA). A significance interval of 95% was used.; NS = not significant. Power calculations were performed using G*Power[17].

SPADE analysis

Flow cytometry files were analyzed in Cytobank (https://www.cytobank.org/) using the SPADE tool for clustering of cells into phenotypic hierarchies to allow for multidimensional analysis as described previously[18]. Populations were pre-gated for transduction marker NGFR, and CD4 or CD8 positivity for SPADE tree generation. Parameters for downsampling and target number of nodes was set to 40% and 12, respectively. Resulting SPADE trees and clusters were manually curated into hi or lo expression of CD45RA and CCR7, followed by coloring of nodes to reflect fold expression of a given marker relative to control.

Antibodies and Recombinant Proteins

Flow cytometry antibodies used: CD4-AF700 (eBioscience; cat#: 56-0048-82); CD4-Pacific Blue (BD Pharmingen; cat#: 558116); CD8-AF700 (eBioscience; cat#: 56-0086-82); CD8-PerCP-Cy5.5 (eBioscience; cat#: 45-0088-42); CD107a-FITC (BD Pharmingen; cat#: 555800); LNGFR-BV421 (BD Pharmingen; cat#: 562582); LNGFR-VioBright FITC (Miltenyi Biotec; cat#: 130-104-893); Human IgG (Fcγ)-PE (Jackson ImmunoResearch; cat#: 109-115-098); IFNγ-APC (BD Pharmingen; cat#: 554702); IL-2-PE (BD Pharmingen; cat#: 554566); TCR αβ-FITC (BD Pharmingen; cat# 555547); TNFα-PE-Cy7 (BD Pharmingen; cat#: 557647); TNFα-FITC (BD Pharmingen; cat#: 554512); rhErbB2/Fc Chimera (R&D Systems; cat# 1129-ER); Protein L-Biotin (Thermo Fisher Scientific; cat#: 29997); Streptavidin-APC (BD Pharmingen; cat#: 554067); CD27-APC-H7 (BD Pharmingen; cat#: 560222); CD28-PE (BD Pharmingen; cat#: 555729); CD45RA-

ECD (Beckman Coulter; cat#: IM2711U); CD62L-APC (BD Pharmingen; cat#: 559772); CD127-PerCP-Cy5.5 (eBioscience; cat#: 45-1278-42); CCR7-PE-Cy7 (BD Pharmingen; cat#: 557648); PD-1-BV421 (BD Horizon; cat#: 562516); TIM-3-PE-CF594 (BD Horizon; cat#: 565560); LAG-3-AF647 (BD Pharmingen; cat#: 565716). IHC antibodies used: CD3 (Abcam Inc.; cat#: ab16669), CD4 (Abcam Inc.; cat#: ab133616), CD8 (Spring Biosciences, Pleasanton, CA; cat#: M3162), HER2 (Cell Signaling Technology, Danvers, MA; cat#: 2242), pan-CK (Sigma Aldrich; cat#: C1801), Ki67 (Spring Biosciences; cat#: M3062, and DAPI, Opal 520, Opal 650, Opal 570, Opal 690, and Opal 620 (Opal 7-ColorfIHC kit; Perkin Elmer; cat# NEL797001KT)

Data availability

The data that support the findings of this study are available from the corresponding author upon reasonable request.

Materials and Methods References

1. Hammill, J. A. *et al.* Designed ankyrin repeat proteins are effective targeting elements for chimeric antigen receptors. *J. Immunother. cancer* **3,** 55 (2015).

2. Dull, T. *et al.* A third-generation lentivirus vector with a conditional packaging system. *J. Virol.* **72,** 8463–71 (1998).

3. Kipriyanov, S. M., Moldenhauer, G., Martin, a C., Kupriyanova, O. a & Little, M. Two amino acid mutations in an anti-human CD3 single chain Fv antibody fragment that affect the yield on bacterial secretion but not the affinity. *Protein Eng.* **10,** 445–453 (1997).

4. Shalaby, M. R. *et al.* Development of humanized bispecific antibodies reactive with cytotoxic lymphocytes and tumor cells overexpressing the HER2 protooncogene. *J. Exp. Med.* **175,** 217–225 (1992).

5. Zhu, Z. & Carter, P. Identification of heavy chain residues in a humanized anti-CD3 antibody important for efficient antigen binding and T cell activation. *J. Immunol.* **155,** 1903–10 (1995).

6. Nicholson, I. C. *et al.* Construction and characterisation of a functional CD19 specific single chain Fv fragment for immunotherapy of B lineage leukaemia and lymphoma. *Mol. Immunol.* **34,** 1157–1165 (1997).

7. Whitlow, M. *et al.* An improved linker for single-chain fv with reduced aggregation and enhanced proteolytic stability. *Protein Eng. Des. Sel.* **6,** 989–995 (1993).

8. Klinger, M. *et al.* Cross-species-specific bispecific binders. (2012). at <http://www.google.com/patents/EP2155788B1?cl=en>

9. Kufer, P., Lutterbüse, R., Kohleisen, B., Zeman, S. & BÄUERLE, P. Pharmaceutical compositions comprising bispecific anti-cd3, anti-cd19 antibody constructs for the treatment of b-cell related disorders. (2004). at <http://www.google.com/patents/WO2004106381A1?cl=en>

10. Brogdon, J., June, C. H., Loew, A., Maus, M. & Scholler, J. Treatment of cancer using humanized anti-cd19 chimeric antigen receptor. (2014). at <http://www.google.com/patents/US20140271635>

11. Hammill, J. A., Afsahi, A., Bramson, J. L. & Helsen, C. W. Viral Engineering of Chimeric Antigen Receptor Expression on Murine and Human T Lymphocytes. *Methods Mol. Biol.* **1458,** 137–57 (2016).

12. Roederer, M., Nozzi, J. L. & Nason, M. C. SPICE: exploration and analysis of post-cytometric complex multivariate datasets. *Cytometry. A* **79,** 167–74 (2011).

13. Bertsimas, D., Johnson, M. & Kallus, N. The Power of Optimization Over Randomization in Designing Experiments Involving Small Samples. *Oper. Res.* **63,** 868–876 (2015).

14. Kwiecien, J. M., Blanco, M., Fox, J. G., Delaney, K. H. & Fletch, a L. Neuropathology of bouncer Long Evans, a novel dysmyelinated rat. *Comp. Med.* **50,** 503–10 (2000).

15. Denkert, C. *et al.* Standardized evaluation of tumor-infiltrating lymphocytes in breast cancer: results of the ring studies of the international immuno-oncology biomarker working group. *Mod. Pathol.* **29,** 1155–64 (2016).

16. Rabinovich, B. A. *et al.* Visualizing fewer than 10 mouse T cells with an enhanced firefly luciferase in immunocompetent mouse models of cancer. *Proc. Natl. Acad. Sci. U. S. A.* **105,** 14342–6 (2008).

17. Faul, F., Erdfelder, E., Lang, A.-G. & Buchner, A. G*Power: A flexible statistical power analysis program for the social, behavioral, and biomedical sciences. *Behav. Res. Methods* **39,** 175–191 (2007).

18. Qiu, P. *et al.* Extracting a cellular hierarchy from high-dimensional cytometry data with SPADE. *Nat. Biotechnol.* **29,** 886–91 (2011).

Supplementary Figure Legends

Supplementary Figure 1:
Biotinylated Protein L is capable of binding CD19 TAC containing the F6A scFv. **A.** Protein L binds the kappa light chain of scFv. HEK 293T-cells were transfected with CD19-TAC-F6A, stained and analyzed for TAC and tNGFR expression by flow cytometry. **B.** CD19-TAC-cells were stimulated with antigen-positive Raji (triangle) or antigen negative K562 (square) tumor cells, respectively. Data are presented as percent of CD4 or CD8 T-cells producing cytokine. Lines represent data medians.

Supplementary Figure 2:
CD3-recruitment domain is required for TAC-engineered T cell function. Full-length and ΔUCHT1 TAC receptors (**A**) were expressed on the surface of primary human T cells (**B**). Relative TAC surface expression is measured by flow cytometry. Cells were stained for CD4, CD8, tNGFR and TAC (via its Myc Tag), and gated on either $CD4^+NGFR^+$ or $CD8^+NGFR^+$; representative TAC expression data are presented as histograms. **C**. HER2-TAC-T cells (bearing huUCHT1 (square) or ΔUCHT1 (triangle)) are stimulated with antigen-positive SK-OV-3 tumor cells. Data are presented as percent of CD4+ or CD8+ T cells producing cytokine. Lines represent data means. **D**. HER2-TAC-T cells (bearing huUCHT1 (square) or ΔUCHT1 (triangle)) and vector control T cells (circles) are co-cultured with SK-OV-3 tumor cells to measure TAC-T cell-mediated cytotoxicity. Data are from 3 independent experiments with 3 different donors; error bars show standard deviation.

Supplementary Figure 3:
TAC-T cells show no evidence of auto-activation in the absence of target antigen. Data originates from the same experiment as Supplemental Figure 2. **A**. HER2-TAC-T cells are stimulated with antigen-positive SK-OV-3 (square) or antigen-negative LOX-IMVI (triangle) tumor cells. Data are presented as percent of CD4+ or CD8+ T cells producing cytokine. Lines represent data means. **B-C**. HER2-TAC-T cells (bearing UCHT1; square) and vector control T cells (circle) are co-cultured with LOX-IMVI or SK-OV-3 tumor cells to measure TAC-T cell-mediated cytotoxicity. Data are from 3 independent experiments with 3 different donors; error bars show standard deviation.

Supplementary Figure 4:
Evaluation of cytosolic TAC domains. (**A**). Schematic representation of CD4 and CD8α TAC constructs containing the anti-HER2 DARPin and UCHT1 CD3-binding domain. (**B**). Cells were stained for CD4, CD8, tNGFR, and TAC expression, and gated on either $CD4^+NGFR^+$ or $CD8^+NGFR^+$; representative TAC expression data are presented as histograms. (**C**) Cytokine production by CD4 TAC- (square) and CD8α TAC- (triangle) T cells stimulated by $HER2^+$ SK-OV-3

tumor cells are shown. Lines represent data means. (**D**) Cytotoxicity was measured by co-culturing $HER2^+$ SK-OV-3 tumor cells with TAC- (CD4 co-receptor (squares) or CD8α co-receptor (triangles)) or vector control (circles) T cells. Data are from 3 independent experiments with 3 different donors; error bars show standard deviation.

Supplementary Figure 5:
First-generation CAR-, second-generation CAR-, and TAC-T cells exhibit similar *in vitro* potency. A. Schematics of TAC and first-generation CAR constructs. **B.** Comparison of cytokine production from CD4+ or CD8+ TAC- (square) and first-generation CAR- (triangle) T cells when stimulated with $HER2^+$ OVCAR-3 tumor cells (minus cytokine production triggered by $HER2^-$ LOX-IMVI tumor cells). Lines represent data means. **C.** Cytotoxicity of TAC- (square) and first-generation CAR- (triangle) relative to vector control (circle) T cells against OVCAR-3 and LOX-IMVI tumor cells. Data are from 3-4 independent experiments; error bars show standard error of the mean. **D.** Schematics of the TAC and 2nd CAR constructs. **E.** Comparison of cytokine production from CD4+ or CD8+ TAC- (square) and second-generation CAR- (inverted triangle) T cells when stimulated with OVCAR-3 (minus cytokine production triggered by $HER2^-$ LOX-IMVI tumor cells). Lines represent data means. **F.** Cytotoxicity of TAC- (square) and second-generation CAR- (inverted triangle) relative to vector control (circle) T cells against LOX-IMVI and OVCAR-3 tumor cells. Data are from 3 independent experiments; error bars show standard error of the mean.

Supplementary Figure 6:
TAC- and CAR-T cells show differential patterns of localization *in vivo*. OVCAR-3 tumor bearing mice were treated with 6.0×10^6 HER2-CAR- or HER2-TAC-T cells, or a matched total number of vector control T cells. At 1, 3, 5, and 7 days post-ACT1 mice (n = 3 per treatment) were perfused and tissues were formalin fixed and paraffin embedded. **A.** Timecourse of H&E (hematoxylin and eosin) stained lung sections at 20X magnification; vasculature are indicated by a "**v**". **B.** CD3 IHC staining of lung sections at 7 days post-ACT1. **C.** H&E and CD3 IHC of cardiac tissue at 7 days post-ACT1. **D.** Timecourse of H&E stained tumor sections at 60X magnification. **E.** CD3 IHC staining of tumor sections at 7 days post-ACT1; arrow indicates a necrotic tumor cell. In all cases, images are representative of observations in all mice (n = 3 each). **F.** CD3 IHC was performed on heart, lung, and tumor tissue; T cell infiltrate was scored as % infiltrate based on tissue area in 10% intervals (score 1 = <1%, score 2 = 1-10%, score 3 = 10-20%, score 4 = 20-30%, score 5 = 30-40%, and score 6 = 40-50%). Data presented as an average score for n = 3 mice per time point.

Supplementary Figure 7:
Single color and composite multicolor IHC tissue analysis. OVCAR-3 tumor bearing mice were treated with 6.0×10^6 HER2-CAR- or HER2-TAC-T cells, or a

matched total number of vector control T cells. At 7 days post-ACT1 mice (n = 3 per treatment) were perfused and tissues were formalin fixed and paraffin embedded for subsequent multicolor IHC analysis (tumor or lung tissues were stained for human cytokeratin (CK, red), cellular proliferation marker Ki-67 (purple), CD8 (cyan), CD4 (yellow), and DAPI (blue)). Representative single-color images are shown alongside 2-color overlay images.

Supplementary Figure 8:
Multicolor IHC of cardiac tissue at 7 days post-ACT1. OVCAR-3 tumor bearing mice were treated with 6.0×10^6 HER2-CAR- or HER2-TAC-T cells, or a matched total number of vector control T cells. At 7 days post-ACT1 mice (n = 3 per treatment) were perfused and tissues were formalin fixed and paraffin embedded for subsequent multicolor IHC analysis (cardiac tissue was stained for cellular proliferation marker Ki-67 (purple), CD8 (cyan), CD4 (yellow), and DAPI (blue)). Representative images are shown.

Supplementary Figure 9:
Statistical analysis of serum cytokine data. An unpaired t-test was used to evaluate the statistical significance of the serum cytokine data (n = 3 for each of HER2-TAC-, HER2-CAR-, and vector control T cells) presented in Figure 6. Pairwise comparisons between the three treatment groups are presented for each of the thirteen cytokines tested. P-values are shown. NS = not significant using a confidence interval of 95%. N/A denotes cases where no analysis was mathematically possible.

Supplementary Figure 10:
Examples of gating strategies used for the analysis of flow cytometry data. A. Gating strategy for phenotypic analysis of engineered T cells. Lymphocytes (SSC-A v. FSC-A) → singlets (FSC-H v. FSC-A) → $CD8^+$ *or* $CD4^+$ cells (CD8-PerCPCy5.5 v. CD4-AF700) → $NGFR^+$ cells (SSC-A v. NGFR-BV421) → TAC receptor expression as a histogram ($ProteinL^+$ with indirect detection via APC-conjugated streptavidin is shown as an example). NGFR+ gates were set based on fully stained, non-transduced T cell controls. B. Gating strategy for functional cytokine production by tumor cell line-stimulated engineered T cells. Lymphocytes (SSC-A v. FSC-A) → singlets (FSC-H v. FSC-A) → $CD8^+$ *or* $CD4^+$ cells (CD8-PerCPCy5.5 v. CD4-AF700) → cytokine positive (SSC-A v. TNF-α-FITC *or* IFN-γ-APC *or* IL-2-PE). Cytokine+ gates were set based on fully stained, PBS- or antigen-negative tumor cell line-stimulated controls.

Figure 1

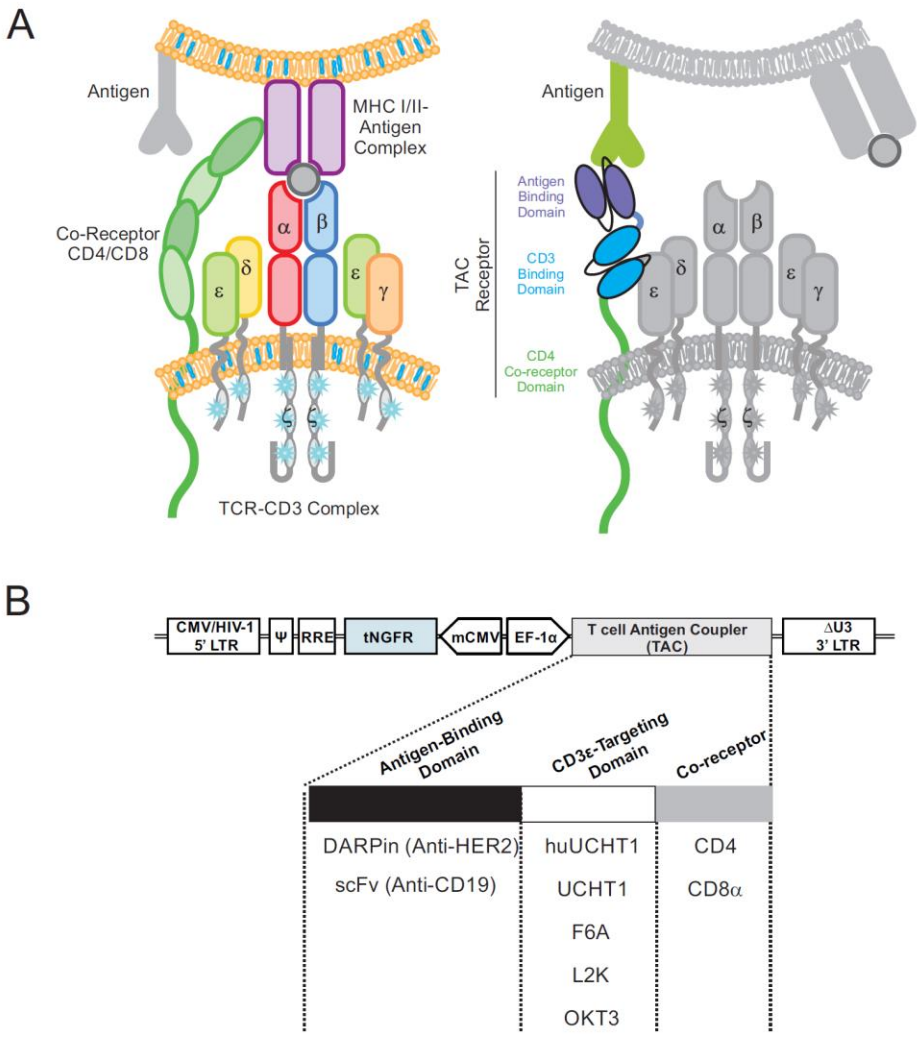
A
Antigen
MHC I/II-Antigen Complex
Co-Receptor CD4/CD8
α
β
δ
ε
ε
γ
ζ
ζ
TCR-CD3 Complex
Antigen
TAC Receptor
Antigen Binding Domain
CD3 Binding Domain
CD4 Co-receptor Domain
B
CMV/HIV-1 5' LTR
Ψ
RRE
tNGFR
mCMV
EF-1α
T cell Antigen Coupler (TAC)
ΔU3 3' LTR
Antigen-Binding Domain
CD3ε-Targeting Domain
Co-receptor
DARPin (Anti-HER2)
scFv (Anti-CD19)
huUCHT1
UCHT1
F6A
L2K
OKT3
CD4
CD8α

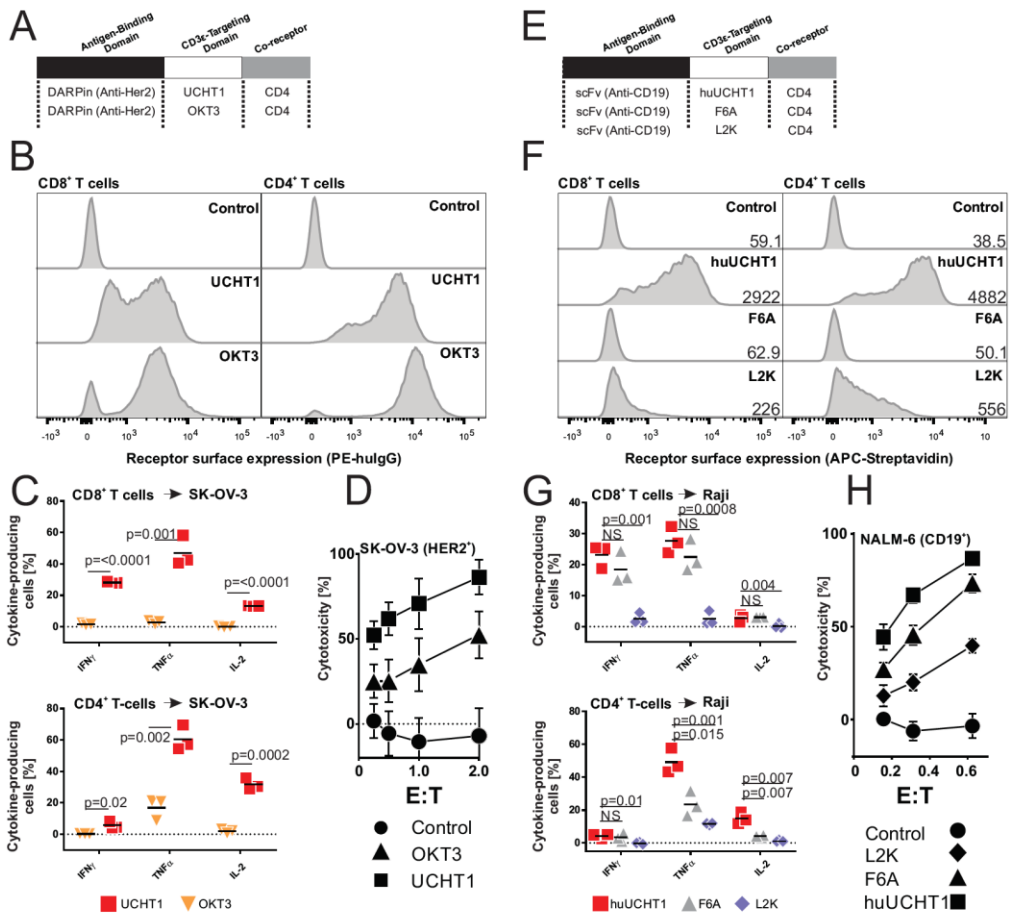
A
Antigen-Binding Domain
CD3ε-Targeting Domain
Co-receptor
DARPin (Anti-Her2)
DARPin (Anti-Her2)
UCHT1
OKT3
CD4
CD4
E
scFv (Anti-CD19)
scFv (Anti-CD19)
scFv (Anti-CD19)
huUCHT1
F6A
L2K
CD4
CD4
CD4
B
CD8+ T cells
CD4+ T cells
Control
UCHT1
OKT3
Receptor surface expression (PE-hulgG)
F
59.1
38.5
huUCHT1
2922
4882
F6A
62.9
50.1
L2K
226
556
Receptor surface expression (APC-Streptavidin)
C
CD8+ T cells → SK-OV-3
Cytokine-producing cells [%]
p=0.001
p=<0.0001
p=<0.0001
IFNγ
TNFα
IL-2
CD4+ T-cells → SK-OV-3
p=0.002
p=0.0002
p=0.02
UCHT1
OKT3
D
SK-OV-3 (HER2+)
Cytotoxicity [%]
E:T
Control
OKT3
UCHT1
G
CD8+ T cells → Raji
p=0.001
NS
p=0.0008
NS
0.004
NS
CD4+ T-cells → Raji
p=0.001
p=0.015
p=0.01
NS
p=0.007
p=0.007
huUCHT1
F6A
L2K
H
NALM-6 (CD19+)
Control
L2K
F6A
huUCHT1

Figure 2

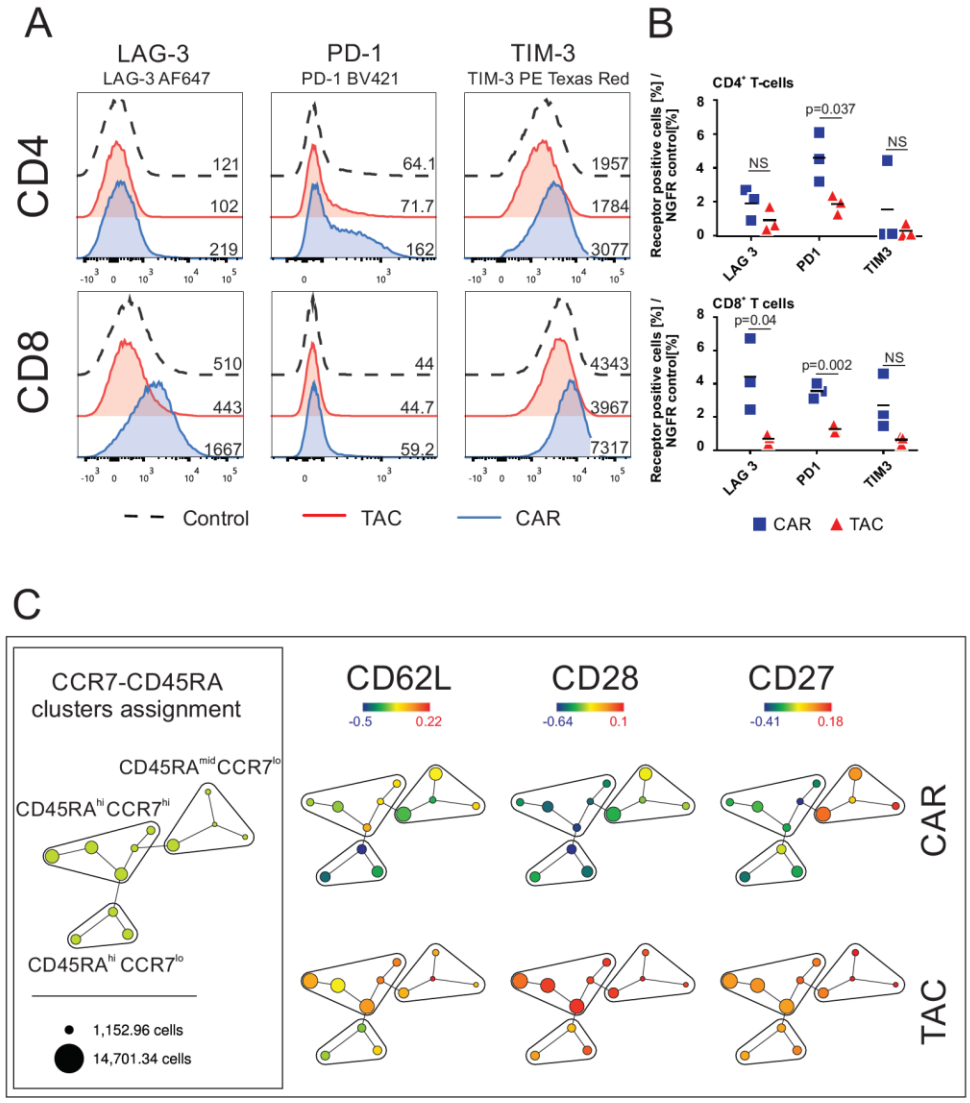
A
LAG-3
LAG-3 AF647
PD-1
PD-1 BV421
TIM-3
TIM-3 PE Texas Red
CD4
CD8
121
102
219
64.1
71.7
162
1957
1784
3077
510
443
1667
44
44.7
59.2
4343
3967
7317
Control
TAC
CAR
B
CD4+ T-cells
CD8+ T cells
Receptor positive cells [%] / NGFR control[%]
p=0.037
NS
p=0.04
p=0.002
LAG 3
PD1
TIM3
CAR
TAC
C
CCR7-CD45RA clusters assignment
CD45RAmidCCR7lo
CD45RAhiCCR7hi
CD45RAhiCCR7lo
1,152.96 cells
14,701.34 cells
CD62L
-0.5
0.22
CD28
-0.64
0.1
CD27
-0.41
0.18
CAR
TAC

Figure 3

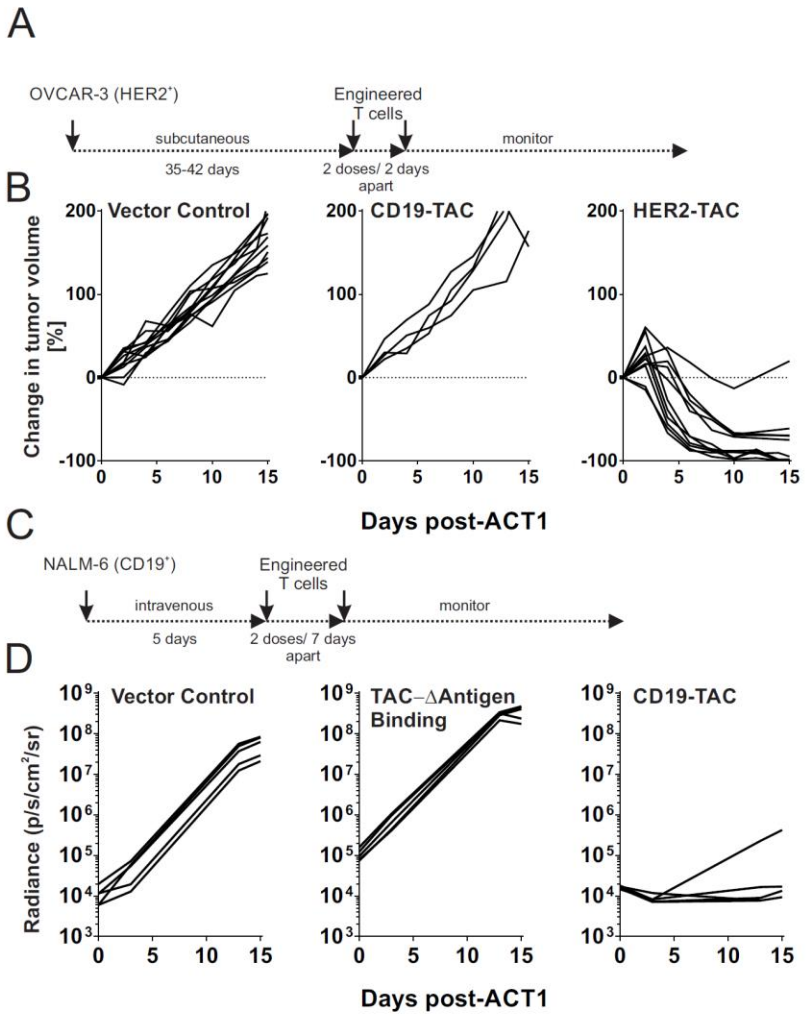
A
OVCAR-3 (HER2+)
subcutaneous
35-42 days
Engineered T cells
2 doses/ 2 days apart
monitor
B
Vector Control
CD19-TAC
HER2-TAC
Change in tumor volume [%]
200
100
0
-100
0 5 10 15
Days post-ACT1
C
NALM-6 (CD19+)
intravenous
5 days
Engineered T cells
2 doses/ 7 days apart
monitor
D
Vector Control
TAC–ΔAntigen Binding
CD19-TAC
Radiance (p/s/cm2/sr)
10^9
10^8
10^7
10^6
10^5
10^4
10^3
0 5 10 15
Days post-ACT1

Figure 4

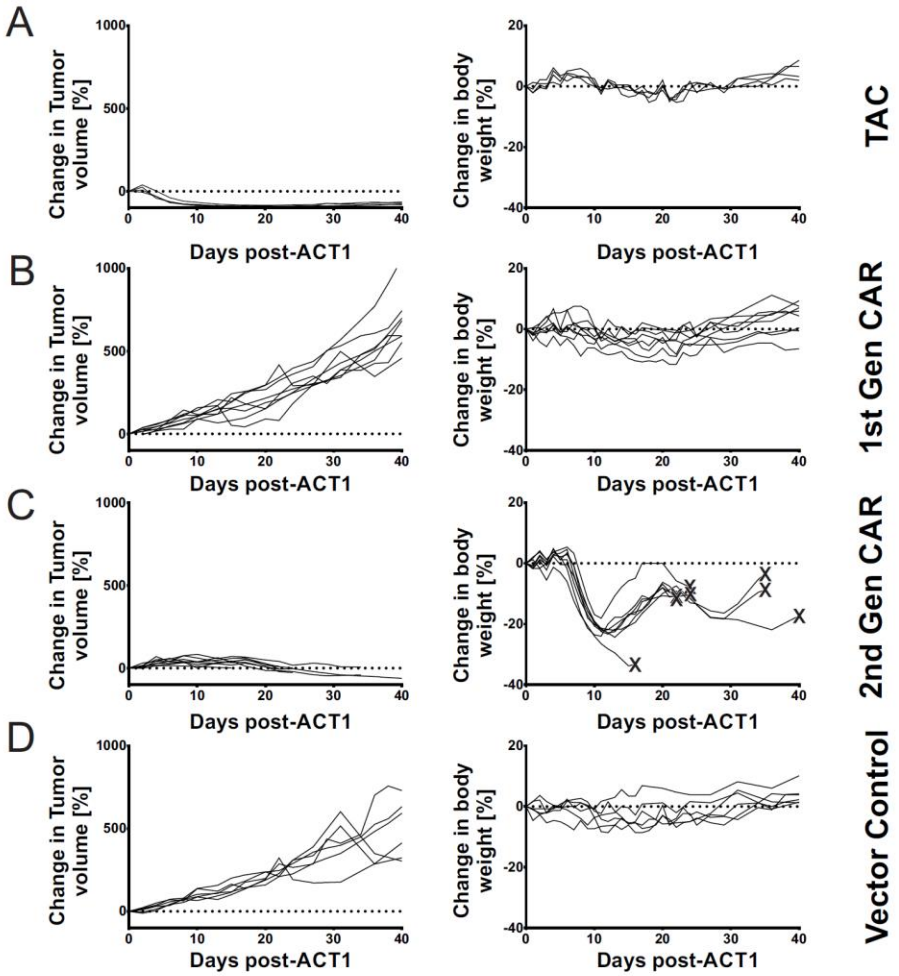
A
B
C
D
Change in Tumor volume [%]
Change in body weight [%]
Days post-ACT1
TAC
1st Gen CAR
2nd Gen CAR
Vector Control

Figure 5

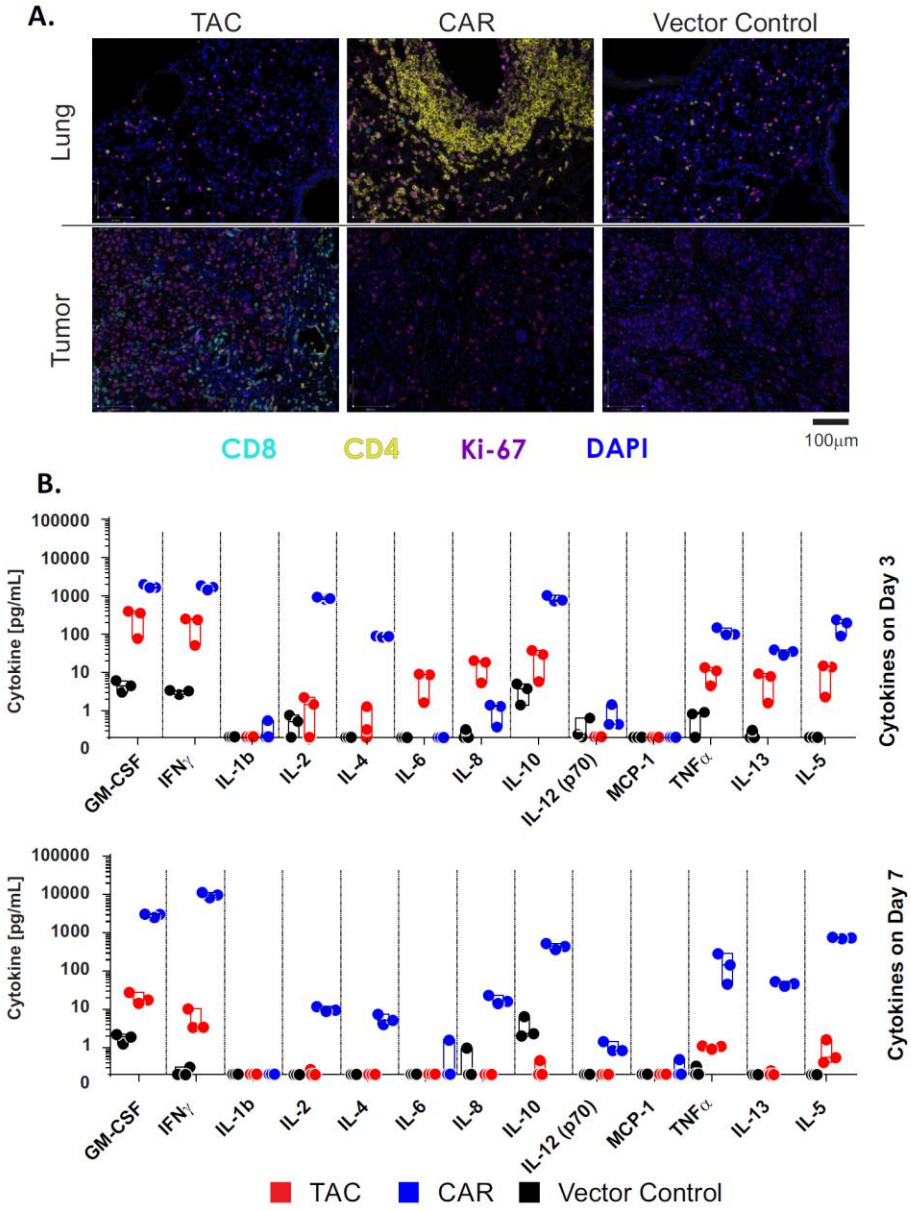
A.
TAC
CAR
Vector Control
Lung
Tumor
CD8
CD4
Ki-67
DAPI
100μm
B.
Cytokine [pg/mL]
100000
10000
1000
100
10
1
0
GM-CSF
IFNγ
IL-1b
IL-2
IL-4
IL-6
IL-8
IL-10
IL-12 (p70)
MCP-1
TNFα
IL-13
IL-5
Cytokines on Day 3
Cytokines on Day 7
TAC
CAR
Vector Control

Figure 6

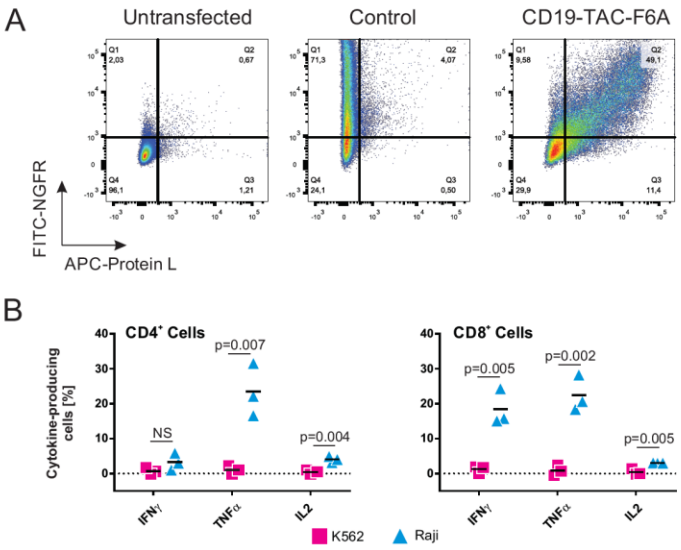

Supplementary- Figure 1

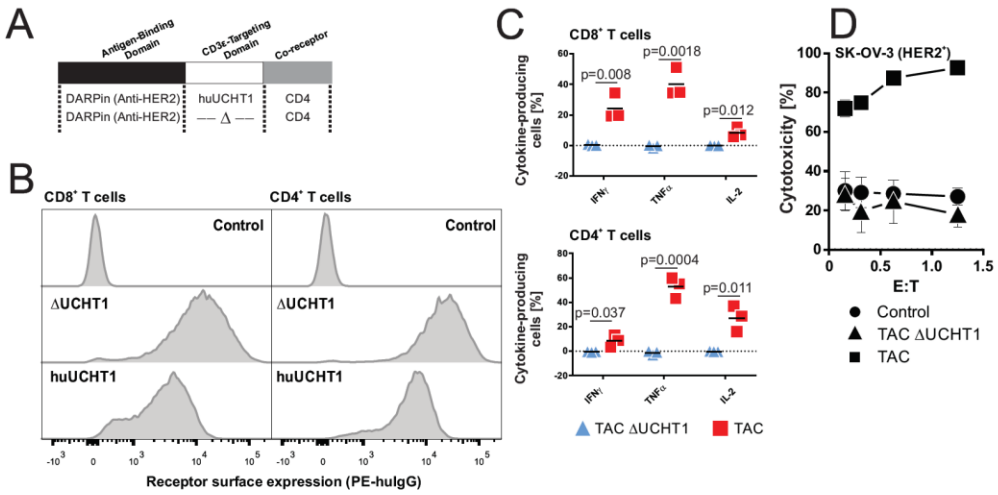

Supplementary- Figure 2

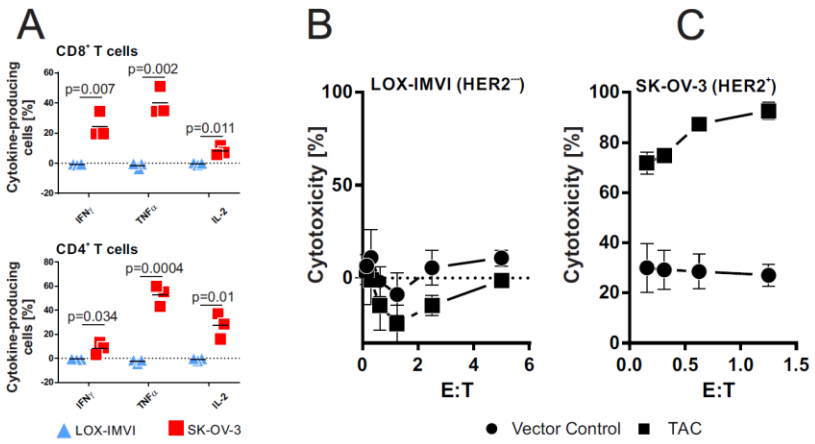

Supplementary- Figure 3

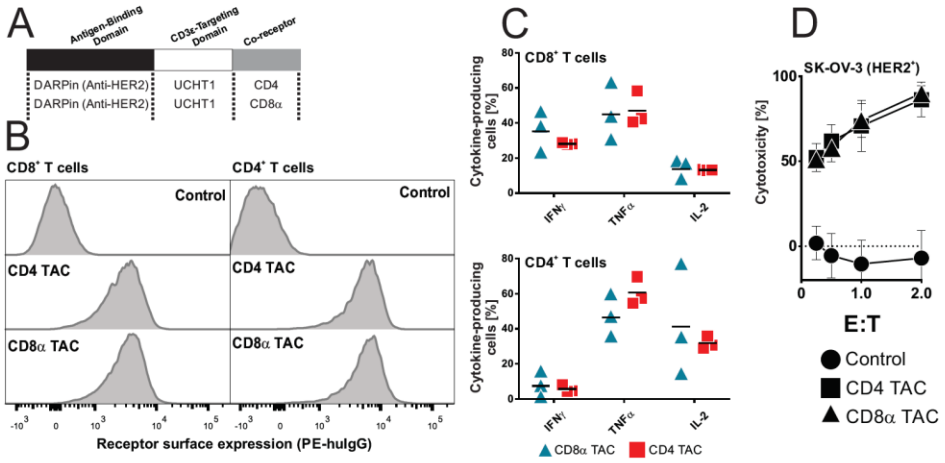

Supplementary- Figure 4

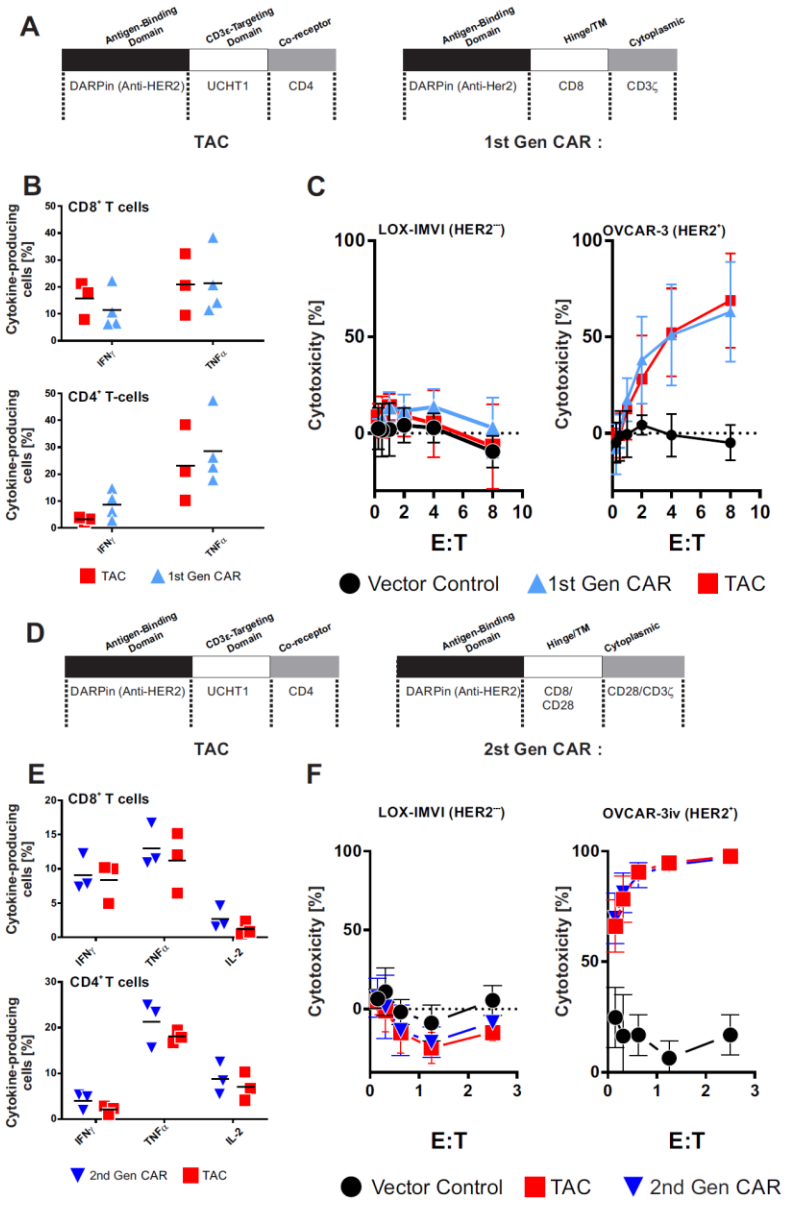

Supplementary- Figure 5

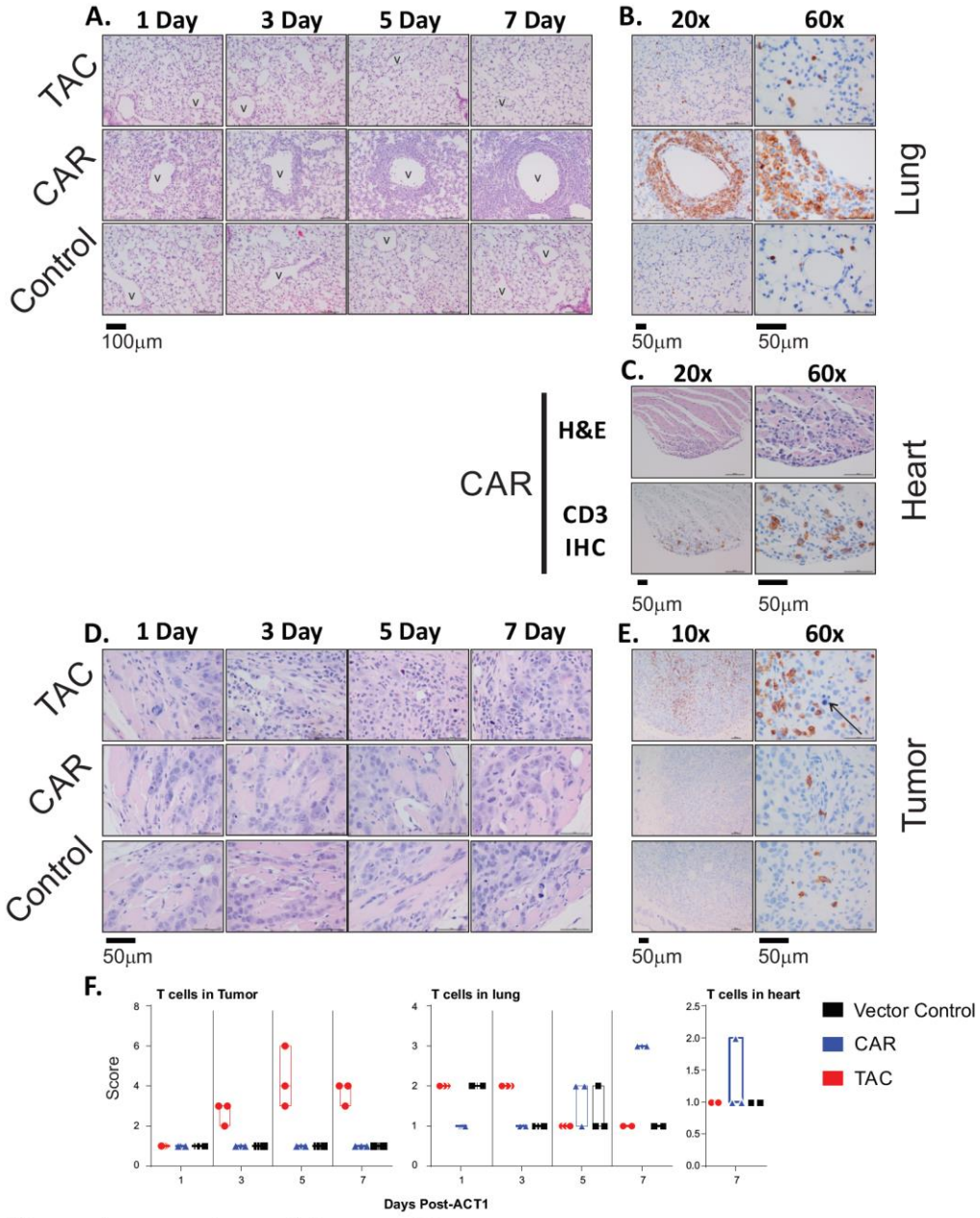

Supplementary-Figure 6

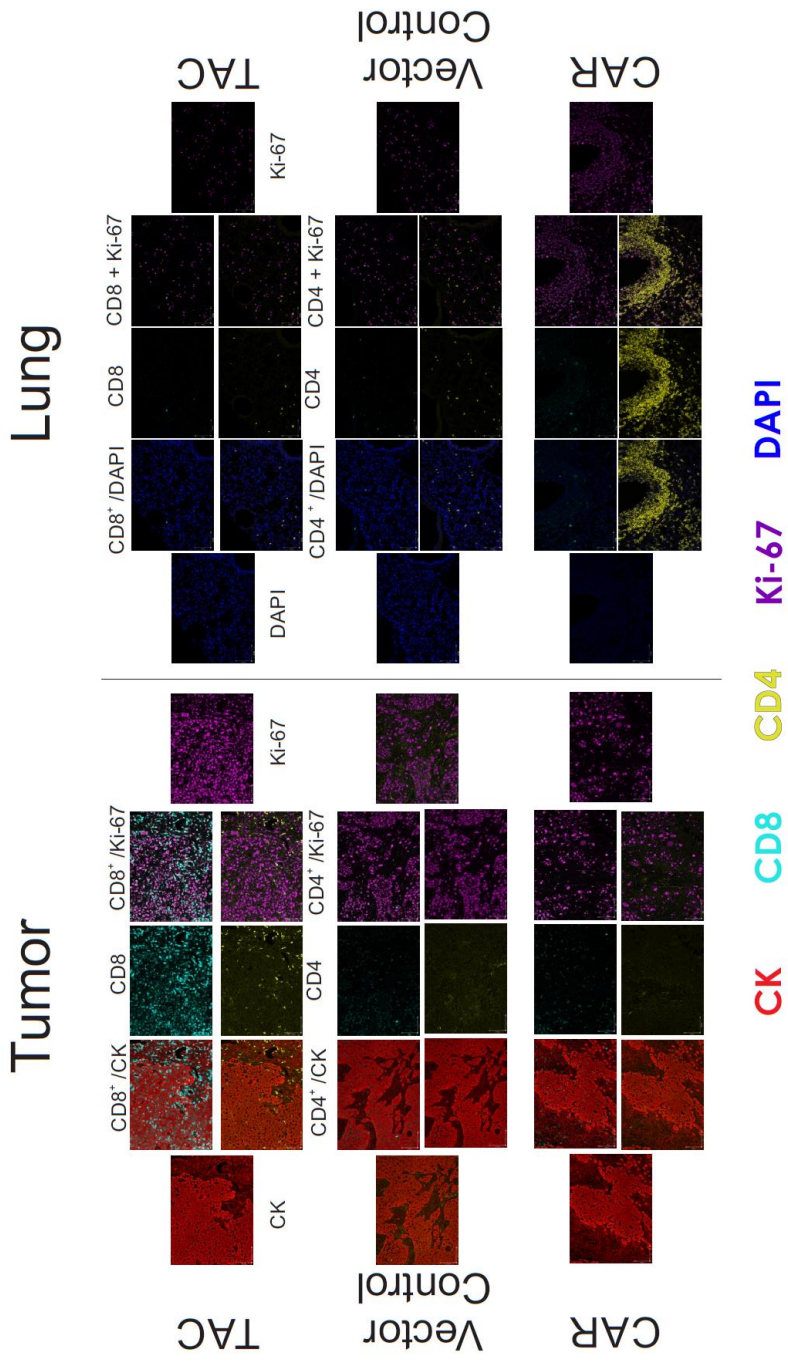

Supplementary-Figure 7

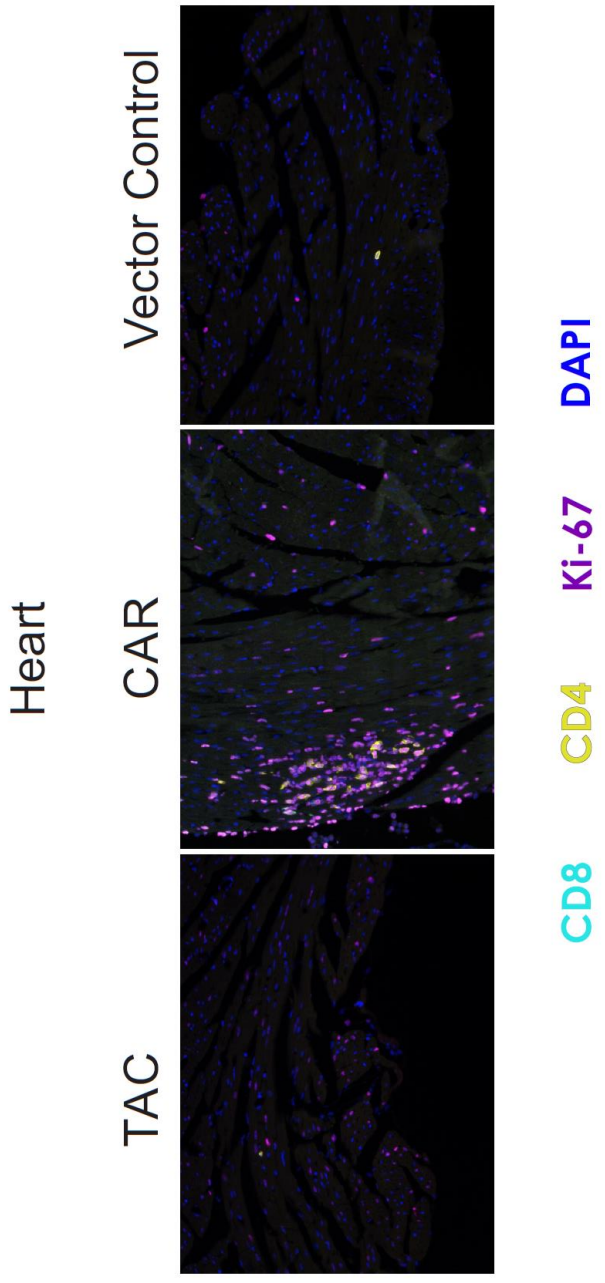

Supplementary-Figure 8

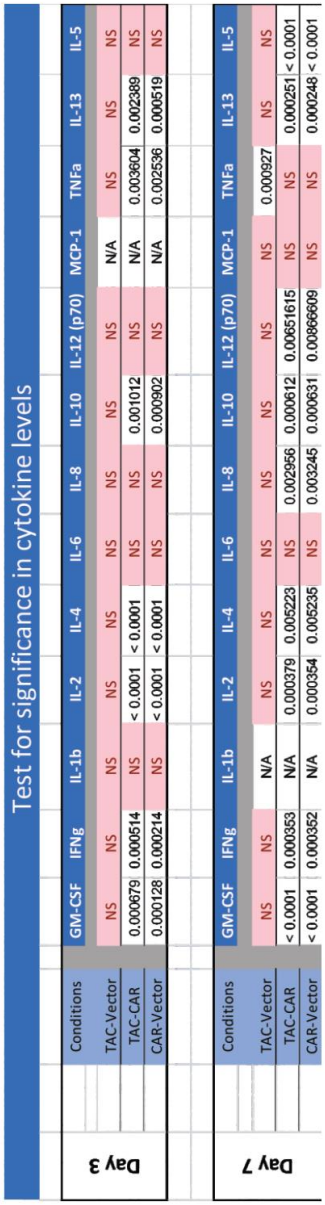

Test for significance in cytokine levels

Day 3

Conditions	GM-CSF	IFNg	IL-1b	IL-2	IL-4	IL-6	IL-8	IL-10	IL-12 (p70)	MCP-1	TNFa	IL-13	IL-5
TAC-Vector	NS	NS	NS	NS	NS	NS	NS	NS	NS	N/A	NS	NS	NS
TAC-CAR	0.000679	0.000514	NS	< 0.0001	< 0.0001	NS	NS	0.001012	NS	N/A	0.003604	0.002389	NS
CAR-Vector	0.000128	0.000214	NS	< 0.0001	< 0.0001	NS	NS	0.000902	NS	N/A	0.002536	0.000519	NS

Day 7

Conditions	GM-CSF	IFNg	IL-1b	IL-2	IL-4	IL-6	IL-8	IL-10	IL-12 (p70)	MCP-1	TNFa	IL-13	IL-5
TAC-Vector	NS	NS	N/A	NS	NS	NS	NS	NS	NS	NS	0.000927	NS	NS
TAC-CAR	< 0.0001	0.000353	N/A	0.000379	0.005223	NS	0.002956	0.000612	0.00651615	NS	NS	0.000251	< 0.0001
CAR-Vector	< 0.0001	0.000352	N/A	0.000354	0.005235	NS	0.003245	0.000631	0.00866609	NS	NS	0.000248	< 0.0001

Supplementary-Figure 9

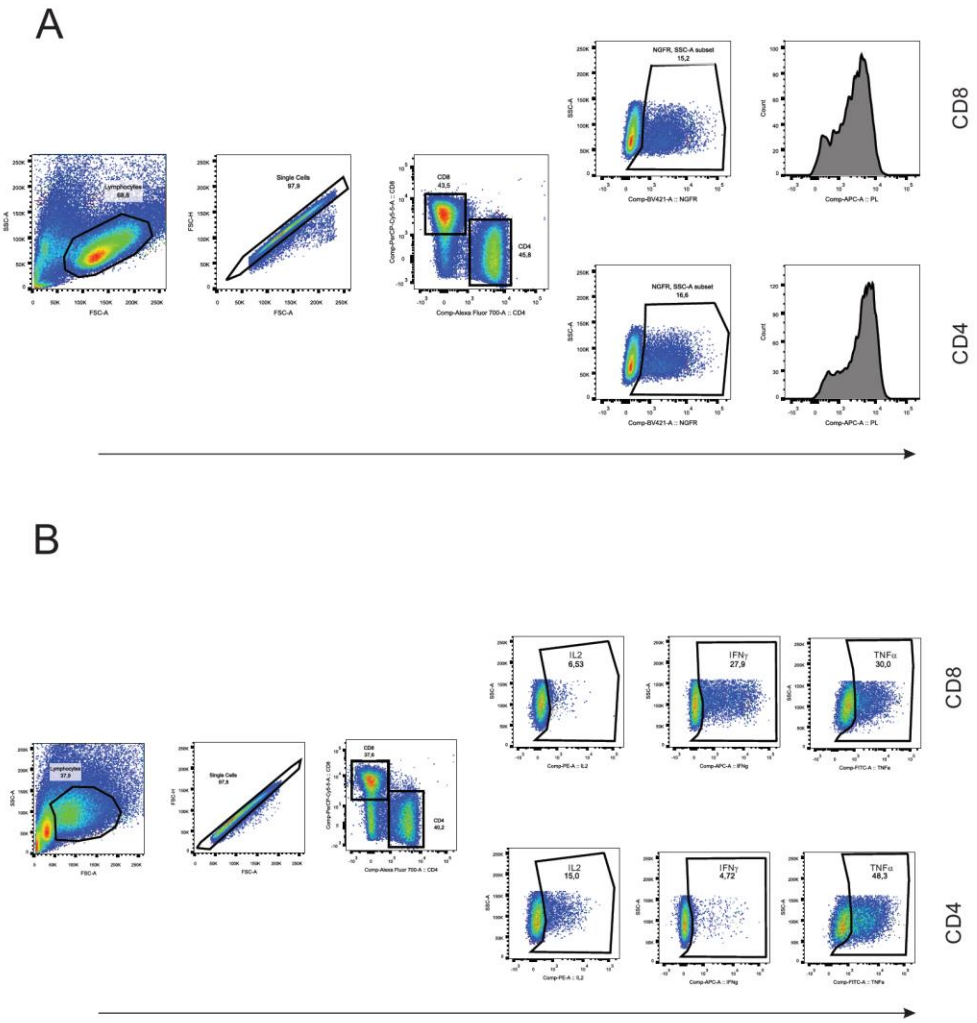

Supplementary-Figure 10

6.0 Chapter Six – Conclusions

The findings of this work echo the CAR-T cell clinical experience thus far – CAR-T cells have the capacity to induce serious toxicities *in vivo*. We arrived at this conclusion in two different small animal models: i) NKG2D-targeted CAR-T cells in a syngeneic model and ii) anti-HER2 DARPin-targeted CAR-T cells in a xenograft model.

6.1 NKG2D-based CAR-T cells can be toxic in vivo

In Chapter Two, using a syngeneic model, we demonstrated for the first time that NKG2D-based CAR-T cells bore the potential to be lethally toxic – in contrast to pre-clinical literature on the subject published prior to our investigations. We concluded that the clinical evaluation of NKG2D-targeted CAR-T cell therapy, which was already in progress, should be undertaken with extreme caution; a sentiment that was echoed by others in response to our publication (267).

Interestingly, subsequent to our publication, the Sentman group (who originally described NKG2D-targeted CARs) published an article describing the toxicities associated with these CAR-T cells (268). Importantly, in reference to our work, these authors agree that "to improve NKG2D CAR design with stronger signaling or the use of immune pre-conditioning should be considered carefully" (268). Given Dr. Sentman's partnerships with those companies responsible for bringing NKG2D-targeted CAR-T cells to trial, our findings have informed clinical practice.

First-in-man phase I clinical trial results of NKG2D-targeted CAR-T cells are beginning to emerge. In a trial of chimeric receptors composed of full-length NKG2D fused to the signaling domain of CD3ζ, used for the treatment of hematological malignancies (NCT02203825), no instances of cytokine release syndrome, neurotoxicity, or auto-immunity were reported (269). The conditions of the trial design were in line with those which produced the lowest levels of toxicity in our syngeneic model. To mitigate risk of toxicity, the trial design included: (i) the initial dose levels of NKG2D-CAR-T cells were markedly lower than those reported in CD19-CAR-T cell trials, (ii) a first-generation CAR-T cell scaffold was used (equivalent to our NKz), and (iii) the trial was conducted in the absence of lympodepleting pre-conditioning (and exclusion criteria included chemo- or radiotherapy received within 3 weeks prior to CAR-T cell infusion) (269). As such, we conclude that the results of these clinical tests were consistent with the predictions of our pre-clinical model. Although the NKG2D-based CAR-T cell product was safe in this trial, there were no objective responses among patients. A follow-up phase I dose escalation and expansion trial is currently recruiting (NCT03018405; THINK trial) (270, 271). Patients in the THINK trial receive increased CAR-T cell doses over multiple infusions; unlike the CD19-CAR-T cell trials, patients in the THINK trial do not receive lymphodepleting conditioning therapy. Again, no major toxicities have been reported and there has been one early

report of a complete response in a single patient treated in the trial (272). Our findings (in our anti-HER2 DARPin-targeted CAR-T cell xenograft toxicity model), and those of others (258), indicate that conventional CAR-T cell preparations have a very narrow therapeutic window. Given the increased dosing and observation of efficacy in the THINK trial, it will be interesting to see whether toxicities are observed upon full disclosure of trial data.

6.2 DARPins can be used to target synthetic receptor-engineered T cells

In Chapter Three, we were the first to demonstrate the utility of DARPins as CAR-targeting elements. The same anti-HER2 DARPin was used in Chapter Five to target a TAC against HER2, proving this capacity is applicable to multiple synthetic receptor designs.

The DARPin-targeting approach has since been confirmed by several other groups in CARs (273, 274) or chimeric costimulatory receptors (274) (akin to CARs but only encoding a source of co-stimulatory signaling) against HER2 (273) and other targets (274).

6.3 Host and T cell source biology contribute to differences in CAR-T cell toxicity

In Chapter Four, using our anti-HER2 DARPin-targeted CARs in a xenograft model, we definitively demonstrated for the first time that biological diversity among human CAR-T cell products could contribute to differential toxicity *in vivo*. Despite having been in development for nearly thirty years, synthetic receptor-engineered T cells are still a young and poorly understood technology. Much of the work done thus far has focused on the feasibility and efficacy of the engineered T cell approach. As such, while most published xenograft pre-clinical CAR-T cell models evaluate multiple donors, they often fail to present data stratified by the T cell donor source. One under-appreciated aspect has been how the differential biology of patients will affect these cellular therapeutics. Currently, tumor burden and antigen status are the only patient-specific features taken into consideration when determining whether a patient is a candidate for CAR-T cell therapy. However, our findings indicate that factors within the T cells used to generate the engineered cell product are contributing to outcomes of CAR-T cell therapy.

We demonstrated that the CD4:CD8 T cell ratio in a CAR-T cell product, which appears to be a biological property that varies from donor-to-donor, is a critical factor contributing to the severity of off-tumor CAR-T cell-associated toxicity. The contribution to toxicity that may be arising from patient-to-patient differences in the adoptive transfer product has only recently been appreciated in clinical trial data. In unpublished data disclosed at the 2017 Society for Immunotherapy of Cancer annual meeting, Juno Therapeutics identified that individuals receiving an increased dose of $CD8^+$ T cells (resulting from variations in the CD19-CAR-T cell adoptive transfer product) significantly correlated with

cerebral edema (i.e. neurotoxicity) arising from an on-tumor response in hematological malignancies (275). Previous reports have linked off-tumor toxicities to $CD4^+$ T cells (276, 277); our data confirms these findings and reveals that donor-specific features within the $CD4^+$ T cells also contribute to the toxicities (e.g. we identified rate of expansion as one contributor – akin to recent clinical findings (278)). Further work is needed to determine exactly what biological factors (whether heritable or non-heritable (279)) underpin these differences, which may allow for the rational design of engineering strategies that correct for toxic potential. Testing DAPRin-28z-CAR-T cells generated from clinical PBMC samples (where patients have a known clinical toxicity outcome) in our model may provide one way to validate the utility of our model as a predictor of this toxic potential.

Consistent with the theme of differential biology impacting toxicity, in Chapter Two the severity of NKG2D-based CAR-T cell toxicity was dependent upon the strain of mice used. We attributed these differences in toxicity to variations in non-tumor NKG2DL expression and CAR-T cell functionality (as measured *in vitro*). As such, our findings in the NKG2D-CAR-T cell model allude to another potential contributor to patient-to-patient differences in toxicity: host microenvironment. It is currently unknown whether differential expression of CAR-targeted tumor associated antigens on non-tumor tissues can contribute to differential severity of on-target, off-tumor toxicity. Our NKG2D-CAR-T cell model suggests this may be a possibility, and indeed healthy tissues show a range of antigen expression across human donors (e.g. pulmonary HER2 expression (280, 281)). This is particularly concerning for CAR-T cell therapeutics targeting tumor associated antigens which are safe only within a narrow therapeutic window; patients expressing TAA at the upper end of the normal distribution may be particularly sensitive to experiencing on-target off-tumor CAR-T cell activation and thus toxicity (282).

The association between efficacy and toxicity with cancer therapeutics is longstanding (recall the toxicities observed with Coley's toxins, for example). The ultimate therapeutic would unlink efficacy and toxicity. Unfortunately, results in our preclinical models suggest that current CAR-T cell products are unable to do so.

6.4 Next-generation synthetic receptor-engineered T cells

In Chapter Five, we introduced a novel synthetic receptor platform, the T cell antigen coupler (TAC), which triggers T cell activation against tumor antigens via the endogenous TCR/CD3 complex in an MHC-independent manner. Unlike equivalent CAR-T cells, anti-HER2 TAC-T cells are efficacious and safe in a solid tumor xenograft model (the same model described in Chapter Four), offering a potential solution to unlink toxicity from efficacy. Whether improved efficacy and safety in treating solid tumors is a general property of TAC-T cells, or an observation unique to this model has yet to be determined; future evaluations of

equivalently targeted TAC- versus CAR-T cells in additional pre-clinical solid tumor and toxicity models are needed.

However, we hypothesize that the TAC platform, through its appropriation of the endogenous TCR for signaling, results in a more natural T cell activation versus a CAR. We further hypothesize that this differential activation will offer TAC-T cells improved solid tumor efficacy and reduced toxicity across a range of targets. Due to their design, CAR-T cells are inherently different in their activation of T cells than a TCR. A CAR containing the CD3ζ activation domain has just three ITAMs per receptor compared to the ten ITAMs per TCR-CD3 complex (204). Furthermore, delivery of activation and co-stimulatory signals are both spatially and temporally concomitant through a CAR, unlike endogenous T cell activation (283). These differences make it unlikely that a CAR-T cell will be capable of mimicking a natural T cell response – a claim that is supported by experimental evidence. Indeed, when CARs were compared to TCRs targeted against the same antigen (a pMHC complex), TCR signaling induced differential T cell activation than the CAR (193). Furthermore, in the absence of antigen, CAR-T cells have been observed to experience low levels of chronic activation leading to exhaustion (284). Lastly, while second generation CARs have demonstrated unprecedented anti-tumor activity in the clinic, their robust proliferative and cytokine responses have led to unprecedented inflammatory toxicities. In Chapter Four, we demonstrated that inclusion of a co-stimulatory domain exacerbates CAR-T cell-associated toxicity; yet, there is no question (based on current data) that inclusion of the co-stimulatory domain is required for CAR-T cell persistence and efficacy in the clinic – a catch-22. Fortunately, the requirement for co-stimulation appears to be unique to the CAR strategy. Natural memory T cells do not necessarily require co-stimulation to effectuate cytokine production, proliferation or cytotoxicity. Indeed, TCR-engineered T cells have been capable of demonstrating efficacy (with reduced observations of toxicities) in clinical trials (252, 285), and we have demonstrated that TAC-T cells (which lack exogenously encoded co-stimulation) are capable of proliferation in response to tumor antigen. In further support of our hypothesis that TAC-T cells experience a more natural activation than their CAR counterparts, data provided in this thesis (and unpublished results) have demonstrated that TAC receptors trigger little to no tonic signalling. Other pre-clinical data are beginning to emerge which also suggest that synthetic T cell activation via co-opting the endogenous TCR-CD3 complex may produce superior efficacy in solid tumors vs CAR-T cells (265, 286). As such, it appears that the future of engineered T cell therapeutics may be in novel synthetic receptor strategies.

6.5 The future of synthetic receptor-engineered T cell therapy for cancer

Amid the diversity of immuno-oncology agents under development, where will synthetic receptor-engineered T cells ultimately fit in?

Given the potent tumor-killing ability of T cells, agents which activate an anti-tumor T cell response are poised to continue to be major players in the

immuno-oncology arena. While immune checkpoint blockade has revolutionized the treatment of melanoma, its use requires an endogenous anti-tumor T cell response (as does TIL therapy). This may limit the patient population capable of benefiting from these therapies to those whose malignancies have high mutational loads (178). In contrast, engineered anti-tumor T cells offer benefit to all patients, regardless of their natural anti-tumor T cell response. Adoptive T cell therapies have the added benefit of being a cellular product (a "living drug") – they are activated *ex vivo*, outside of the local immunosuppressive microenvironment, and are capable of *in vivo* amplification and persistence. Synthetic receptor-engineered T cells (as opposed to TCR-engineered T cells) are particularly appealing given their ability to trigger anti-tumor cytotoxicity in an MHC-independent manner.

However, given the heterogeneous nature of human tumors and their ability of to evolve in response to the selective pressure of the immune system or a therapeutic agent (287), it is unlikely that an engineered T cell which solely functions to induce cytotoxicity against a single target will be capable of uniformly producing durable complete regressions, especially in solid tumors. Indeed, clinical relapses of $CD19^+$ hematological malignancies treated with CD19-CAR-T cells have been associated with antigen loss (221). Instead, the induction of durable complete responses will be better mediated by combinatorial approaches, as is the consensus opinion among immuno-oncologists (288, 289).

One strategy to resist tumor escape to CAR-T cell therapy has been to generate a T cell product which permits a simultaneous response against multiple tumor antigens (e.g. T cells bearing multiple CARs, CARs with multiple tumor antigen-binding domains, and pooled CAR-T cell products) (221). However, with CAR-T cells, targeting an increased number of antigens may increase the occurrence of toxicity. Even if TAC-T cells prove to be a safer option, permitting multi-targeting strategies, how many antigens must be targeted to guarantee complete elimination of a tumor?

As previously mentioned, the ultimate goal of immuno-oncology is to revert the tumor microenvironment to a state promoting immunological tumor elimination rather than escape. Reinstating this natural homeostasis allows for the generation of endogenous anti-tumor immune responses which are capable of evolving alongside a tumor, rather than static agents which treat a single aspect of tumor biology, leaving a patient susceptible to relapse. For this reason, the most successful combinatorial treatment strategies will likely promote the elimination of tumors alongside a correction of the immunosuppressive microenvironment. Several strategies as such have been pioneered (in the pre-clinical setting) with CAR-T cells. For example, CAR-T cells can be engineered to express additional genetic payload (e.g. IL-12) (290) or used to carry an oncolytic virus (291). Such strategies will likely pair well with next-generation synthetic receptor-engineered T cell strategies (like the TAC) which offer the advantage of improved safety profiles.

Synthetic receptor-engineered T cells will ultimately serve to be a tool as a part of systemically active combinatorial immuno-oncology treatment regimens –

we anticipate that our contributions towards an improved understanding of CAR-T cell toxicities and novel receptor strategies, as described in this thesis, will contribute towards the development of safer engineered T cell therapies for this purpose.

7.0 Chapter Seven – References

1. Coley, W.B. 1891. Contribution to the knowledge of sarcoma. *Annals of Surgery* 14: 199–220.

2. Ibrahim, F., and T. Khan. 2015. Bacterial Skin Infections. *Primary Care: Clinics in Office Practice* 42: 485–499.

3. Coley, W.B. 1893. The treatment of malignant tumors by repeated inoculations of erysipelas. *The American Journal of the Medical Sciences* 105: 487–511.

4. Mellman, I., G. Coukos, and G. Dranoff. 2011. Cancer immunotherapy comes of age. *Nature* 480: 480–489.

5. Coley, W. B. 1910. The Treatment of Inoperable Sarcoma by Bacterial Toxins (the Mixed Toxins of the Streptococcus erysipelas and the Bacillus prodigiosus). *Proceedings of the Royal Society of Medicine* 3: 1–48.

6. Balkwill, F. 2009. Tumour necrosis factor and cancer. *Nat Rev Cancer* 9: 361–371.

7. McCarthy, E. F. 2006. The toxins of William B. Coley and the treatment of bone and soft-tissue sarcomas. *The Iowa orthopaedic journal* 26: 154–158.

8. Nauts, H. C., and J. R. McLaren. 1990. Coley toxins--the first century. *Adv Exp Med Biol* 267: 483–500.

9. U.S. National Institutes of Health, National Cancer Institute. Surveillance, Epidemiology and End Results (SEER) Training Modules. Available online at: *https://training.seer.cancer.gov/* (accessed Aug 25, 2017).

10. Canadian Cancer Society's Advisory Committee on Cancer Statistics. 2017. Canadian cancer statistics 2017. Toronto, ON: Canadian Cancer Society. Available online at: *http://www.cancer.ca/~/media/cancer.ca/CW/cancer%20information/cancer%20101/Canadian%20cancer%20statistics/Canadian-Cancer-Statistics-2017-EN.pdf?la=en* (accessed October 10, 2017).

11. Knudson, A. G. 1971. Mutation and Cancer: Statistical Study of Retinoblastoma. *Proceedings of the National Academy of Sciences* 68: 820–823.

12. Hanahan, D., and R. A. Weinberg. 2000. The Hallmarks of Cancer. *Cell* 100: 57–70.

13. Hanahan, D., and R. A. Weinberg. 2011. Hallmarks of cancer: the next generation. *Cell* 144: 646–674.

14. Martelotto, L. G., C. K. Y. Ng, S. Piscuoglio, B. Weigelt, and J. S. Reis-Filho. 2014. Breast cancer intra-tumor heterogeneity. *Breast Cancer Res* 16: 210. doi: 10.1186/bcr3658.

15. Marusyk, A., V. Almendro, and K. Polyak. 2012. Intra-tumour heterogeneity: a looking glass for cancer? *Nat Rev Cancer* 12: 323–334.

16. Wu, J. M., M. J. Fackler, M. K. Halushka, D. W. Molavi, M. E. Taylor, W. W. Teo, C. Griffin, J. Fetting, N. E. Davidson, A. M. De Marzo, J. L. Hicks, D. Chitale, M. Ladanyi, S. Sukumar, and P. Argani. 2008. Heterogeneity of breast cancer metastases: comparison of therapeutic target expression and promoter methylation between primary tumors and their multifocal metastases. *Clin Cancer Res* 14: 1938–1946.

17. Junttila, M. R., and F. J. de Sauvage. 2013. Influence of tumour micro-environment heterogeneity on therapeutic response. *Nature* 501: 346–354.

18. Catalano, V., A. Turdo, S. Di Franco, F. Dieli, M. Todaro, and G. Stassi. 2013. Tumor and its microenvironment: a synergistic interplay. *Semin Cancer Biol* 23: 522–532.

19. Wang, M., J. Zhao, L. Zhang, F. Wei, Y. Lian, Y. Wu, Z. Gong, S. Zhang, J. Zhou, K. Cao, X. Li, W. Xiong, G. Li, Z. Zeng, and C. Guo. 2017. Role of tumor microenvironment in tumorigenesis. *J Cancer* 8: 761–773.

20. Miller, K. D., R. L. Siegel, C. C. Lin, A. B. Mariotto, J. L. Kramer, J. H. Rowland, K. D. Stein, R. Alteri, and A. Jemal. 2016. Cancer treatment and survivorship statistics, 2016. *CA Cancer J Clin* 66: 271–289.

21. Sudhakar, A. 2010. History of Cancer, Ancient and Modern Treatment Methods. *J Cancer Sci Ther* 1: 1–4.

22. Canadian Cancer Society. Treatment. Available online at: *http://www.cancer.ca /en/cancer-information/diagnosis-and-treatment/treatment/?region=on* (accessed October 5, 2017).

23. Slater, J. M. 2012. From X-Rays to Ion Beams: A Short History of Radiation Therapy. In *Ion Beam Therapy* vol. 320. U. Linz, ed. Springer, Berlin, Heidelberg. 3–16.

24. Baskar, R., J. Dai, N. Wenlong, R. Yeo, and K.-W. Yeoh. 2014. Biological response of cancer cells to radiation treatment. *Front Mol Biosci* 1: 24. doi: 10.3389/fmolb.2014.00024.

25. Schaue, D., and W. H. McBride. 2015. Opportunities and challenges of radiotherapy for treating cancer. *Nature reviews Clinical oncology* 12: 527–540.

26. Fu, D., J. A. Calvo, and L. D. Samson. 2012. Balancing repair and tolerance of DNA damage caused by alkylating agents. *Nat Rev Cancer* 12: 104–120.

27. Emadi, A., R. J. Jones, and R. A. Brodsky. 2009. Cyclophosphamide and cancer: golden anniversary. *Nature reviews Clinical oncology* 6: 638–647.

28. Speers, C., and L. J. Pierce. 2016. Postoperative Radiotherapy After Breast-Conserving Surgery for Early-Stage Breast Cancer. *JAMA Oncology* 2: 1075–1082.

29. Anampa, J., Della Makower, and J. A. Sparano. 2015. Progress in adjuvant chemotherapy for breast cancer: an overview. *BMC Med* 13: 195. doi: 10.1186/s12916-015-0439-8.

30. Yardley, D. A. 2013. Drug resistance and the role of combination chemotherapy in improving patient outcomes. *Int J Breast Cancer* 2013: 137414. doi: 10.1155/2013/137414.

31. Bailey, A. M., Y. Mao, J. Zeng, V. Holla, A. Johnson, L. Brusco, K. Chen, J. Mendelsohn, M. J. Routbort, G. B. Mills, and F. Meric-Bernstam. 2014. Implementation of biomarker-driven cancer therapy: existing tools and remaining gaps. *Discov Med* 17: 101–114.

32. Tsimberidou, A. M., A. M. M. Eggermont, and R. L. Schilsky. 2014. Precision cancer medicine: the future is now, only better. *Am Soc Clin Oncol Educ Book* 34: 61–69.

33. Puhalla, S., S. Bhattacharya, and N. E. Davidson. 2012. Hormonal therapy in breast cancer: a model disease for the personalization of cancer care. *Mol Oncol* 6: 222–236.

34. Wong, Y. N. S., R. Ferraldeschi, G. Attard, and J. de Bono. 2014. Evolution of androgen receptor targeted therapy for advanced prostate cancer. *Nature reviews Clinical oncology* 11: 365–376.

35. Otto, T., and P. Sicinski. 2017. Cell cycle proteins as promising targets in cancer therapy. *Nat Rev Cancer* 17: 93–115.

36. Gharwan, H., and H. Groninger. 2015. Kinase inhibitors and monoclonal antibodies in oncology: clinical implications. *Nature reviews Clinical oncology* 13: 209–227.

37. Vasudev, N. S., and A. R. Reynolds. 2014. Anti-angiogenic therapy for cancer: current progress, unresolved questions and future directions. *Angiogenesis* 17: 471–494.

38. Couzin-Frankel, J. 2013. Breakthrough of the year 2013. Cancer immunotherapy. *Science* 342: 1432–1433.

39. Klein, G. 2012. Tumor resistance. *Oncoimmunology* 1: 1355–1359.

40. C. P. Rhoads. 1954. Paul Ehrlich and the cancer problem. *Annals of the New York Academy of Sciences* 59: 190–197.

41. Ribatti, D. 2016. The concept of immune surveillance against tumors. The first theories. *Oncotarget* 8: 7175–7180.

42. R. T. Prehn, and J. M. Main. 1957. Immunity to methylcholanthrene-induced sarcomas. *J Natl Cancer Inst* 18: 769–778.

43. E. J. Foley. 1953. Antigenic properties of methylcholanthrene-induced tumors in mice of the strain of origin. *Cancer Res* 13: 835–837.

44. Burnet, F. M. 1967. Immunological aspects of malignant disease. *The Lancet* 289: 1171–1174.

45. Dunn, G. P., A. T. Bruce, H. Ikeda, L. J. Old, and R. D. Schreiber. 2002. Cancer immunoediting: from immunosurveillance to tumor escape. *Nat Immunol* 3: 991–998.

46. Shankaran, V., H. Ikeda, A. T. Bruce, J. M. White, P. E. Swanson, L. J. Old, and R. D. Schreiber. 2001. IFNgamma and lymphocytes prevent primary tumour development and shape tumour immunogenicity. *Nature* 410: 1107–1111.

47. Mortaz, E., P. Tabarsi, D. Mansouri, A. Khosravi, J. Garssen, A. Velayati, and I. M. Adcock. 2016. Cancers Related to Immunodeficiencies: Update and Perspectives. *Frontiers in Immunology* 7: 365. doi: 10.3389/fimmu.2016.00365.

48. Chapman, J. R., A. C. Webster, and G. Wong. 2013. Cancer in the transplant recipient. *Cold Spring Harb Perspect Med* 3. doi: 10.1101/cshperspect.a015677.

49. Mittal, D., M. M. Gubin, R. D. Schreiber, and M. J. Smyth. 2014. New insights into cancer immunoediting and its three component phases--elimination, equilibrium and escape. *Curr Opin Immunol* 27: 16–25.

50. Teng, M. W. L., J. Galon, W.-H. Fridman, and M. J. Smyth. 2015. From mice to humans: developments in cancer immunoediting. *J Clin Invest* 125: 3338–3346.

51. Schreiber, R. D., L. J. Old, and M. J. Smyth. 2011. Cancer Immunoediting: Integrating Immunity's Roles in Cancer Suppression and Promotion. *Science* 331: 1565–1570.

52. Boissonnas, A., L. Fetler, I. S. Zeelenberg, S. Hugues, and S. Amigorena. 2007. In vivo imaging of cytotoxic T cell infiltration and elimination of a solid tumor. *J Exp Med* 204: 345–356.

53. Ritter, A. T., Y. Asano, J. C. Stinchcombe, N. M. G. Dieckmann, B.-C. Chen, C. Gawden-Bone, S. van Engelenburg, W. Legant, L. Gao, M. W. Davidson, E. Betzig, J. Lippincott-Schwartz, and G. M. Griffiths. 2015. Actin depletion initiates events leading to granule secretion at the immunological synapse. *Immunity* 42: 864–876.

54. Gabrielson, A., Y. Wu, H. Wang, J. Jiang, B. Kallakury, Z. Gatalica, S. Reddy, D. Kleiner, T. Fishbein, L. Johnson, E. Island, R. Satoskar, F. Banovac, R. Jha, J. Kachhela, P. Feng, T. Zhang, A. Tesfaye, P. Prins, C. Loffredo, J. Marshall, L. Weiner, M. Atkins, and A. R. He. 2016. Intratumoral CD3 and CD8 T-cell Densities Associated with Relapse-Free Survival in HCC. *Cancer Immunol Res* 4: 419–430.

55. Bachmayr-Heyda, A., S. Aust, G. Heinze, S. Polterauer, C. Grimm, E. I. Braicu, J. Sehouli, S. Lambrechts, I. Vergote, S. Mahner, D. Pils, E. Schuster, T. Thalhammer, R. Horvat, C. Denkert, R. Zeillinger, and D. C. Castillo-Tong. 2013. Prognostic impact of tumor infiltrating CD8+ T cells in association with cell proliferation in ovarian cancer patients--a study of the OVCAD consortium. *BMC Cancer* 13: 422. doi: 10.1186/1471-2407-13-422.

56. Sharma, P., Y. Shen, S. Wen, S. Yamada, A. A. Jungbluth, S. Gnjatic, D. F. Bajorin, V. E. Reuter, H. Herr, L. J. Old, and E. Sato. 2007. CD8 tumor-infiltrating lymphocytes are predictive of survival in muscle-invasive urothelial carcinoma. *Proc Natl Acad Sci USA* 104: 3967–3972.

57. Naito, Y., K. Saito, K. Shiiba, A. Ohuchi, K. Saigenji, H. Nagura, and H. Ohtani. 1998. CD8+ T cells infiltrated within cancer cell nests as a prognostic factor in human colorectal cancer. *Cancer Res* 58: 3491–3494.

58. Liu, S., J. Lachapelle, S. Leung, D. Gao, W. D. Foulkes, and T. O. Nielsen. 2012. CD8+ lymphocyte infiltration is an independent favorable prognostic indicator in basal-like breast cancer. *Breast Cancer Res* 14: R48. doi: 10.1186/bcr3148.

59. Mahmoud, S. M. A., E. C. Paish, D. G. Powe, R. D. Macmillan, M. J. Grainge, A. H. S. Lee, I. O. Ellis, and A. R. Green. 2011. Tumor-infiltrating CD8+ lymphocytes predict clinical outcome in breast cancer. *J Clin Oncol* 29: 1949–1955.

60. Hérin, M., C. Lemoine, P. Weynants, F. Vessière, A. Van Pel, A. Knuth, R. Devos, and T. Boon. 1987. Production of stable cytolytic T-cell clones directed against autologous human melanoma. *Int J Cancer* 39: 390–396.

61. Housseau, F., D. A. Langer, S. D. Oberholtzer, A. Moorthy, H. I. Levitsky, D. M. Pardoll, and S. L. Topalian. 2002. Tumor-specific CD8+ T lymphocytes derived from the peripheral blood of prostate cancer patients byin vitro stimulation with autologous tumor cell lines. *Int J Cancer* 98: 57–62.

62. Coulie, P. G., V. Brichard, A. Van Pel, T. Wölfel, J. Schneider, C. Traversari, S. Mattei, E. De Plaen, C. Lurquin, J. P. Szikora, J. C. Renauld, and T. Boon. 1994. A new gene coding for a differentiation antigen recognized by autologous cytolytic T lymphocytes on HLA-A2 melanomas. *J Exp Med* 180: 35–42.

63. Brichard, V., A. Van Pel, T. Wolfel, C. Wolfel, E. De Plaen, B. Lethe, P. G. Coulie, and T. Boon. 1993. The tyrosinase gene codes for an antigen recognized by autologous cytolytic T lymphocytes on HLA-A2 melanomas. *Journal of Experimental Medicine* 178: 489–495.

64. Knuth, A., T. Wölfel, E. Klehmann, T. Boon, and K. H. M. zum Büschenfelde. 1989. Cytolytic T-cell clones against an autologous human melanoma: specificity study and definition of three antigens by immunoselection. *Proc Natl Acad Sci USA* 86: 2804–2808.

65. Zippelius, A., P. Batard, V. Rubio-Godoy, G. Bioley, D. Liénard, F. Lejeune, D. Rimoldi, P. Guillaume, N. Meidenbauer, A. Mackensen, N. Rufer, N. Lubenow, D. Speiser, J.-C. Cerottini, P. Romero, and M. J. Pittet. 2004. Effector function of human tumor-specific CD8 T cells in melanoma lesions: a state of local functional tolerance. *Cancer Res* 64: 2865–2873.

66. Dadmarz, R., M. K. Sgagias, S. A. Rosenberg, and D. J. Schwartzentruber. 1995. CD4+ T lymphocytes infiltrating human breast cancer recognise autologous tumor in an MHC-class-II restricted fashion. *Cancer Immunol Immunother* 40: 1–9.

67. Robbins, P. F., M. El-Gamil, Y. F. Li, G. Zeng, M. Dudley, and S. A. Rosenberg. 2002. Multiple HLA Class II-Restricted Melanocyte Differentiation Antigens Are Recognized by Tumor-Infiltrating Lymphocytes from a Patient with Melanoma. *The Journal of Immunology* 169: 6036–6047.

68. Bos, R., and L. A. Sherman. 2010. CD4+ T-cell help in the tumor milieu is required for recruitment and cytolytic function of CD8+ T lymphocytes. *Cancer Res* 70: 8368–8377.

69. Haabeth, O. A. W., K. B. Lorvik, C. Hammarström, I. M. Donaldson, G. Haraldsen, B. Bogen, and A. Corthay. 2011. Inflammation driven by tumour-specific Th1 cells protects against B-cell cancer. *Nat Commun* 2: 240. doi: 10.1038/ncomms1239.

70. Perez-Diez, A., N. T. Joncker, K. Choi, W. F. N. Chan, C. C. Anderson, O. Lantz, and P. Matzinger. 2007. CD4 cells can be more efficient at tumor rejection than CD8 cells. *Blood* 109: 5346–5354.

71. Quezada, S. A., T. R. Simpson, K. S. Peggs, T. Merghoub, J. Vider, X. Fan, R. Blasberg, H. Yagita, P. Muranski, P. A. Antony, N. P. Restifo, and J. P. Allison. 2010. Tumor-reactive CD4(+) T cells develop cytotoxic activity and eradicate large established melanoma after transfer into lymphopenic hosts. *J Exp Med* 207: 637–650.

72. Zhang, M., Y. He, X. Sun, Q. Li, W. Wang, A. Zhao, and W. Di. 2014. A high M1/M2 ratio of tumor-associated macrophages is associated with extended survival in ovarian cancer patients. *J Ovarian Res* 7: 19. doi: 10.1186/1757-2215-7-19.

73. Panni, R. Z., D. C. Linehan, and D. G. DeNardo. 2013. Targeting tumor-infiltrating macrophages to combat cancer. *Immunotherapy* 5: 1075–1087.

74. Gardner, A., and B. Ruffell. 2016. Dendritic Cells and Cancer Immunity. *Trends Immunol* 37: 855–865.

75. Morvan, M. G., and L. L. Lanier. 2015. NK cells and cancer: you can teach innate cells new tricks. *Nat Rev Cancer* 16: 7–19.

76. Tugues, S., S. H. Burkhard, I. Ohs, M. Vrohlings, K. Nussbaum, J. V. Berg, P. Kulig, and B. Becher. 2014. New insights into IL-12-mediated tumor suppression. *Cell Death Differ* 22: 237–246.

77. Parker, B. S., J. Rautela, and P. J. Hertzog. 2016. Antitumour actions of interferons: implications for cancer therapy. *Nat Rev Cancer* 16: 131–144.

78. Kumar, V., S. Patel, E. Tcyganov, and D. I. Gabrilovich. 2016. The Nature of Myeloid-Derived Suppressor Cells in the Tumor Microenvironment. *Trends Immunol* 37: 208–220.

79. Noy, R., and J. W. Pollard. 2014. Tumor-associated macrophages: from mechanisms to therapy. *Immunity* 41: 49–61.

80. Whiteside, T. L. 2014. Induced regulatory T cells in inhibitory microenvironments created by cancer. *Expert Opin Biol Ther* 14: 1411–1425.

81. Takeuchi, Y., and H. Nishikawa. 2016. Roles of regulatory T cells in cancer immunity. *Int Immunol* 28: 401–409.

82. Noguchi, T., J. P. Ward, M. M. Gubin, C. D. Arthur, S. H. Lee, J. Hundal, M. J. Selby, R. F. Graziano, E. R. Mardis, A. J. Korman, and R. D. Schreiber. 2017.

Temporally Distinct PD-L1 Expression by Tumor and Host Cells Contributes to Immune Escape. *Cancer Immunol Res* 5: 106–117.

83. Chen, L., and D. B. Flies. 2013. Molecular mechanisms of T cell co-stimulation and co-inhibition. *Nat Rev Immunol* 13: 227–242.

84. Flavell, R. A., S. Sanjabi, S. H. Wrzesinski, and P. Licona-Limón. 2010. The polarization of immune cells in the tumour environment by TGFbeta. *Nat Rev Immunol* 10: 554–567.

85. Dennis, K. L., N. R. Blatner, F. Gounari, and K. Khazaie. 2013. Current status of interleukin-10 and regulatory T-cells in cancer. *Curr Opin Oncol* 25: 637–645.

86. Mumm, J. B., J. Emmerich, X. Zhang, I. Chan, L. Wu, S. Mauze, S. Blaisdell, B. Basham, J. Dai, J. Grein, C. Sheppard, K. Hong, C. Cutler, S. Turner, D. LaFace, M. Kleinschek, M. Judo, G. Ayanoglu, J. Langowski, D. Gu, B. Paporello, E. Murphy, V. Sriram, S. Naravula, B. Desai, S. Medicherla, W. Seghezzi, T. McClanahan, S. Cannon-Carlson, A. M. Beebe, and M. Oft. 2011. IL-10 elicits IFNγ-dependent tumor immune surveillance. *Cancer Cell* 20: 781–796.

87. Wucherpfennig, K. W., E. Gagnon, M. J. Call, E. S. Huseby, and M. E. Call. 2010. Structural biology of the T-cell receptor: insights into receptor assembly, ligand recognition, and initiation of signaling. *Cold Spring Harb Perspect Biol* 2: a005140. doi: 10.1101/cshperspect.a005140.

88. Balakrishnan, A., and G. P. Morris. 2015. The highly alloreactive nature of dual TCR T cells. *Curr Opin Organ Transplant* 21: 22–28.

89. Nicolas, L., G. Monneret, A. L. Debard, A. Blesius, M. C. Gutowski, G. Salles, and J. Bienvenu. 2001. Human gammadelta T cells express a higher TCR/CD3 complex density than alphabeta T cells. *Clin Immunol* 98: 358–363.

90. Schodin, B. A., T. J. Tsomides, and D. M. Kranz. 1996. Correlation between the number of T cell receptors required for T cell activation and TCR-ligand affinity. *Immunity* 5: 137–146.

91. Sykulev, Y., A. Brunmark, M. Jackson, R. J. Cohen, P. A. Peterson, and H. N. Eisen. 1994. Kinetics and affinity of reactions between an antigen-specific T cell receptor and peptide-MHC complexes. *Immunity* 1: 15–22.

92. Lythe, G., R. E. Callard, R. L. Hoare, and C. Molina-París. 2015. How many TCR clonotypes does a body maintain? *J Theor Biol* 389: 214–224.

93. Laydon, D. J., C. R. M. Bangham, and B. Asquith. 2015. Estimating T-cell repertoire diversity: limitations of classical estimators and a new approach. *Philos Trans R Soc Lond, B, Biol Sci* 370. doi: 10.1098/rstb.2014.0291.

94. Zarnitsyna, V. I., B. D. Evavold, L. N. Schoettle, J. N. Blattman, and R. Antia. 2013. Estimating the diversity, completeness, and cross-reactivity of the T cell repertoire. *Frontiers in Immunology* 4: 485. doi: 10.3389/fimmu.2013.00485.

95. Arstila, T. P., A. Casrouge, V. Baron, J. Even, J. Kanellopoulos, and P. Kourilsky. 1999. A direct estimate of the human alphabeta T cell receptor diversity. *Science* 286: 958–961.

96. Sewell, A. K. 2012. Why must T cells be cross-reactive? *Nat Rev Immunol* 12: 669–677.

97. Masopust, D., and J. M. Schenkel. 2013. The integration of T cell migration, differentiation and function. *Nat Rev Immunol* 13: 309–320.

98. N. Yudanin, Y. Ohmura, M. Kubota, B. Grinshpun, T. Sathaliyawala, T. Kato, H. Lerner, Y. Shen, and D. L. Farber. 2014. Spatial map of human T cell compartmentalization and maintenance over decades of life. *Cell* 159: 814–828.

99. Koch, U., and F. Radtke. 2011. Mechanisms of T cell development and transformation. *Annu Rev Cell Dev Biol* 27: 539–562.

100. Krueger, A., N. Ziętara, and M. Łyszkiewicz. 2016. T Cell Development by the Numbers. *Trends Immunol* 38: 128–139.

101. Murphy, K., P. Travers, and M. Walport. 2008. *Janeway's Immunobiology*, Seventh Edition. Garland Science, New York, NY.

102. Gascoigne, N. R. J., V. Rybakin, O. Acuto, and J. Brzostek. 2016. TCR Signal Strength and T Cell Development. *Annu Rev Cell Dev Biol* 32: 327–348.

103. Weinreich, M. A., and K. A. Hogquist. 2008. Thymic Emigration: When and How T Cells Leave Home. *The Journal of Immunology* 181: 2265–2270.

104. Resop, R. S., and C. H. Uittenbogaart. 2015. Human T-Cell Development and Thymic Egress: An Infectious Disease Perspective. *For Immunopathol Dis Therap* 6: 33–49.

105. Stone, J. D., A. S. Chervin, and D. M. Kranz. 2009. T-cell receptor binding affinities and kinetics: impact on T-cell activity and specificity. *Immunology* 126: 165–176.

106. Tseng, S. Y., J. C. Waite, M. Liu, S. Vardhana, and M. L. Dustin. 2008. T Cell-Dendritic Cell Immunological Synapses Contain TCR-dependent CD28-CD80 Clusters That Recruit Protein Kinase C. *The Journal of Immunology* 181: 4852–4863.

107. Dudek, A. M., S. Martin, A. D. Garg, and P. Agostinis. 2013. Immature, Semi-Mature, and Fully Mature Dendritic Cells: Toward a DC-Cancer Cells Interface That Augments Anticancer Immunity. *Frontiers in Immunology* 4: 438. doi: 10.3389/fimmu.2013.00438.

108. Crespo, J., H. Sun, T. H. Welling, Z. Tian, and W. Zou. 2013. T cell anergy, exhaustion, senescence, and stemness in the tumor microenvironment. *Curr Opin Immunol* 25: 214–221.

109. Smith-Garvin, J. E., G. A. Koretzky, and M. S. Jordan. 2009. T cell activation. *Annu Rev Immunol* 27: 591–619.

110. Farber, D. L., N. A. Yudanin, and N. P. Restifo. 2013. Human memory T cells: generation, compartmentalization and homeostasis. *Nat Rev Immunol* 14: 24–35.

111. Chang, J. T., E. J. Wherry, and A. W. Goldrath. 2014. Molecular regulation of effector and memory T cell differentiation. *Nat Immunol* 15: 1104–1115.

112. Farber, D. L., M. G. Netea, A. Radbruch, K. Rajewsky, and R. M. Zinkernagel. 2016. Immunological memory: lessons from the past and a look to the future. *Nat Rev Immunol* 16: 124–128.

113. Buchholz, V. R., T. N. M. Schumacher, and D. H. Busch. 2015. T Cell Fate at the Single-Cell Level. *Annu Rev Immunol* 34: 65–92.

114. Geginat, J., M. Paroni, F. Facciotti, P. Gruarin, I. Kastirr, F. Caprioli, M. Pagani, and S. Abrignani. 2013. The CD4-centered universe of human T cell subsets. *Seminars in Immunology* 25: 252–262.

115. DuPage, M., and J. A. Bluestone. 2016. Harnessing the plasticity of CD4(+) T cells to treat immune-mediated disease. *Nat Rev Immunol* 16: 149–163.

116. Geginat, J., M. Paroni, S. Maglie, J. S. Alfen, I. Kastirr, P. Gruarin, M. De Simone, M. Pagani, and S. Abrignani. 2014. Plasticity of human CD4 T cell subsets. *Frontiers in Immunology* 5: 630. doi: 10.3389/fimmu.2014.00630.

117. Yang, Z.-Z., D. M. Grote, S. C. Ziesmer, B. Xiu, N. R. Yates, F. J. Secreto, L. S. Hodge, T. E. Witzig, A. J. Novak, and S. M. Ansell. 2013. Soluble and membrane-bound TGF-β-mediated regulation of intratumoral T cell differentiation and function in B-cell non-Hodgkin lymphoma. *PLoS ONE* 8: e59456. doi: 10.1371/journal.pone.0059456.

118. Martínez-Lostao, L., A. Anel, and J. Pardo. 2015. How Do Cytotoxic Lymphocytes Kill Cancer Cells? *Clin Cancer Res* 21: 5047–5056.

119. Voskoboinik, I., J. C. Whisstock, and J. A. Trapani. 2015. Perforin and granzymes: function, dysfunction and human pathology. *Nat Rev Immunol* 15: 388–400.

120. L. W. Collison, and C. J. Workman. 2008. How regulatory T cells work. *Nat Rev Immunol* 8: 523–532.

121. Galluzzi, L., A. Buqué, O. Kepp, L. Zitvogel, and G. Kroemer. 2015. Immunological Effects of Conventional Chemotherapy and Targeted Anticancer Agents. *Cancer Cell* 28: 690–714.

122. Chen, G., and L. A. Emens. 2013. Chemoimmunotherapy: reengineering tumor immunity. *Cancer Immunology, Immunotherapy* 62: 203–216.

123. Park, B., C. Yee, and K.-M. Lee. 2014. The effect of radiation on the immune response to cancers. *Int J Mol Sci* 15: 927–943.

124. Apetoh, L., F. Ghiringhelli, A. Tesniere, M. Obeid, C. Ortiz, A. Criollo, G. Mignot, M. C. Maiuri, E. Ullrich, P. Saulnier, H. Yang, S. Amigorena, B. Ryffel, F. J. Barrat, P. Saftig, F. Levi, R. Lidereau, C. Nogues, J.-P. Mira, A. Chompret, V. Joulin, F. Clavel-Chapelon, J. Bourhis, F. André, S. Delaloge, T. Tursz, G. Kroemer, and L. Zitvogel. 2007. Toll-like receptor 4-dependent contribution of the immune system to anticancer chemotherapy and radiotherapy. *Nat Med* 13: 1050–1059.

125. Vincent, J., G. Mignot, F. Chalmin, S. Ladoire, M. Bruchard, A. Chevriaux, F. Martin, L. Apetoh, C. Rébé, and F. Ghiringhelli. 2010. 5-Fluorouracil selectively kills tumor-associated myeloid-derived suppressor cells resulting in enhanced T cell-dependent antitumor immunity. *Cancer Res* 70: 3052–3061.

126. Ghiringhelli, F., C. Menard, P. E. Puig, S. Ladoire, S. Roux, F. Martin, E. Solary, A. Le Cesne, L. Zitvogel, and B. Chauffert. 2006. Metronomic cyclophosphamide regimen selectively depletes CD4+CD25+ regulatory T cells and restores T and NK effector functions in end stage cancer patients. *Cancer Immunol Immunother* 56: 641–648.

127. Rosenberg, S. A. 2014. IL-2: the first effective immunotherapy for human cancer. *J Immunol* 192: 5451–5458.

128. Disis, M. L. 2014. Mechanism of action of immunotherapy. *Semin Oncol* 41 Suppl 5: S3–S13. doi: 10.1053/j.seminoncol.2014.09.004.

129. Rosenberg, S. A., J. C. Yang, D. E. White, and S. M. Steinberg. 1998. Durability of Complete Responses in Patients With Metastatic Cancer Treated With High-Dose Interleukin-2. *Annals of Surgery* 228: 307–317.

130. Schwartzentruber, D. J. 2001. Guidelines for the safe administration of high-dose interleukin-2. *J Immunother* 24: 287–293.

131. Panelli, M. C., R. White, M. Foster, B. Martin, E. Wang, K. Smith, and F. M. Marincola. 2004. Forecasting the cytokine storm following systemic interleukin (IL)-2 administration. *J Transl Med* 2: 17. doi: 10.1186/1479-5876-2-17.

132. Vacchelli, E., J. Pol, N. Bloy, A. Eggermont, I. Cremer, W. H. Fridman, J. Galon, A. Marabelle, H. Kohrt, L. Zitvogel, G. Kroemer, and L. Galluzzi. 2015. Trial watch: Tumor-targeting monoclonal antibodies for oncological indications. *Oncoimmunology* 4: e985940. doi: 10.4161/2162402X.2014.985940.

133. Weiner, G. J. 2015. Building better monoclonal antibody-based therapeutics. *Nat Rev Cancer* 15: 361–370.

134. Kontermann, R. E., and U. Brinkmann. 2015. Bispecific antibodies. *Drug Discovery Today* 20: 838–847.

135. Huehls, A. M., T. A. Coupet, and C. L. Sentman. 2014. Bispecific T-cell engagers for cancer immunotherapy. *Immunol Cell Biol* 93: 290–296.

136. Przepiorka, D., C.-W. Ko, A. Deisseroth, C. L. Yancey, R. Candau-Chacon, H.-J. Chiu, B. J. Gehrke, C. Gomez-Broughton, R. C. Kane, S. Kirshner, N. Mehrotra, T. K. Ricks, D. Schmiel, P. Song, P. Zhao, Q. Zhou, A. T. Farrell, and R. Pazdur. 2015. FDA Approval: Blinatumomab. *Clin Cancer Res* 21: 4035–4039.

137. Maher, J., and A. A. Adami. 2013. Antitumor immunity: easy as 1, 2, 3 with monoclonal bispecific trifunctional antibodies? *Cancer Res* 73: 5613–5617.

138. Garber, K. 2014. Bispecific antibodies rise again. *Nat Rev Drug Discov* 13: 799–801.

139. Ribas, A. 2015. Releasing the Brakes on Cancer Immunotherapy. *N Engl J Med* 373: 1490–1492.

140. Teng, M. W. L., S. F. Ngiow, A. Ribas, and M. J. Smyth. 2015. Classifying Cancers Based on T-cell Infiltration and PD-L1. *Cancer Res* 75: 2139–2145.

141. Topalian, S. L., J. M. Taube, R. A. Anders, and D. M. Pardoll. 2016. Mechanism-driven biomarkers to guide immune checkpoint blockade in cancer therapy. *Nat Rev Cancer* 16: 275–287.

142. Boutros, C., A. Tarhini, E. Routier, O. Lambotte, F. L. Ladurie, F. Carbonnel, H. Izzeddine, A. Marabelle, S. Champiat, A. Berdelou, E. Lanoy, M. Texier, C. Libenciuc, A. M. M. Eggermont, J.-C. Soria, C. Mateus, and C. Robert. 2016.

Safety profiles of anti-CTLA-4 and anti-PD-1 antibodies alone and in combination. *Nature reviews Clinical oncology* 13: 473–486.

143. Lichty, B. D., C. J. Breitbach, D. F. Stojdl, and J. C. Bell. 2014. Going viral with cancer immunotherapy. *Nat Rev Cancer* 14: 559–567.

144. Kaufman, H. L., F. J. Kohlhapp, and A. Zloza. 2015. Oncolytic viruses: a new class of immunotherapy drugs. *Nat Rev Drug Discov* 14: 642–662.

145. Kaufman, H. L., D. W. Kim, G. DeRaffele, J. Mitcham, R. S. Coffin, and S. Kim-Schulze. 2009. Local and distant immunity induced by intralesional vaccination with an oncolytic herpes virus encoding GM-CSF in patients with stage IIIc and IV melanoma. *Ann Surg Oncol* 17: 718–730.

146. Rehman, H., A. W. Silk, M. P. Kane, and H. L. Kaufman. 2016. Into the clinic: Talimogene laherparepvec (T-VEC), a first-in-class intratumoral oncolytic viral therapy. *Journal for ImmunoTherapy of Cancer* 4: 53. doi: 10.1186/s40425-016-0158-5.

147. Bridle, B. W., J. E. Boudreau, B. D. Lichty, J. Brunellière, K. Stephenson, S. Koshy, J. L. Bramson, and Y. Wan. 2009. Vesicular stomatitis virus as a novel cancer vaccine vector to prime antitumor immunity amenable to rapid boosting with adenovirus. *Mol Ther* 17: 1814–1821.

148. Butterfield, L. H. 2015. Cancer vaccines. *BMJ* 350: h988. doi: 10.1136/bmj.h988.

149. Melero, I., G. Gaudernack, W. Gerritsen, C. Huber, G. Parmiani, S. Scholl, N. Thatcher, J. Wagstaff, C. Zielinski, I. Faulkner, and H. Mellstedt. 2014. Therapeutic vaccines for cancer: an overview of clinical trials. *Nature reviews Clinical oncology* 11: 509–524.

150. Melief, C. J. M., T. van Hall, R. Arens, F. Ossendorp, and S. H. van der Burg. 2015. Therapeutic cancer vaccines. *J Clin Invest* 125: 3401–3412.

151. Kantoff, P. W., C. S. Higano, N. D. Shore, E. R. Berger, E. J. Small, D. F. Penson, C. H. Redfern, A. C. Ferrari, R. Dreicer, R. B. Sims, Y. Xu, M. W. Frohlich, and P. F. Schellhammer. 2010. Sipuleucel-T immunotherapy for castration-resistant prostate cancer. *N Engl J Med* 363: 411–422.

152. Yee, C. 2005. Adoptive T cell therapy: Addressing challenges in cancer immunotherapy. *J Transl Med* 3: 17. doi: 10.1186/1479-5876-3-17.

153. Restifo, N. P., M. E. Dudley, and S. A. Rosenberg. 2012. Adoptive immunotherapy for cancer: harnessing the T cell response. *Nat Rev Immunol* 12: 269–281.

154. McGray, A. J. R., R. Hallett, D. Bernard, S. L. Swift, Z. Zhu, F. Teoderascu, H. VanSeggelen, J. A. Hassell, A. A. Hurwitz, Y. Wan, and J. L. Bramson. 2013. Immunotherapy-induced CD8+ T cells instigate immune suppression in the tumor. *Mol Ther* 22: 206–218.

155. Rosenberg, S. A., and N. P. Restifo. 2015. Adoptive cell transfer as personalized immunotherapy for human cancer. *Science* 348: 62–68.

156. Eberlein, T. J., M. Rosenstein, and S. A. Rosenberg. 1982. Regression of a disseminated syngeneic solid tumor by systemic transfer of lymphoid cells expanded in interleukin 2. *J Exp Med* 156: 385–397.

157. Rosenberg, S. A., B. S. Packard, P. M. Aebersold, D. Solomon, S. L. Topalian, S. T. Toy, P. Simon, M. T. Lotze, J. C. Yang, C. A. Seipp, C. Simpson, C. Carter, S. Bock, D. Schwartzentruber, J. P. Wei, and D. E. White. 1988. Use of Tumor-Infiltrating Lymphocytes and Interleukin-2 in the Immunotherapy of Patients with Metastatic Melanoma. *New England Journal of Medicine* 319: 1676–1680.

158. Goff, S. L., M. E. Dudley, D. E. Citrin, R. P. Somerville, J. R. Wunderlich, D. N. Danforth, D. A. Zlott, J. C. Yang, R. M. Sherry, U. S. Kammula, C. A. Klebanoff, M. S. Hughes, N. P. Restifo, M. M. Langhan, T. E. Shelton, L. Lu, M. L. M. Kwong, S. Ilyas, N. D. Klemen, E. C. Payabyab, K. E. Morton, M. A. Toomey, S. M. Steinberg, D. E. White, and S. A. Rosenberg. 2016. Randomized, Prospective Evaluation Comparing Intensity of Lymphodepletion Before Adoptive Transfer of Tumor-Infiltrating Lymphocytes for Patients With Metastatic Melanoma. *J Clin Oncol* 34: 2389–2397.

159. Radvanyi, L. G., C. Bernatchez, M. Zhang, P. S. Fox, P. Miller, J. Chacon, R. Wu, G. Lizee, S. Mahoney, G. Alvarado, M. Glass, V. E. Johnson, J. D. McMannis, E. Shpall, V. Prieto, N. Papadopoulos, K. Kim, J. Homsi, A. Bedikian, W.-J. Hwu, S. Patel, M. I. Ross, J. E. Lee, J. E. Gershenwald, A. Lucci, R. Royal, J. N. Cormier, M. A. Davies, R. Mansaray, O. J. Fulbright, C. Toth, R. Ramachandran, S. Wardell, A. Gonzalez, and P. Hwu. 2012. Specific lymphocyte subsets predict response to adoptive cell therapy using expanded autologous tumor-infiltrating lymphocytes in metastatic melanoma patients. *Clin Cancer Res* 18: 6758–6770.

160. Pilon-Thomas, S., L. Kuhn, S. Ellwanger, W. Janssen, E. Royster, S. Marzban, R. Kudchadkar, J. Zager, G. Gibney, V. K. Sondak, J. Weber, J. J. Mulé, and A. A. Sarnaik. 2012. Efficacy of Adoptive Cell Transfer of Tumor-infiltrating Lymphocytes After Lymphopenia Induction for Metastatic Melanoma. *Journal of Immunotherapy* 35: 615–620.

161. Rosenberg, S. A., J. C. Yang, R. M. Sherry, U. S. Kammula, M. S. Hughes, G. Q. Phan, D. E. Citrin, N. P. Restifo, P. F. Robbins, J. R. Wunderlich, K. E. Morton,

C. M. Laurencot, S. M. Steinberg, D. E. White, and M. E. Dudley. 2011. Durable complete responses in heavily pretreated patients with metastatic melanoma using T-cell transfer immunotherapy. *Clin Cancer Res* 17: 4550–4557.

162. Stevanović, S., L. M. Draper, M. M. Langhan, T. E. Campbell, M. L. Kwong, J. R. Wunderlich, M. E. Dudley, J. C. Yang, R. M. Sherry, U. S. Kammula, N. P. Restifo, S. A. Rosenberg, and C. S. Hinrichs. 2015. Complete regression of metastatic cervical cancer after treatment with human papillomavirus-targeted tumor-infiltrating T cells. *J Clin Oncol* 33: 1543–1550.

163. Turcotte, S., A. Gros, E. Tran, C.-C. R. Lee, J. R. Wunderlich, P. F. Robbins, and S. A. Rosenberg. 2013. Tumor-reactive CD8+ T cells in metastatic gastrointestinal cancer refractory to chemotherapy. *Clin Cancer Res* 20: 331–343.

164. Tran, E., S. Turcotte, A. Gros, P. F. Robbins, Y.-C. Lu, M. E. Dudley, J. R. Wunderlich, R. P. Somerville, K. Hogan, C. S. Hinrichs, M. R. Parkhurst, J. C. Yang, and S. A. Rosenberg. 2014. Cancer immunotherapy based on mutation-specific CD4+ T cells in a patient with epithelial cancer. *Science* 344: 641–645.

165. Sarnaik, A., H. Kluger, J. Chesney, J. Sethuraman, M. Lotze, B. Larsen, I. Gorbatchevsky, N. L. Samberg, S. Suzuki, L. Wang, M. Mirgoli, M. Fardis, and B. Curti. 2017. Efficacy of Single Administration of Tumor Infiltrating Lymphocytes (TIL) in Heavily Pre-Treated Metastatic Melanoma Patients Following Checkpoint Therapy. Poster presentation at: *ASCO 2017*. Available online at: *http://www.iovance.com/wp-content/uploads/2017/05/LION-Bio_ASCO2017_Poster_FINAL.pdf* (accessed Oct 26, 2017).

166. Rosenberg, S. A. 2011. Cell transfer immunotherapy for metastatic solid cancer--what clinicians need to know. *Nature reviews Clinical oncology* 8: 577–585.

167. Alexandrov, L. B., S. Nik-Zainal, D. C. Wedge, S. A. J. R. Aparicio, S. Behjati, A. V. Biankin, G. R. Bignell, N. Bolli, A. Borg, A.-L. Børresen-Dale, S. Boyault, B. Burkhardt, A. P. Butler, C. Caldas, H. R. Davies, C. Desmedt, R. Eils, J. E. Eyfjörd, J. A. Foekens, M. Greaves, F. Hosoda, B. Hutter, T. Ilicic, S. Imbeaud, M. Imielinski, M. Imielinsk, N. Jäger, D. T. W. Jones, D. T. W. Jones, S. Knappskog, M. Kool, S. R. Lakhani, C. López-Otín, S. Martin, N. C. Munshi, H. Nakamura, P. A. Northcott, M. Pajic, E. Papaemmanuil, A. Paradiso, J. V. Pearson, X. S. Puente, K. Raine, M. Ramakrishna, A. L. Richardson, J. Richter, P. Rosenstiel, M. Schlesner, T. N. Schumacher, P. N. Span, J. W. Teague, Y. Totoki, A. N. J. Tutt, R. Valdés-Mas, M. M. van Buuren, L. van 't Veer, A. Vincent-Salomon, N. Waddell, L. R. Yates, J. Zucman-Rossi, P. A. Futreal, U. McDermott, P. Lichter, M. Meyerson, S. M. Grimmond, R. Siebert, E. Campo, T. Shibata, S. M. Pfister, P.

J. Campbell, and M. R. Stratton. 2013. Signatures of mutational processes in human cancer. *Nature* 500: 415–421.

168. Bobisse, S., P. G. Foukas, G. Coukos, and A. Harari. 2016. Neoantigen-based cancer immunotherapy. *Ann Transl Med* 4: 262. doi: 10.21037/atm.2016.06.17.

169. Debets, R., E. Donnadieu, S. Chouaib, and G. Coukos. 2016. TCR-engineered T cells to treat tumors: Seeing but not touching? *Seminars in Immunology* 28: 10–21.

170. Johnson, L. A., R. A. Morgan, M. E. Dudley, L. Cassard, J. C. Yang, M. S. Hughes, U. S. Kammula, R. E. Royal, R. M. Sherry, J. R. Wunderlich, C.-C. R. Lee, N. P. Restifo, S. L. Schwarz, A. P. Cogdill, R. J. Bishop, H. Kim, C. C. Brewer, S. F. Rudy, C. VanWaes, J. L. Davis, A. Mathur, R. T. Ripley, D. A. Nathan, C. M. Laurencot, and S. A. Rosenberg. 2009. Gene therapy with human and mouse T-cell receptors mediates cancer regression and targets normal tissues expressing cognate antigen. *Blood* 114: 535–546.

171. Robbins, P. F., S. H. Kassim, T. L. N. Tran, J. S. Crystal, R. A. Morgan, S. A. Feldman, J. C. Yang, M. E. Dudley, J. R. Wunderlich, R. M. Sherry, U. S. Kammula, M. S. Hughes, N. P. Restifo, M. Raffeld, C.-C. R. Lee, Y. F. Li, M. El-Gamil, and S. A. Rosenberg. 2014. A pilot trial using lymphocytes genetically engineered with an NY-ESO-1-reactive T-cell receptor: long-term follow-up and correlates with response. *Clin Cancer Res* 21: 1019–1027.

172. Leone, P., E.-C. Shin, F. Perosa, A. Vacca, F. Dammacco, and V. Racanelli. 2013. MHC class I antigen processing and presenting machinery: organization, function, and defects in tumor cells. *J Natl Cancer Inst* 105: 1172–1187.

173. Garrido, F., N. Aptsiauri, E. M. Doorduijn, A. M. G. Lora, and T. van Hall. 2016. The urgent need to recover MHC class I in cancers for effective immunotherapy. *Curr Opin Immunol* 39: 44–51.

174. Seliger, B. 2011. Novel insights into the molecular mechanisms of HLA class I abnormalities. *Cancer Immunol Immunother* 61: 249–254.

175. Jackson, H. J., S. Rafiq, and R. J. Brentjens. 2016. Driving CAR T-cells forward. *Nature reviews Clinical oncology* 13: 370–383.

176. Johnson, L. A., and C. H. June. 2016. Driving gene-engineered T cell immunotherapy of cancer. *Cell Res* 27: 38–58.

177. Sadelain, M., R. Brentjens, and I. Riviere. 2013. The basic principles of chimeric antigen receptor design. *Cancer Discov* 3: 388–398.

178. Sadelain, M., I. Riviere, and S. Riddell. 2017. Therapeutic T cell engineering. *Nature* 545: 423–431.

179. Hammill, J. A., A. Afsahi, J. L. Bramson, and C. W. Helsen. 2016. Viral Engineering of Chimeric Antigen Receptor Expression on Murine and Human T Lymphocytes. In *The Tumor Microenvironment. Methods in Molecular Biology* vol. 1458. J. Ursini-Siegel, and N. Beauchemin, eds. Humana Press, New York, NY. 137–157.

180. Gross, G., T. Waks, and Z. Eshhar. 1989. Expression of immunoglobulin-T-cell receptor chimeric molecules as functional receptors with antibody-type specificity. *Proc Natl Acad Sci USA* 86: 10024–10028.

181. Eshhar, Z., T. Waks, G. Gross, and D. G. Schindler. 1993. Specific activation and targeting of cytotoxic lymphocytes through chimeric single chains consisting of antibody-binding domains and the gamma or zeta subunits of the immunoglobulin and T-cell receptors. *Proceedings of the National Academy of Sciences* 90: 720–724.

182. Till, B. G., M. C. Jensen, J. Wang, E. Y. Chen, B. L. Wood, H. A. Greisman, X. Qian, S. E. James, A. Raubitschek, S. J. Forman, A. K. Gopal, J. M. Pagel, C. G. Lindgren, P. D. Greenberg, S. R. Riddell, and O. W. Press. 2008. Adoptive immunotherapy for indolent non-Hodgkin lymphoma and mantle cell lymphoma using genetically modified autologous CD20-specific T cells. *Blood* 112: 2261–2271.

183. Louis, C. U., B. Savoldo, G. Dotti, M. Pule, E. Yvon, G. D. Myers, C. Rossig, H. V. Russell, O. Diouf, E. Liu, H. Liu, M.-F. Wu, A. P. Gee, Z. Mei, C. M. Rooney, H. E. Heslop, and M. K. Brenner. 2011. Antitumor activity and long-term fate of chimeric antigen receptor-positive T cells in patients with neuroblastoma. *Blood* 118: 6050–6056.

184. Pule, M. A., B. Savoldo, G. D. Myers, C. Rossig, H. V. Russell, G. Dotti, M. H. Huls, E. Liu, A. P. Gee, Z. Mei, E. Yvon, H. L. Weiss, H. Liu, C. M. Rooney, H. E. Heslop, and M. K. Brenner. 2008. Virus-specific T cells engineered to coexpress tumor-specific receptors: persistence and antitumor activity in individuals with neuroblastoma. *Nat Med* 14: 1264–1270.

185. Kershaw, M. H., J. A. Westwood, L. L. Parker, G. Wang, Z. Eshhar, S. A. Mavroukakis, D. E. White, J. R. Wunderlich, S. Canevari, L. Rogers-Freezer, C. C. Chen, J. C. Yang, S. A. Rosenberg, and P. Hwu. 2006. A phase I study on adoptive immunotherapy using gene-modified T cells for ovarian cancer. *Clin Cancer Res* 12: 6106–6115.

186. Lamers, C. H. J., S. Sleijfer, A. G. Vulto, W. H. J. Kruit, M. Kliffen, R. Debets, J. W. Gratama, G. Stoter, and E. Oosterwijk. 2006. Treatment of metastatic renal cell carcinoma with autologous T-lymphocytes genetically retargeted against carbonic anhydrase IX: first clinical experience. *J Clin Oncol* 24: e20–e22.

187. Milone, M. C., J. D. Fish, C. Carpenito, R. G. Carroll, G. K. Binder, D. Teachey, M. Samanta, M. Lakhal, B. Gloss, G. Danet-Desnoyers, D. Campana, J. L. Riley, S. A. Grupp, and C. H. June. 2009. Chimeric Receptors Containing CD137 Signal Transduction Domains Mediate Enhanced Survival of T Cells and Increased Antileukemic Efficacy In Vivo. *Molecular Therapy* 17: 1453–1464.

188. Finney, H. M., A. D. Lawson, C. R. Bebbington, and A. N. Weir. 1998. Chimeric receptors providing both primary and costimulatory signaling in T cells from a single gene product. *J Immunol* 161: 2791–2797.

189. Carpenito, C., M. C. Milone, R. Hassan, J. C. Simonet, M. Lakhal, M. M. Suhoski, A. Varela-Rohena, K. M. Haines, D. F. Heitjan, S. M. Albelda, R. G. Carroll, J. L. Riley, I. Pastan, and C. H. June. 2009. Control of large, established tumor xenografts with genetically retargeted human T cells containing CD28 and CD137 domains. *Proc Natl Acad Sci USA* 106: 3360–3365.

190. Porter, D. L., B. L. Levine, M. Kalos, A. Bagg, and C. H. June. 2011. Chimeric antigen receptor-modified T cells in chronic lymphoid leukemia. *N Engl J Med* 365: 725–733.

191. Kalos, M., B. L. Levine, D. L. Porter, S. Katz, S. A. Grupp, A. Bagg, and C. H. June. 2011. T cells with chimeric antigen receptors have potent antitumor effects and can establish memory in patients with advanced leukemia. *Sci Transl Med* 3: 95ra73. doi: 10.1126/scitranslmed.3002842.

192. Rosenberg, S. A. 2014. Finding suitable targets is the major obstacle to cancer gene therapy. *Cancer Gene Ther* 21: 45–47.

193. Oren, R., M. Hod-Marco, M. Haus-Cohen, S. Thomas, D. Blat, N. Duvshani, G. Denkberg, Y. Elbaz, F. Benchetrit, Z. Eshhar, H. Stauss, and Y. Reiter. 2014. Functional comparison of engineered T cells carrying a native TCR versus TCR-like antibody-based chimeric antigen receptors indicates affinity/avidity thresholds. *J Immunol* 193: 5733–5743.

194. Maus, M. V., J. Plotkin, G. Jakka, G. Stewart-Jones, I. Riviere, T. Merghoub, J. Wolchok, C. Renner, and M. Sadelain. 2016. An MHC-restricted antibody-based chimeric antigen receptor requires TCR-like affinity to maintain antigen specificity. *Mol Ther Oncolytics* 3: 16023. doi: 10.1038/mto.2016.23.

195. Govers, C., Z. Sebestyén, J. Roszik, M. van Brakel, C. Berrevoets, Á. Szöőr, K. Panoutsopoulou, M. Broertjes, T. Van, G. Vereb, J. Szöllősi, and R. Debets. 2014. TCRs genetically linked to CD28 and CD3ε do not mispair with endogenous TCR chains and mediate enhanced T cell persistence and anti-melanoma activity. *J Immunol* 193: 5315–5326.

196. Locke, F. L., S. S. Neelapu, N. L. Bartlett, T. Siddiqi, J. C. Chavez, C. M. Hosing, A. Ghobadi, L. E. Budde, A. Bot, J. M. Rossi, Y. Jiang, A. X. Xue, M. Elias, J. Aycock, J. Wiezorek, and W. Y. Go. 2017. Phase 1 Results of ZUMA-1: A Multicenter Study of KTE-C19 Anti-CD19 CAR T Cell Therapy in Refractory Aggressive Lymphoma. *Mol Ther* 25: 285–295.

197. Morgan, R. A., J. C. Yang, M. Kitano, M. E. Dudley, C. M. Laurencot, and S. A. Rosenberg. 2010. Case report of a serious adverse event following the administration of T cells transduced with a chimeric antigen receptor recognizing ERBB2. *Mol Ther* 18: 843–851.

198. Urbanska, K., C. Stashwick, M. Poussin, and D. J. Powell. 2015. Follicle-Stimulating Hormone Receptor as a Target in the Redirected T-cell Therapy for Cancer. *Cancer Immunol Res* 3: 1130–1137.

199. VanSeggelen, H., J. A. Hammill, A. Dvorkin-Gheva, D. G. M. Tantalo, J. M. Kwiecien, G. F. Denisova, B. Rabinovich, Y. Wan, and J. L. Bramson. 2015. T Cells Engineered With Chimeric Antigen Receptors Targeting NKG2D Ligands Display Lethal Toxicity in Mice. *Mol Ther* 23: 1600–1610.

200. Zhang, T., B. A. Lemoi, and C. L. Sentman. 2005. Chimeric NK-receptor-bearing T cells mediate antitumor immunotherapy. *Blood* 106: 1544–1551.

201. Nikiforow, S., L. Werner, J. Murad, M. Jacobs, L. Johnston, S. Patches, R. White, H. Daley, H. Negre, J. Reder, C. L. Sentman, T. Wade, A. Schmucker, F. F. Lehmann, S. Snykers, R. Allen, H. Dipietro, K. Cummings, I. Galinsky, N. C. Munshi, R. L. Schlossman, R. M. Stone, D. S. Neuberg, R. J. Soiffer, G. Dranoff, J. Ritz, and S. H. Baumeister. 2016. Safety data from a first-in-human phase 1 trial of NKG2D chimeric antigen receptor-T cells in AML/MDS and multiple myeloma. Poster presentation at: *ASH 58th Annual Meeting & Exposition*. Available online at: *https://www.celyad.com/files/library/posters/DFCI-Celdara-Celyad-NKG2D-Poster-ASH-final-version-12_4_16(1).pdf* (accessed Aug 29, 2017).

202. Urbanska, K., E. Lanitis, M. Poussin, R. C. Lynn, B. P. Gavin, S. Kelderman, J. Yu, N. Scholler, and D. J. Powell. 2012. A universal strategy for adoptive immunotherapy of cancer through use of a novel T-cell antigen receptor. *Cancer Res* 72: 1844–1852.

203. Bezverbnaya, K., A. Mathews, J. Sidhu, C. W. Helsen, and J. L. Bramson. 2016. Tumor-targeting domains for chimeric antigen receptor T cells. *Immunotherapy* 9: 33–46.

204. Harris, D. T., and D. M. Kranz. 2016. Adoptive T Cell Therapies: A Comparison of T Cell Receptors and Chimeric Antigen Receptors. *Trends in Pharmacological Sciences* 37: 220. doi: 10.1016/j.tips.2015.11.004.

205. Turtle, C. J., L.-A. Hanafi, C. Berger, T. A. Gooley, S. Cherian, M. Hudecek, D. Sommermeyer, K. Melville, B. Pender, T. M. Budiarto, E. Robinson, N. N. Steevens, C. Chaney, L. Soma, X. Chen, C. Yeung, B. Wood, D. Li, J. Cao, S. Heimfeld, M. C. Jensen, S. R. Riddell, and D. G. Maloney. 2016. CD19 CAR–T cells of defined CD4+:CD8+ composition in adult B cell ALL patients. *Journal of Clinical Investigation* 126: 2123–2138.

206. Fesnak, A. D., C. H. June, and B. L. Levine. 2016. Engineered T cells: the promise and challenges of cancer immunotherapy. *Nat Rev Cancer* 16: 566–581.

207. Savoldo, B., C. A. Ramos, E. Liu, M. P. Mims, M. J. Keating, G. Carrum, R. T. Kamble, C. M. Bollard, A. P. Gee, Z. Mei, H. Liu, B. Grilley, C. M. Rooney, H. E. Heslop, M. K. Brenner, and G. Dotti. 2011. CD28 costimulation improves expansion and persistence of chimeric antigen receptor-modified T cells in lymphoma patients. *J Clin Invest* 121: 1822–1826.

208. Kawalekar, O. U., R. S. O'Connor, J. A. Fraietta, L. Guo, S. E. McGettigan, A. D. Posey, P. R. Patel, S. Guedan, J. Scholler, B. Keith, N. W. Snyder, N. W. Snyder, I. A. Blair, I. A. Blair, M. C. Milone, and C. H. June. 2016. Distinct Signaling of Coreceptors Regulates Specific Metabolism Pathways and Impacts Memory Development in CAR T Cells. *Immunity* 44: 380–390.

209. Zhao, Z., M. Condomines, F. Perna, C. C. Kloss, G. Gunset, J. Plotkin, and M. Sadelain. 2015. Structural Design of Engineered Costimulation Determines Tumor Rejection Kinetics and Persistence of CAR T Cells. *Cancer Cell* 28: 415–428.

210. U.S. Food & Drug Administration. 2017. FDA approves tisagenlecleucel for B-cell ALL and tocilizumab for cytokine release syndrome. Available online at: *https://www.fda.gov/drugs/informationondrugs/approveddrugs/ucm574154.htm* (accessed Nov 2, 2017).

211. U.S. Food & Drug Administration. 2017. FDA approves CAR-T cell therapy to treat adults with certain types of large B-cell lymphoma. Available online at: *https://www.fda.gov/NewsEvents/Newsroom/PressAnnouncements/ucm581216.htm* (accessed Nov 2, 2017).

212. Davila, M. L., I. Riviere, X. Wang, S. Bartido, J. Park, K. Curran, S. S. Chung, J. Stefanski, O. Borquez-Ojeda, M. Olszewska, J. Qu, T. Wasielewska, Q. He, M. Fink, H. Shinglot, M. Youssif, M. Satter, Y. Wang, J. Hosey, H. Quintanilla, E. Halton, Y. Bernal, D. C. G. Bouhassira, M. E. Arcila, M. Gonen, G. J. Roboz, P. Maslak, D. Douer, M. G. Frattini, S. Giralt, M. Sadelain, and R. Brentjens. 2014. Efficacy and toxicity management of 19-28z CAR T cell therapy in B cell acute lymphoblastic leukemia. *Sci Transl Med* 6: 224ra25. doi: 10.1126/scitranslmed.3008226.

213. Maude, S. L., N. Frey, P. A. Shaw, R. Aplenc, D. M. Barrett, N. J. Bunin, A. Chew, V. E. Gonzalez, Z. Zheng, S. F. Lacey, Y. D. Mahnke, J. J. Melenhorst, S. R. Rheingold, A. Shen, D. T. Teachey, B. L. Levine, C. H. June, D. L. Porter, and S. A. Grupp. 2014. Chimeric Antigen Receptor T Cells for Sustained Remissions in Leukemia. *New England Journal of Medicine* 371: 1507–1517.

214. Lee, D. W., J. N. Kochenderfer, M. Stetler-Stevenson, Y. K. Cui, C. Delbrook, S. A. Feldman, T. J. Fry, R. Orentas, M. Sabatino, N. N. Shah, S. M. Steinberg, D. Stroncek, N. Tschernia, C. Yuan, H. Zhang, L. Zhang, S. A. Rosenberg, A. S. Wayne, and C. L. Mackall. 2014. T cells expressing CD19 chimeric antigen receptors for acute lymphoblastic leukaemia in children and young adults: a phase 1 dose-escalation trial. *Lancet* 385: 517–528.

215. Turtle, C. J., L. A. Hanafi, C. Berger, M. Hudecek, B. Pender, E. Robinson, R. Hawkins, C. Chaney, S. Cherian, X. Chen, L. Soma, B. Wood, D. Li, S. Heimfeld, S. R. Riddell, and D. G. Maloney. 2016. Immunotherapy of non-Hodgkins lymphoma with a defined ratio of CD8+ and CD4+ CD19-specific chimeric antigen receptor-modified T cells. *Sci Transl Med* 8: 355ra116. doi: 10.1126/scitranslmed.aaf8621.

216. Turtle, C. J., K. A. Hay, L.-A. Hanafi, D. Li, S. Cherian, X. Chen, B. Wood, A. Lozanski, J. C. Byrd, S. Heimfeld, S. R. Riddell, and D. G. Maloney. 2017. Durable Molecular Remissions in Chronic Lymphocytic Leukemia Treated With CD19-Specific Chimeric Antigen Receptor-Modified T Cells After Failure of Ibrutinib. *J Clin Oncol* 35: 3010–3020. doi: 10.1200/JCO.2017.72.8519.

217. Kochenderfer, J. N., M. E. Dudley, S. H. Kassim, R. P. T. Somerville, R. O. Carpenter, M. Stetler-Stevenson, J. C. Yang, G. Q. Phan, M. S. Hughes, R. M. Sherry, M. Raffeld, S. Feldman, L. Lu, Y. F. Li, L. T. Ngo, A. Goy, T. Feldman, D. E. Spaner, M. L. Wang, C. C. Chen, S. M. Kranick, A. Nath, D. A. N. Nathan, K. E. Morton, M. A. Toomey, and S. A. Rosenberg. 2014. Chemotherapy-Refractory Diffuse Large B-Cell Lymphoma and Indolent B-Cell Malignancies Can Be Effectively Treated With Autologous T Cells Expressing an Anti-CD19

Chimeric Antigen Receptor. *Journal of Clinical Oncology* 33: 540. doi: 10.1200/JCO.2014.56.2025.

218. Dudley, M. E., J. R. Wunderlich, J. C. Yang, R. M. Sherry, S. L. Topalian, N. P. Restifo, R. E. Royal, U. Kammula, D. E. White, S. A. Mavroukakis, L. J. Rogers, G. J. Gracia, S. A. Jones, D. P. Mangiameli, M. M. Pelletier, J. Gea-Banacloche, M. R. Robinson, D. M. Berman, A. C. Filie, A. Abati, and S. A. Rosenberg. 2005. Adoptive cell transfer therapy following non-myeloablative but lymphodepleting chemotherapy for the treatment of patients with refractory metastatic melanoma. *J Clin Oncol* 23: 2346–2357.

219. Dudley, M. E., J. C. Yang, R. Sherry, M. S. Hughes, R. Royal, U. Kammula, P. F. Robbins, J. Huang, D. E. Citrin, S. F. Leitman, J. Wunderlich, N. P. Restifo, A. Thomasian, S. G. Downey, F. O. Smith, J. Klapper, K. Morton, C. Laurencot, D. E. White, and S. A. Rosenberg. 2008. Adoptive Cell Therapy for Patients With Metastatic Melanoma: Evaluation of Intensive Myeloablative Chemoradiation Preparative Regimens. *Journal of Clinical Oncology* 26: 5233–5239.

220. Gattinoni, L., S. E. Finkelstein, C. A. Klebanoff, P. A. Antony, D. C. Palmer, P. J. Spiess, L. N. Hwang, Z. Yu, C. Wrzesinski, D. M. Heimann, C. D. Surh, S. A. Rosenberg, and N. P. Restifo. 2005. Removal of homeostatic cytokine sinks by lymphodepletion enhances the efficacy of adoptively transferred tumor-specific CD8+ T cells. *J Exp Med* 202: 907–912.

221. Ruella, M., and M. V. Maus. 2016. Catch me if you can: Leukemia Escape after CD19-Directed T Cell Immunotherapies. *Comput Struct Biotechnol J* 14: 357–362.

222. Fry, T. J., N. N. Shah, R. J. Orentas, M. Stetler-Stevenson, C. M. Yuan, S. Ramakrishna, P. Wolters, S. Martin, C. Delbrook, B. Yates, H. Shalabi, T. J. Fountaine, J. F. Shern, R. G. Majzner, D. F. Stroncek, M. Sabatino, Y. Feng, D. S. Dimitrov, L. Zhang, S. Nguyen, H. Qin, B. Dropulic, D. W. Lee, and C. L. Mackall. 2017. CD22-targeted CAR T cells induce remission in B-ALL that is naive or resistant to CD19-targeted CAR immunotherapy. *Nat Med*. 24: 20–28.

223. Zhang, W.-Y., Y. Wang, Y.-L. Guo, H.-R. Dai, Q.-M. Yang, Y.-J. Zhang, Y. Zhang, M.-X. Chen, C.-M. Wang, K.-C. Feng, S.-X. Li, Y. Liu, F.-X. Shi, C. Luo, and W.-D. Han. 2016. Treatment of CD20-directed Chimeric Antigen Receptor-modified T cells in patients with relapsed or refractory B-cell non-Hodgkin lymphoma: an early phase IIa trial report. *Signal Transduction and Targeted Therapy* 1: 16002. doi: 10.1038/sigtrans.2016.2.

224. Till, B. G., M. C. Jensen, J. Wang, X. Qian, A. K. Gopal, D. G. Maloney, C. G. Lindgren, Y. Lin, J. M. Pagel, L. E. Budde, A. Raubitschek, S. J. Forman, P. D.

Greenberg, S. R. Riddell, and O. W. Press. 2012. CD20-specific adoptive immunotherapy for lymphoma using a chimeric antigen receptor with both CD28 and 4-1BB domains: pilot clinical trial results. *Blood* 119: 3940–3950.

225. Luo, Y., L. J. Chang, Y. Hu, L. Dong, G. Wei, and H. Huang. 2015. First-in-man CD123-specific chimeric antigen receptor-modified T cells for the treatment of refractory acute myeloid leukemia. *Blood* 126: 3778–3778.

226. Ali, S. A., V. Shi, I. Maric, M. Wang, D. F. Stroncek, J. J. Rose, J. N. Brudno, M. Stetler-Stevenson, S. A. Feldman, B. G. Hansen, V. S. Fellowes, F. T. Hakim, R. E. Gress, and J. N. Kochenderfer. 2016. T cells expressing an anti-B-cell maturation antigen chimeric antigen receptor cause remissions of multiple myeloma. *Blood* 128: 1688–1700.

227. Berdeja, J. G., Y. Lin, N. S. Raje, D. Siegel, N. C. Munshi, M. Liedtke, S. Jagannath, M. V. Maus, A. Turka, L. P. Lam, K. Hege, R. Morgan, M. T. Quigley, and J. N. Kochenderfer. 2017. First-in-human multicenter study of bb2121 anti-BCMA CAR T-cell therapy for relapsed/refractory multiple myeloma: Updated results. Abstract presented at: *2017 ASCO Annual Meeting*. *Journal of Clinical Oncology*. doi: 10.1200/JCO.2017.35.15_suppl.3010.

228. Fan, F., W. Zhao, J. Liu, A. He, Y. Chen, X. Cao, N. Yang, B. Wang, P. Zhang, Y. Zhang, F. Wang, B. Lei, L. Gu, X. Wang, Q. Zhuang, and W. Zhang. 2017. Durable remissions with BCMA-specific chimeric antigen receptor (CAR)-modified T cells in patients with refractory/relapsed multiple myeloma. Abstract presented at: *2017 ASCO Annual Meeting. Journal of Clinical Oncology* doi: 10.1200/JCO.2017.35.18_suppl.LBA300.

229. Junghans, R. P. 2017. The challenges of solid tumor for designer CAR-T therapies: a 25-year perspective. *Cancer Gene Ther* 24: 89–99.

230. Johnson, L. A., and C. H. June. 2016. Driving gene-engineered T cell immunotherapy of cancer. *Cell Res* 27: 38–58.

231. Katz, S. C., R. A. Burga, E. McCormack, L. J. Wang, W. Mooring, G. R. Point, P. D. Khare, M. Thorn, Q. Ma, B. F. Stainken, E. O. Assanah, R. Davies, N. J. Espat, and R. P. Junghans. 2015. Phase I Hepatic Immunotherapy for Metastases Study of Intra-Arterial Chimeric Antigen Receptor-Modified T-cell Therapy for CEA+ Liver Metastases. *Clin Cancer Res* 21: 3149–3159.

232. Beatty, G. L., A. R. Haas, M. V. Maus, D. A. Torigian, M. C. Soulen, G. Plesa, A. Chew, Y. Zhao, B. L. Levine, S. M. Albelda, M. Kalos, and C. H. June. 2013. Mesothelin-Specific Chimeric Antigen Receptor mRNA-Engineered T Cells

Induce Antitumor Activity in Solid Malignancies. *Cancer Immunol Res* 2: 112–120.

233. Ahmed, N., V. S. Brawley, M. Hegde, C. Robertson, A. Ghazi, C. Gerken, E. Liu, O. Dakhova, A. Ashoori, A. Corder, T. Gray, M.-F. Wu, H. Liu, J. Hicks, N. Rainusso, G. Dotti, Z. Mei, B. Grilley, A. Gee, C. M. Rooney, M. K. Brenner, H. E. Heslop, W. S. Wels, L. L. Wang, P. Anderson, and S. Gottschalk. 2015. Human Epidermal Growth Factor Receptor 2 (HER2) -Specific Chimeric Antigen Receptor-Modified T Cells for the Immunotherapy of HER2-Positive Sarcoma. *J Clin Oncol* 33: 1688–1696.

234. Bellone, M., and A. Calcinotto. 2013. Ways to enhance lymphocyte trafficking into tumors and fitness of tumor infiltrating lymphocytes. *Frontiers in oncology* 3: 231. doi: 10.3389/fonc.2013.00231.

235. Casucci, M., R. E. Hawkins, G. Dotti, and A. Bondanza. 2014. Overcoming the toxicity hurdles of genetically targeted T cells. *Cancer Immunology, Immunotherapy* 64: 123–130.

236. Linette, G. P., E. A. Stadtmauer, M. V. Maus, A. P. Rapoport, B. L. Levine, L. Emery, L. Litzky, A. Bagg, B. M. Carreno, P. J. Cimino, G. K. Binder-Scholl, D. P. Smethurst, A. B. Gerry, N. J. Pumphrey, A. D. Bennett, J. E. Brewer, J. Dukes, J. Harper, H. K. Tayton-Martin, B. K. Jakobsen, N. J. Hassan, M. Kalos, and C. H. June. 2013. Cardiovascular toxicity and titin cross-reactivity of affinity-enhanced T cells in myeloma and melanoma. *Blood* 122: 863–871.

237. Lee, D. W., R. Gardner, D. L. Porter, C. U. Louis, N. Ahmed, M. Jensen, S. A. Grupp, and C. L. Mackall. 2014. Current concepts in the diagnosis and management of cytokine release syndrome. *Blood* 124: 188–195.

238. Kochenderfer, J. N., M. E. Dudley, S. A. Feldman, W. H. Wilson, D. E. Spaner, I. Maric, M. Stetler-Stevenson, G. Q. Phan, M. S. Hughes, R. M. Sherry, J. C. Yang, U. S. Kammula, L. Devillier, R. Carpenter, D.-A. N. Nathan, R. A. Morgan, C. Laurencot, and S. A. Rosenberg. 2011. B-cell depletion and remissions of malignancy along with cytokine-associated toxicity in a clinical trial of anti-CD19 chimeric-antigen-receptor-transduced T cells. *Blood* 119: 2709–2720.

239. Kochenderfer, J. N., W. H. Wilson, J. E. Janik, M. E. Dudley, M. Stetler-Stevenson, S. A. Feldman, I. Maric, M. Raffeld, D. A. N. Nathan, B. J. Lanier, R. A. Morgan, and S. A. Rosenberg. 2010. Eradication of B-lineage cells and regression of lymphoma in a patient treated with autologous T cells genetically engineered to recognize CD19. *Blood* 116: 4099–4102.

240. Bonifant, C. L., H. J. Jackson, R. J. Brentjens, and K. J. Curran. 2016. Toxicity and management in CAR T-cell therapy. *Mol Ther Oncolytics* 3: 16011. doi: 10.1038/mto.2016.11.

241. Howard, S. C., D. P. Jones, and C.-H. Pui. 2011. The Tumor Lysis Syndrome. *New England Journal of Medicine* 364: 1844–1854.

242. Kochenderfer, J. N., M. E. Dudley, R. O. Carpenter, S. H. Kassim, J. J. Rose, W. G. Telford, F. T. Hakim, D. C. Halverson, D. H. Fowler, N. M. Hardy, A. R. Mato, D. D. Hickstein, J. C. Gea-Banacloche, S. Z. Pavletic, C. Sportes, I. Maric, S. A. Feldman, B. G. Hansen, J. S. Wilder, B. Blacklock-Schuver, B. Jena, M. R. Bishop, R. E. Gress, and S. A. Rosenberg. 2013. Donor-derived CD19-targeted T cells cause regression of malignancy persisting after allogeneic hematopoietic stem cell transplantation. *Blood* 122: 4129–4139.

243. Grupp, S. A., M. Kalos, D. Barrett, R. Aplenc, D. L. Porter, S. R. Rheingold, D. T. Teachey, A. Chew, B. Hauck, J. F. Wright, M. C. Milone, B. L. Levine, and C. H. June. 2013. Chimeric antigen receptor-modified T cells for acute lymphoid leukemia. *N Engl J Med* 368: 1509–1518.

244. Brudno, J. N., and J. N. Kochenderfer. 2016. Toxicities of chimeric antigen receptor T cells: recognition and management. *Blood* 127: 3321–3330.

245. Maude, S. L., D. Barrett, D. T. Teachey, and S. A. Grupp. 2014. Managing cytokine release syndrome associated with novel T cell-engaging therapies. *Cancer J* 20: 119–122.

246. Teachey, D. T., S. F. Lacey, P. A. Shaw, J. J. Melenhorst, S. L. Maude, N. Frey, E. Pequignot, V. E. Gonzalez, F. Chen, J. Finklestein, D. M. Barrett, S. L. Weiss, J. C. Fitzgerald, R. A. Berg, R. Aplenc, C. Callahan, S. R. Rheingold, Z. Zheng, S. Rose-John, J. C. White, F. Nazimuddin, G. Wertheim, B. L. Levine, C. H. June, D. L. Porter, and S. A. Grupp. 2016. Identification of Predictive Biomarkers for Cytokine Release Syndrome after Chimeric Antigen Receptor T-cell Therapy for Acute Lymphoblastic Leukemia. *Cancer Discov* 6: 664–679.

247. Bedoya, F., M. J. Frigault, and M. V. Maus. 2017. The Flipside of the Power of Engineered T Cells: Observed and Potential Toxicities of Genetically Modified T Cells as Therapy. *Mol Ther* 25: 314–320.

248. Feng, K., Y. Liu, Y. Guo, J. Qiu, Z. Wu, H. Dai, Q. Yang, Y. Wang, and W. Han. 2017. Phase I study of chimeric antigen receptor modified T cells in treating HER2-positive advanced biliary tract cancers and pancreatic cancers. *Protein Cell*. doi: 10.1007/s13238-017-0440-4.

249. Thistlethwaite, F. C., D. E. Gilham, R. D. Guest, D. G. Rothwell, M. Pillai, D. J. Burt, A. J. Byatte, N. Kirillova, J. W. Valle, S. K. Sharma, K. A. Chester, N. B. Westwood, S. E. R. Halford, S. Nabarro, S. Wan, E. Austin, and R. E. Hawkins. 2017. The clinical efficacy of first-generation carcinoembryonic antigen (CEACAM5)-specific CAR T cells is limited by poor persistence and transient pre-conditioning-dependent respiratory toxicity. *Cancer Immunol Immunother* 66: 1425–1436. doi: 10.1007/s00262-017-2034-7.

250. Park, J. H., M. B. Geyer, and R. J. Brentjens. 2016. CD19-targeted CAR T-cell therapeutics for hematologic malignancies: interpreting clinical outcomes to date. *Blood* 127: 3312–3320.

251. Teachey, D. T., S. R. Rheingold, S. L. Maude, G. Zugmaier, D. M. Barrett, A. E. Seif, K. E. Nichols, E. K. Suppa, M. Kalos, R. A. Berg, J. C. Fitzgerald, R. Aplenc, L. Gore, and S. A. Grupp. 2013. Cytokine release syndrome after blinatumomab treatment related to abnormal macrophage activation and ameliorated with cytokine-directed therapy. *Blood* 121: 5154–5157.

252. Mackall, C. L., S. P. D'Angelo, M. C. Cristea, K. Odunsi, E. Norry, L. Pandite, T. Holdich, G. Kari, I. R. Ramachandran, L. Ribeiro, G. K. Binder-Scholl, and R. G. Amado. 2016. Cytokine release syndrome (CRS) in patients treated with NY-ESO-1c259 TCR. Abstract presented at: *2016 ASCO Annual Meeting*. *Journal of Clinical Oncology*. doi: 10.1200/JCO.2016.34.15_suppl.3040.

253. Liu, X., S. Jiang, C. Fang, S. Yang, D. Olalere, E. C. Pequignot, A. P. Cogdill, N. Li, M. Ramones, B. Granda, L. Zhou, A. Loew, R. M. Young, C. H. June, and Y. Zhao. 2015. Affinity-Tuned ErbB2 or EGFR Chimeric Antigen Receptor T Cells Exhibit an Increased Therapeutic Index against Tumors in Mice. *Cancer Res* 75: 3596–3607.

254. Park, S., E. Shevlin, Y. Vedvyas, M. Zaman, S. Park, Y.-M. S. Hsu, I. M. Min, and M. M. Jin. 2017. Micromolar affinity CAR T cells to ICAM-1 achieves rapid tumor elimination while avoiding systemic toxicity. *Sci Rep* 7. doi: 10.1038/s41598-017-14749-3.

255. Freeth, J., J. Soden, A. Bourdeau, J. Rottman, P. Kasperkovitz, K. Friedman, and C. Horvath. 2017. Nonclinical safety assessment in cancer immunotherapy: Off-target profiling of whole CAR T cells using plasma membrane protein arrays. Poster presentation at: *Society of Toxicology 56th Annual Meeting and ToxExpo*. Available online at: *https://www.retrogenix.com/wp-content/uploads/2017/04/Poster-SOT-2017-Retrogenix-CAR-T-cell-specificity-screening.pdf* (accessed Nov 6, 2017).

256. Kloss, C. C., M. Condomines, M. Cartellieri, M. Bachmann, and M. Sadelain. 2012. Combinatorial antigen recognition with balanced signaling promotes selective tumor eradication by engineered T cells. *Nat Biotechnol* 31: 71–75.

257. Le Tourneau, C., J. J. Lee, and L. L. Siu. 2009. Dose escalation methods in phase I cancer clinical trials. *J Natl Cancer Inst* 101: 708–720.

258. Hay, K. A., L.-A. Hanafi, D. Li, J. Gust, W. C. Liles, M. M. Wurfel, J. A. López, J. Chen, D. Chung, S. Harju-Baker, S. Cherian, X. Chen, S. R. Riddell, D. G. Maloney, and C. J. Turtle. 2017. Kinetics and biomarkers of severe cytokine release syndrome after CD19 chimeric antigen receptor-modified T-cell therapy. *Blood* 130: 2295–2306.

259. Tasian, S. K., S. S. Kenderian, F. Shen, M. Ruella, O. Shestova, M. Kozlowski, Y. Li, A. Schrank-Hacker, J. J. D. Morrissette, M. Carroll, C. H. June, S. A. Grupp, and S. Gill. 2017. Optimized depletion of chimeric antigen receptor T cells in murine xenograft models of human acute myeloid leukemia. *Blood* 129: 2395–2407.

260. Gargett, T., and M. P. Brown. 2014. The inducible caspase-9 suicide gene system as a "safety switch" to limit on-target, off-tumor toxicities of chimeric antigen receptor T cells. *Frontiers in Pharmacology* 5. doi: 10.3389/fphar.2014.00235.

261. Paszkiewicz, P. J., S. P. Fräßle, S. Srivastava, D. Sommermeyer, M. Hudecek, I. Drexler, M. Sadelain, L. Liu, M. C. Jensen, S. R. Riddell, and D. H. Busch. 2016. Targeted antibody-mediated depletion of murine CD19 CAR T cells permanently reverses B cell aplasia. *J Clin Invest* 126: 4262–4272.

262. Neelapu, S. S., S. Tummala, P. Kebriaei, W. Wierda, C. Gutierrez, F. L. Locke, K. V. Komanduri, Y. Lin, N. Jain, N. Daver, J. Westin, A. M. Gulbis, M. E. Loghin, J. F. de Groot, S. Adkins, S. E. Davis, K. Rezvani, P. Hwu, and E. J. Shpall. 2017. Chimeric antigen receptor T-cell therapy - assessment and management of toxicities. *Nature reviews Clinical oncology* 15: 47–62.

263. Fitzgerald, J. C., S. L. Weiss, S. L. Maude, D. M. Barrett, S. F. Lacey, J. J. Melenhorst, P. Shaw, R. A. Berg, C. H. June, D. L. Porter, N. V. Frey, S. A. Grupp, and D. T. Teachey. 2017. Cytokine Release Syndrome After Chimeric Antigen Receptor T Cell Therapy for Acute Lymphoblastic Leukemia. *Critical Care Medicine* 45: e124–e131. doi: 10.1097/CCM.0000000000002053.

264. Zitvogel, L., J. M. Pitt, R. Daillère, M. J. Smyth, and G. Kroemer. 2016. Mouse models in oncoimmunology. *Nat Rev Cancer* 16: 759–773.

265. TCR^2 Therapeutics. A novel class of T cell therapies that exploit the natural signaling power of T cell receptors to fight cancer. Available online at: *http://www.tcr2.com/innovation/* (accessed Oct 31, 2017).

266. Li, V. 2017. TRuCs vs. CARs. Available online at: *https://www.biocentury.com/biocentury/emerging-company-profile/2017-06-23/why-tcr2s-trucs-could-beat-out-car-t-therapies-solid-* (accessed Nov 6, 2017).

267. Lynn, R. C., and D. J. Powell. 2015. Strain-dependent Lethal Toxicity in NKG2D Ligand-targeted CAR T-cell Therapy. *Mol Ther* 23: 1559–1561.

268. Sentman, M.-L., J. M. Murad, W. J. Cook, M.-R. Wu, J. Reder, S. H. Baumeister, G. Dranoff, M. W. Fanger, and C. L. Sentman. 2016. Mechanisms of Acute Toxicity in NKG2D Chimeric Antigen Receptor T Cell-Treated Mice. *J Immunol* 197: 4674–4685.

269. Nikiforow, S., L. Werner, J. Murad, M. Jacobs, L. Johnston, R. White, S. Patches, H. Daley, H. Negre, J. Reder, C. L. Sentman, T. Wade, A. Schmucker, F. F. Lehmann, S. Snykers, R. Allen, H. Dipietro, K. Cummings, I. Galinsky, N. C. Munshi, R. L. Schlossman, R. M. Stone, D. S. Neuberg, R. J. Soiffer, G. Dranoff, J. Ritz, and S. H. Baumeister. 2016. Safety Data from a First-in-Human Phase I Trial of NKG2D Chimeric Antigen Receptor-T Cells in AML/MDS and Multiple Myeloma. Poster presentation at: *ASH 58th Annual Meeting & Exposition*. Available online at: *https://www.celyad.com/files/library/posters/DFCI-Celdara-Celyad-NKG2D-Poster-ASH-final-version-12_4_16(1).pdf* (accessed Aug 29, 2017).

270. Verma, B., A. Awada, J.-P. H. Machiels, J. B. Brayer, D. A. Sallman, T. Kerre, K. Odunsi, C. Lonez, D. E. Gilham, and F. F. Lehmann. 2017. A NKG2D-based CAR-T therapy in a Multinational Phase 1 Dose Escalation and Expansion Study Targeting Multiple Solid and Hematologic Tumor Types. Poster presentation at: *2017 ASCO Annual Meeting*. Available online at: *https://www.celyad.com/files/library/Investors/celyad_ASCO2017-final.pdf* (accessed Aug 29, 2017).

271. Celyad. 2017. CAR T NKR-2: Leveraging the Breadth of Innate Immunity. Available online at: *http://www.celyad.com/files/library/CART-NKR-2-White-Paper-March-2017.pdf* (accessed Nov 13, 2017).

272. Celyad. 2017. Celyad reports a first complete response in a relapsed refractory AML patient in the THINK trial. Available online at: *https://www.celyad.com/en/news/celyad-reports-a-first-complete-response-in-a-relapsed-refractory-aml-patient-in-the-think-trial* (accessed Nov 13, 2017).

273. Siegler, E., S. Li, Y. J. Kim, and P. Wang. 2017. Designed Ankyrin Repeat Proteins as Her2 Targeting Domains in Chimeric Antigen Receptor-Engineered T Cells. *Hum Gene Ther*. doi: 10.1089/hum.2017.021.

274. Balakrishnan, A., A. I. Salter, A. Plückthun, and S. R. Riddell. 2016. Abstract A75: Designed Ankyrin Repeat Proteins (DARPins) as recognition motifs in chimeric antigen receptors. Abstract presented at: *AACR Special Conference on Tumor Immunology and Immunotherapy*. *Cancer Immunology Research.* doi: 10.1158/2326-6074.TUMIMM16-A75.

275. Dengler, R. 2017. Cancer immunotherapy company tries to explain deaths in recent trial. Available online at: *http://www.sciencemag.org/news/2017/11/cancer-immunotherapy-company-tries-explain-deaths-recent-trial* (accessed Nov 27, 2017).

276. Lamers, C. H., S. Sleijfer, S. van Steenbergen, P. van Elzakker, B. van Krimpen, C. Groot, A. Vulto, M. den Bakker, E. Oosterwijk, R. Debets, and J. W. Gratama. 2013. Treatment of metastatic renal cell carcinoma with CAIX CAR-engineered T cells: clinical evaluation and management of on-target toxicity. *Mol Ther* 21: 904–912.

277. Chinnasamy, D., Z. Yu, M. R. Theoret, Y. Zhao, R. K. Shrimali, R. A. Morgan, S. A. Feldman, N. P. Restifo, and S. A. Rosenberg. 2010. Gene therapy using genetically modified lymphocytes targeting VEGFR-2 inhibits the growth of vascularized syngenic tumors in mice. *J Clin Invest* 120: 3953–3968.

278. DeAngelo, D. J., A. Ghobadi, J. H. Park, S. N. Dinner, G. N. Mannis, M. A. Lunning, S. K. Khaled, A. T. Fathi, I. Gojo, E. S. Wang, M. R. Bishop, H. Hughes, C. Sutherland, W. Brown, J. Smith, S. Blackman, J. Whitmore, L. Wang, K. Rogers, N. S. Trede, M. Gilbert, and W. G. Wierda. 2017. Clinical outcomes for the phase 2, single-arm, multicenter trial of JCAR015 in adult B-ALL (ROCKET study). Poster presentation at: *SITC 32nd Annual Meeting*. Available online at: *https://www.congress-posters.com/uploads/DeAngelo%20et%20al.%20(ROCKET)%202017%20SITC%20Annual%20Meeting%20(P217).pdf* (accessed Nov 18, 2017).

279. Brodin, P., and M. M. Davis. 2016. Human immune system variation. *Nat Rev Immunol* 17: 21–29.

280. Uhlen, M., P. Oksvold, L. Fagerberg, E. Lundberg, K. Jonasson, M. Forsberg, M. Zwahlen, C. Kampf, K. Wester, S. Hober, H. Wernerus, L. Björling, and F. Ponten. 2010. Towards a knowledge-based Human Protein Atlas. *Nat Biotechnol* 28: 1248–1250.

281. Human Protein Atlas. ERBB2 Tissue Atlas - Primary Data - Lung. Available online at: *https://www.proteinatlas.org/ENSG00000141736-ERBB2/tissue/lung* (accessed Nov 14, 2017).

282. Majzner, R. G., A. J. Walker, M. Murgai, L. Zhang, A. H. Long, K. M. Wanhainen, R. J. Orentas, and C. L. Mackall. 2016. Abstract 2648: Chimeric antigen receptor T-cell therapy against anaplastic lymphoma kinase (ALK) is limited by target antigen density and CAR surface expression. Abstract presented at: *Proceedings of the 107th Annual Meeting of the American Association for Cancer Research. Cancer Research.* 76: 2648. doi: 10.1158/1538-7445.AM2016-2648.

283. Dustin, M. L. 2014. The immunological synapse. *Cancer Immunol Res* 2: 1023–1033.

284. Long, A. H., W. M. Haso, J. F. Shern, K. M. Wanhainen, M. Murgai, M. Ingaramo, J. P. Smith, A. J. Walker, M. E. Kohler, V. R. Venkateshwara, R. N. Kaplan, G. H. Patterson, T. J. Fry, R. J. Orentas, and C. L. Mackall. 2015. 4-1BB costimulation ameliorates T cell exhaustion induced by tonic signaling of chimeric antigen receptors. *Nat Med* 21: 581–590.

285. Rapoport, A. P., E. A. Stadtmauer, G. K. Binder-Scholl, O. Goloubeva, D. T. Vogl, S. F. Lacey, A. Z. Badros, A. Garfall, B. Weiss, J. Finklestein, I. Kulikovskaya, S. K. Sinha, S. Kronsberg, M. Gupta, S. Bond, L. Melchiori, J. E. Brewer, A. D. Bennett, A. B. Gerry, N. J. Pumphrey, D. Williams, H. K. Tayton-Martin, L. Ribeiro, T. Holdich, S. Yanovich, N. Hardy, J. Yared, N. Kerr, S. Philip, S. Westphal, D. L. Siegel, B. L. Levine, B. K. Jakobsen, M. Kalos, and C. H. June. 2015. NY-ESO-1-specific TCR-engineered T cells mediate sustained antigen-specific antitumor effects in myeloma. *Nat Med* 21: 914–921.

286. TCR^2 Therapeutics. 2017. TCR^2 Therapeutics presents positive solid tumor data for its novel TRuC engineered T cell therapies at the World Preclinical Congress. Available online at: *https://static1.squarespace.com/static/581760e96b8f5b0e59bf9daa/t/59a58d2746c3c4b644966fa4/1504021800444/TCR2+PR+%2813JUN2017%29.pdf* (accessed Nov 6, 2017).

287. Holohan, C., S. Van Schaeybroeck, D. B. Longley, and P. G. Johnston. 2013. Cancer drug resistance: an evolving paradigm. *Nat Rev Cancer* 13: 714–726.

288. Sharma, P., S. Hu-Lieskovan, J. A. Wargo, and A. Ribas. 2017. Primary, Adaptive, and Acquired Resistance to Cancer Immunotherapy. *Cell* 168: 707–723.

289. Spranger, S., and T. Gajewski. 2013. Rational combinations of immunotherapeutics that target discrete pathways. *Journal for ImmunoTherapy of Cancer* 1: 16. doi: 10.1186/2051-1426-1-16.

290. Chmielewski, M., and H. Abken. 2015. TRUCKs: the fourth generation of CARs. *Expert Opin Biol Ther* 15: 1145–1154.

291. VanSeggelen, H., D. G. Tantalo, A. Afsahi, J. A. Hammill, and J. L. Bramson. 2015. Chimeric antigen receptor-engineered T cells as oncolytic virus carriers. *Mol Ther Oncolytics* 2: 15014. doi: 10.1038/mto.2015.14.